AN ABSTRACT OF THE THESIS OF

Abel Hernandez-Guerrero for the degree of Doctor of Philosophy in Mechanical Engineering presented on July 23, 1991.

Title: A Study of Ignition and Propagation of Combustive Synthesis Reaction Between Titanium and Carbon

Abstract Approved: Redacted for Privacy
Dr. A. Murty Kanury

Combustive Synthesis or Self-Propagating High-Temperature Synthesis (SHS), is an energy-efficient combustion method of producing metallic, ceramic and composite materials from their constituent powders.

This thesis presents the results of an experimental and numerical evaluation of the propagation velocity for the SHS solid-solid reaction of titanium and carbon, as well as a study of the ignition process for the reaction.

The experimental results show the dependency trend of the wave propagation speed on various parameters: diameter of the reactant compact, density of the compact, reactant mixture composition, and dilution of the reactant mixture with the inert product TiC. Conditions at which the reaction ceases to propagate in a self-supporting manner are also identified.

This thesis attempts to generalize the existing experimental observations of the gasless SHS process by means of a dimensional analysis, thus offering a mechanistic framework within which future developments can be correlated. The implementation of the new reaction kinetics model of Kanury and some suitable dimensionless variables permit the main factors affecting the process to be embedded in a single key parameter, the Da number. This parameter includes the overall effects of thermal properties, stoichiometry of the reaction, carbon particle size, a process constant, a compression effect and the diffusion of one reactant through an intermediate complex. The study of propagation covers a broad range of possible Da numbers that could arise for different conditions found in experiments. A section in numerical calculations of the preheated length is included as well.

Comparison of the numerical and experimental results for propagation are found to be in reasonable agreement, thus validating the suitability of the analytical model.

The numerical study includes an examination of the ignition problem for a stoichiometric mixture, using a prescribed surface temperature boundary condition. For this condition, an ignition threshold curve is determined above which ignition will always occur and below which no ignition is possible.

A Study of Ignition and Propagation of Combustive Synthesis Reaction between Titanium and Carbon

By

Abel Hernandez-Guerrero

A THESIS

submitted to

Oregon State University

in partial fulfillment of
the requirements for the
degree of

Doctor of Philosophy

Completed July 23, 1991

Commencement June 1992

APPROVED

Redacted for Privacy

Professor of Mechanical Engineering in charge of major

Redacted for Privacy

Head of Department of Mechanical Engineering

Redacted for Privacy

Dean of Graduate School

Date thesis is presented July 23, 1991

Typed by Abel Hernandez-Guerrero for Abel Hernandez-Guerrero

ACKNOWLEDGEMENTS

I thank God that Rita and I succeeded in happily ending our adventure in a foreign land. As we return to our own country may He take us through paths in which we can use our knowledge to promote education and understanding.

I dedicate this work to the memory of my father Eutimio Hernandez and to my mother Francisca Guerrero. My father finished the fourth grade and my mother had only two years of schooling. It was their dream that their sons receive advanced education. As the youngest of their sons it is my joy to have fulfilled their dream. I can never repay my mother's unflagging praying for the success of our studies.

I would like to thank Dr. James Welty from the ME Department (OSU) and Dr. Arturo Lara from FIMEE (Universidad de Guanajuato, Mexico) because thanks to them I was offered the opportunity to undertake both my Masters and Ph.D. programs at Oregon State. Along the road to the end of both programs many people contributed one way or another, both in the academic and non-academic fields. To them I am deeply indebted.

I wish to acknowledge my major advisor, Dr. Kanury, for all the help and guidance offered by him throughout this work. I am grateful for the assistance of Dr. Lorin Davis, Dr. Gordon Reistad and Dr. Joel Davis. Special thanks go to Dr. Charles Wicks who was essential in the final stage of my work. I thank also Dr. Warnes for his help in the heat-

treatment stage of the experiments and Dr. Paasch for letting me make use of his SUN computer.

What can I say? Rita has always been there for me. Her love and understanding always allowed me to overcome any adversity. Our team work is finally crowned with her Masters degree and this thesis.

The discussions with my friend of many years, Salvador, also played a key role in improving the understanding of the academic problems at hand.

Lastly, but not least, I thank our families for all their support and encouragement. Any single letter from them kept us going throughout our stay in this "never-ending-rain" Oregon.

TABLE OF CONTENTS

LIST OF FIGURES

LIST OF TABLES

LIST OF APPENDIX FIGURES

LIST OF APPENDIX TABLES

A Study of Ignition and Propagation of Combustive Synthesis Reaction between Titanium and Carbon.

CHAPTER 1

THE SELF-PROPAGATING HIGH-TEMPERATURE SYNTHESIS

1.1 Introduction.

The combustion science has come a long way since the pioneering days when the concepts of the nature of combustion were initially presented in the remarkable work of N. N. Semenov in 1928 on the critical conditions of a thermal explosion. This work revealed the principal feature of combustion processes: a relationship between heat release due to chemical reaction and heat losses. Later, Zeldovich, Frank-Kamenestskii, Damkohler, and others, carried out investigations that laid the foundations of the modern theory of combustion.

The science of combustion has been influenced by the enormous problems of energy production and propulsion. Scientists studied the most efficient methods of burning the various fuels and prepared energy-rich fuel compositions. This also resulted in a limited number of systems and processes studied. At the present times the theory and practice of combustion processes has entered a new stage of

development since combustion science now offers a variety of powerful and novel methods for studying the phenomena involving complicated reactions mechanisms coupled with physical processes. This permits the involvement of and application of combustion processes in many other fields. Significant advances have been made in the development of the theory of combustion, thanks to improvement of experimental techniques and extensive use of high-speed computers, among others.

The attention of investigators has been restricted for a long time primarily to gasifying systems; hence, the theory of combustion of condensed systems is in a less known state than the theory of combustion of gases. Most of the research on the theory of combustion of condensed systems, both theoretical and experimental, has been accomplished by Russian scientists over the last few decades [1, 2, 3]. Recently, attention has been focused in one particular case of the condensed systems, the so-called gasless combustion, in which all of the reactants and products are in the condensed state. The possibility of producing a wide variety of industrially and strategically important solid materials in a non-conventional manner caught the attention of researchers in the western hemisphere [4-24] relating to the phenomena of condensed systems known as self-propagating high-temperature synthesis, of which the gasless combustion is a part.

Reactions involving solids as reactants can be organized into four distinct groups. The first and second groups pertain to oxidations occurring either at the surface of the solid or within the pores of it. In the first group, the reaction is of the type: solid + gas --> gas; the product is a gas so that the mass of the solid gradually decreases with time as the reaction proceeds. The solid gradually diminishes in size (or its pores gradually enlarge). Combustion of graphite and of porous char in air are examples of the first group.

Reactions of the type solid + gas --> solid constitute the second group. Since the product is a solid, the mass of the solid gradually increases with time as the reaction proceeds. The solid may gradually increase in size (or its pores may gradually close). Oxidation (rusting, scaling, tarnishing) of metals and metal sponges in air are examples of this group. In both the first and second groups, the concentration distribution of the oxidant gas near the surface plays a crucial role in determining the overall reaction rate. Metal nitride formation reactions also pertain to this group.

The third group of reactions involving solids is of the type solid --> solid + gas; these are known as decomposition reactions. When prompted thermally, decomposition reactions are also known as pyrolysis reactions. Some of the products

of decomposition are gaseous so that the mass of the decomposing solid decreases with time as the reaction progresses. Charring of wood offers an example of this group.

The fourth group of reactions, solid + solid -> solid, is of direct concern in this thesis. The reactants are all solids and the products are also solids. These reactions are thus, in principle, gasless reactions. The reactant mass remains invariant with time, but the volume may change. Reactions between any of the transition metals of the chemical groups IV (titanium, zirconium and hafnium), V (vanadium, niobium and tantalum) and VI (molybdenum, tungsten and chromium) and any of the non-metals such as carbon, sulfur, silicon and boron, form part of this fourth kind of reactions. These reactions appear to be sufficiently exothermic to result in a self-supporting propagation.

1.2 Characteristics of the SHS Reaction.

Self-propagating high-temperature synthesis, known in the United States by the acronym SHS, is a combustion method for producing materials from their constituent powders. Such reaction is characterized by an exothermic heat release which suffices to self-propagate the combustion-front through a compact of the powder reactants once the reaction is initiated in some region by an external heat source.

Synthesis, during which chemical bonds form, and structurization, during which the formation of the product takes place, occur simultaneously. Some of the typical characteristics of the process are [25]:

- Temperatures, 1,500 °C to 4,000 °C;
- Propagation rate, 0.1 to 15 cm/s;
- Thickness of synthesis zone, 0.1 to 5 mm;
- Rate of heating, 1,000 °C/s to 10^6 °C/s;
- Duration of initiation, .05 to 4 sec;
- Extreme thermal gradients, as high as 10^5 K/cm;
- Preservation of the external shape of the starting compact [26].

This last characteristic is due to the fact that even though part of the materials in the reaction zone may be molten, because of the high melting points of refractory materials, a lattice of rigid refractory material forms preserving the initial shape.

The SHS process can be classified in three cases: 1) the gasless case, in which the materials before and after are exclusively in the solid or condensed phase; 2) the filtration case, in which the nonmetallic gaseous reactant spontaneously enters into the reaction zone after being transported through the pores of the pressed-metal-powder reactant; and 3) the condensation case, in which the reaction proceeds in the gas phase and is accompanied by

condensation of the final product. The gasless case is the specific phenomenon which will be investigated in this thesis.

1.3 Applications and Advantages of SHS Products.

SHS reactions have become attractive for a variety of reasons. Investigation on this type of reactions, besides the interest of the theoretical aspect, has reached higher levels of recognition due to practical considerations. This kind of reactions provide an energy-efficient approach to the synthesis of simple and complex materials including metallic, ceramic and composite materials.

Some of the more practical advantages of the SHS method over those of conventional methods include higher purity of the products, relative simplicity of the process, possibility of simultaneous formation and densification of the materials, and possibility of obtaining complex or metastables phases. Some other advantages have being claimed to this process, but some of these advantages have not been experimentally confirmed. However we can list some of the current and potential applications of the SHS process to prepare materials such as [12]:

1) Abrasives, cutting tools, polishing powders; examples of it are TiC, cemented carbides, and carbonitrides.
2) Resistive heating elements, like $MoSi_2$.

3) High-temperature lubricants, like molybdenum chalcogenides.
4) Solid lubricants, e.g., sulfides.
5) Neutron attenuators (shielding nuclear radiation), like refractory metal hydrides and ferro-alloys.
6) Shape-memory alloys, like TiNi.
7) High temperature structural alloys, like nickel aluminides.
8) Steel processing additives, like nitrided ferroalloys.
9) Electrodes for electrolysis of corrosive media, like TiN and TiB_2.
10) Coatings for containment of liquid metals and corrosive media, example of which are products of aluminum and iron oxide thermite reactions.
11) Powders for further ceramic processing, like Si_3N_4.
12) Alloys to produce superconductors, like MoS_2 alloyed with Nb [25].

Some of these listed materials have important industrial applications. They are conventionally produced by sintering a mixture of powders in a furnace heated by gas plasmas, microwave-electromagnetics, induction-coupled plasmas or hollow cathode discharges. Contrary to the characteristics of the SHS process given above, these conventional methods are expensive and energy-intensive, with a process

that is difficult to control, that has a long reaction time, and that is not always reliable in terms of the purity of the final product or of properties sought. For example, a process for preparing titanium carbide needs to employ sophisticated power-consuming equipment, the productivity of the process is low (0.5 kg/hr per furnace), and the quality of the final product is poor (there will be some percent of unreacted material in the final product) [27].

The SHS process avoids some of the practical problems of conventional methods showing that:

a) processing times are of the order of seconds or minutes rather than hours,
b) any contaminants in the reactants are vaporized away so that the products are generally purer,
c) process permits production of seamless linings of the product over complicated substrate surface contours,
d) potential for simultaneous materials synthesis and product fabrication by forming the precursor green compacts into the shape of the desired piece, among other things.

The explanation of the SHS process requires the combined concepts of thermodynamics, theory of combustion, chemical engineering, metallurgy, and material science.

1.4 The Issue Addressed in this Thesis.

The not-so-well understood complexity of the intrinsic chemical kinetics in the SHS reactions, and the multiplicity of factors that influence the propagation of the combustion wave have made it difficult to establish theoretically the mechanisms controlling the velocity of the front (a main problem from the viewpoint of the theory of combustion) and the limits of the synthesis so that a behavior of the reaction can be predicted for practical and optimal reactor design purposes. This thesis provides the results of our particular experimental findings in the propagation speed for the SHS reaction that produces titanium carbide. In the thesis we also make a numerical study of the factors that affect this gasless SHS reaction by means of a dimensionless analysis. Our focus is on thermal, physical and chemical mechanisms, embedded in key dimensionless parameters, which culminate in the SHS process. Dimensional analysis offers a study tool to generalize the existing and future experimental observations of the gasless SHS process and to offer a mechanistic frame-work within which future developments can be correlated. Our task is to delineate experimentally the dependency of the steady propagation speed of the SHS reaction wave on such parameters as initial density of the mixture, reactant ratio, dilution with product and diameter of the samples. Analytically the

task will be to determine the dependency of ignition and propagation on an important dimensionless parameter (introduced in Chapter 4), the Damkohler number Da. This parameter encircles the effects of thermal properties (density ρ, thermal conductivity K, and specific heat C_p), composition, carbon particle size, process constant ß, a "compression" effect and the diffusion of titanium through an intermediate complex (as described in Chapter 3).

An important element in the SHS processes is the chemical kinetics of the reaction. Some of the known kinetic models are discussed in Chapter 3. Currently, most of the available kinetic models for solid-solid reactions follow a trend imposed by definitions of kinetic rates from the Soviet literature. Even though most of the essential elements of physics and chemistry appear to be considered in these models, detailed explanation of the models is lacking. This makes the implementation of these Soviet kinetics models a bit ambiguous. In this thesis we implement the new kinetic model for solid + solid -> solid reactions developed by Kanury [28]. This model is based on experimental observations of the mechanism of reaction by the Russian scientists Aleksandrov and Korchagin [29, 30].

Summarizing, the overall purpose of this thesis is to contribute towards an improved understanding of the manner in which the exothermic SHS reactions develop and propagate.

1.5 Planned Presentation Within this Thesis.

This dissertation will be presented in the following order: Chapter 2 gives an examination of the existing literature on the development of the Self-Propagating High-Temperature Synthesis, SHS. Important contributions on both experimental and theoretical fields are asserted and some insights on the process and its specific features are reiterated or clarified.

In Chapter 3, the kinetics of the problem are fully discussed, depicting some models that have been used by earlier investigators. The kinetics model to be used in this thesis is introduced and explained.

Chapter 4 shows the analysis of the governing equations and boundary conditions, first in a 2-d format and then, based on some non-radial effect assumptions, reduced to a 1-d format. Nondimensional variables and parameters are introduced. The Damkohler number, an important parameter of the problem,is identified. Assumptions and approximations are discussed in some detail. The ignition problem is addressed as well.

In Chapter 5, the numerical model is formulated and the governing equations are discretized. Chapter 6 deals with the description of the experimental method and the instrumental setup used in this investigation. Some experimental drawbacks encountered through the development of this work

are indicated.

The experimental results are presented in Chapter 7 while the numerical results are divided into two parts; Chapter 8 presents the numerical results on ignition and Chapter 9 presents the numerical results on propagation speed and their comparison with the experimental values.

The study ends in Chapter 10 with conclusions of both, numerical and experimental investigations. Remarks are given on future directions for experimental or theoretical research believed to be necessary as a consequence of the present investigation.

CHAPTER 2

LITERATURE SURVEY

2.1 Introduction.

This chapter reviews the efforts by other scientists and engineers on the development of Self-Propagating High-Temperature Synthesis (SHS). Important contributions are asserted and some insights on the process and its specific features are reiterated or clarified. This is done by first presenting an overall review of the works on experimental research and then a review on some of the theoretical approaches. Most of the papers on the SHS problem are from the Russian literature and in journals which are not readily accessible. Throughout most of this chapter, rather than to follow a chronological order of the progress in the understanding and contributions to the SHS process, an arrangement of ideas is pursued.

2.2 Beginnings of SHS Investigations.

According to Merzhanov [31], the possibility of gasless combustion was first conjectured by the Russian scientists Belyaev and Komkova. They found that for a single thermite

system the burning velocity does not depend on pressure [3]. Merzhanov was experimenting with powder combustion as early as 1959-1960 [1, 2]. Merzhanov proved the reality of gasless combustion in 1965, when he developed a gasless composition based on the ferric oxide-aluminum thermite. However, the process with thermites was too complex to attempt to prove that the rate of combustion was determined solely by the reaction taking place. Accordingly, Merzhanov and coworkers chose a mixture of titanium and boron for their experiments. To their surprise, the product of combustion retained its original shape, and was exception-ally hard and dense. Pure TiB_2 was formed. The Soviet researchers were quick to realize the potential of the process and initiated further research efforts at the Soviet Institute of Chemical Physics in 1967 under the direction of Merzhanov. Eventually, their efforts had a transition from basic to applied research. Illustrations of such transition are found in 1973 and 1979 United States patents claimed by Merzhanov and co-workers [27, 32] on their process. According to Crider [25], seventy compounds had been synthesized by 1974, and by 1976 there were 30 different Soviet facilities engaged in investigating the process as well as studying ceramic products made with the SHS technique. The size of reactors available by 1972 for the SHS process were up to 10 kg of material per reaction. By the late 70's more than 200 ceramic compounds

(using both gas and gasless reaction) and refractory compounds had been produced. At least two SHS materials have reached industrial production in the Soviet Union: TiC abrasives as a substitute for diamond products and $MoSi_2$ for heating elements. Table 2.1 presents a list of some materials prepared by the SHS method [33].

Table 2.1 Some Refractory Compounds Produced by Self-Propagating High-Temperature Synthesis (SHS)

Strongly Exothermic	
Carbides	TiC, ZrC, HfC, VC, NbC, Ta_2C
Borides	TiB_2, ZrB_2, HfB_2, VB_2, NbB_2, TaB_2, MoB
Nitrides	AlN, BN, Si_3N_4, TiN, ZrN, Ta_2N
Silicides	$TiSi_3$, ZrSi, $MoSi_2$
Chalcogenides	MgS, $NbSe_2$, $TaSe_2$, MoS_2, WS_2
Hydrides	TiH_2, ZrH_2, NbH_2, IH_2
Intermetallics	NiAl, CoAl
Weakly Exothermic	
Carbides	B_4C, Al_4C_3, SiC, Mo_2C
Borides	MoB_4, Mo_2B, W_2B_5
Germanide	$NbGe_2$

It was not until 1973 that the SHS process was first confirmed in the United States in a notable work by Hardt [15], of the Lockheed Missiles and Space Co. However, a process very similar to the SHS method was already claimed by McKenna [17] for the preparation of tungsten monocarbide. It is interesting to note that even in Holt's 1982 paper [34], all the references are from the Russian literature and none were from the United States. An extensive research program was eventually initiated in the United States, but mainly under the auspices of state agencies, army, navy, DARPA [18], or national laboratories. Imminently a few private industrial organizations became involved (see references). Currently, a few known academic institutions are doing work in the SHS problem (Kanury [20, 21, 22, 28, 35, 36] here at OSU).

2.3 Literature In Experimental Research.

In one of the first western works, Hardt, Phung, and Holsinger [15, 37] studied the propagation rate in metal powder mixtures to form intermetallic alloys. These researchers identified that the mass diffusion coefficients involved in solid-solid reactions were strongly concentration dependent. However, in their conclusions they noted that the magnitude of the diffusion coefficients might vary over a wide range without producing large change in the

calculated propagation rate. Based on their experiments the investigators acknowledged how sensitive the mixing procedure was to the process; this has been further verified in this investigation (described in Chapters 6 and 7).

Holt, one of the best known SHS researchers, initially worked synthesizing TiC, TiN, and TiB_2 [34]. He examined the microstructure of TiC, the effects of initial porosity, combustion temperature, and titanium particle size on the density of the final product. Using high-speed photography, he reported a propagation speed of 0.35 cm/s for TiC. He demonstrated that the porosity of the initial compact as well as the initial temperature of the sample and the stoichiometry have very little influence, if any, on the final density of the TiC. An interesting finding was that nonstoichiometric samples with carbon/titanium ratios less than 0.6 or greater than 1.67 could not be ignited.

In a later investigation, Holt and Munir (Munir is another well known SHS researcher in the United States), united efforts in experimenting with titanium carbide formation [38]. However, they did not address the issue of reaction mechanism, and they did not give conclusive experimental results concerning the rate of propagation or measured properties. Basically their investigations centered in determining the adiabatic combustion temperature under different conditions.

Shkiro et al. [39, 40] worked on the SHS process for preparing tantalum carbides (which has one of the highest known melting points: TaC 4,270 K, Ta_2C 3,770 K). Tantalum carbides are used in producing high melting point alloys and heat resistant construction materials. They found that for this particular system a redistribution of the components through capillary spreading was not possible. Shkiro and coworkers obtained experimental data that showed that as the diameter of a cylindrical sample decreased, the amount of unreacted carbon grew and the propagation decreased to a quenching point (at about 8-10 mm). This unreacted amount was shown to decrease if the initial temperature of the sample was increased. When dilution with final product increased there was an increase in the amount of unreacted carbon. In their experiments they found that by using two particle sizes of Ta, 2 μm and 45 μm, in the reaction, quenching occurred. Evidently the large metal particles acted as an inert diluent. Their results also included the effect of inert argon pressure and density.

In another experimental set-up, Henshaw and Niiler [41] observed three cases of gasless combustion (for all cases, T_a is the adiabatic temperature and T_m is the melting temperature):

1) T_a is greater than T_m for one reactant. Rigid materials with fine pores were produced, including TiC, ZrC,

ZrB_2, TiB, and SiC.

2) T_a is greater than T_m for both reactants and the product. This case resulted in severely distorted solid materials, including AlNi, TiSi, ZrSi, and TiNi.

3) T_a is less than T_m for both reactants and the product. This case resulted in a powdery final material, such as B_4C and WC.

Henshaw and Niiler reported a propagation speed of 4.7 cm/s for TiC; a high-speed 120 frames/sec video system was used to determine the speed. From the light spectra, the continuum radiation was analyzed to yield a very precise value for the temperature of the reaction zone (although they did not report it).

Another investigation performed by Hardt [26] reported the effect of various variables on the morphology of TiC and TiB_2, and on eliminating porosity; he found that densification of the products would not take place without compaction (a fact already mentioned by Holt [34]). He found that reduction of gaseous impurities by pre-treatment of the starting mixtures in a vacuum did not appear to be as beneficial as the Russian literature claimed. He also provided a description on coloration and expansion of products.

Kumar et al. [5], studied both theoretically and experimentally the combustion characteristics of the

molybdenum-silicon system. They evaluated the overall heat transfer coefficient and found that it was almost independent of the combustion temperature for a given specimen diameter. For larger specimen diameters the radial temperature gradients were significantly reduced since the system was closer to being adiabatic. They also reported expansion of the specimens.

Contrary to the statements of Merzhanov [3], Hardt [26] claimed that by increasing the ambient pressure the thermal conductivity of the gas surrounding the sample increases; therefore, the time and energy required for ignition will also increase. Experiments by Shkiro [39,40] also revealed that the combustion rate for tantalum carbides increases with increase in argon pressure, and then became "saturated" at a certain point. However the increase only occurred for low argon pressures (below 1 atm).

In a major work, Aleksandrov and Korchagin [29, 30] from the Institute of Solid State Chemistry and Mineral Refining, tried to follow one of the principles of solid state chemistry that requires that in the study of reaction mechanism and kinetics, account must be taken of the actual structures of solids. When the solids are composed of powders, their structure and reactivity are determined by the properties (including geometry) of the constituent particles. To such effect they developed a procedure that

used a transmission-type electron microscope "in situ" on model particle-film samples (that is, the formation of phases and products are followed in real time at the moment of their appearance). Even though they acknowledged the extreme difficulty in determining the mechanism of reaction one of their goals was to change the "soft" methodology used by all researchers of the mechanisms of reaction; this "soft" method involves stopping the reactions by rapid cooling [42, 43] and uses metallographic methods and x-ray spectral analysis. According to Aleksandrov, Korchagin and Boldyrev, these methods can not detect intermediate products and structures. They presented convincing experimental arguments in favor of their proposed mechanism. This mechanism considered that the reactions between the solid components begins only after a liquid phase appears (i.e. a solid + liquid reaction takes place). A more detailed description of their mechanism is given in Chapter 3. All systems studied by Aleksandrov and Korchagin showed an appreciable delay in the formation of the phase final product. Ten systems were studied: MoO_3-Al, Fe_2O_3-Al, Ni-Al, Ti-C, Nb-C, Ta-C, Ti-B, Nb-B, Ta-B, Hf-B. In all, except MoO_3-Al the layer was formed and one reactant melted.

Maksimov et al. [43], argued that the technique used by Aleksandrov and Korchagin [29, 30] did not really model the conditions of interactions at the front, and asserted that

the method of metallographic study of specimens with a combustion front fixed by quenching the sample is the most simple and accessible technique. They conducted investigations on the Ti-B system but their conclusions do not really seem to give any insight of the true mechanism, only in what they assumed to have happened when they quenched the sample. Thus, their arguments against the work of Aleksandrov and Korchagin are not strong enough and do not provide a better technique.

The electron microscope observations of Rogachev et al. [42] on the systems Ti-C and Ti-B showed that the onset of reaction coincides with the appearance of a metallic melt which spreads over the surface of the carbon in the form of a thin film less than 10^{-7} m thick. At the same time, a reaction takes place on the boundary between the carbon material and the melt leading to the formation of finely dispersed particles ($< 10^{-6}$ m) of titanium carbide within the liquid film. Using an innovative experimental method they placed the mixture of reactants into a wedge-shaped cavity in a cooper block. In this way, the combustion wave was extinguished as it approached the apex due to higher heat losses dictated by an increasing surface to volume ratio. One important thing that Rogachev [42] observed is that the structure or particle size of the carbide (or boride) formed did not correlate to the structure or size of

the initial reactants, but it was completely determined by the combustion parameters. Some more insights on this effect were given by the study of Mullins [14] on the effect of carbon morphology on the combustion synthesis of titanium carbide. He found some cases in which some morphology is preserved.

Experiments from Holt [34], and Riley and Niiler [44] using scanning electron micrographs, SEM, proved that the mechanism of the Ti + C reaction to form TiC is the movement of molten titanium to solid carbon. Since some theoretical analysis of these reactions involve diffusional mass transport, the fact that it is the titanium rather than the carbon diffusing, provides important information.

Contrary to these experiments, Khusid [45] claimed that from his studies of the Ti-C system the carbon diffuses in the melt with a diffusivity of the order of 10^{-9} m^2/s. The review by Munir and Anselmi-Tamburini [11] also reported a work by Kirdyashkin that may bring controversy to the consensus on the mechanism of reaction. According to these investigators, Kirdyashkin concluded that the dominant mechanism for the combustion synthesis of TiC was the diffusion of carbon through the initial TiC layer. This conclusion was based primarily on the apparent agreement between the activation energy for combustion and that for the diffusion of carbon in TiC. The works of Kirdyashkin and

Kushids are the only ones that claim such a reaction mechanism.

Vadchenko and Merzhanov [46] made another attempt to elucidate the mechanism of reaction. Using carbon-coated titanium (also for the system Zr+C) wires, they investigated the mechanism of the ignition and the combustion processes between these elements under conditions involving intense heat loss and high power level in the heat source. They concluded that the combustion process was is preceded by the melting of titanium, after which the titanium flowed into and filled the pores between the particles of carbon. The formation of the carbide took place in a subsequent crystallization from a molten phase. They mentioned that the coefficients of diffusion of atoms of Ti and Zr through the corresponding carbide film were 10^4 times less than for atoms of carbon. With a somewhat similar experimental method Knyazik and Merzhanov [47] tried to determine the macrokinetics of the interaction Ti-C under electrothermal explosion conditions. This method consisted of heating the sample by the passage of an electrical current through the specimen itself. A characteristic feature that they found was the almost linear increase in temperature from 2,000 to 3,000 K. Realizing that with such rapid heating of the specimen the external heat losses were low, they concluded that the reaction rate was independent of the temperature in

the investigated range; accordingly, the reaction was of zeroth order and mathematically inactivated. They explained that these effects were by solution of graphite into the melt. At temperatures below the Ti melting point they explained that carbide was formed as a result of a solid-state reaction.

Azatyan et al. [48] studied the combustion of titanium with silicon and showed that increasing the titanium particle size lowers the maximum temperature attainable and therefore the propagation rate. Another effect of increasing the particle size is that the product of combustion changes from the expected Ti_5Si_3 to $TiSi_2$ (particle change from <100 μm to > 100 μm). However, as the combination of Ti and Si powders gives a multiphase product, their results are not totally related to our single phase product analysis.

Maksimov et al. [49] presented some experimental indications that the spin mode of combustion can also arise in gasless systems. The spin combustion mode happens when the chemical reaction focus moves over the side surface of the specimen describing a spiral; it is observed mainly for cases of combustion of metals in gases like nitrogen. They observed that the spin regime lies near the combustion limit (with respect to the ratio of reactants) for the systems Ti-Al and Ti-ferroboron. However, they did not explain why the spin combustion mode was not observed in all gasless

systems. Merzhanov was the first to report [50, 51] that the phenomenon of spin combustion for gas-solid systems was influenced by specimen density, specimen diameter and nitrogen/argon ratio in the gas mixture, and that the phenomena existed close to the limit of propagation. He also reported auto-oscillatory combustion, which is the propagation of a planar flame front in a pulsating regime with a specific frequency. He pointed out that its burning rate and frequency were affected by the degree of dilution of the initial mixture with inert additives, by the specimen density, and by specimen diameter.

Repeated combustion is another phenomenon reported [51]. This consists of the passage of a second flame front along the already burned substance, following the propagation of the first flame. It is said that this phenomenon is influen-ced by the nitrogen pressure, specimen density, metal parti-cle size, and incomplete conversion of the substance at the combustion front. When hafnium burns in a nitrogen-argon mixture, a second slower moving front appears approximately 4 seconds after passage of the first front.

Merzhanov [31] was clear in remarking that i) diffusion transfer of the combustion product did not occur, that ii) there was no similarity between the concentration and temperature fields (in contrast to the combustion of gases), and

iii) the processes occurring in the burnout zone did not affect the rate of propagation of the combustion wave. Merzhanov [51], also noted the existence of filtering combustion for the case of combustion with nitrogen gas; filtration of the gas takes place under the action of the pressure difference arising due to nitrogen absorption in the reaction zone. This filtration gives raise to two effects: when the characteristic time of combustion is much greater than the characteristic time of filtration, combustion takes place in layers; otherwise, surface combustion occurs.

The only known work on the combustion of gasless systems at cryogenic temperatures was reported by Strunina et.al [52]. This is of interest for outer space applications. They analyzed changes in combustion regime with critical initial temperatures.

Japan is another country which is doing research in the SHS process. The Japanese have developed a new method for ceramic-to-metal welding [53] as well as a different ignition process for the synthesis of SiC [54]. There is a disadvantage in the ceramic-to-metal welding in that it has to be performed at pressures of about 3 GPa. For the synthesis of SiC, the new ignition process helps the weak reaction to proceed, something that the heat released from the exothermicity of the reaction is not able to do; this

special reaction shows a weak release of heat (69 KJ/mol compared to 293 kJ/mol for TiB_2). Weakly exothermic compounds, like SiC, B_4C, Al_4C_3, Mo_2C, MoB_4, MoB_2, Mo_2B, WB, W_2B_5, WB_4, $TaSi_2$, Mo_3Si, etc., are characterized by low bonding energies between the atoms, and hence require external source of heat for the reaction to persevere. The Japanese also found that a mixed reactant of powders with relatively large particle size could not be ignited.

The primary objective of the majority of investigations on combustion synthesis is the production of powders. Despite their intrinsic advantages, SHS produced powders must be further processed to form dense bodies and shapes. Reports of successful experiments to consolidate ceramic bodies to full densities after being formed by the SHS reactions are sparse. A technique to accomplish this consolidation was devised by the Yamada et al. [55], who synthesized and simultaneously applied high pressure to compact the material, obtaining up to 95% of theoretical densities. This method has the potential to shorten the overall process and to minimize the energy input. Another technique to densify the product while synthesizing was tried by Riley and Niiler [44], using pressures no higher than 0.4 GPa; these pressures are considered relatively low for compaction. It is interesting to note that two of the above methods cited, welding-to-metal and pressing while

heating, were already claimed in a 1965 patent by Williams [16], from Australia, although in a more empirical basis.

From the observations of the previously mentioned experiments to densify the powders, it is found that pressureless sintering during combustion is not sufficient in magnitude to cause the formation of highly dense products. There are two basic reasons for this observation. The first reason relates to the time the material is held at high temperatures. Although the temperature of the combustion front of many SHS reactions is extremely high, the exposure time of the material to such conditions is relatively short. The second reason, and perhaps the most important, is the evolution of gases during the passage of the combustion front. The same process that is responsible for the purification of SHS produced materials (the expulsion of volatile impurities) can lead to the formation of entrapped gases, and hence the swelling of the product (a phenomenon that was observed in our experiments as well as in another investigations [41]). Rice [8], based on simple analytical calculations, erroneously argues that there is a volume decrease of the sample, an indication that practice does not exactly follow theory in this case.

The steps that can be taken to lessen the effect of gas evolution during reaction are the outgassing of the reactants prior to combustion and/or the application of a high

inert gas pressure during combustion. Kecskes and Niiler [10] identified the solid and gaseous impurities on constituent powders to form TiC and studied the effects of their evolution. The main gas species evolved from the graphite are: CO, N_2, C_2H_4, H_2O, CO_2, C_3H_8, O^+, CH_4, and from titanium are: H_2O, OH^+, H_2, H^+, CO, N_2. Carbon monoxide and carbon dioxide need baking temperatures above 1,000 °C to be evolved. The major constituents of impurity gases ejected during reaction consisted of free hydrogen, carbon monoxide, free oxygen, carbon dioxide, and hydrocarbons. Water vapor was driven off as soon as the compact reaches 100 °C, followed by the release of hydrogen from TiH_2 at 400 °C, oxygen from the dissociation of TiO_2 at about 2,000 °C, and CO and CO_2 throughout the temperature range. They observed that if the combustion wave velocity is so fast that the impurities can not escape out of the sample in the heated region ahead of the front, the very sudden release of the vapors at the reaction front can violently disrupt the process. They also analyzed the condensable impurities deposited around the sample. The sources of condensables were as follows: tungsten, sodium, sulfur, chlorine, potassium and calcium from the filament used to ignite the samples; titanium from the Ti powder, iron, nickel, copper, manganese, and chromium as impurities in the aluminum substrates that were positioned near the sample; silicon and

potassium from the mica stage that held the samples, and calcium from the graphite powder. These researchers pre-heated the sample at 800 °C by operating the heating filament at a power level of 200 W for 10 minutes with the pressure reduced down to a pressure base of 10^{-2} Pa. When they did not do this heat-treatment, they encountered samples which would explode due to the violent outgassing. (This was also encountered in our experiments. In our experiments, as described in a later chapter, their recommendations were followed to purge impurities in a vacuum oven for several hours in the 500 °C range.) Hardt [26] pre-treated his samples in vacuum up to a temperature close to 700 °C. Holt and Munir [38] and Shkiro [39, 40] also presented analysis of gas evolutions.

In another study, Hansen et al. [9] did some elaborated investigation of SHS by three different means: (1) thermo-chemical computer modeling, (2) time-resolved quadrupole mass spectrometry, and (3) optical multichannel analysis. The computer modeling was based on the minimi-zation of the total free energy of the system under the constraints of constant temperature, pressure, and mass. However, only titanium, carbon and oxygen were considered to form the system. The other two techniques were based on the irradiation of a laser beam on the surface of the sample. In case (2), the vapors evolved from the sample were passed

through the ionization region of the mass spectrometer, while in case (3) the light emissions from the sample during laser ignition were analyzed using an optical multichannel analyzer (OMA). The second technique found that the impurities H_2, O_2, N_2, and H_2O were easily removed from the reaction mass and should make minor contributions to the overall mechanism of the reaction. The information using the OMA technique did not give conclusive results.

Products obtained by the SHS method have been compared to commercially obtained products by ways of comparing their densification rates or their structures after some heat treatment; this was done by Quabdesselam and Munir [56] for titanium diboride, and by Manley, Holt and Munir [57] for titanium carbide. In the case of the diboride the investigators found little differences, while the commercial carbide could be more densified that the synthesized carbide. An overall observation is that SHS produced powders are not as easy to sinter as powders prepared by conventional means [38].

An analysis of the mechanism of densification is presented by Ristic [13]. In terms of abrasive properties, the synthesized titanium carbide shows better results than conventionally-made titanium carbide, as tested by Merzhanov et al. [27]. Due to the "self-purification" characteristic of the SHS process, the oxygen impurities are reduced (a by-

product of conventionally produced powder), resulting in a significantly reduction of the hardness and yield strength of refractory ceramics [41].

Data on the chemical and physical properties of SHS products are consistently absent from reports in SHS. Even for the most studied reactions, the production of titanium carbide and titanium diboride, the controlling kinetic and property values for the powders compact are difficult to find. For example, the thermal conductivity of the powders, which has an important role in controlling the characteristics of the reaction, has not been fully determined for a system. One of the few exceptions is the thermochemical data measured by Hardt and Phung [15]. Additional experimental data available on SHS powder compacts is the data provided by Butakova et al.[58], for the thermal conductivity of the systems $2Fe_2O_3 + 3Ti + 2.26TiO_2$, $2Cr_2O_3 + 3Zr + 2.8ZrO_2$, and $Cr_2O_3 + 2Al + .64Al_2O_3$, as a function of density, percentage dilution by reaction product and particle size. Butakova's experimental results show an increase in the thermal conductivity with increasing compact density.

The somewhat similar process involving reaction of powders of intermetallic systems also suffers also from the lack of data available on thermophysical parameters or the dependence on composition, pressing density, etc. [59].

The reactant powder compact densities are a major

factor in the rate of propagation. Rice et al. [60] studied the effect of percent theoretical density for 4 reactions involving titanium and observed that with increasing compact density up to a maximum value at about 60 ± 10 % of the theoretical density there is an increase in the propagation velocity. They also found that at higher densities the propagation rates not only decreased, but terminated due to self-extinction; at certain high densities the reaction even failed to propagate. They argued that the maximum point in propagation rate is due to the following inverse trends as a function of density: (i) increasing availability of reactants species (porosity decreases as density increases), and (ii) larger density producing larger heat losses. Heat transfer ahead of the combustion front has the consequence of lowering the temperature to which the sample is preheated by the reaction before ignition and thus lowers the combustion temperature. They also found that larger particles affect ignitability and propagation in an adverse manner. The trend found by Rice after the maximum point is contrary to the results of the numerical model of Kottke and Niiler [19]. (In our experiments the same trends as reported by Rice were determined (see Chapter 7).) The results of Azatyan et al. [48] also showed this trend with a maximum at about 70% relative density. The results of Shkiro et al. [39, 40] showed the decreasing-side trend with density for

tantalum carbides, but did not show a maximum.

One feature in the study of these high-temperature reactions is the difficulty associated with trying to measure the combustion temperature of some of the reactions. A proof of this statement is the work of Holt [34] who had to use an indirect measurement of positioning inside the samples pieces of materials to observe if they melted. If the materials did not melt then their melting temperatures could be considered as an upper limit of the reaction. However, this method is not conclusive at all. The same problem of melting occurs when some type of thermocouples are inserted to try to monitor the combustion temperature, since at some point of temperature, they will melt. Hardt [26] reported using tungsten-rhenium thermocouples but could not trace the peak temperatures because the specimen reacted with the thermocouples. Pyrometers offer another method of measuring the temperature, but they have the problem that the evolution of gases from the compact will produce "clouds" inside the chamber, and thus interfere with the pyrometer readings.

In regards to the decrease and control of the high temperatures, and hence the propagation rates, the Russians researchers introduced the method of diluting the product material with the normal reactants. This method produced a product of fairly uniform and fine particles size and good

purity, but poor mechanical strength. Another practical technique that the Russians introduced is the use of a "chemical furnace" [26]. This furnace is simply a layer of another SHS mixture which surrounds the test specimen. The heat output of the thermal blanket ignites the specimen and maintains it for a prolonged period at an elevated temperature.

The next section presents an overview of the theoretical approaches to the SHS problem.

2.4 Literature on Theoretical Research.

Probably one of the first mathematical models related to the SHS process was that of Aldushin and Merzhanov [61]. Most of their basic qualitative results can be applied to the process. The mechanism of their model and other proposed models are explained later in Chapter 3.

Kovalenko [62] made a very complex mathematical analysis of the gasless combustion with large heat transfer at a wall (enclosed systems) for reaction of the system PbO_2-WO_2, but without any concern about the kinetics or stoichiometry of the reaction. This approach is very common in the output of SHS papers from the Soviet Union. Strunina et al. [63] used the same kind of approach to mathematically study the influence of heat losses and thermophysical parameters, but for a double system of reactions. Two

different powder systems were put together so that one served as the igniter for the other. They extended their theoretical work further by studying the conditions under which the second system would ignite [64]. It seems a little premature to try to analyze two systems at once, since there is still a need for a consistent model for a single system.

An analysis on the problem of stability for a gasless system with heat losses was made by Strunina et al. [65]. They used four different variations of the kinetic function of the type described in the general kinetics model in chapter 3. Most of their analysis was done for a one dimensional system and the remainder of their analysis was for a flat 2-D specimen with a simple first order kinetics. Dvoryankin et al. [66] also addressed the combustion stability and proposed their model. They compared the type of stability which might exists, imposing two types of conditions at the surface of a sample: a normal Newtonian type of heat losses and an ideal thermal contact with an inert material.

Hardt and Phung [15] made a study of a SHS propagation with a one-dimensional model with no heat losses. The process is governed by diffusion through a film of product separating the reactants. Their kinetic analysis is described in detail in Chapter 3. They made the simplifying assumptions that the reactant geometry can be approximated

by a structure of alternating layers of components whose relative thicknesses are dependent on the reaction stoichiometry and density. Accordingly, their derivation showed that the reaction rate is dependent on these thicknesses. Their paper is unique in that it reports measured thermochemical data.

Another mathematical investigation is that of Lyubhenko [67] et al. who constructed a somewhat complex 1-d numerical model, involving a simple kinetic reaction model. Their analysis was very mathematically involved but, according to the authors, it predicts well some experimental trends for the iron-aluminum thermite reaction. The conditions for the degeneration of the steady propagation of a thermal combustion wave were investigated by Aldushin et al. [68].

The trend of using kinetic equations of first order appears repeatedly in analytical models, even the more recent investigation of Boddington et al. [7], from England. They developed a simple 1-D numerical model with convection losses. Their reported numerical results were surprisingly close to the experimental results for mixtures of tungsten and potassium dichromate. The unexpected accuracy is questionable based on the fact that the thermal and kinetics properties are themselves difficult to assess accurately. The authors themselves acknowledge how fortuitous their results were; however, it should be pointed out in their

behalf that the model seems to satisfactorily predict the observed trends of the SHS process as well as to predict conditions leading to combustion failure. From their numerical findings it was determined that steady state is reached early (at about 20 ms) and not far away from the hot boundary (.2 mm).

Aleksandrov et al. [69] also used a first order kinetics in their analysis of the influence of two-dimensionality and heat losses in gasless combustion. They developed some criteria under which approximate values of the propagation rate can be estimated, and compared those parametric values with computational runs. The kinetics (explained in detail in chapter 3) derived from Aleksandrov and Korchagin [29, 30] was adapted by Huque et al. [22] for the analysis of the synthesis of TiC.

Even one of the latest modeling studies, by Varma et al. [70], assumed simply a first order kinetic reaction with respect to one reactant and a zeroth order with respect to the other reactant without any further examination of the mechanism of reaction. They failed to interpret how the cylindrical sample is positioned since convective and radiative losses at the base of the sample were used. The range of validity of parameters used in their study were given without any explanation of what were the "typical property values of SHS reactions," or how they might be

obtained. Their numerical results were not compared with any actual experimental result.

Another numerical modeling that used first order kinetics is that of Hlavacek, Puszynski and co-workers [4, 5, 6]. They found that, in the adiabatic case, the heating-up time associated with an insignificant degree of conversion at the beginning of the reaction was short. They mentioned that the concentration profiles were steep for high values of the activation energy E, but for low values of E, the propagation wave degenerated. They performed their high-order finite-difference scheme on supercomputers at national laboratories. They discussed the following analytically developed stability criteria for gasless combustion:

1) If $\mu < \mu_{cr}$ there is constant-pattern profile

2) if $\mu > \mu_{cr}$ there is oscillatory behavior

where $\mu = E(T_a - T_o)/(RT_a^2)$, T_a is the adiabatic temperature, T_o is the initial temperature of the sample, E is the activation energy, and R is the universal gas constant. This criterion was based on the assumption that the reaction zone is infinitely narrow. They also included another criterion for stability:

1) if $T_a/T_o > 2$, an increase in the reaction heat results in a more stable combustion,

2) if $T_a/T_o < 2$, an increase in the reaction heat gives raise to a less stable combustion process.

For non-adiabatic conditions they found that for high values of the cooling parameters there will be an extinction of the propagation. They described oscillatory behavior when temperatures overshoot the adiabatic temperature and perturb the steady propagation. Some simplifications were also presented.

In connection to the criteria between steady-state and auto-oscillatory conditions, Merzhanov [31] determined the following criteria:

$$\alpha=9.1\ (C_p/Q)\ (RT_a^2/E)\ [1-.27\ Q/(C_p\ T_a)]$$

if $\alpha>1$ steady-state combustion occurs

if $\alpha<1$ auto-oscillatory combustion takes place.

Holt and Munir [38], however, observed some doubts about the validity of this criteria. It has been mentioned [12] that the reactions will not be self-sustaining unless $T_a \geq 1800$ K based on data which compares T_a for several compounds against their ratio of $\Delta H°/C_p$. This range of temperatures corresponds to a minimum ratio of $\Delta H°/C_p \geq 2X10^3$ K. From this study, Munir concluded that there is a low sensitivity of C_p to temperature for several compounds.

Kottke and Niiler [19] performed an investigation on the possible effects of the thermal conductivity on the reaction Ti+C. They measured the thermal conductivity of the

compacted powders against the density of the sample at room temperature. However, their modeling analysis could be strongly questioned, since in no part of their model was there any mention whatsoever of the kinetics mechanism nor of an internal heat source term. Other than that, their paper is an excellent exercise in modeling conductivity in a block without internal heat sources. Their modeling results predicted that the SHS propagation velocity has a linear dependence on the thermal conductivity of the precursor powder for highly compact products.

In the theoretical work of Kumar et al. [5] on the molybdenum-silicon system, the investigators proposed a simple surface reaction controlled model for systems in which the product layers exhibits a porous microstructure. They acknowledged how difficult it was to quantitatively simulate solid-solid reactions due to the lack of information on the reaction mechanism and in the physical and kinetic properties of the systems. Interestingly, some of their numerical results were strikingly close or equal to the experimental results. Their formulation of the mechanism of reaction assumed that the reaction rate was proportional to the surface area of the fraction of unreacted nonmelting compound. This is explained later in Chapter 3.

Kanury [21] emphasized that an approach to the analysis of the SHS process can evolve on the basis of the developed

knowledge of the combustion science. He showed that the observed global patterns [24] of the process can be predicted by combustion theory. Ignition, reaction wave propagation and quenching were part of his analysis. Some of his conclusions were: (i) an increase in reactant particle size causes a decrease in propagation speed, since smaller particle sizes provide larger surface areas conducive to larger reaction rates; (2) increase in sample diameter results in an increase in the wave speed to an asymptotic value due to a relative gradual reduction of lateral heat losses; (3) in contrast, if the sample thickness is below a certain critical value, the lateral heat loss will be sufficiently intense to preclude ignition; (4) a high thermal conductivity of the compact will make ignition more difficult while making propagation easier; (5) dilution with inerts, products or excess reactants tends to decrease the effective heat of combustion and reaction temperature and, thereby, the propagation speed; (6) there exists rich and lean limits of composition only between which propagation is possible; (7) preheating the reactants increases the reaction temperature and hence the propagation speed.

2.5 Closing Comments.

As it is evident from this review, the vast majority of SHS process literature resulted from Russian Investigations.

However, while we see that in those papers the essential physics and chemistry appear, they lack detail in their reports. We should add, however, that most of the existing research on the process was done by metallurgist and materials science people, and that their work was primarily highly descriptive and empirical. Mechanisms were seldom stressed with no attempt to account for reaction kinetic rate processes, and only a few investigations involving mechanism as a significative feature.

A National Science Foundation Workshop on SHS was recently held [71]. The workshop succeeded in bringing together most of the United States SHS researchers. Corbin [33] had already talked of the need to combine efforts for the study of this phenomenon and of the need of major experimental efforts to determine the total characteristics of starting powders and kinetics of reaction. He also spoke of the necessity of developing a unified model to simulate the process. Microscopic models and mechanistic descriptions of the sequence of the initial reaction, nucleation and product growth are virtually nonexistent [71].

The outcome of the NSF workshop calls for a major thrust on basic research. The participants quote Merzhanov as saying: "The task is (1) the development of precise experimental methods for investigating the dynamics of structural conversion that occur in SHS, and methodology for

comprehensive diagnostics of the process, and (2) the development of reliable mathematical models . . ..".

A short list of some of the existent basic research needs is presented in Table 2.2.

Table 2.2 Current Basic Research Needs in the SHS Process.

A. Determination of high temperature thermophysical and thermochemical data for reactants and products: enthalpy of formation, specific heat, thermal and mass diffusivities, etc.
B. Characterization of the three zones of combustion, warming zone, reaction zone and afterburn zone.
C. Execution of experiments to determine chemical and physical mechanisms; basic quantities to be measured: burning velocity, temperature profile, degree of conversion, pressure of composition of gases.
D. Development of new techniques for dynamical measurement of temperature, elemental composition and structure.
E. Study methods of densification, understand effects of gradients, determine influence of defects, etc.

Point A in this table stresses the unavailability of accurate values of the thermal and kinetic properties. This imposes an immense problem if some kind of accurate modeling is sought. However, no ranking in the table should be emphasized and all points in the research needs should be considered.

For some more insights in the SHS process, the reviews by Munir and Anselmi-Tamburini [11] (which also includes gases-solids reactions), Munir [12], Munir and Holt [23], Sheppard [24], Crider [25], and Corbin [33], are suggested. For an introduction to surface reactions references [72-80] are suggested.

We close this chapter by also quoting a comment from a 1988 paper [19]: ". . . definitive experimental measurements of propagation velocity as a function of green compact density remain to be performed . . .," from which we infer that the SHS process still needs to be further studied.

CHAPTER 3

KINETICS OF THE PROBLEM

3.1 Introduction.

In this chapter, the chemical kinetic characteristics for the solids --> solids reaction are discussed. Initially, a summary of gas reaction kinetics is presented so some of its conclusions can be drawn to better comprehend the kinetics of the solid --> solid reaction. A description of some of the kinetics models which have been proposed to explain the SHS process is presented. The new kinetics model, proposed by Kanury [28], is introduced and its merits are discussed.

3.2 Overall Description of the Kinetics Problem.

Specialists of the SHS process are basically interested in two questions: (i) determining the factors controlling the velocity of the reaction front and (ii) clarifying the factors determining the rate of reaction and formation of the desired product. As mentioned in the preceding chapters, there is very little existing knowledge related to the chemical kinetics of the combustion of solids in the

reaction: solid + solid --> solid. The importance of understanding the chemical kinetics is obvious, since it is one of the more important factors influencing the ignition and propagation or non-propagation of the combustion wave in the compact of reactants.

One basic problem is to establish relationships between reactivity of solids and the structure of the reactant mixture. This requires studying microprocesses in regions with dimensions of the order of the size of the particles of the powder. Mutual arrangement, structure, chemical and phase composition (before, during and after reaction) should be taken into account. Such studies are extremely difficult because of the rapid rate of the reactions, as well as the high temperatures under which they occur. Limitations also exist in the available experimental methods and equipment which would yield information on the governing mechanisms.

Numerous attempts exist in the literature trying to elucidate the mechanism of reaction. Several models have been proposed involving distinctive different features on how the reaction proceeds, each model is based on some simplifying assumptions of geometry or conclusions based on experimental observations. Some ideas about the mechanism of interaction are based on assumptions which are in the best case supported by data from indirect experiments or are based on theoretical calculations relating to the rate of

combustion with the kinetic parameters of the reaction. Since the kinetic parameters are often unknown, there is always the chance that some factors have been ignored. The fact that there exist several proposed mechanisms that are based upon knowledge gained from gas-phase reactions indicates that the current knowledge of the kinetics of solids -> solids is not complete.

3.3 Summary of Gas Reaction Kinetics.

By doing a quick review of gas phase kinetics, we facilitate an easier understanding of the solid reactions. Complex mechanisms of gas-phase reactions are sufficiently well understood. Modern technology allow both experimental and analytical studies to investigate the variables of the gas phase reaction within acceptable accuracy.

By using some of the results of the kinetic theory of gas reactions rates, a qualitative understanding of the influence of some of the parameters of the reaction can be obtained. This success is largely due to the conceptual clarity associated with the collisions and interactions amongst the atomic or molecular gaseous reactants. For an elementary reaction rate, the reaction rate N'''_A (kmoles of species A/(m^3 s)) for a reaction such as:

$$n\,A + m\,B \rightarrow \text{product} \qquad (3.1)$$

is given by the Arrhenius exponential law:

$$N'''_A = -k_o C_A^n C_B^m e^{-\frac{E}{RT}} \qquad (3.2)$$

where the pre-exponential factor k_o is dependent on the nature of the particles of A and B, C_A and C_B are molar concentrations of the reacting species, E is the activation energy, R is the universal gas constant and T is the absolute temperature. The stoichiometry given above also describes the precise manner in which the species particles interact in the elementary reaction, since n and m are the same as the orders of the reaction. Values of k_o and E can be theoretically estimated for elementary gas phase reactions and the effect of gas pressure is found proportional to $P^{(n+m)}$.

A mechanism composed of several elementary steps, each with its own elementary rate equation can be integrated to obtain the overall rate of depletion of a reactant or generation of a product. When mechanism of this sort become complicated or unavailable, the equation given above is usually assumed to hold for the rate of the global reaction with kinetic constants k_o, m, n, and E. The resultant empirical global rate equation correctly contains the dependencies of the reaction rate on reactant composition, pressure and temperature.

3.4 Characteristics of Solid Reactions.

As mentioned earlier, Kanury and Huque [20], gave an excellent review on the kinetics models. The following presentations in Sections 3.4 and 3.5 are based on some of their observations.

Of the four groups of solid reactions identified in Chapter 1, the collision theory concepts may be extended to arrive at some viable rate mechanism for only the first group. The effect of temperature on the heterogeneous reaction rate continues to be described by the Arrhenius exponential (as in Equation (3.2)). In the remaining three groups, the detail of interaction among the reactants is not so clear. This thesis involves only the fourth group, however, some of the following observations relate to the second and third groups.

A number of molecules are generally held together to form the crystalline or polymeric structure of a solid. To result in oxidation in which the product oxide is a solid (i.e., the second group identified earlier), the reactant gas attacks the crystalline solid either at the surface or in the interior after the gas diffuses into the crystal through any existent defects. Once the reaction in a solid layer is initiated, the reaction can be continued only if either the ionic metal diffuses outwards to the gas or the oxidant gas diffuses inwards through the oxide layer to the

metal. The resistance to this diffusion gradually increases with time as the oxide layer thickens. The rate of increase of the oxide layer thickness is inversely proportional to the thickness itself so that thickness is proportional to $(\text{time})^{1/2}$. Thus, the overall chemical reaction rate is determined by a physical diffusional process. The coefficient of diffusion in solids is expected [73, 74] to depend on temperature according to the relation:

$$D \alpha T^{1/2} e^{-E/(RT)}.$$

In reactions of the third group, the crystalline units of the solid undergo violent vibrations in response to heating. With sufficiently intense heating, the vibrations may become so strong as to rupture the crystal or the molecule. Such a process is known as thermal decomposition or pyrolysis. The products generally are a lower density solid and a mixture of gases and vapors. The effect of temperature on the pyrolysis reaction rate is traditionally taken to follow the Arrhenius exponential law. This is justified by the fact that a higher temperature leads to an intensified vibration and thereby to an increased rupture of the molecules.

In the second, third as well as the fourth types of solid reactions, the notion of the order of the reaction has a rather limited physical meaning. It does, however, serve to incorporate into the rate law the fact that the reaction

ceases when one or more of the reactants is depleted.

To describe the fourth (as well as the second) type of solid reactions, the phenomena of migration of cations, isotopic exchange, self-diffusion, preferential diffusion along grain boundaries and defects have to be considered. The theory shows that the transport coefficients pertaining to these diffusion are temperature-dependent again in an inverse negative way [75-78].

For the reactions of the fourth group, i.e. of the type solid + solid --> solid, which is the one of our interest, lets us consider a uniform powder mixture of species A and B. The reaction rate can be defined as the rate of change of mass per unit volume of one of the species, say A, in units of $kg/(m^3 s)$. If the particles are small, of the order of angstroms, the reaction may follow a rate equation of the type given by Equation (3.2). The concentrations are interpreted to be the partial densities of the two species of the mixture. For the simplest case when $n \approx m \approx 1$ and the mixture has a total density ρ, it follows that $C_B = (\rho - C_A)$. Equation (3.2) is transformed to:

$$N'''_A = -k_o C_A (\rho - C_A) e^{-\frac{E}{RT}} \qquad (3.3)$$

If the particles are not small, the reaction rate at the very initial stages of the reaction is expected to

depend on the size and shape of the particles; it is perhaps proportional to the number of points of contact between the reactant species. However, the solid product of the reaction poses a barrier between the reactants A and B. The thicker this barrier gets, the lower the subsequent reaction rate becomes. There exists several other models and, in turn, other rate equations that account for the effect of this formed solid layer and for the effect of temperature [20].

3.5 Kinetic Models of Gasless Combustion.

The primary factors that make difficult the study of the reaction mechanism of SHS processes are the high rates of local heating, high temperatures and limitations of the available experimental methods. Most of the SHS kinetics hypotheses are thus verifiable by the alternate route of indirect experimental observations. Some of these observations have evolved in the proposed mechanisms of reaction. Let us consider some of the proposed kinetic models reported in the literature. In the following models $\eta=0$ will denote the state of the initial reactants, while $\eta=1$ denotes that of the final products.

3.5.1 Merzhanov Model.

The basis for the Merzhanov model is that the advance of the reaction depends upon diffusion of the reactants

across an ever-growing product layer. The final rate equation is invalid if the product layer is not a continuously growing solid layer, as one may encounter when the product either forms bridges and filaments between the reactant particles or is ruptured and decomposed as soon as it is formed.

Merzhanov et al. [31, 61, 68] used the so-called logarithmic law to describe the SHS kinetics:

$$\frac{\partial \eta}{\partial t} = k_o \exp\left(-\frac{E}{RT}\right) \exp(-\beta\eta) \qquad (3.4)$$

where t is the time, k_o is a constant for the system under consideration, E is the activation energy, R is the universal gas constant, T is the absolute temperature, and ß is the kinetic parameter or self-inhibition constant. ß characterizes the inhibition of the reaction as δ increases. η is the extent of conversion $\eta = \delta/\delta_{max}$, where δ is the product layer thickness and δ_{max} is the maximum value that δ can achieve. ß is a function of the probability of a blister barrier being situated within a certain thickness element dδ evolving in a time element dt.

This equation is applicable to SHS processes if the products (and some of the reactants) neither melt nor vaporize at the process temperatures. These systems, in general, are heterogeneous from both thermal and chemical

points of view. If the particles are sufficiently fine, the temperature gradients within the particles can be reduced or even eliminated.

3.5.2 General Kinetics Model.

We have called this the general model, since most papers in the literature use a variant (order) of it. In fact, the Merzhanov model and the Aleksandrov and Korchagin [29. 30] model could be considered an adaptation of it; the first order reaction equation can be applied if particles are extremely small, as discussed in Section 3.4.

$$\frac{\partial \eta}{\partial t} = k_o \exp\left(-\frac{E}{RT}\right) \phi(\eta) \qquad (3.5)$$

The last factor in this equation, $\phi(\eta)$, is called the kinetic function, and is defined by one of the following functions [65]:

$(1-\eta)$	for a first order reaction
$(1-\eta)^2$	second order reaction
$(1-\eta)(\eta+\eta_o)$	reaction with acceleration
$S(\eta)\ f(\eta)$	complex reaction
$e^{-\beta\eta}$	Merzhanov model

where η_o is a ratio of the rate constants, $S(\eta)$ is the specific reaction surface, and $f(\eta)$ is a function characterizing the kinetic law of interaction through the

product layers. As indicated in the review chapter, most researchers use this kinetics without really questioning it, or without regards of what the origin of the mechanism of reaction is. The fact that some investigators have obtained good theoretical results in agreement with their experimental results would explain its broad use. Unfortunately, this kind of kinetics does not account for particle size variation, different stoichiometry, dilution with an inert, etc.

3.5.3 Kumar et al. Model [5].

In this model one of the reactants is considered to be a solid, a liquid or a gas, and the other reactant is a solid which does not melt; the product exhibits a porous microstructure. It is considered that the more "mobile" reactant has good access into the unreacted core of the second, solid reactant. The diffusion of the "mobile" reactant through the product layer is limited to the diffusion through the submicron products layers formed on the micrograins of the porous particles. Kumar et.al conclude that this type of diffusion should not be affected by the particle size of a nonmelting reactant. Based on the fact that the complete conversion of a single particle is obtained within milliseconds, their model assumes that the reaction rate is proportional to the surface area of the

fraction of unreacted nonmelting compound.

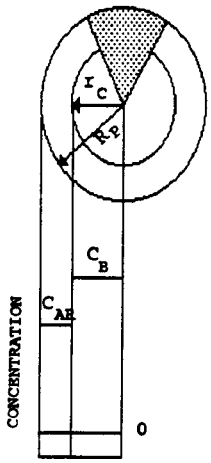

Figure 3.1 The porous Structure of Metal Particle and Intraparticle Reactant Concentrations During the Combustion Synthesis [5].

For a reaction described by:

n A(solid,liquid and/or gas) + B(solid) --> P(solid)

The reaction rate is,

$$-\frac{d\,N_A}{dt} = k_o\, e^{-\frac{E}{RT}}\, 4\pi r_c^2\, C_{AR}\, M_A \qquad (3.6)$$

where: M_A, M_B -molecular weight of reactants, kg/kmole

ρ_B -density of nonmelting reactant, kg/m^3

k_o -pre-exponential factor, m/s

E -activation energy, J/mole

R -universal gas constant, J/(mole K)

n -stoichiometric coefficient

R_p -average particle radius, m

r_c -reaction front interface position, m

C_{AR} -initial concentration of more "mobile" reactant, kg/m^3

The molar rate of consumption is,

$$\frac{dN_B}{dt} = \frac{1}{n}\frac{dN_A}{dt} = \rho_B M_B 4\pi r_c^2 \frac{dr_c}{dt} \qquad (3.7)$$

These investigators define η, the extent of conversion of the solid particle, by the following relation:

$$\eta = 1-(\frac{r_c}{R_p})^3 \qquad (3.8)$$

Adapting this definition into the previous two equations and rearranging, they obtain the kinetics rate equation as:

$$\frac{d\eta}{dt} = \frac{M_A k_o e^{-\frac{E}{RT}} C_{AR}}{n M_B \rho_B R_p} (1-\eta)^{.667} \qquad (3.9)$$

3.5.4 Hardt and Phung Model [15].

This model was initially intended to describe the reaction rates of intermetallics. In view that in a pressed

specimen most particles appear flat and irregular, a slab geometry seemed most appropriate for the Hardt and Phung model (see Figure 3.2).

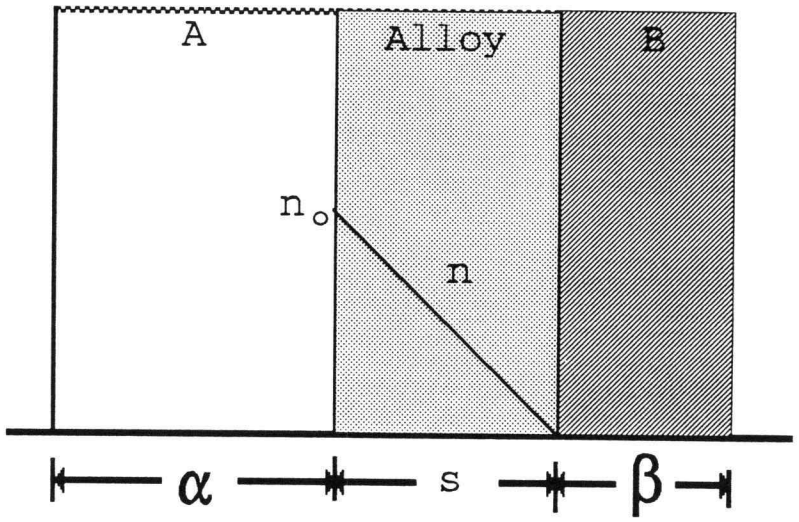

Figure 3.2 Interparticle Diffusion.

In Figure 3.2, α is current thickness of metal A, s is current thickness of alloy layer, ß is current thickness of metal B, n_o is concentration of A in pure A layer, and n is concentration of A in alloy layer. Alternate parallel layers of A and B represent adjacent particles of the two metals. For simplicity, a single particle size is assumed for each metal. Mass diffusion involved identical units, consisting of one-half of a particle of each kind. Such units will be called diffusion cells whereas the term particle denotes a

grain of either metal powder. The initial thickness of the two layers of a diffusion cell is determined by stoichiometry, atomic weights, and densities. If α_o is the thickness of metal A in a cell, then the thickness of metal B is given by:

$$ß_o = \alpha_o \frac{N_B M_B \rho_A}{N_A M_A \rho_B} \qquad (3.10)$$

where N_A, M_A, and ρ_A are respectively the stoichiometric fraction, the atomic weight, and the density of metal A, and N_B, M_B, and ρ_B are those of metal B. To react, the metals must diffuse through the layer of alloy product being formed. As the product layer thickness s increases, the reactant thicknesses α and ß decrease with time. The corresponding differential decrease in thickness ß of the B metal is:

$$dß = \frac{ß_o}{\alpha_o} d\alpha \qquad (3.11)$$

As the reaction proceeds, the product grows at the expense of the two unreacted layers. The product layer does not need to contain exclusively the reacted atoms of the two kinds in the stoichiometric ratio. On the side of metal A is an excess of unreacted A atoms moving toward metal B;

similarly, near metal B, the alloy layer contains an excess of B metal moving toward metal A.

The rate of increase of the product layer thickness ds/dt is the sum of the rates of diminishment of the layers α and ß. Thus,

$$\frac{ds}{dt} = -\frac{d\alpha}{dt} - \frac{d\beta}{dt} \qquad (3.12)$$

The rate of diffusion across the layer s gives the rate of consumption of A as:

$$\frac{d\alpha}{dt} = -\left(\frac{D}{s}\right) \qquad (3.13)$$

where $D=D_o\ e^{-E/(RT)}$ is the coefficient of diffusion of species A across the product layer. Combining these relations, one obtains,

$$\frac{ds}{dt} = \frac{1 + \frac{\beta_o}{\alpha_o}}{\frac{D}{s}} \qquad (3.14)$$

Finally, by defining the extent of reaction as $\eta = s/\beta_o$, the following rate equation for the model is obtained:

$$\frac{\partial \eta}{\partial t} = \frac{\alpha_o+\beta_o}{\alpha_o\ \beta_o^2}\ \frac{D_o}{\eta}\ e^{-\frac{E}{RT}} \qquad (3.15)$$

3.5.5 Aleksandrov and Korchagin Model [29, 30].

Aleksandrov, Korchagin and Boldyrev claim to provide unequivocal experimental evidence to support their mechanism of reaction. In this mechanism the reaction between the components begins only after a liquid phase appears, i.e. a solid + liquid reaction takes place. The reaction proceeds by diffusion of atoms of liquid phase B into solid phase A until solid solutions or intermetallic compounds, whose melting point is lower than that of the solid component, form in the boundary layer. Thus, these compounds can pass into the liquid phase by melting. The resulting layer of intermediate products AB' grows steadily at the A/AB' boundary and passes into the liquid phase at the opposite B/AB' boundary. The investigators observed that after a layer of certain width is attained, the intermediate product is absorbed by the liquid component, and simultaneously from the other side (at the interface with the solid) its growth continues. Here the width of the layer of primary products stays practically constant and is independent of the amount of liquid phase. See Figure 3.3.

Two factors contribute to a gradual reduction of the reaction rate: first, the surface area at which the reaction occurs is gradually decreased. Second, the concentration of species A in the outer melt is gradually reduced due to

continuous dilution with the intermediate species AB'.

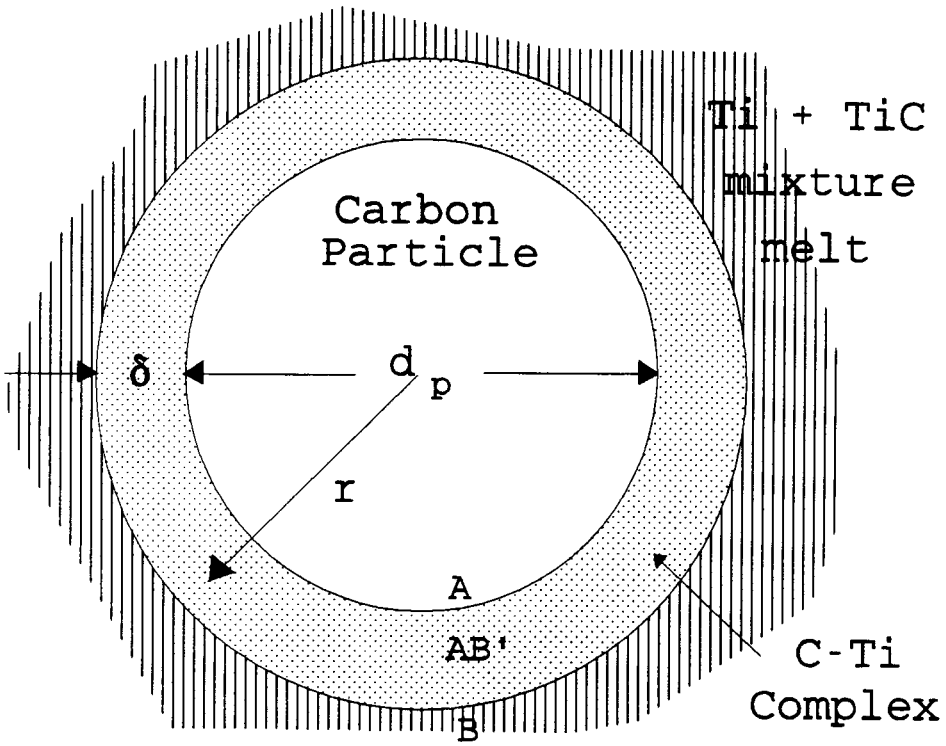

Figure 3.3 Schematic of Aleksandrov and Korchagin Model.

With η, as before, representing the extent of reaction; t the time; k the effective rate constant of the reaction; C_B the concentration of the substance B on the outer surface of the layer of intermediate products; and S the area of the interphase surface AB'/A, these investigators write the following kinetic equation:

$$\frac{d\eta}{dt} = k\, C_B\, S \qquad)$$

S varies in the course of the process as described by the equation for a shrinking surface:

$$S = k' (1-\eta)^{2/3} \qquad (3.17)$$

In the case of a stoichiometric mixture, the concentration of the component B in the liquid phase is given by:

$$C_B = k'' (1-\eta) \qquad (3.18)$$

Since the rate of diffusion, and the entire process as a whole, varies in this case according to the change of C_B and the cross sectional area of the diffusion flux, the equation for a stoichiometric mixture is:

$$\frac{d\eta}{dt} = k(T) (1-\eta)^{5/3} \qquad (3.19)$$

If the mixture is not stoichiometric, let μ, the composition factor of the mixture, be equal to the ratio of the coefficient in front of B in the stoichiometric reaction equation to the molar coefficient for this component in the given mixture ($\mu\eta < 1$). Let j be an index equal to 0, 1 and 2 to account respectively for a plane, cylindrical, and spherical shape of the particles. The Aleksandrov and Kor-

chagin model is described by the general rate equation in the form:

$$\frac{\partial \eta}{\partial t} = k(T)\ (1-\mu\eta)\ (1-\eta)^{\frac{j}{j+1}} \qquad (3.20)$$

According to their observations, the diffusion coefficients of the liquid component, estimated from the growth rate and the width of the layer of primary products, exceed the known values for bulk bimetallic samples by several orders of magnitude; however Aleksandrov and Korchagin do not provide a specific value for any case. In their mechanism, the final reaction product should form at the later stages of the reaction, via crystallization from the melt as the liquid component becomes saturated by dissolution of the layer of primary products. These conclusions are also confirmed by data obtained [30] with a synchrotronic illumination diffractometer with which they found an appreciable delay in the formation of the phase of final product.

3.6 Discussion of the Kinetic Models.

Literature [3, 31, 79] contains other models for solid state reactions, but nearly all models involve a reaction rate determined by the diffusional resistance offered by the product layer (as in some of the previously described models). In Merzhanov's model, the product layer gradually

grows; such a growth brings with it blisters which randomly obstruct the diffusion of the reactant. The consequence of this blistering is a progressively strong self-inhibition of the reaction.

In the Hardt and Phung model, the product layer gradually thickens as the reactant diffuses across it to produce the reaction. The reactant concentration on the side of species A is taken to be constant while that on the side of species B is taken to be zero, thus inferring the intrinsic chemical reaction to be fast compared to diffusion.

In contrast, the Aleksandrov and Korchagin model considers the intermediate product layer to be of constant thickness (0.1 to 10 μm), as a result of the formation of the intermediate due to the reaction on the solid side and its continuous dissolution into the molten species A on the outer side. While the diffusional resistance remains invariant in this situation, the concentration of species A in the outer liquid decreases with time to reduce the diffusion rate, and hence, the reaction rate. An additional factor which reduces the net reaction rate is the gradual reduction in the surface area of the solid species B as it gets gradually consumed.

However, in spite of the considered diffusion through a layer, if the models assume kinetic processes of zero, first or second order, then these models still do not take

into account explicitly the effect of reactant particle size, and presumably any effect not considered which will be contained in the empirically determined constant. The diffusion model on the other hand, requires a knowledge of the geometry of the reactants, and hence includes particle size as a parameter.

Kumar's model takes a different approach and considers the reaction to be limited by how much area of reaction exists; by neglecting any resistance due to diffusion it infers that the model can only be used for highly porous particles. Kumar's model does not involve any possible dilution with inerts, but it does include the effect of particle size.

In the case of the general kinetics model, any effects that are not considered are assumed to be imbedded in the highly empirical value of k_o; therefore, any ambiguity can always be originated.

Being based on extensive experimental observations of the reaction mechanism, the model of Aleksandrov and Korchagin appears to be the most desirable for incorporation in our studies. Their synchrotron radiation and electron microscope techniques [29, 30] are by far the most informative in terms of describing a step-by-step mechanism of reaction. The experimental studies of Holt [34], Rogachev [42], Riley and Niiler [44], Vadchenko and Merzhanov [46],

and other researchers present independent evidence to confirm the melting of titanium particles, surface-tensional flow of this melt around graphite particles and reaction of the melt with graphite.

3.7 Mechanism Selected for this Investigation. The Kanury Model [28].

Kanury developed a new kinetics model for the reactions solid + solid --> solid, in which the important sequential features include the diffusion of the melted metal into the carbon phase, the subsequent melting reaction of this phase, and finally the precipitation of the product. The experimental observations of Aleksandrov and Korchagin [29, 30] confirm that:

i) in all systems studied, melts and gases play an important role, and an interaction solid-solid with formation of solid products only, is not achieved;

ii) the SHS reaction has an unusual mass transport mechanism, consisting of the motion of particles of one reagent along the surface of another with simultaneous reaction and formation of a layer of primary (intermediate) products. The rate at which this intermediate dissolves in the metal-melt side is such that the thickness of the complex is proportional to the instantaneous diameter of the nonmetal particle (see Figure 3.3).

iii) the component predominantly transferred by the molecular diffusion method is usually the more easily melting component;

iv) the coefficients of diffusion of the components of most systems, evaluated based on the rate of growth of the layer of primary products and its width, are close to the values of the coefficients of surface diffusion;

v) the melt immediately forms intermediate products, separating the reagents.

After the thickness of this layer reaches a definite value (from 0.1 μm for Ta-C up to ≈10 μm for Ni-Al) absorption of this layer by the liquid phase starts and at the same time the layer begins to grow on the other side where there is a boundary with the other solid component.

Since the diffusion resistance of the layer of primary products AB' is much greater than that of the liquid, the concentration of the melting substance B on the outer boundary is virtually equal to its concentration in the liquid. The concentration of B on the inner boundary is equal or close to zero, since the rate of the chemical reaction is incommensurably higher than the rate of diffusion.

The systems investigated by Aleksandrov and Korchagin were MoO_3-Al, Fe_2O_3-Al, Ni-Al, Ti-C, Nb-C, Ta-C, Ti-B, Nb-B, Ta-B and Hf-B. In all, except in MoO_3-Al, the intermediate

layer was formed and one reactant melted.

3.7.1 Assumptions.

Some of the main assumptions of Kanury's model [28] are as follows:

i) The thickness of the layer of intermediate product is proportional to the instantaneous diameter of the nonmetal particle.

ii) The time to establish a steady state in the mechanism of reaction (characterized by the thickness of the layer of primary products) is much shorter than the duration of the interaction process as a whole. Thus we can assume that the layer is formed almost from the beginning.

iii) All particles are of the same size.

iv) All particles have a spherical shape.

v) The concentration of the melting reagent is zero at the outer surface of the surrounded nonmetal particle; this means that the reaction on the surface of the particle is very fast.

vi) The initial mixture of C, Ti and TiC is uniform.

3.7.2 Formulation of the Possible Kinetics Explained by the Kanury Model.

Suppose that the sample to analyze will be a mixture of:

1 (kmol of C) + a (kmol of Ti) + b (kmol of TiC)

where a is a factor that represents the stoichiometric or excess amount of titanium (or shortage); for stoichiometric conditions a=1; b is the factor that represents dilution of the mixture with product TiC. The following mixture combinations arise:

i) a stoichiometric mixture with no product dilution (a=1, b=0)

$$C + Ti \longrightarrow TiC$$

ii) a metal rich mixture with no product present (a>1, b=0)

$$C + a\,Ti \longrightarrow TiC + (a-1)\,Ti$$

iii) a metal lean mixture with no product present (a<1), b=0)

$$C + a\,Ti \longrightarrow (1-a)\,TiC + (1-a)\,C$$

iv) a stoichiometric mixture with some product diluted (a=1)

$$C + Ti + b\,TiC \longrightarrow (b+1)\,TiC$$

v) a metal rich mixture with some product diluted (a>1)

$$C + a\,Ti + b\,TiC \longrightarrow (b+1)\,TiC + (a-1)\,Ti$$

vi) a metal lean mixture with some product diluted (a<1)

$$C + a\,Ti + b\,TiC \longrightarrow (b+1-a)\,TiC + (1-a)\,C$$

It is necessary to determine quantitatively how the concentrations of either reactant vary with respect to time

to account for how much mass reacts and, in turn, how much heat is generated. The heat generation term in the energy equation (see Chapter 4) couples the energy equation with the kinetics to describe the process. The concentrations are determined by invoking the basics of stoichiometry and mass diffusion.

In the following paragraphs the deduction of the concentration of the reactants as function of the initial number of moles present, densities and molecular weights is presented as previously described by Kanury [28]. A steady-diffusion analysis is added to calculate the diffusion rate of Ti through the intermediate layer. With these concentrations and diffusion rate, the rate of reactant consumption can be determined.

3.7.3 Stoichiometry, Analysis of Concentrations.

By definition, the number of moles is calculated as number of moles= mass/M=(volume ρ)/M, where M represents the molecular weight. Thus, <u>per each particle of C present at time zero</u> the number of moles present are respectively:

moles of S	moles of L	moles of P
$\frac{\pi d_{po}^3}{6}\frac{\rho_c}{M_c}$	$\frac{\pi d_{po}^3}{6}\frac{\rho_c}{M_c}$ a	$\frac{\pi d_{po}^3}{6}\frac{\rho_c}{M_c}$ b

here d_{po} represents the initial diameter of the particle of carbon (recall that particles are assumed spherical). M_c and ρ_c are the molecular weight and density of carbon respectively. After the reaction starts, there will be a reduction of volume of the carbon particle, and hence an equal reduction in the number of moles of carbon and titanium present as dictated by the stoichiometry of the reaction and at the same time this number of moles of product will be produced. Therefore, at time t>0:

moles of C consumed	moles of Ti consumed	moles of TiC produced
$\frac{\pi}{6}(d_{po}^3-d_p^3)\frac{\rho_c}{M_c}$	$\frac{\pi}{6}(d_{po}^3-d_p^3)\frac{\rho_c}{M_c}$	$\frac{\pi}{6}(d_{po}^3-d_p^3)\frac{\rho_c}{M_c}$

where d_p represents the instantaneous diameter of the carbon particle. Subtracting this consumption from the initial number of moles of carbon and titanium, and adding the initial amount of TiC to the TiC produced up to this time, one obtains the number of moles that are present in the mixture:

moles of C	moles of Ti	moles of TiC
$\frac{\pi}{6}d_p^{\,3}\frac{\rho_c}{M_c}$	$\frac{\pi}{6}[(a-1)d_{po}^3+d_p^{\,3}]\frac{\rho_c}{M_c}$	$\frac{\pi}{6}[(b+1)d_{po}^3-d_p^3]\frac{\rho_c}{M_c}$

From the definition of moles, volume = (moles)(M/ρ), the volume of remains can be calculated as:

volume left of C	volume left of Ti	volume left of TiC
$\frac{\pi d_p^3}{6}$	$\frac{\pi}{6}[(a-1)d_{po}^3+d_p^3]\frac{\rho_C}{M_C}\frac{M_{Ti}}{\rho_{Ti}}$	$\frac{\pi}{6}[(b+1)d_{po}^3-d_p^3]\frac{\rho_C}{M_C}\frac{M_{TiC}}{\rho_{TiC}}$

From the definition for concentration in a molar base, concentration=moles/volume, the concentration of titanium can be determined as:

$$C_{Ti} = \frac{\frac{\pi}{6}[(a-1)d_{po}^3+d_p^3]\frac{\rho_C}{M_C}}{\text{volume of the melt present}} \qquad (3.21)$$

that is:

$$C_{Ti} = \frac{[(a-1)+\frac{d_p^3}{d_{po}^3}]}{[(a-1)+\frac{d_p^3}{d_{po}^3}]\frac{M_{Ti}}{\rho_{Ti}} + [(b+1)-\frac{d_p^3}{d_{po}^3}]\frac{M_{TiC}}{\rho_{TiC}}} \qquad (3.22)$$

From this equation the ratio d_p/d_{po} appears; this ratio can be defined into a dimensionless variable as:

$$\Delta = \frac{d_p}{d_{po}} \qquad (3.23)$$

Substituting Δ in Equation (3.22) and rearranging, we obtain the final form for the concentration of titanium as a function of the stoichiometric constants and of molecular weights and densities:

$$C_{Ti} = \frac{[(a-1)+\Delta^3]}{[(a-1)+\Delta^3]\frac{M_{Ti}}{\rho_{Ti}} + [(b+1)-\Delta^3]\frac{M_{TiC}}{\rho_{TiC}}} \qquad (3.24)$$

The ideal limiting cases (i.e at the beginning and end of the reaction) for the concentration of Ti at the outer melt are as follows:

i) Stoichiometric case, no product dilution (a=1, b=0)

$$C_{Tio} = \frac{\rho_{Ti}}{M_{Ti}} \qquad C_{Ti\infty} = 0 \qquad (3.25)$$

ii) Stoichiometric case, some product dilution (a=1, b=b)

$$C_{Tio} = \frac{1}{\frac{M_{Ti}}{\rho_{Ti}} + b\frac{M_{TiC}}{\rho_{TiC}}} \qquad C_{Ti\infty} = 0 \qquad (3.26)$$

iii) Metal rich case (a > 1), some product diluted

$$C_{Tio} = \frac{a}{a\frac{M_{Ti}}{M_{Ti}} + b\frac{M_{TiC}}{\rho_{TiC}}} \qquad C_{Ti\infty} = \frac{a-1}{(a-1)\frac{M_{Ti}}{\rho_{Ti}} + (b+1)\frac{M_{TiC}}{\rho_{TiC}}} \quad (3.27)$$

iv) Metal L lean case (a < 1), dilution with product

$$C_{Tio} = \frac{a}{a\frac{M_{Ti}}{\rho_{Ti}} + b\frac{M_{TiC}}{\rho_{TiC}}}$$

$$C_{Ti\infty} = \frac{a-1+\Delta^3}{[a-1+\Delta^3]\frac{M_{Ti}}{\rho_{Ti}} + [b+1-\Delta^3]\frac{M_{TiC}}{\rho_{TiC}}} = 0 \quad (3.28)$$

For this case, we can determine the final dimensionless diameter of the non-melting carbon particle as:

$$\Delta^3_{\infty} = 1 - a \quad (3.29)$$

3.7.4 Steady Diffusion of Melted Ti Across the Complex.

With the assumption that the concentration of the melting titanium at the surface of the carbon particle is zero (due to a fast local reaction), and with the aid of Figure 3.3, we can solve for the concentration profile of titanium across the layer of intermediate product. The differential equation that describes this concentration change is:

$$\frac{1}{r^2}\frac{d}{dr}\left(r^2\frac{dC_{Ti}}{dr}\right) = 0 \qquad (3.30)$$

with conditions:

$$\begin{aligned} &\text{(i) at } r = \frac{d_p}{2} \rightarrow C_{Ti} = 0 \text{ (fast surface reaction)} \\ &\text{(ii) at } r = \frac{d_p}{2}+\delta \rightarrow C_{Ti} = C_{Tim} \end{aligned} \qquad (3.31)$$

where δ is the thickness of the intermediate product and C_{Tim} represents the concentration of titanium in the melt. The second condition assumes that the titanium remains uniform at all times in the melt. The solution gives the rate of diffusion of titanium across the intermediate complex, in kmoles/s, as:

$$4\pi r^2 D \frac{dC_{Ti}}{dr} = \pi \frac{d_p (d_p + 2\delta)}{\delta} D C_{Tim} \qquad (3.32)$$

where D is the coefficient of diffusivity of Ti across the intermediate product. The stoichiometry of the problem indicates that the consumption rate of the non-melting carbon reactant is equal to the diffusion rate of the melting titanium reactant. This equality gives a relation between the concentration of titanium in the melt and the shrinking of the carbon particle. The carbon reactant consumption rate, in kmol/sec, is:

$$-\frac{1}{M_c}\frac{d}{dt}\left(\rho_c \frac{\pi d_p^3}{6}\right)$$

By equating this rate with the rate of diffusion of titanium across the intermediate, we obtain:

$$-\frac{1}{M_c}\frac{d}{dt}\left(\rho_c\frac{\pi d_p^3}{6}\right) = \pi \frac{d_p(d_p+2\delta)}{\delta} D\, C_{Tim} \qquad (3.33)$$

To simplify the writing, from here after, C_{Tim} will be written as C_{Ti}. As mentioned earlier, one of the assumptions of Kanury's model is that the thickness δ of the intermediate product is directly proportional to the instantaneous diameter of the carbon particle d_p. Thus, by definition:

$$ß = \frac{\delta}{d_p} \qquad (3.34)$$

Introducing this definition as well as the definition for Δ, Equation (3.33), and $D=D_o\, e^{-E/(RT)}$, we obtain after algebraic rearrangement:

$$\frac{d\Delta^3}{dt} = -6\frac{M_c}{\rho_c}\frac{(1+2ß)}{ß}\frac{1}{d_{po}^2} D_o e^{-\frac{E}{RT}} C_{Ti}\, \Delta \qquad (3.35)$$

This equation coupled with the equation for C_{Ti}, Equation (3.24), will allow the determination of both Δ and C_{Ti} for a given temperature. Once these values are calculated, the rate of heat evolution per unit volume can be calculated as shown in Section 3.8.

If we introduce the following definition:

$$\phi = \frac{C_{Ti}}{C_{Tio}} \tag{3.36}$$

Equations (3.24) and (3.35) can be reduced in a dimensionless fashion to:

$$\phi = \frac{[(a-1)+\Delta^3]}{[(a-1)+\Delta^3]\frac{M_{Ti}}{\rho_{Ti}}+[(b+1)-\Delta^3]\frac{M_{TiC}}{\rho_{TiC}}} \frac{1}{C_{Tio}} \tag{3.37}$$

$$\frac{d\Delta^3}{dt} = -6\frac{M_c C_{Tio}}{\rho_c} \frac{D_o}{d_{po}^2} \frac{(1+2\beta)}{\beta} e^{-\frac{E}{RT}} \phi \Delta \tag{3.38}$$

This last two equations can be solved for the two unknown variables ϕ and the dimensionless volume ratio of the carbon particle Δ as a function of time. The consumption rates and hence the rate of energy generation (see next section) can be determined once the time variation of Δ and ϕ is known.

The range for the variables ϕ and Δ is between 0 and 1. Just before the reaction, $C_{Ti} = C_{Tio}$ then $\phi = 1$ and $\Delta = 1$. At the other end of the range, we have two different situations when the reaction is to be considered as finished. If we have a lean metal case ($a < 0$) then the reaction will cease when the concentration of Ti has been deplenished ($\phi=0$), but the value of Δ will not reach the zero value since there will still be some non-melting carbon reactant left. The other situation is when we have a rich melting titanium case ($a>0$); in this case, there will be still some Ti reactant (ϕ is not zero) while the non melting carbon has already been deplenished and Δ is 0.

3.8 Determination of the Mass Consumption Rate.

The mass consumption rate of a carbon particle in a unit volume, is given by:

$$\dot{W} = -\frac{d}{dt}\left(\frac{\pi}{6} d_p^3 \rho_c\right) \qquad (3.39)$$

If we multiply by N_{pC}, the total number of particles of carbon, and divide by the volume of the mixture, the result is the volumetric mass consumption rate of carbon in $kg/(m^3 s)$:

$$\dot{W}''' = -\frac{d}{dt}\left(\frac{\pi}{6} d_p^3 \rho_c\right) \frac{N_{pC}}{V_{mix}} \qquad (3.40)$$

The number of carbon particles present is simply equal to the mass of carbon in the mixture divided by the mass per particle of carbon. The V_{mix} is calculated as the total mass of the mixture divided by its density. If use is made of the Δ definition, the above equation can be reduced to:

$$\dot{W}''' = \rho_{mix} \frac{m_c}{m_{mix}} \left(-\frac{d\Delta^3}{dt}\right) \qquad (3.41)$$

This expression multiplied by h_{cc}, the enthalpy of combustion per kg of carbon, yields the rate of energy evolution per unit volume needed in the energy equation (described in Chapter 4):

$$\dot{S}''' = h_{cc}\ \rho_{mix} \frac{m_c}{m_{mix}} \left(-\frac{d\Delta^3}{dt}\right) \qquad (3.42)$$

3.9 Closing Comments.

In this chapter the current status in the kinetic modeling of the SHS reactions is presented. Several kinetics models are described as well the new kinetic model developed by Kanury [28]. This model will be incorporated in this study to mathematically study the propagation process of the

reaction wave. Kanury's model, based on experimental results, develops two coupled equations for determining the instantaneous diameter of the carbon particle and the concentration of titanium as functions of time. A reaction rate can be then determined as dependent on temperature, particle size, reactant proportions, and inert product.

CHAPTER 4

MODEL FORMULATION

4.1 Introduction.

In this chapter, we present the mathematical model. The energy equation is coupled to the kinetics equations described in Chapter 3 to portray the exothermic reaction of the type: solid + solid --> solid, for a mixture of titanium and carbon powders. First the equations and their boundary conditions are developed for a 2-dimensional system. Then the impact of radial effects on the speed of propagation of the reaction wave is examined to suggest the reduction of the analysis to a 1-dimensional form. The problem is then nondimensionalized so as to generalize the model and its analysis.

4.2 Governing Equations.

Consider two sets of Ti and C powders. The powders are thoroughly mixed and compacted into a cylindrical shape as shown in Figure 1.

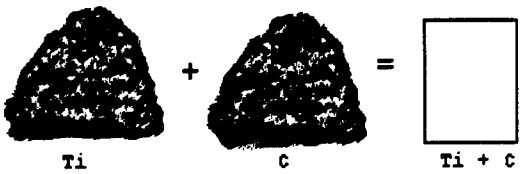

Figure 4.1 Powders are Compacted into a Cylindrical Shape.

The sample is then positioned vertically in a reaction chamber in a quiescent atmosphere of an inert gas. The top surface of the sample is heated by an external source to a sufficiently high temperature to induce the conditions to reach ignition. By furnishing this energy we provide the means for reaction to start on the layer adjacent to the external source. Ignition will occur when this layer achieves a temperature at which the rate of heat generation exceeds the energy transfer by conduction to the next layer and the heat losses to the surroundings. The excess heat increases the temperature of the layer, which in turn leads to a higher reaction rate, until a high heat evolution rate is attained and ignition is then said to have occurred.

The energy that is released in the reaction of the first layer will be transferred by conduction to the next adjacent layer so that it will also start reacting and

consequently a self-propagating process is under way along the extent of the sample.

The phenomenon is expected to be governed by the following fundamental processes:

(i) Thermal inertia.

(ii) Thermal conduction in both radial and axial directions.

(iii) Energy release due to reaction.

(iv) Peripheral surface losses to the surrounding gas.

The presence of a gas in the reaction environment is inconsequential in terms of the kinetics as long as no solid species react with the gas. An inert atmosphere (such as argon) is assumed to surround the system. When carbon is involved as a reactant, oxygen-bearing gas environments may be undesirable.

The following assumptions are made to develop the model:

(a) Temperature variations in the circumferential direction are absent. The external source is applied uniformly all around the top surface, therefore the assumption of no changes in the circumferential direction is reasonable.

(b) All physical properties are function of temperature and composition.

(c) The kinetics model of Kanury [28] discussed in Section 3.7 applies.

(d) The conditions at the end of the sample, far ahead of

the reaction wave, are not crucial. This assumption applies if the length of the sample under scrutiny is long enough such that whatever conditions imposed on this boundary do not play a role in the propagation rate. Thus the length of the sample can be treated like that of a "semi-infinite" body.

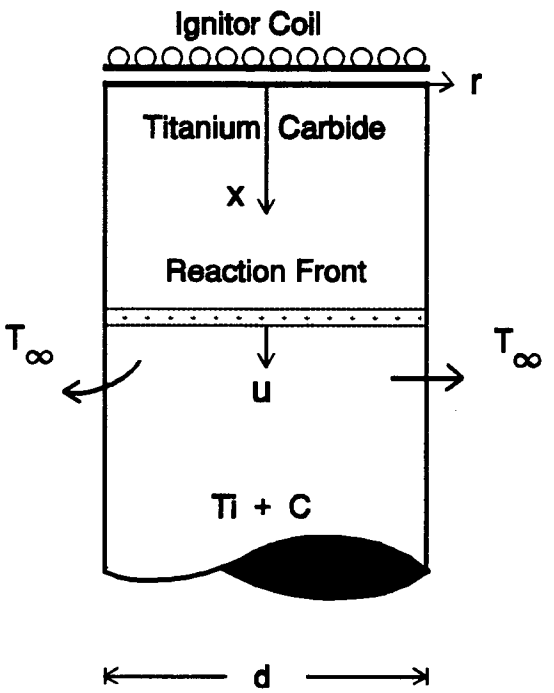

Figure 4.2 Schematic of the Coordinates of the Compact.

With these assumptions, the energy equation for the cylindrical sample can be written as follows, see Figure 4.2:

$$\rho_{mix} C_{pmix} \frac{\partial T}{\partial t} = \frac{\partial}{\partial x}(K_{mix} \frac{\partial T}{\partial x}) + \frac{1}{r} \frac{\partial}{\partial r}(K_{mix} r \frac{\partial T}{\partial r}) + \dot{S}''' \quad (4.1)$$

where x and r are the axial and radial coordinates along the sample, t is time, and T is temperature. K_{mix}, C_{pmix} and ρ_{mix} are respectively the thermal conductivity, specific heat and density of the compact. The term on the left hand side represents the transient heating; the first two terms of the right hand side represent the conduction transfer in the axial and radial coordinates, respectively. The last term in the right hand side represent the rate of energy evolution per unit volume due to the reaction.

This rate of energy evolution per unit volume is given by:

$$\dot{S}''' = h_{cc} \rho_{mix} \frac{m_c}{m_{mix}} (-\frac{d\Delta^3}{dt}) \quad (4.2)$$

where h_{cc} is the enthalpy of combustion per kg of carbon, m_c is the mass of carbon in the mixture, m_{mix} is the total mass of the compact and Δ, defined in Chapter 3, is the ratio of the instantaneous diameter to the initial diameter of the carbon particle. The factor in parenthesis is given by Kanury's kinetic model, presented in detail in Section 3.7, as:

$$\frac{d\Delta^3}{dt} = -6\frac{M_C C_{Tio}}{\rho_C}\frac{D_o}{d_{po}^2}\left(\frac{1+2\beta}{\beta}\right) e^{-\frac{E}{RT}} \phi\, \Delta \qquad (4.3)$$

where M_C is the molecular weight of carbon, C_{Tio} is the initial concentration of titanium in the mixture, d_{po} is the initial carbon particle diameter, β is a constant for a given reaction, E is the activation energy, R is the universal gas constant and ϕ is the ratio of the instantaneous to the initial concentration of titanium in the mixture. Equation (4.3) shows the connection of the three variables of the problem, T, Δ and ϕ. The equation for ϕ is

$$\phi = \frac{[(a-1)+\Delta^3]}{[(a-1)+\Delta^3]\frac{M_{Ti}}{\rho_{Ti}} + [(b+1)-\Delta^3]\frac{M_{TiC}}{\rho_{TiC}}}\frac{1}{C_{Tio}} \qquad (4.4)$$

as derived in Chapter 3. Thus, clearly, the variables of the problem are functions of position (x,r) and time t.

The combined energy-kinetic rate equations, Equations (4.1), (4.3) and (4.4), define the governing equations of the model. The energy equation is coupled to the kinetics of reaction via the source term. For a given temperature field, the source term can be found by solving the two kinetic equations (i.e. (4.3) and (4.4)) for the variables Δ and ϕ.

These kinetics variables vary between 1 and 0; the upper value meaning no reaction has taken effect and the lower value indicating full consumption of reactants (in fact, $\Delta=0$ indicates that the particle of carbon has been deplenished whereas $\phi=0$ indicates full consumption of the titanium melt).

As the reaction progresses through the sample we find four different zones: a first zone where reaction already ceased (i.e. the concentration of Ti is already zero or the non-melting carbon particles are all consumed), a second region where there are steep gradients of temperature and concentration (where the reaction is considered to be sitting upon), a third warm-up zone where thermal effects start being felt and slow reactions are taking place, and a fourth zone where no heating effect has been felt and the temperature remains unaltered with respect to the initial condition. See Figure 4.3.

If the speed of propagation is fast then the propagation front will be thinner yielding a steeper temperature gradient. The model should be able to show that for a faster propagation the "thermal thickness" will decrease. The conditions for a reaction wave to propagate faster are that the compact be one of high conductivity, high energy release, and low volumetric specific heat. A high initial temperature of the compact should also yield an exponentially higher

energy release, and thus a faster propagation speed.

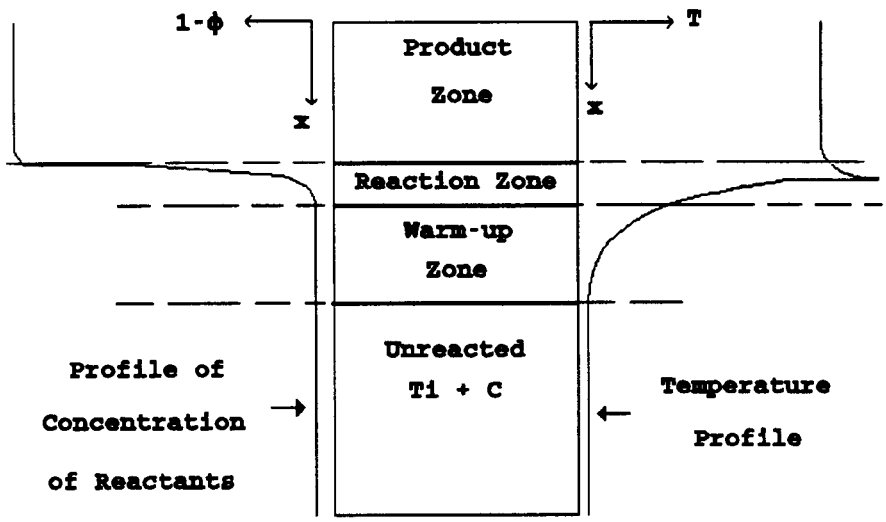

Figure 4.3 Characteristic Regions in the Compact with Corresponding Temperature and Species Profiles.

4.2.1 Initial and Boundary Conditions.

To solve the set of governing equations, initial and boundary conditions that properly describe the physics of the problem are required. Advancing in time, once a solution for the temperature field is known, we should be able to determine the values for Δ and ϕ.

The initial conditions at $t \leq 0$, are that the temperature distribution is uniform and constant throughout the sample

and that no reaction has developed:

$$T(x,r,0) = T_o \tag{4.5}$$

$$\Delta(x,r,0) = 1 \tag{4.6}$$

$$\phi(x,r,0) = 1 \tag{4.7}$$

In order to produce ignition, an external energy source is imposed to maintain the top layer at a prescribed surface temperature. Thus,

$$T(0,r,t) = T_{hot}, \quad \text{a constant} \tag{4.8}$$

As mentioned previously, for modeling purposes it is assumed that the far end of the sample is of no relevance; hence we could model it as being insulated, at a constant temperature, or simply model it as a semi-infinite length sample. Taking this last condition:

$$T(x\to\infty,r,t) = T_o, \quad \text{a constant} \tag{4.9}$$

The condition of symmetry at the x-axis dictates that

$$\frac{\partial T(x,r,t)}{\partial r}\Big|_{r=0} = 0 \tag{4.10}$$

On the periphery of the sample, there is heat loss to the surroundings by convection and radiation; accordingly,

$$-K_{mix} A \frac{\partial T(x,r)}{\partial r}\Big|_{r=R} = hA\,[T(x,R)-T_\infty] + A\sigma\varepsilon F\,[T(x,R)^4-T_\infty^4] \tag{4.11}$$

where A is the surface area, h is the convective coefficient, σ is the Stefan-Boltzmann constant, ε is the emissivity and F is the radiative view factor.

4.3 Reduction to One-dimensional Model.

The foregoing governing equations with their initial and boundary conditions complete the modeling of the problem in a 2-d format. Our experience in preliminary numerical analyses, as well as the investigations reported by other researchers [4, 7, 22, 67, 70], suggest that radial effects produce a negligible impact on the propagation wave. Radial effects have been found to occur only at diameters which are impractically small [22]. The time for propagation of the reaction wave is generally much shorter than the time needed to propagate radial heat loss effects. Therefore, for our modeling purposes the 2-d model given above can be reduced to a 1-dimension model by replacing the conductive radial term in the energy equation with the energy loss terms given in Equation (4.11).

An energy analysis of one section of the compact (the

control volume in Figure 4.4) yields,

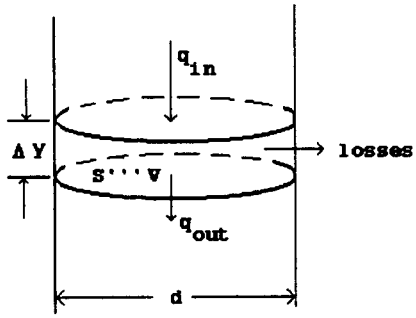

Figure 4.4 Control Volume for a 1-d Propagation.

rate of energy accumulation in control volume	=	net transfer of energy by conduction	+	rate of internal energy evolution	+	net energy transfer to the surroundings

This energy analysis translates into:

$$\rho_{mix} C_{pmix} \frac{\partial T}{\partial t} = \frac{\partial}{\partial x}\left(K_{mix}\frac{\partial T}{\partial x}\right) + \dot{S}''' - \frac{4}{d}h(\dot{T}-T_{\infty}) - \frac{4}{d}\sigma\varepsilon F(T^4-T_{\infty}^4) \qquad (4.12)$$

This equation shows that the reduction of the model from a 2-d format to a 1-d format makes the condition at the boundary r=R, as defined in Equation (4.11), to be now a

part of the energy equation. The kinetics equations (i.e. Equations (4.3) and (4.4)) still apply, but the variables Δ and ϕ are now dependents only on the axial position x and time t. The initial condition as well as the boundary conditions at the top and bottom of the compact remain the same, but dependent only on the axial position x. The initial conditions for T, Δ and ϕ, at $t \leq 0$, are:

$$T(x,0) = T_o \quad \text{uniform throughout the sample} \tag{4.13}$$

$$\Delta(x,0) = 1 \tag{4.14}$$

$$\phi(x,0) = 1 \tag{4.15}$$

and the boundary conditions at the top layer and at the far end of the sample are:

$$T(0,t) = T_{hot} \tag{4.16}$$

$$T(x \to \infty, t) = T_o \quad \text{a constant} \tag{4.17}$$

4.4 Nondimensionalization.

The introduction of suitable definitions will render the model in a dimensionless fashion. By doing so, the

analysis of the model will center in investigating the combined effects of the parameters evolved. The set of dimensionless variables to use in this model is:

$$\theta = \frac{E}{R\,T_r^2}\,(T-T_r) \tag{4.18}$$

$$y = \frac{x}{L_r} \tag{4.19}$$

$$\tau = \frac{t}{L_r^2/\alpha_r} \tag{4.20}$$

$$\hat{C}_p = \frac{C_{pmix}}{C_{pr}} \tag{4.21}$$

$$\hat{\rho} = \frac{\rho_{mix}}{\rho_r} \tag{4.22}$$

$$\hat{K} = \frac{K_{mix}}{K_r} \tag{4.23}$$

In these dimensionless definitions, the subscript r alludes to reference values for physical properties ρ, C_p

and K, and for temperature and length. The reference values are discussed in next chapter.

When these definitions are installed in the energy equation the following parameters, known as the Zeldovich and Stefan numbers, appear quite naturally:

$$Z = \frac{E}{RT_r} \tag{4.24}$$

$$H = \frac{h_{cc}}{C_{pr}\, T_r} \tag{4.25}$$

Thus, the energy equation gets transformed to:

$$\hat{\rho}\, C_{\hat{p}}\, \frac{\partial \theta}{\partial \tau} = \frac{\partial}{\partial y}\left(\hat{K}\, \frac{\partial \theta}{\partial y}\right) + \frac{Z}{T_r}\frac{L_r^2}{K_r}\dot{S}''' - ()_1 - ()_2 \tag{4.26}$$

where parenthesis 1, the convective loss term, is written as:

$$()_1 = 4\, \frac{hL_r}{K_g}\, \frac{K_g}{K_r}\, \frac{L_r}{d}(\theta - \theta_\infty) \tag{4.27}$$

K_g is the thermal conductivity of the surrounding inert gas and d is the diameter of the sample. Parenthesis 2, the radiation loss term, is:

$$()_2 = \frac{4}{Z^3} \frac{\varepsilon\sigma F L_r T_r^3}{K_g} \frac{K_g}{K_r}\frac{L_r}{d} [(\theta+Z)^4 - (\theta_\infty+Z)^4] \qquad (4.28)$$

Substituting the heat evolution rate, Equation (4.2) (in dimensionless time format), and the definition for thermal diffusivity, the energy equation becomes

$$\hat{\rho}\ \hat{C}_p \frac{\partial\theta}{\partial\tau} = \frac{\partial}{\partial y}(\hat{K}\frac{\partial\theta}{\partial y}) + H\ Z \frac{\rho_{mix}}{\rho_r} \frac{m_c}{m_{mix}} (-\frac{\partial\Delta^3}{\partial\tau}) - ()_1 - ()_2 \qquad (4.29)$$

This equation as written, represents the general dimensionless energy equation for the self-propagating high-temperature of solids + solids -> solids. In this general equation, variations in the physical properties of a particular mixture can be taken into account as well as losses by convection and radiation.

Now we apply the dimensionless definitions to the kinetics equations. Equation (4.3) transforms to:

$$\frac{d\Delta^3}{d\tau} = -\frac{D_o e^{-Z}}{\alpha_r} \frac{L_r^2}{d_{po}^2} \frac{6M_c C_{Tio}}{\rho_c} \frac{1+2\beta}{\beta} e^{\frac{z\theta}{\theta+z}} \phi\ \Delta \qquad (4.30)$$

The equation for the variable ϕ, Equation (4.4), remains unaltered but being now a function of dimensionless position y and time τ.

Equations (4.29), (4.30) and (4.4) constitute the

governing equations of the 1-d model. One could go ahead and solve the system as given up to this point with its corresponding dimensionless boundary conditions (provided in following section). However, some more insight can be obtained if me make the introduction of the following definition, known as the Damkohler number, a ratio of the characteristic chemical rate to the characteristic physical rate of the process:

$$Da = \frac{\rho_{mix}}{\rho_r} \frac{m_c}{m_{mix}} \frac{D_o e^{-z}}{\alpha_r} \frac{L_r^2}{d_{po}^2} \frac{6M_c C_{Tio}}{\rho_c} \frac{1+2\beta}{\beta} \qquad (4.31)$$

This definition of the Damkohler number encircles the effects of thermal properties ρ, K and C_p, composition, carbon particle size, process constant ß, a "compression effect" and the diffusion of titanium through the intermediate complex (as described in Chapter 3).

The composition effect is brought in by the factors m_c/m_{mix} and C_{Tio}, which contain the molar coefficients a and b; the "compression" effect is that given by the ratio ρ_{mix}/ρ_r.

Incorporating this Damkohler number definition to the energy and kinetics equations, we can now fully write the governing equations in their final form as:

$$\hat{\rho}\,\hat{C}_p\,\frac{\partial\theta}{\partial\tau} = \frac{\partial}{\partial y}\left(\hat{K}\frac{\partial\theta}{\partial y}\right) + H\,Z\,Da\,e^{\frac{z\theta}{\theta+z}}\,\phi\,\Delta - ()_1 - ()_2 \qquad (4.32)$$

$$\frac{d\Delta^3}{d\tau} = -\frac{Da}{\frac{\rho_{mix}}{\rho_r}\frac{m_c}{m_{mix}}}\,e^{\frac{z\theta}{z+\theta}}\,\phi\,\Delta \qquad (4.33)$$

$$\phi = \frac{[(a-1)+\Delta^3]}{[(a-1)+\Delta^3]\frac{M_{Ti}}{\rho_{Ti}} + [(b+1)-\Delta^3]\frac{M_{TiC}}{\rho_{TiC}}}\,\frac{1}{C_{Tio}} \qquad (4.34)$$

Here we can clearly see the interaction of the variables θ, Δ and ϕ, and also of the parameters affecting the process. This interaction can be expressed in a functional form as:

$$\theta,\Delta,\phi = f\left(a,b,Da,H,Z,\frac{hL_r}{K_g},\frac{K_g}{K_r},\frac{L_r}{d},\frac{\varepsilon\sigma FL_rT_r^3}{K_g}\right) \qquad (4.35)$$

This functional relation lists 9 different parameters. The boundary conditions are not listed since for a long sample after ignition occurs, whatever conditions used for the top and bottom boundaries will be of no relevance in the propagation process.

Having thus determined the governing equations of the

1-dimensional model, equations (4.32), (4.33) and (4.34), we can now proceed to determine how the nondimensionalization procedure affects the boundary conditions.

4.4.1 Dimensionless Conditions.

The initial condition, when transferred to the dimensionless time τ becomes

$$\theta(y,0) = \theta_o, \quad \text{a constant} \tag{4.36}$$

$$\Delta(y,0) = 1 \tag{4.37}$$

$$\phi(y,0) = 1 \tag{4.38}$$

The boundary conditions at the top and far end of the compact transform respectively to

$$\theta(o,\tau) = \theta_{hot} \tag{4.39}$$

and

$$\theta(+\infty,\tau) = \theta_o \tag{4.40}$$

As we advance in time for a particular temperature distribution through the sample we are able to determine the value of Δ, the ratio of the instantaneous to the initial

diameter of the carbon particles, since this variable depends on the temperature. Determining this value of Δ enables us to use Equation (4.34) to calculate ϕ, the ratio of the instantaneous concentration to the initial concentration of titanium. Therefore the solution of the set of governing equations has to be done simultaneously for each time step.

The range for both variables, ϕ and Δ, is between 0 and 1. Just before reaction, $CTi=C_{Tio}$, accordingly $\phi=1$ and $\Delta=1$. At the other end of the range we have two different situations for the reaction to be considered finished. If we have a lean titanium case ($a<1$) then the reaction will cease when the concentration of Ti has been deplenished ($\phi=0$), but the value of Δ will not reach the zero value since there will still be some carbon left. The other situation arises when we have a rich titanium case ($a>1$). In this case, there will still be some Ti reactant left (ϕ is not zero) while the particle of carbon has already been deplenished and Δ is 0. These two conditions will therefore determine the very existence of the source term in the energy equation, since when either Δ or ϕ become zero no more heat generation is possible.

4.5 Governing Equations for this Study.

Equation (4.35) clearly states the overall functiona-

lity of the problem. However, based on the experimental results obtained in this study and in previous analysis found in the literature, the heat losses terms can be considered of small or no influence in the propagation of the reacting front. While solving the whole problem embedded in the functionality given in Equation (4.35) represents a great challenge, the most important characteristics and effects of the dimensionless parameters of the problem can be studied without considering the heat losses terms of Equations (4.27) and (4.28).

Additionally, it was mentioned in Section 4.1 that the thermal properties are a function of temperature and composition. However, the thermal conductivity is expected to depend on the density of the compact as well. Given the present state of knowledge on this dependency K-ρ, and given that our objective in this study is to gain an understanding of the characteristics of the SHS problem while testing Kanury's new kinetic model, the values for thermal conductivity and density will be considered constants throughout this study. Not having a relation K-ρ for the powdery mixture Ti + C the "compaction" effect becomes of no relevance since it will only make the value of volumetric heat capacity vary while not affecting the value of thermal conductivity.

With these further simplifications, the governing

equations under scrutiny in this study will be as follows:

$$\hat{C}_p \frac{\partial \theta}{\partial \tau} = \frac{\partial^2 \theta}{\partial y^2} + H\ Z\ Da\ e^{\frac{z\theta}{\theta+z}}\ \phi\ \Delta \qquad (4.41)$$

$$\frac{d\Delta^3}{d\tau} = -\frac{Da}{\frac{m_c}{m_{mix}}}\ e^{\frac{z\theta}{\theta+z}}\ \phi\ \Delta \qquad (4.42)$$

$$\phi = \frac{[(a-1)+\Delta^3]}{[(a-1)+\Delta^3]\frac{M_{Ti}}{\rho_{Ti}} + [(b+1)-\Delta^3]\frac{M_{TiC}}{\rho_{TiC}}}\ \frac{1}{C_{Tio}} \qquad (4.43)$$

Thus, the functionality of Equation (4.35) gets reduced to:

$$\theta, \Delta, \phi = f(a, b, Da, H, Z) \qquad (4.44)$$

With the Damkohler number being the essential parameter since it encircles the majority of effects that could of some impact in the SHS process: thermal properties, composition, particle size, process constant and diffusion of titanium through the intermediate complex formed. The boundary conditions will not change from those given in Section 4.4.1.

4.6 The Ignition Problem.

The governing equations, Equations (4.41), (4.42) and (4.43), will also allow the study of the ignition problem. Ignition is a transition from a nonreactive to a reactive state in which external stimuli lead to a thermochemical runaway followed by a rapid transition to self-sustained combustion of the sample. Here we will investigate the ignitability of the stoichiometric powder compact under the influence of a constant-temperature source for different physical and chemical parameters (i.e. those that combine to form the Damkohler number) at adiabatic conditions.

In general, ignition of a solid compact is a complex phenomenon which involves many physicochemical processes. When the net heat evolved from the initial chemical reactions overcomes heat losses, sustained ignition is achieved. It is generally understood that ignition is incomplete if steady-state combustion does not follow the ignition event after the removal of the external energy source [81]. The time period from the start of the external stimulus to the instant of sustained ignition, called the ignition delay, is one of the most important parameters in the study of ignition.

Selection of a proper ignition criteria is a controversial issue in ignition studies. Many different

criteria are proposed in theoretical models as well as in experimental studies. This is due to the fact that each criterion is employed according to the characteristics of the model/experiment.

Some of the ignition criteria for theoretical studies are [82]:

- when the surface temperature exceeds a critical value
- when the rate of rise of the surface temperature exceeds a critical value
- when there is a point of inflection in the surface-temperature-time trace
- when the subsurface value at a given distance exceeds a critical value
- when the light emitted by the sample exceeds a critical intensity
- when the heat generation is balanced with the heat losses, etc.,

and some of the ignition criteria used in experimental studies are:

- first appearance of flame recorded in high-speed motion pictures
- onset of light emission detected by a photocell
- attainment of a certain light intensity detected by a photodiode
- abrupt rise in a thermocouple output

- abrupt change in voltage-current characteristics of an electrically heated wire
- onset of signal from an ionization pin which is submerged immediately below the upper surface in contact with the igniting source, etc.,

The experimental study of ignition is just as complex as the theory [83]. The time period of the entire ignition event is very short and the region of major activity is extremely small. Because it is difficult to probe and observe the ignition region, no experimental data was obtained in our experiments to correlate with analytical analysis.

It is expected that the ignition delay will be larger if the igniting source temperature is decreased, if the reactants are not at stoichiometric composition and if the thermal conductivity of the compact is large.

For this study, the criteria to use will follow the established fact (see Kanury [84]) that there is always some temperature of the reacting mixture at which the rate of heat generation exceeds the loss rate. Since we will be modeling the SHS problem in a semi-infinite cylinder at adiabatic conditions, the heat loss implies the loss of energy by conduction to the semi-infinite cylinder. This condition is reached when:

$$\frac{\partial T}{\partial x}\Big|_{x=0} = 0 \qquad (4.45)$$

or in dimensionless format:

$$\frac{\partial \theta}{\partial y}\Big|_{y=0} = 0 \qquad (4.46)$$

For stoichiometric conditions (i.e. a=1, b=0), the functionality of Equation (4.44) reduces to being a function of only H, Z, and Da. For constant values of H and Z (see next chapter) our only independent parameter is the Da number. Hence our study of the ignition problem for the SHS reaction of Ti + C compacts will be to find, for a given Da number, the minimum constant temperature of the igniting source under which the system will always be ensured to attain propagation. Below this minimum temperature no ignition/propagation will occur. Reducing the temperature increases the time to attain ignition conditions. For some temperatures the time of ignition becomes so large that the reactants deplenish and any attainment of the gradient given in Equation (4.46) will only mean that conduction from the hot igniting source to the adjacent layer has taken place. Here is where the Da number becomes an essential parameter since it is the ratio of the characteristic reaction rate to the characteristic conduction rate. Thus, large Da numbers will clearly lead to very small times to reach ignition

conditions while low Da numbers will take extremely large times to reach ignition conditions.

Two different outcomes are expected from this analysis: (i) a plot of temperature of the hot source versus the time to reach the ignition conditions (i.e. Equation (4.46)) for a broad range of Da numbers (determined in Chapter 5), and (ii) a chart of Da number versus the minimum temperature of the igniting source. This chart must present a curve above which we will encounter the zone where any combination Da-temperature will always produce ignition and below the curve the zone where no combination will be able to ignite the compact. This second plot is obtained by determining from (i) what are the asymptotic points of minimum temperature for a given Da number. The plot obtained in (i) is typical of data obtained in experiments [85].

The ignition analysis carries a heavier burden than the propagation analysis since the computational times become very large due to the fact that we will be working at or near the conditions that will need simulation of longer "semi-infinite" bodies (i.e. an increasingly larger number of nodes is required).

CHAPTER 5

NUMERICAL FORMULATION

5.1 Introduction.

In this chapter we present the approach taken to solve the system of governing equations presented in Chapter 4. These governing equations are in the form of a nonlinear partial differential equation coupled with a nonlinear differential equation and with an explicit equation for the ϕ variable. Due to these nonlinearities, an analytical solution is not feasible and the problem has to be solved numerically. Furthermore, the exponentiality of the source term makes the numerical solution difficult since the temperature and concentration profiles are expected to change rapidly in the region where the reaction front is passing.

A finite-difference approach is used. The equations are discretized so that the variables are considered to exist only at discrete points. Derivatives are approximated by differences resulting in algebraic representations of the partial differential equations.

To ensure that the solutions do not pose stability

problems an implicit method is implemented. Enough number of nodes are used to guarantee the semi-infinite length condition of the far end of the sample. The problem of selection of time increments is solved by investigating the behavior of the solution as the time step is varied. The optimum value of time increment is determined by checking on the convergence of the time needed to reach ignition conditions using smaller and smaller values of time increment. It is important to comply with a small time increment so as to insure that the approximation of continuous time evolution is valid, but at the same time a large step size is needed to avoid enormous computer running times.

The values of the input parameters to use in this study are also determined in this chapter.

5.2 Finite-Difference Discretization.

5.2.1 Explicit Scheme.

The first step in establishing a finite-difference procedure is to replace the continuous problem domain by a finite difference approximation of the derivatives appearing in the governing equations. Details of the finite-difference schemes applied to heat transfer are well known and can be found in the literature [86].

Using a forward-difference representation for the time

derivatives and a central-difference formula for the second derivatives, we can approximate the governing equations by:

$$\hat{C}_p \frac{\theta_{i,j+1}-\theta_{i,j}}{\Delta\tau} = \frac{\theta_{i+1,j}-2\theta_{i,j}+\theta_{i-1,j}}{\Delta y^2} + H\ Z\ Da \exp\left(\frac{Z\theta_{i,j}}{Z+\theta_{i,j}}\right) \phi_{i,j}\Delta_{i,j} \tag{5.1}$$

$$\frac{\Delta^3_{i,j+1}-\Delta^3_{i,j}}{\Delta\tau} = -\frac{Da}{m_c/m_{mix}} \exp\left(\frac{Z\theta_{i,j}}{Z+\theta_{i,j}}\right) \phi_{i,j}\ \Delta_{i,j} \tag{5.2}$$

$$\phi_{i,j} = \frac{a\ -1+\Delta^3_{i,j}}{[a\ -1+\Delta^3_{i,j}]\frac{M_{Ti}}{\rho_{Ti}} + [b\ +1-\Delta^3_{i,j}]\frac{M_{Tic}}{\rho_{Tic}}} \frac{1}{C_{Tio}} \tag{5.3}$$

where the subindex i indicates the i-th nodal position and subindex j indicates the time level.

The initial conditions, Equations (4.36) to (4.38), are written in a discretized manner as:

$$\theta_{i,0} = \theta_0 \tag{5.4}$$

$$\Delta_{i,0} = 1 \tag{5.5}$$

$$\phi_{i,0} = 1 \tag{5.6}$$

While the boundary conditions, Equations (4.39) to (4.40), are written as:

$$\theta_{0,j} = \theta_{hot} \tag{5.7}$$

$$\theta_{N,j} = \theta_{o} \tag{5.8}$$

The value of N is chosen large enough so that conditions at the far node end do not affect the reaction process.

This discretization clearly leads to an explicit form of solution. An explicit scheme is one for which only one unknown appears in the difference equation in a manner which permits evaluation in terms of known quantities. This form of solution is easy to understand and program. This method was programmed and tested for several runs. However, these tests showed that in order to have consistent solutions both the time step and the spacing between nodes had to be reduced. The tests used time increments of $1x10^{-2}$, $5x10^{-3}$, $1x10^{-3}$, $5x10^{-4}$, and $1x10^{-4}$, while the space sizings tested were 1.2, 1, 0.75, 0.5, 0.3, 0.2, 0.1 and 0.05. The results indicated that the time increments had to be reduced by several orders of magnitude (in the range $1x10^{-4}$ and $5x10^{-5}$) to have dependable solutions. Out of concern for stability it was decided that an implicit scheme was to be used instead of the above explicit scheme. Thus, round-off or truncation errors are not permitted to grow in the sequence

of numerical procedures as the calculation proceeds from one step to the next. Rounding-off errors were also minimized by using double precision numerical schemes.

5.2.2 Implicit Scheme.

If the second derivative term in the energy equation is approximated by θ's at the j+1 time level, three unknowns would appear in the difference scheme and the procedure can be modified to an implicit solution. This indicates that the algebraic formulation would now require the simultaneous solution of several equations involving the unknowns.

The fully implicit approximation produces the following finite-difference energy equation:

$$\hat{C}_p \frac{\theta_{i,j+1}-\theta_{i,j}}{\Delta\tau} = \frac{\theta_{i+1,j+1}-2\theta_{i,j+1}+\theta_{i-1,j+1}}{\Delta y^2} + H\ Z\ Da \exp\left(\frac{Z\ \theta_{i,j}}{Z+\theta_{i,j}}\right) \phi_{i,j}\ \Delta_{i,j} \qquad (5.9)$$

The finite difference equations, Equations (5.2) and (5.3), remain unaltered. The θ field can be determined from the above equation by solving a tridiagonal system of simultaneous equations, which can be accomplished quite efficiently. Tridiagonal systems commonly occur in connection with the use of implicit difference schemes for second order partial differential equations.

If all the terms at the j+1 time level are moved to the

left hand side, one obtains:

$$-A_1 \theta_{i-1,j+1} + (1+2A_1)\ \theta_{i,j+1} - A_1\ \theta_{i+1,j+1} = \theta_{i,j} + B_1\ H\ Z\ DA \exp\left(\frac{Z\ \theta_{i,j}}{Z + \theta_{i,j}}\right) \phi_{i,j} \Delta_{i,j} \quad (5.10)$$

where the constants A_1 and B_1 are defined as:

$$A_1 = \frac{\Delta\tau}{\hat{C}_p\ \Delta y^2} \quad (5.11)$$

$$B_1 = \frac{\Delta\tau}{\hat{C}_p} \quad (5.12)$$

The boundary conditions can now be applied to Equation (5.10). The condition at the node i=1, next to the ignitor, will transform Equation (5.10) to:

$$(1+2A_1)\ \theta_{1,j+1} - A_1\ \theta_{2,j+1} = A_1\ \theta_{hot} + \theta_{1,j} + B_1\ H\ Z\ Da \exp\left(\frac{Z\ \theta_{1,j}}{Z + \theta_{1,j}}\right) \phi_{1,j} \Delta_{1,j} \quad (5.13)$$

And the condition of semi-infinite body is implemented as:

$$-A_1\ \theta_{N-2,j+1} + (1+2A_1)\ \theta_{N-1,j+1} = A_1\ \theta_{N,j} + \theta_{N-1,j} + B_1\ H\ Z\ Da \exp\left(\frac{Z\ \theta_{N-1,j}}{Z + \theta_{N-1,j}}\right)\ \phi_{n-1,j}\ \Delta_{N-1,j} \quad (5.14)$$

Equations (5.10), (5.13) and (5.14) when put together

for the range i=1 to i=N-1 form a system of equations which can be represented in a matrix form as shown in Figure 5.1.

This system of equations is solved for the variable θ at the same time step as Equations (5.2) and (5.3) for the variables Δ and ϕ respectively. The system is initialized using the initial conditions as given in Equations (5.4), (5.5) and (5.6). Appendix 2 provides a listing of the numerical FORTRAN code used to analyze the problem.

5.3 Input Values for Parameters of the Problem.

No matter how much a numerical method simulation program is tested and verified, it is an inescapable reality that the simulated results depend directly on the input parameters. For this simulation input values are required such as specific heat, thermal conductivity, enthalpy of reaction, density, molecular weights, etc., to determine the value of the dimensionless parameters. Table 5.1 provides values for some of the parameters of the reaction.

The specific heat of the mixture can be calculated from the mass weighted average of the individual components ($Cp=\Sigma Y_i C_{pi}$), and will be different for different values of the stoichiometry parameters a and b. The value for thermal conductivity of the mixed titanium and carbon powder compact is about 1.67 W/(mK).

Table 5.1 Some Properties of the Reaction.

Molecular weight of C	12
Molecular weight of Ti	47.9
Molecular weight of TiC	59.9
Density of carbon graphite ρ_c, in g/cm^3	2.2
Density of titanium ρ_{Ti}, in g/cm^3	4.54
Density of titanium carbide ρ_{TiC}, in g/cm^3	4.95
Activation energy E, in J/mole	137,940
Diffusion coefficient D_o, in m^2/s	2.04×10^{-7}
Enthalpy of reaction h_{cC}, in J/kg of C	1.525×10^7
Enthalpy of reaction h_{cTiC}, in J/kg of TiC	3.0514×10^6

5.3.1 Reference Parameters.

In the definitions of Equations (4.18) to (4.23) reference values for physical properties ρ, C_p, and K and for temperature and length were introduced. To avoid giving trivial values to these parameters it is of more interest, when possible, to choose values that reflect the properties of the problem on hand. The value for ρ_r, reference density, is thus chosen to be the value for the density of carbon

(see Table 5.1). C_{pr}, reference specific heat, is chosen as that of a mixture in stoichiometric proportions without product dilution. The most complete information of individual specific heat values for carbon graphite, titanium and titanium carbide is found in the TPRC Data Series [87]. For a stoichiometric mixture without product dilution C_p=950 J/(kg K). The reference thermal conductivity will be the same as that of the mixture, making the ratio K/K_r equal to 1.

The reference temperature will be taken as the adiabatic temperature for a stoichiometric mixture without product dilution. Assuming complete conversion of C and Ti to TiC, the adiabatic reaction temperature can be obtained from the first law of thermodynamics as:

$$T_{ad} = T_o + \frac{h_c}{(a-1)C_{pTi} + (1+b)C_{pTiC}} \qquad \text{if } a \geq 1 \qquad (5.15)$$

$$T_{ad} = T_o + \frac{a\,h_c}{(1-a)C_{pC} + (a+b)C_{pTiC}} \qquad \text{if } a \leq 1 \qquad (5.16)$$

Thus, for our reference temperature:

$$T_r = 300 + \frac{3.0514 \times 10^6}{950} = 3512 \text{ K} \qquad (5.17)$$

Mixtures with a≠1 and b≠0 obviously lead to lower reaction temperatures.

Ideally the reference length would be equal to the measured "thermal thickness" of a reaction obtained under adiabatic stoichiometric undiluted conditions; however, this experimental information is not available. Nevertheless, from the theory of flame propagation it is known that this thickness is of the order of α/u [84]. Thus, our reference length will be of the order of α_r/u, α_r being the reference thermal diffusivity $\{\alpha_r=K_r/(\rho_r\ C_{pr})\}$ and u being a typical measured value from our experiments. For stoichiometric undiluted conditions u is of the order of 1 cm/s.

5.3.2 Range for the Values of Independent Parameters.

The functionality given in Equation (4.44) gives a, b, Da, H, and Z as the independent parameters of the problem. As defined in Equation (4.25), the Stefan number H directly involves the enthalpy of the reaction, an intrinsic constant value of the Ti + C reaction. Accordingly the Stefan number becomes an intrinsic constant parameter of the problem. In the same way the Zeldovich number, as defined in Equation (4.24), relates directly to the activation energy E, also a constant of the reaction. This relationship of H and Z to constants of the reaction makes them constants of the dimensionless problem. Thus, the only three parameters to

vary in the analysis are a, b and Da. The values for H and Z are determined as:

$$Z=E/(RT_r)=138000/(8.314 \times 3512) = 4.72$$

$$H=h_{cc}/(C_pT_r)=1.5257\times10^7/(950 \times 3512) = 4.57$$

From our experiments, which will be described in the next two chapters, it has been found that the reaction quenches for mole fractions (ratio of moles of titanium per mole of carbon in the initial mixture) larger than 1.6 and less than about 0.6. We select therefore a range for a as $0.5 \leq a \leq 1.6$.

In the same way the quenching of the reaction occurs for dilution of the initial mixture with TiC exceeding 27.5 weight %. This weight % is translated to the b moles used in the analysis by the following relation:

$$\text{weight \% of TiC} = \frac{b\, M_{TiC}}{M_C + aM_{Ti} + bM_{TiC}} \qquad (5.18)$$

The 27.5 weight % is equal to b=0.333. Hence, the range for b in this study will be $0 \leq b \leq 1/3$

To determine the upper and lower values of the Da number range to be covered in this study one must ascertain what are the upper and lower values of each factor forming the Da number (even though some of these factors will remain constant in this study). These factors are ρ_{mix}/ρ_r, m_C/m_{mix}, D_o/α_r, e^{-Z}, L_r^2/d_{po}^2, M_C/ρ_C, C_{Tio}. Their ranges are determined

next:

$$\rho_{mix}/\rho_r = 1700/2200 = 0.777$$

$$= 2700/2200 = 1.22$$

where the values 1700 and 2200 kg/m^3 represent the lower and upper values of density to which the samples were compressed in the experiments. Accordingly, the selected range for this factor is: $1/2 < \rho_{mix}/\rho_r < 3/2$

$$m_c/m_{mix} = 12/(12+48a+60b) = 0.294 \text{ if } a=0.6,\ b=0$$

$$= 2 \text{ if } a=1,\ b=0$$

$$= 0.15 \text{ if } a=1,\ b=1/3$$

$$= 0.1351 \text{ if } a=1.6,\ b=0$$

Accordingly the range here is selected as: $0.1 < m_c/m_{mix} < 0.2$

$$D_o/\alpha_r = 2.04\times10^{-7}/(1.67/2200/950) = 0.2553.$$

The order of magnitude yields, $0.1 < D_o/\alpha_r < 1$

Now, for the exponential factor,

$$e^{-2} \approx e^{-5}, \text{ since } Z=4.7$$

$$L_r^2/\ d_{po}^2 \approx (\alpha_r/u)^2\ /(40\times10^{-6})^2 \approx (7.99\times10^{-7}/.01)/(40\times10^{-6})^2$$

$$\approx 4$$

Here a representative size of 40 microns for the carbon particle is used. Due to its order of magnitude the selected range becomes: $0.1 < L_r^2/\ d_{po}^2 < 10.$

$$M_c/\rho_c = 12/2.2$$

$$C_{Tio} = a/(aM_{Ti}/\rho_{Ti}+bM_{TiC}/\rho_{TiC} = 0.0945 \text{ for all a, b=0}$$

$$= 0.0684 \quad \text{for a=1, b=1/3}$$

These last two factors combine to form a factor $(M_c/\rho_c)(C_{Tio})$ of the order of 1. Finally, $(1+2ß)/ß \approx 400$.

Accordingly, the lower values for the Da range will be determined by using the lower value of the range (calculated above) of each of the factors forming the Da number:

$$Da > (1/2)(0.1)(0.1)e^{-5}(0.1)(6)(1)(400) = 0.8$$

and the upper value of Da will be determined by using the upper value of the range of each of its forming factors:

$$Da < (3/2)(0.2)(1)e^{-5}(10)(6)(1)(400) = 48.5$$

From these values, and in order to have a symmetric range for Da, the selected range of Da to be covered in this study is:

$$10^{-2} < Da < 10^{2}$$

Thus embodying most of the possible Da values that could arise for different conditions found in experiments.

5.3.3 Values for Boundary and Initial Conditions.

Equation (4.36) gives the initial condition for temperature as θ_o. While this is a dimensionless quantity, it should still reflect an initial condition in real temperature. Room temperature is selected to reflect the

conditions under which the experiments were performed. However, it is feasible that higher initial temperatures could be imposed on the model if the sample had been pre-heated. From the dimensionless temperature definition and the values given in previous sections we determine θ_o=-4.32. This value holds also for the far end of the sample.

The upper end of the surface condition establishes θ_{hot} as the temperature of the source next to it. For the propagation study this value will be hold simply at the adiabatic temperature. Thus, from the θ definition, θ_{hot}=0. For the ignition study the value of θ_{hot} can vary between the θ range: $-4.32 < \theta_{hot} < 0$, depending on the Da number used.

5.4 Time and Space Increments.

As mentioned before, the steep gradients that appear around the region where the reaction front is located produce abrupt changes in the profiles of the variables. Two ways were implemented to overcome these abrupt changes. The first forced the convergence of the θ temperature to within 1% between a computation at the time-level j and the computation at the time-level j+1 (decreasing the time step until convergence is achieved). The second approach was to simply decrease the time step to a value that did not produce essentially any difference in the solution and that did not produce high overshooting (see Figure 5.2). Both

approaches gave identical results.

Overshooting was always observed if time increments were large. Figure 5.2 shows such a case. Large time steps indirectly produce sharp temperature variations due to the exponential source term.

Very small time increments and small nodal distances are preferred for the sake of more accurate results, however, in order to keep computer times to a minimum, it is necessary to determine the largest possible values for time and space increments. The cases that are expected to cause the most problems with stability and accuracy are those of a fast moving reaction wave since they have the shortest reaction zones/thermal thicknesses and therefore the steepest gradients. A fast moving reaction wave is expected to be one with a high Da number and in stoichiometric proportions. Thus, the determination of the optimum $\Delta\tau$ and Δy to be used has to be based on these conditions: the upper value of the Da range (Da=100) and stoichiometric conditions with no dilution (a=1, b=0). For conditions other than these, the gradients of temperature and composition are not as steep and therefore even larger time increments or larger nodal distances may not cause instabilities.

To determine the optimum values of $\Delta\tau$ and Δy, several combinations were tested. Table 5.2 shows how these combinations affect the determination of the propagation speed.

Table 5.2 Calculated Dimensionless Speeds for Different Combinations of $\Delta\tau$ and Δy.

Δy	$\Delta\tau=1x10^{-3}$	$\Delta\tau=1x10^{-4}$	$\Delta\tau=5x10^{-5}$
.05	overshooting	9.6	9.3
.1	overshooting	9.5	9.1
.2	overshooting	7.2	7
.5	overshooting	4.05	4.3
1.0	overshooting	2.46	2.41

Time increments smaller than $\Delta\tau=5x10^{-5}$ do not significantly change the propagation speeds obtained with this $\Delta\tau$. Therefore, this is the optimum time increment to use. At this order of magnitude, a smaller $\Delta\tau$ will heavily increase computational running times. However, from Table 5.2, one may observe that values of $\Delta\tau=1x10^{-4}$ are reasonably accurate as those given by $\Delta\tau=5x10^{-5}$.

The effect of the nodal distance nodal Δy on the determination of the ignition conditions was also investigated. For this effect, in order to keep running times low, $\Delta\tau$ was chosen to be $1x10^{-4}$ and the same conditions as before were kept; that is, the Damkohler number equal to 100 and a=1, b=0. The same FORTRAN code given in Appendix 2

with small variations was used to record the times to reach ignition conditions for the nodes i=1 and i=2. Figures 5.3 and 5.4 show this times versus nodal distance.

In these figures, several values of θ_{hot} are shown. Since different values for the temperature at the top surface are used in the ignition conditions calculations, it is necessary to check if a reduced value of θ_{hot} will influence significantly the behavior of the plot.

In the figures, the upper lines are lines of low dimensionless temperature (in the θ scale, θ=-4.32 is equivalent to room temperature) and the lower ones are lines of hotter temperature, closer to the adiabatic dimensionless temperature (i.e. θ=0).

It is clear from Figures 5.3 and 5.4 that for smaller values of the top surface temperature it is possible to use larger values for Δy while for values close to the adiabatic temperature the best values to use are either Δy=0.1 or Δy=0.05.

To verify the effect of nodal distance Δy, a check of the times to reach ignition conditions at the top surface is made with Da=1. Only two values of Δy are used for this check, Δy=0.2 and Δy=0.1 and the time increment is kept constant at $\Delta\tau=5x10^{-5}$. The results are shown in Table 5.3.

Table 5.3 Effect of Nodal Increment on the Time to Reach Ignition Conditions at the Top Surface.

Δy	θ_{hot}=-0.94	θ_{hot}=-1.41	θ_{hot}=-1.89
0.1	4.85	7.28	15.7
0.2	4.857	7.33	15.85

Again it is observed that a value of Δy=0.1 seems to be a reasonable value to use in the calculations. From the results in this table it is verified that larger nodal increments can be accommodated without loosing accuracy in the result. Hence, it could be feasible to make arrangements to use different time and nodal increments as Da number varies. However in numerical analyses, it is necessary to maintain some consistency in the procedure to ensure reliable results. Thus, based on these analyses, it is established that the optimum values to use in calculations are $\Delta\tau=5x10^{-5}$ and Δy=0.1.

5.5 Number of Nodes.

The two boundary conditions imposed on the system can have an affect, within some distance, on the propagation speed results. Propagation speeds have to be determined far enough away from the hot upper surface but also at a distance far enough away from the bottom "semi-infinite" far

end. Given the multiple number of cases that will be analyzed, a fix pre-established number of nodes have to be consistently used. To maintain the condition that at the far end of the sample the mixture still remains at the initial conditions requires the use of a fairly large number of nodes (to simulate semi-infinite lengths); this leads to very long computer run times.

Based on an extensive number of test performed it was found that, while for fast propagating reactions a smaller number of nodes is required, for some cases a relatively high number of nodes is needed to simulate the conditions of a semi-infinite length. This is specially true for cases when it take long time to start reacting and when the reaction front moves very slowly. For these cases there will be enough time for thermal heating effects to spread farther towards the far end of the sample; under these conditions, this "semi-infinite" end will act as a thermal sink.

Figures 5.5 and 5.6 show typical temperature profiles along the length of the sample. We see in Figure 5.5 that a "safe region" can be found in which the effects of the "hot" and "cold" boundaries do not affect the propagation of the reacting wave front. In this region a value for the propagation speed can be determine without regards to the effects of boundary conditions. In both figures 400 nodes are used. For most of the cases tested, the "safe region"

extended from about the node 100 to the node 300. Actually, for high Da numbers (as in Figure 5.5) this region was broader (say between the node 60 to node 340), but for low Da numbers the length of 400 nodes became too small to fully simulate a semi-infinite length. For very low Da numbers (<1) the nodal distance was increased to 600 or more. In Figure 5.5 the profile plotted was recorded at a very late stage in the propagation (near to where the effect of the "cold" boundary may be felt). At this time the effect of the top surface had enough time to propagate downstream; but as the figure shows, its effect has not even reached the node 100. For all propagation runs, a θ_{hot} value of 0 is taken as the temperature of the igniting source; however, for this figure, a smaller value of θ_{hot} was taken so to check on the effect that it could have on the propagation front. With $\theta_{hot}=0$ and stoichiometric cases the top boundary will be clearly of no effect, since the maximum reaction temperature is equal to the top boundary; however, for nonstoichiometric cases the maximum reaction temperature is lower than the top surface temperature and it is where the upper boundary could have some effect, specially for slow reacting mixtures.

In Figure 5.6 the temperature profile was recorded when the propagation was at an early stage (near the node 150). One can see that the modeling of semi-infinite body is fully accomplish since far ahead of the propagation front

the sample is still at the initial conditions. The effect of the upper surface is not fell either as indicated by the horizontal profile upstream of the reaction front.

5.6 Concluding Remarks.

This chapter has presented the numerical approach taken to analyze the problem. Both explicit and implicit finite difference techniques are discussed and examined so as to determine which one can provide a more appropriate method for the study. Several tests, using both methods, are performed to check on the consistency of solution. It is found that the implicit finite-differencing technique provides a more suitable method for the analysis.

After several runs the values for nodal space and time steps are determined "sufficiently" small ("sufficiently" is a quantity always hard to estimate) to ensure continuity of the solution and at the same time large enough to avoid huge computational times. These values are respectively $\Delta y=0.1$ and $\Delta\tau=5\times10^{-5}$. Overshooting is found to occur at larger values of either Δy or $\Delta\tau$.

An optimum value of 400 nodes for "medium" to "large" Damkohler numbers (≥ 1) and 600 nodes for smaller Da numbers is found sufficient to overcome possible boundary effects. The results of the numerical runs will be shown and discussed in Chapters 8 and 9.

$$\begin{bmatrix} (1+2\,A_1) & -A_1 & 0 & 0 & \cdot & \cdot & \cdot & 0 \\ -A_1 & (1+2\,A_1) & -A_1 & 0 & \cdot & \cdot & \cdot & 0 \\ 0 & \searrow & \searrow & \searrow & \cdot & \cdot & \cdot & \cdot \\ \cdot & \cdot & \searrow & \searrow & \searrow & \cdot & \cdot & \cdot \\ \cdot & \cdot & \cdot & \cdot & \searrow & \searrow & \searrow & 0 \\ \cdot & \cdot & \cdot & \cdot & \cdot & -A_1 & (1+2A_1) & -A_1 \\ 0 & 0 & 0 & 0 & 0 & 0 & -A_1 & (1+2A_1) \end{bmatrix} \begin{bmatrix} \theta_{1,j+1} \\ \theta_{2,j+1} \\ \cdot \\ \theta_{i,j+1} \\ \cdot \\ \theta_{N-2,j+1} \\ \theta_{N-1,j+1} \end{bmatrix} = \begin{bmatrix} A_1\theta_{hot}+\theta_{1,j}+source_{1,j} \\ \theta_{2,j}+source_{2,j} \\ \cdot \\ \theta_{i,j} \\ \cdot \\ \theta_{N-2,j}+source_{N-2,j} \\ A_1\theta_o+\theta_{N-1,j}+source_{N-1,j} \end{bmatrix}$$

Where the term "source" is given by:

$$source_{i,j} = B_1\ H\ Z\ Da\ \exp\left(\frac{Z\ \theta_{i,j}}{Z + \theta_{i,j}}\right)$$

Figure 5.1 Matrix Representation of the Implicit System of Equations.

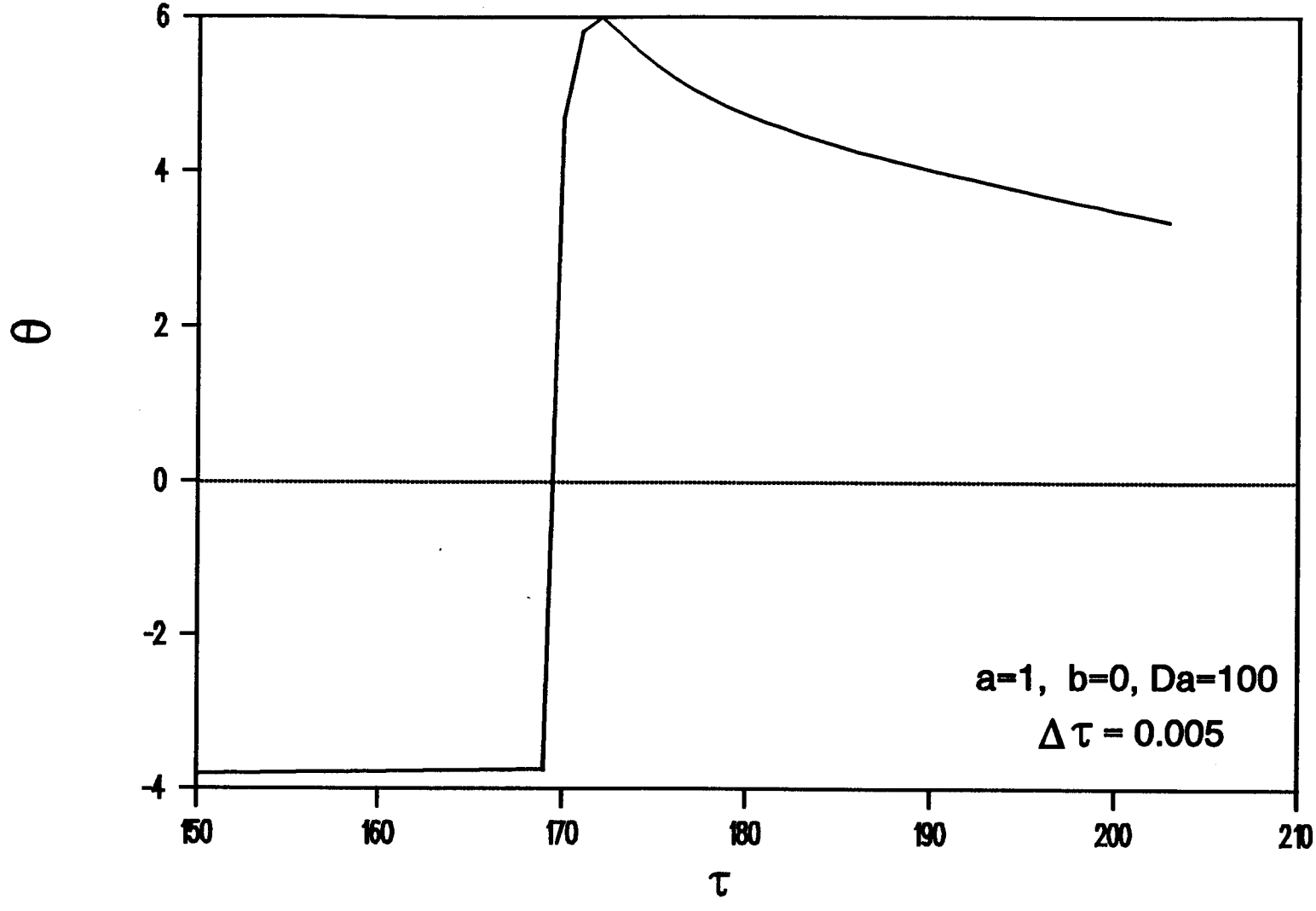

Figure 5.2 Example of Overshooting when Time Increments are Large.

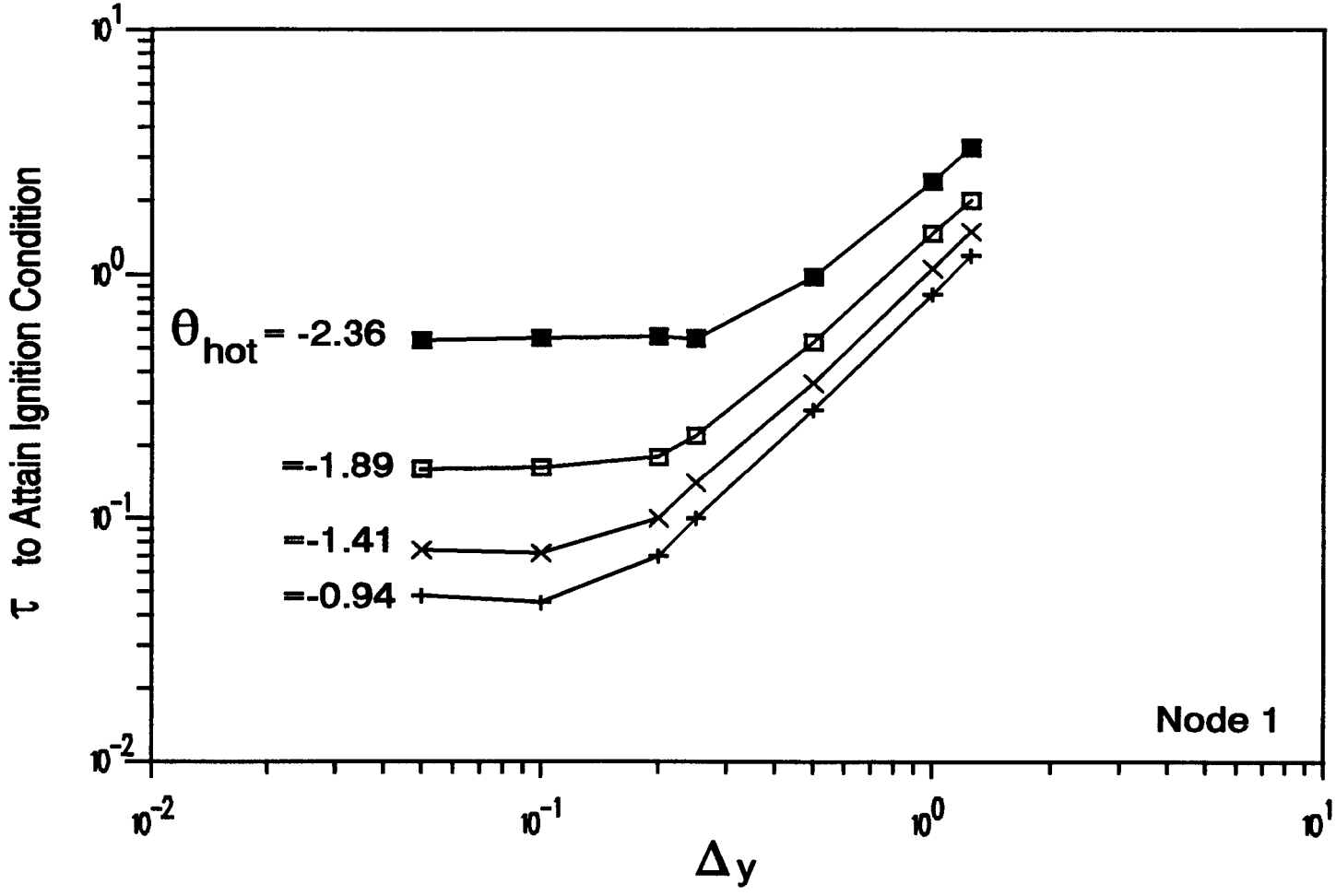

Figure 5.3 Effect of Nodal Distance on the Time to Attain Ignition Conditions. Node 1.

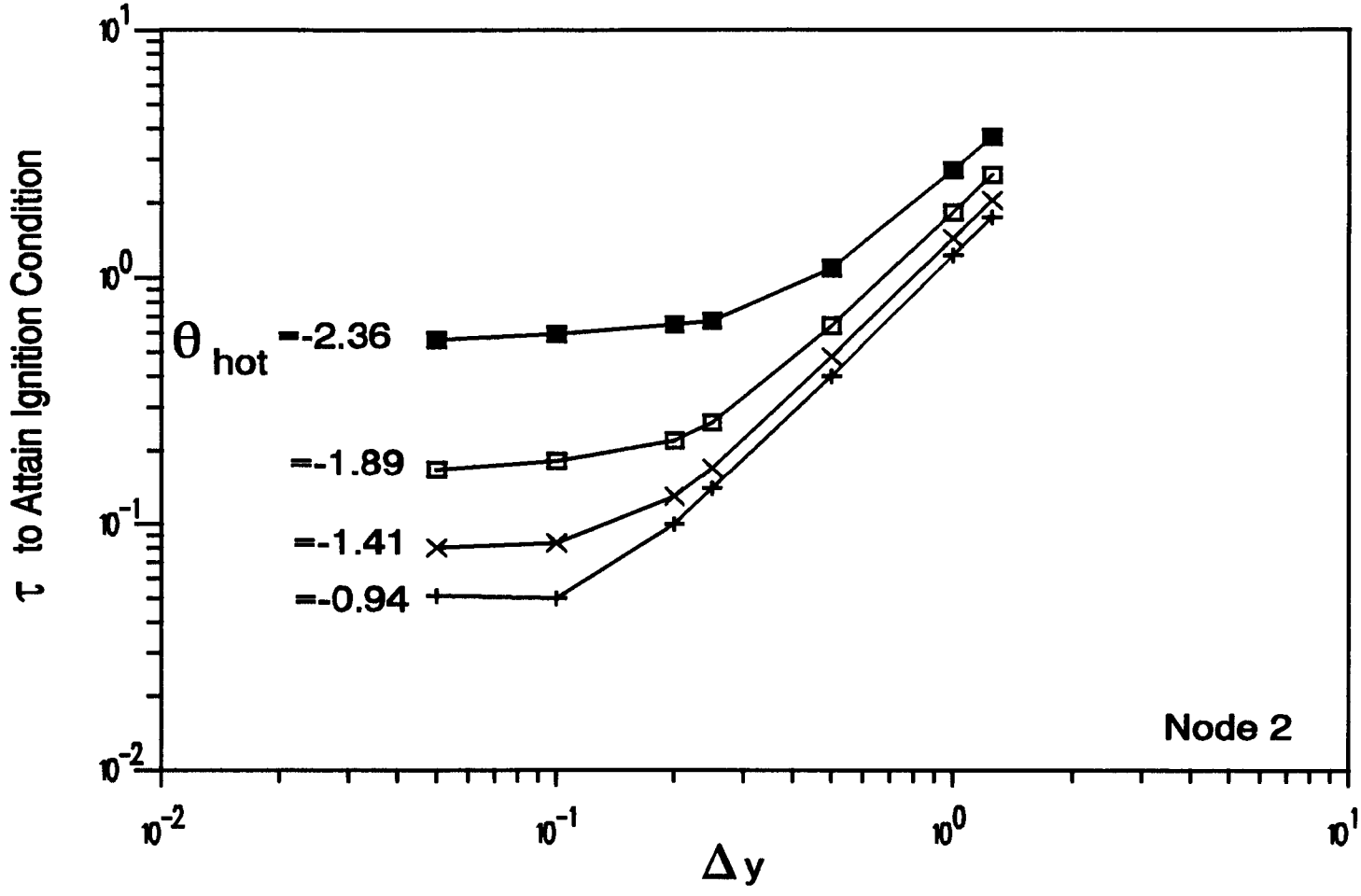

Figure 5.4 Effect of Nodal Distance on the Time to Attain Ignition Conditions. Node 2.

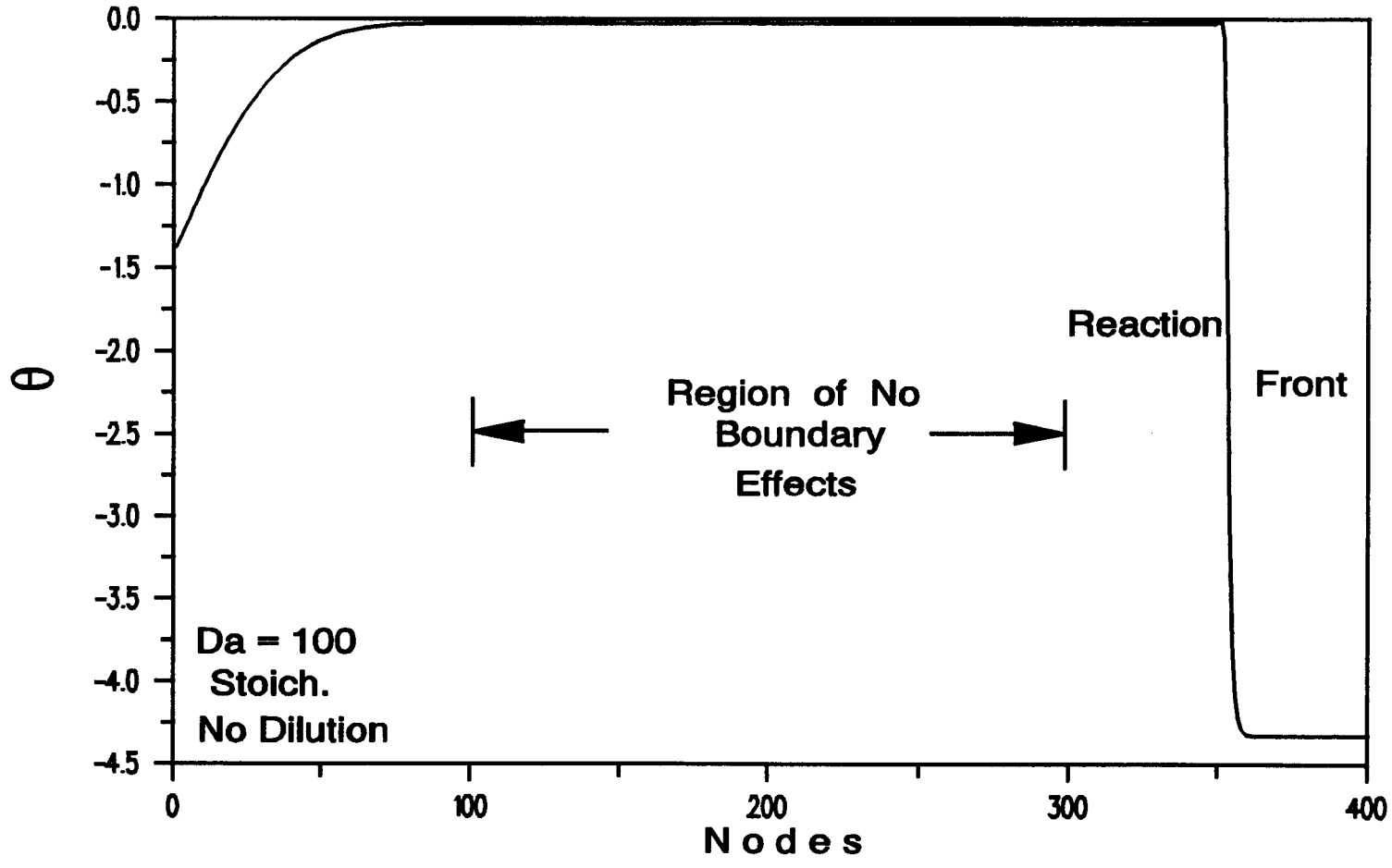

Figure 5.5 Typical Temperature Profile Showing the No-effect of the "Hot" and "Cold" Boundaries on the Propagating Front.

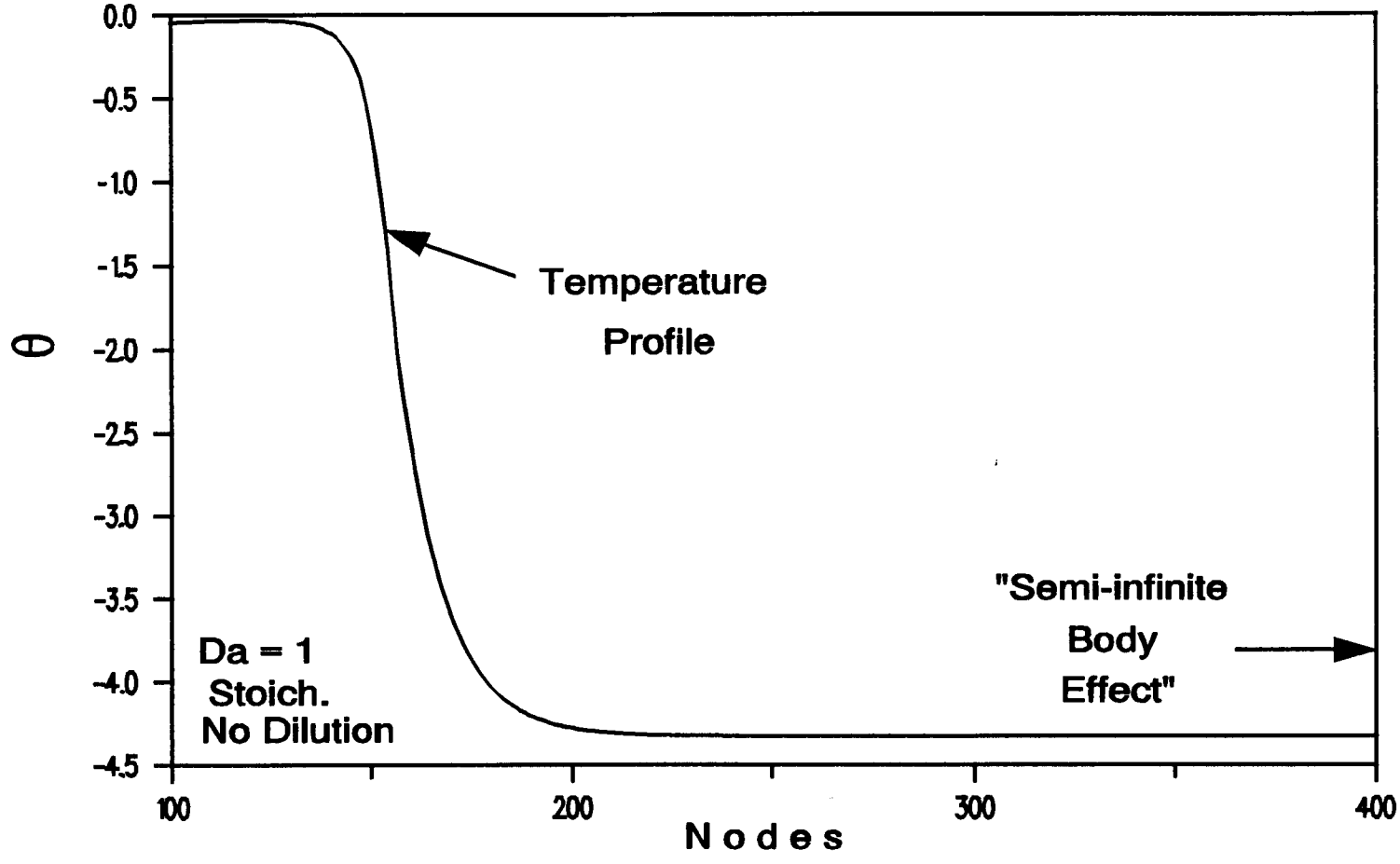

Figure 5.6 Effect of the "Cold End" of the Semi-infinite Sample.

CHAPTER 6

EXPERIMENTAL SCHEME

6.1 Introduction.

In this chapter the experimental apparatus used to perform the experiments is explained as well as the description of how the experiments were accomplished.

The main object of the experimental investigation was to determine the effects of several sample variables in the speed of propagation of the combustive synthesis of titanium carbide and when some of those conditions are sufficient to quench the propagation. The sample parameters included: sample diameters, reactant mole ratios, density of the sample and dilution of the initial stoichiometric mixture with inert product. Whereas the samples to be combusted had different sizes or compositions, the overall experimental setup did not changed much with the exception of minor details in the methodology of preparing the samples. Some of these details are also explained in this chapter.

6.2 Experimental Setup.

The experimental setup was devised to satisfy the

following requirements:

1) To have a central apparatus that could be assembled and dismantled easily and efficiently so many experiments could be performed without the need of major changes.

2) To have a proper data acquisition device and a computerized technique for collecting and storing data from each experiment.

3) To prepare the samples with a proper heat treatment in vacuum before the combustive synthesis.

The main ensemble consisted of a reaction chamber connected to a computerized data acquisition device. The reaction chamber had many entry-ports through which it could be attached to any other devices if needed. Three of those ports were used to connect the main chamber to a supply of argon gas, to a power supply and to a vacuum pump and its vacuum gauge system. See Figure 6.1.

Some auxiliary systems used to prepare the samples were: a vacuum furnace to heat-treat the samples, scales to measure the powders and compacts of Ti and C, a hydraulic press dies-and-plungers system to compact the powders and a capacitive discharge thermocouple welder.

6.3 Main Components of the Experimental Apparatus.

6.3.1 Reaction Chamber.

The reaction chamber consisted of a circular stainless

steel base on top of which a glass bell is positioned. The metal base is equipped with electrical connections through which power can be supplied to the interior.

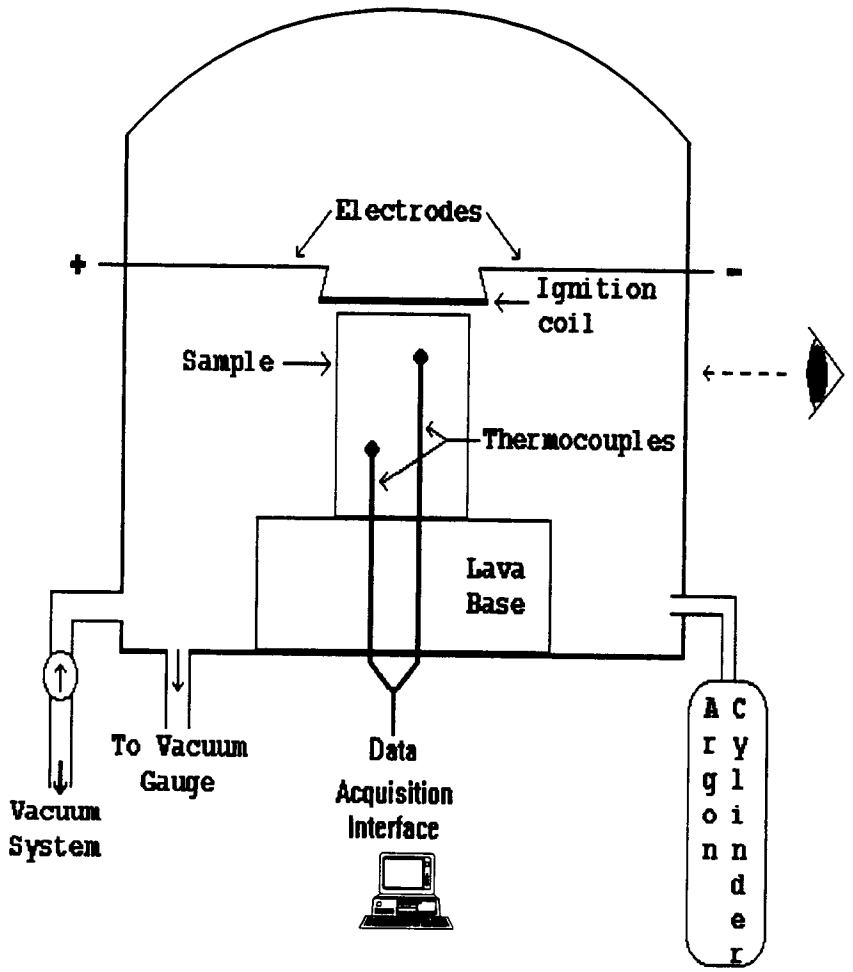

Figure 6.1 Scheme of Main Ensemble.

The main chamber is also equipped with eight entry-ports on the sides and two on the bottom. Some of these ports were used to connect the chamber to the data acquisition device, to a vacuum pump, to a thermocouple vacuum gage and to an argon cylinder; the rest of the ports were epoxy-sealed. Both the diameter of the steel base and the height of the 5 mm thick bell are 61 cm.

6.3.2 Data Acquisition System.

The temperature measurements were accomplished by using data acquisition boards from Data Translation, Inc., PCLab software and a IBM personal computer, as shown in Figure 6.2.

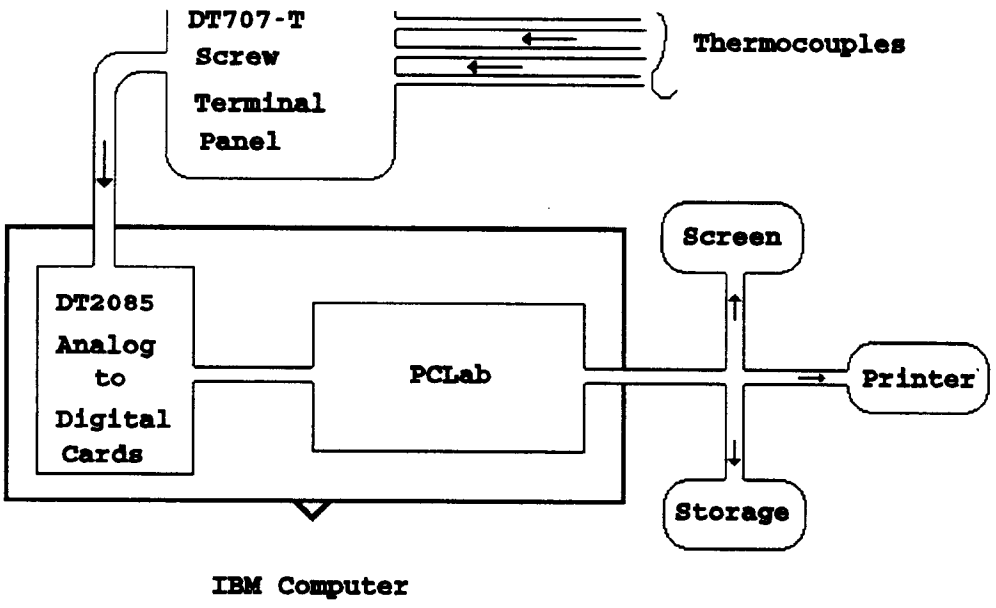

Figure 6.2 Temperature Monitoring System.

The hardware and software were calibrated and adjusted according to the specifications in their manuals [88, 89]. The thermocouple leads were connected to a DT707-T screw terminal with a cold junction compensation circuit board and a frequency range of 25-13000 Hz. When the voltages across the thermocouples were sensed by the DT707-T, the signals were fed into DT2085 analog-to-digital cards. These cards were installed inside the IBM personal computer.

A computer program, as shown in Appendix 3, was written to employ the PCLab subroutines. This program converts the digital voltage output from the DT2085 cards into degrees Kelvin.

Once the data is translated, it can be send to the screen, to memory or to the printer.

From the wide range of thermocouples available none can stand as high a temperature as the tungsten-rhenium thermocouple. This type of thermocouple is normally used at high temperature in reducing or vacuum environments, but never in an oxidizing atmosphere because of the high oxidation rates. Pure tungsten becomes very brittle when heated above its recrystallization temperature. To make the wire easier to handle, rhenium alloys are used in both thermocouple legs. The selected thermocouple used in the experiments was a .01 inch., type C. which consisted of one wire of tungsten-5% rhenium and one wire of tungsten-26%

rhenium, and had an upper range around 2800 °C. The standard error rating given by the OMEGA ENGINEERING company is of ±4.4 °C between 0 and 427 °C and ±1% between 427 and 2316 °C. The thermocouples were connected to the data acquisition board via extension grade wires. A DCC Corporation "Hot Spot" thermocouple welder was used to prepare the thermocouple beads [90].

6.3.3 Vacuum Pump System.

The main chamber was equipped with a .33 hp CENCO HYVAC 7 vacuum pump with a rated speed of 525 RPM. This pump has a pumping capacity of 35 l/min at 1 mTorr. The vacuum created in the main chamber was monitored with a CENCO thermocouple vacuum gauge with a measuring range of 1-1000 mtorr.

6.3.4 Vacuum Furnace for Heat Treatment.

Due to the high cost of vacuum furnaces a simple device was developed to provide heat treatment to the titanium and carbon samples. It consists of a simple furnace inside which a vacuum chamber is inserted. This vacuum chamber embodies a half nipple with a fixed flange on one end and closed at the other end with a circular stainless steel plate. The open end of the half nipple is closed by means of a nonrotatable-tapped mini flange through which a port is

drilled to connect the chamber to the vacuum pump and vacuum gage system. The vacuum chamber was made leak-proof by using a high-temperature cooper gasket ring between the fixed flange and the tapped flange. The furnace was equipped with a temperature control panel. See Figure 6.3

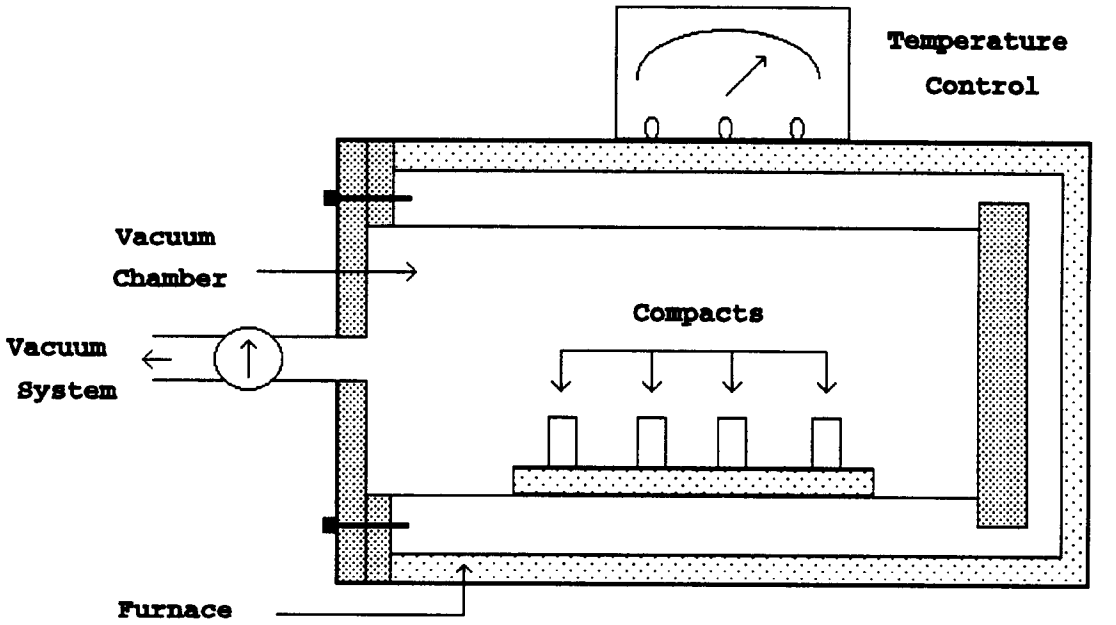

Figure 6.3 Setup for Heat Treatment of Samples in Vacuum.

The specifications of the furnace are:

-type: Thermolyne 150 model F-D1525M.

-interior dimensions: 4.5 inch. X 4.5 inch. X 9 inch.

-temperature range: continuous heating up to 1200 °C.

The specifications of the half nipple and flanges are:

-material: stainless steel type 304,

-half-nipple dimensions: 3 inch. o.d./10 inch. length

-flanges: 4.62 inch. o.d., 1 fixed to nipple.

The half-nipple with fixed flange, the nonrotatable-tapped mini flange, and the cooper gaskets were acquired from the MDC Vacuum Products Corporation.

6.3.5 Power Supply.

The energy needed for the samples to start reacting was supplied by means of a 1/25 inch tungsten coil. Due to the different sizes of samples tested in the experiments, coils of either 1/4 inch or 7/8 inch were used. The wire diameter of these coils is rated by the manufacturer, R. D. Mathis Co., as capable of reaching up to 2700 °C if a current of 65 amps at 24 volts is supplied. The coils were connected to the power source through electrodes installed in the combustion chamber base. The current provided to the coils could be controlled in the AC/DC 25 volts Sureweld Chemetron Corporation (model S409794) power supply connected to the reaction chamber.

6.3.6 Secondary Equipment.

The thermocouples were prepared using a DCC Corporation "Hot Spot" capacitive discharge welder, which generates an electric arc for fusing standard couple elements and/or welding them to any thickness metal. The specifications of the welder are:

-store weld energy: 5 to 50 Watt seconds.

-wire gauge: welds all standard wire between 16 to 30 gauge.

-cycle time: can perform 5 to 10 welds per minute.

-power: either 120 VAC 60 Hz lines or self-charging battery.

Another secondary equipment used was a common precision analytical scale (AB-4 model A14118) manufactured by the Torsion Balance Company. The scale could read a minimum of 0.1 mg. This precision was more than adequate for our purposes of measuring the powders to specific mixtures ratios and for weighing the samples before and after reaction.

The powders were compacted by means of a 20-tons per square inch coaxial-load hydraulic press. As different sizes of samples were required, stainless steel cylinder and rams were manufactured between 8 and 20 mm (I.D. of cylinder). A floating-cylinder method was implemented to reduce stress

concentrations on the sample ends. The method can be explained with the following steps and the help of Figure 6.4:

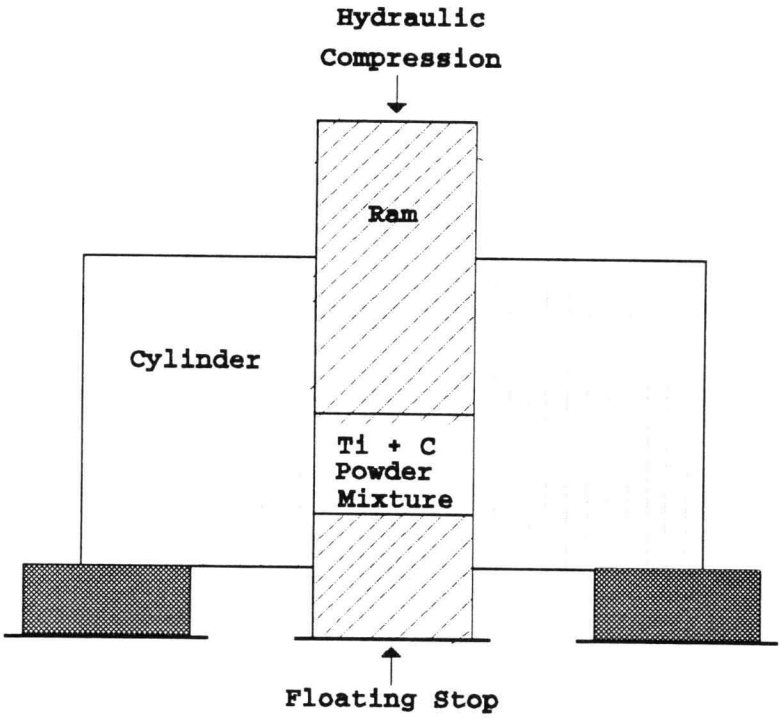

Figure 6.4 The Floating-Cylinder Method.

-The cylinder is initially mounted on a foundation which allows for the central part of the cylinder to move freely

up and down. A small ram is positioned inside the cylinder and let fall to hit the bottom surface; this will act as a floating stop later on in the compression process.

-The powders are then poured inside the cylinder.

-the other ram (top) is inserted and some initial pressure is applied after which the foundation on which the cylinder was resting is removed.

-The pressing continues; since now the cylinder can move, the stresses generated on the lower end of the compacted powders are lessened.

-After the compaction process is finished the sample has to be removed in a way that does not produce additional stresses and that at the same time does not break the sample (some of which will have relatively small compaction). This is done by resting the rams-cylinder pieces on a hollow cylinder and slowly applying small pressure to the top ram until the bottom stop and the sample are ejected.

Some other secondary devices included photographic equipment as well as a video-recording camera. The videos were tested to verify the feasibility of determining the propagation speeds from the recorded reactions. It became clear that this could be possible only if a high-speed camcorder was available.

6.4 Experimental Methodology.

The aim of each experimental run was to determine the velocity at which the reaction front will propagate along the sample. In order to accomplish this, it was needed to establish a temperature history of the sample to be tested. Thus, it was decided that two thermocouples would be positioned inside the sample at two known positions parallel to the axial axis. The velocity of propagation can be determined by dividing this known distance between thermocouples by the time that it takes the reaction front to reach the thermocouples.

6.4.1 Step-by-step Procedure.

Due to the many different combinations of parameters tested in the experiments, the investigative runs were scheduled so the same type of parameter was varied at a time. In this way only powders of one combination had to be prepared, or the same diameter of samples, or the same density, etc. The following steps exemplify how the experiments were performed.

Step 1: calculation of how much reactant was needed to adjust to a typical 20 mm height cylindrical compact. This step was no longer needed after experience was gained in earlier runs.

Step 2: measurement of the reactant powders to conform a

specific mixture composition.

Step 3: mixing of the reactants until no more coarse parts were observed. This was accomplished by mixing with a mortar and pestle and then by shaking the powders inside a glass container for about 20-30 minutes.

Step 4: compaction of the powders in the hydraulic press.

Step 5: measurement of height and weight of the sample.

Step 6: drilling of holes for later insertion of the thermocouples. This was a very delicate step since the holes had to be drilled very carefully, specially in the cases of relatively low density of the sample. The two holes were drilled longitudinally at the same radial distance from the center in a diametrically opposite manner.

Step 7: measurement of weight of sample.

Step 8: heat treatment of sample in the vacuum furnace. This step was generally performed overnight since the samples required at least five hours of treatment at above 500 °C to ensure that most of the volatile impurities were removed.

Step 9: thermocouple insertion and placement of the sample in the center of the combustion chamber.

Step 10: placement of the heating coil. The coil was positioned generally at a distance of about 3-5 mm above the sample to accommodate the possibility of expansion of the specimen and avoid breaking the hot sensitive coil. This was a tricky trade off since placing the coil closer to the

sample will permit a prompt start of reaction, but the cost of coils remained a constraint.

Step 11: mounting of the bell glass on the steel base. To assure that the chamber had no leaks a rubber gasket was attached to the glass and the steel base was coated with high vacuum grease.

Step 12: activation of the main chamber vacuum system. This step lapsed in about 30-40 minutes or when a vacuum of about 200 mTorr was achieved (1 atm=760 Torr).

Step 13: filling of main chamber with argon up to atmospheric pressure.

Step 14: adjustment of DC power supply to 24 Volts at 65 A.

Step 15: set up the data acquisition system (frequency and maximum recording time).

Step 16: preparation of photographic or video recording equipment (in some cases).

Step 17: the power source and the data acquisition system start concurrently (this is the nucleus of the experiment).

Step 18: cooling of the reaction chamber and subsequent dismantling of the setup to prepare for another experiment.

6.4.2 Data Collection.

After each experiment the data collected was stored in the hard disk unit for a later analysis. Due to the uncertainty of the time that would take for the top layer of

the sample to start reacting, the data taken could be very large if the chosen maximum recording time was too large compared to the time taken for the whole sample to be consumed. Therefore, the whole data taken had to be reduced to only the data taken while the ignition-propagation process was under way. This uncertainty became less of a problem as the experiments progressed. To lessen the problem, the computer program for data acquisition was modified to write only a given range of data for storage.

Several frequencies were used so the data storing (a very time consuming process) could be minimized since the number of experiments were on the order of hundreds. Ultimately the frequency used for all experiments was 400 Hz and data taken for about 60 seconds (which means 24000 data values to store per experiment!). While some experiments would take only a few seconds some will take a time larger than the maximum recording time.

6.4.3 Sample Length and Thermocouple Settings.

The length of the compressed sample, of course, depends on the amount of powder mixture loaded into the cylinder and the final achieved density. Typically, the 20 mm diameter sample lengths ranged between 22 and 26 mm; 16 mm diameter samples, between 17 and 28 mm; 12 mm diameter samples, between 18 and 26 mm; and 8 mm diameter samples between 18

and 25 mm.

Three considerations went into the determination of the minimum acceptable length between the upper surface, thermocouples and bottom surface of the sample. First, there must be sufficient distance between the top surface (where ignition is done) and the upper thermocouple to ensure that it is below the zone of initial, ignition-related, transient behavior of the propagation front. Estimates lead us to surmise that 7-8 mm is the minimum required length between the top surface and the upper thermocouple bean (Boddington [7] claims from his numerical results that 0.2 mm from the hot surface is all that is required to attain steady state combustion). Second, a gap between the two thermocouples of about 7 to 10 mm is found to give a reasonable resolution in temperature measurement to obtain the propagation speed. Finally, the bottom thermocouple must be sufficiently upstream so as not to be influenced by the boundary condition at the bottom end of the sample. Typically, the temperature profile ahead of the SHS wave decays within a distance of 3-7 mm. The faster the wave, the shorter this decay distance.

6.4.4 Heat Treatment.

As mentioned previously, the green compacts need to be subjected to heat-treatment in vacuum to remove volatile

impurities. These impurities cause a disturbance of the propagation front or avoid its initiation. Experiments performed without heat-treating the sample gave frustrating results. In some cases, the compact would "crack" and halt the propagation, while in some others the readings given by the thermocouples were erratic. In some other cases there simply was not an ignition of the compact. According to Shkiro et. al [40] the purity of the starting components played an important role in the pop-corning effect of the powders in their investigation of the system Ta_2C and TaC.

The samples were baked in the heat-treatment setup shown in Figure 6.3 for more than five hours at above 500 °C. Kecskes and Niiler [10] experimentally found that the samples needed to be vacuum-treated at a temperature exceeding 500 °C in order to remove most of the H_2, water vapor, and a variety of hydrocarbons. Holt and Munir [38] also identified the evolved gases to contain CO, N_2, and CH_4. In our experiments we found that heat-treatment at about 350 °C is inadequate (just as if no heat-treatment occurred).

6.4.5 Additional Comments on Experimental Approach.

Drilling of the two holes in which the two thermocouples were to be inserted resulted in a very time consuming process since there was a high percent of breaking of the samples, specially in low density samples. In short,

the limit of the low density range was set by whether a sample could endure the drilling of two holes at very close locations without breaking the sample. Breaking of samples caused a very tedious problem since additional samples had to be prepared when this occurred.

While in some cases researchers have determined the propagation speeds by means of video recording equipment it was found in our experiments that this approach was not very reliable due to the gases that evolved during the process which obscure any recording. A high-speed video cameras would be also needed with a very dependable ratio of frame by frame timing as compare with real time. Photographic equipment has the very important barrier of not knowing ahead of time at what moment the propagation would start to trigger the shutter. Some of our experiments were photographed while the propagation was going, but it became clear that additional equipment was needed to overcome the brightness radiating from the sample.

Experiments carry out in an evacuated chamber show that the compact literally blows apart following ignition, an effect also reported in [10]. The effect was even more violent in unbaked samples.

The mixing and shaking process takes anywhere from 30 minutes to over an hour. The time of mixing could possibly be a parameter of the SHS problem since too short a mixing

process may fail to ensure mixture uniformity while too long a mixing would allow oxidation of the reactants (because the mixing bottle contains air). Maslov [91] uses a mixing time of 6-8 hours in a porcelain drum. Ideally, if we were to do it again with appropriate resources, we will choose a ball-mill with an inert atmosphere.

6.5 Concluding Remarks.

This chapter has presented the methodology used in the experimental part of this thesis. A step-by-step approach is used to explain the method and some insights in particular problems encountered in those steps are provided. The instrumentation used is described as well as some other devices employed to perform the experiments.

CHAPTER 7

EXPERIMENTAL RESULTS

7.1 Introduction.

This chapter describes the results of the measurements of the propagation of the reaction front using the experimental setup described in Chapter 6. These results show the dependency of the steady propagation speed on: (i) supply mixture composition, (ii) dilution of the reactant mixture with the inert product TiC, (iii) the diameter of the reactant compact, and (iv) the density of the compact. The effects of these parameters on the density of the final product are also presented. Conditions at which the reaction wave ceases to propagate in a self-supporting manner are also identified.

7.2 Procedure.

The basic step-by-step methodology to carry out the experiments was fully explained in Chapter 6. This section now describes the conditions under which the experiments were divided to scrutinize separately the effect of each of the parameters listed in Section 7.1

To establish the conditions for conducting the experiments, we define a set of standard conditions as shown in Table 7.1. In the entirety of experiments performed, all conditions other than the property under examination were kept constant at the standard values.

Table 7.1. Numerical Values of the Parameters at "Standard" Conditions.

Parameter	Numerical Value
Sample diameter	1.6 cm
Sample density	2.5 g/cm^3
Initial temperature	300 K
Mixture ratio	Stoichiometric
Product dilution	None
Sample length	1.22-2.5 times sample diameter (see Chap. 6)

While the diameter, initial temperature, mixture ratio and product dilution are parameters that can be totally controllable, the density and sample length are parameters that are fully dependent on the manufacturing-pressing processes. However, after many experimental trials-and-errors, both parameters were set to fit within a reasonable

deviation from the corresponding "standard" condition value listed in Table 7.1

7.3 Temperature Histories Readings from Data Acquisition.

The temperature readings of the impregnated thermocouples were recorded with a data acquisition system which was turned on concurrently with the ignition power source. Figure 7.1 shows the temperature histories at two locations as given by the two thermocouples in a typical experiment. This figure shows that the reaction front is quite abrupt. The rapid increase in temperature indicates the arrival of the reaction front at both locations.

From the temperature histories of the two thermocouples, the difference in time at which the temperature reaches some established values is determined. Time differences are taken within the range of 1,500 to 3,000 °C and speeds are measured by dividing the known distance between the two thermocouple locations by this time difference. An average of these values is taken as the observed speed of the reaction wave. Repeated experiments under nominally similar conditions yielded consistent speeds indicating an achievement of steady propagation by the time the top thermocouple is encountered by the wave.

The low temperature portions of Figure 7.1 are shown with broken lines due to limitations in the data acquisition

process. [Both the thermocouples show constant readings after reaching about 3,500 K, an unfortunate consequence of the upper limit of the temperature range of the thermocouples.]

The positioning of the hot igniting coil on top of the sample presented always a slight difficulty since it could not be fixed at a definite distance in all experiments. After the first or second experiment, the coils would become partially twisted (but still in workable conditions). To compensate this twisting, the distance to the sample had to be varied. The distance was also varied since not all the samples were of the same length. These experimental details coupled with the variation in the physical properties and kinetics make the reading times different for each case. Figure 7.2 shows another temperature readout for an experiment having the same conditions as those of Figure 7.1; however, it is very likely that in the experiment shown in Figure 7.2 the igniting coil was much closer to the top surface of the sample than for the case of Figure 7.1. Cases for which long ignition times (more than 60 seconds) are needed were not taken into consideration since, in these cases, the sample reacts literally in a volumetric manner.

7.4 Effect of Supply Mixture Composition.

The effect of the reactant mixture composition on the

propagation speed is presented in Figure 7.3. At every mole ratio, a number of experiments were performed in order to see the reproducibility of the results. At each point, some scatter in the data is observed. This scatter is believed to be mainly due to the unavoidable nonuniformity in the mixing of the reactant powders. The line shown in Figure 7.3 is the best fit curve passing through the data points. This is explained in Section 7.10.

When the sample involves stoichiometric proportions, all the reactants are converted into the product upon reaction under the constraint only of thermochemical equilibrium. If either of the reactants is in excess in the initial mixture, that excess amount is not converted into product. While not contributing to energy release, the excess reactant absorbs some of the released energy of reaction to reduce the maximum attained temperature. This, in turn, reduces the speed at which the reaction propagates.

For stoichiometric conditions the measured speed is around 1 cm/sec at a nominal density of 2.5 g/cm^3. Hardt and Holsinger [37] report measurements of 1.2 to 1.6 cm/sec. Considering the complexity of the propagation process, the agreement is deemed reasonable. Especially so, for there exist differences between these two investigations in such experimental parameters as the reactant particle size, composition of the carbon constituent and compact density.

Hardt and Holsinger report a speed of 1.5 cm/sec when the carbon reactant is a mix of 2/3 graphite and 1/3 lampblack. When 100% lampblack carbon is used, but with various reactant particle sizes, they report speeds in the range 1.2 to 1.6 cm/sec. In our experiments only graphite was used.

Scatter of measured data is unavoidable even in experiments conducted by the same investigator due to the lack of perfect uniformity of mixture composition and compaction density in the sample. Data scatter, as evident in Figures 7.3 to 7.6, is quite typical.

At sufficiently large departure from stoichiometry, the reaction ceases to propagate altogether. This is the quenching condition. Experimentally determined quenching conditions for reactants composition are more than 1.6 moles of titanium per mole of carbon and less than 0.6 moles of titanium per mole of carbon. These results are in agreement with Holt [34].

7.5 Effect of Dilution with the Inert Product.

Figure 7.4 shows the measured propagation speed as dependent on the degree of dilution with the product (i.e., TiC) which is presumed inert. Dilution is presented as percentage of weight of the reactant mixture [wt. of TiC/wts. of (C+Ti+TiC)]. (The line passing through the scattered data points again represents the best fit curve of

the data.) The diluent not only acts as a heat sink but also reduces the total energy released per unit mass of the initial mixture. Thus, dilution reduces the maximum attained temperature. Addition of inert TiC thus leads to a progressive reduction in the reaction wave propagation speed and an eventual failure of the combustion. Experimentally, failure is observed if the percent by weight of TiC exceeds 27.5. The samples with 27.5 percent of TiC can be ignited but the reaction becomes quenched part way through the samples.

7.6 Effect of Diameter.

The ratio of the surface area to the volume decreases as the sample diameter increases; accordingly the lateral heat loss becomes progressively less significant compared to volumetric heat generation. The effect of lateral heat loss is expected to reduce the propagation speed below that encountered under adiabatic conditions. Ultimately an asymptotic value [21] for the sample diameter will be reached above which there is no noticeable effect of lateral heat loss on the propagation speed. This asymptotic propagation speed is analogous to the adiabatic flame speed. On the other hand, a gradual decrease in the diameter will lead to a smaller value of the propagation speed because of a progressively increasing heat loss; ultimately a critical

diameter is reached below which the wave ceases to propagate altogether.

The effect of diameter on propagation speed is shown in Figure 7.5. It is evident from this figure that the effect of heat loss on propagation speed is insignificant for all sample diameters above 8 mm. A sample diameter less than 8 mm was not investigated in our experiments due to problems in preparing these samples and in making holes in them for the thermocouples.

Of peripheral concern is the effect of the insertion of the high-thermal-conductivity thermocouple wires on the propagation speed. Let K and A, respectively, be thermal conductivity and cross sectional area. The product (KA) is proportional to the heat conduction rate. The ratio of (KA) of the two thermocouple-leads to the (KA) of the sample is estimated to be 0.012 under the worst operating conditions. The thermocouple wires are thus expected to increase the propagation speed by no more than 0.6%. This small error can be ignored in the light of various other uncertainties involved in the experiment.

7.7 Effect of Initial Density of the Compact.

The effect of sample initial density on propagation speed is shown in Figure 7.6. (The scattered points represent the data while the line represents a least square

curve fit of the data.) Samples with initial densities ranging from 1.59 to 2.75 g/cm^3 were tested. The limits of this density range correspond respectively to about 42 to 73% of the maximum possible density of 3.75 g/cm^3 to which an initial sample can be compressed. Results show that the propagation speed attains a maximum value at a density near 2.1 g/cm^3; this corresponds to about 56% of the theoretical density. At low densities, the speed is found to increase as density of the sample increases. At high densities, the speed is found to decrease as density increases. This trend is attributed to the two opposing effects of density: (1) increased density increases the thermal conductivity which in turn increases the speed; and (2) increased density increases the volumetric heat capacity which in turn reduces the speed. Within the tested density range, the results are in excellent qualitative agreement with those reported by Rice, et al.[60], who establish that the propagation speed of a titanium and carbon system, with 10 weight % excess titanium, attains a maximum value at approximately 60% of theoretical density. Our results, however, contradict the observations of Kottke and Niiler [19] who showed that the speed of propagation continuously increases as the density increases. Eslamloo-Grami and Munir [92] in their work with titanium nitride showed that the combustion wave velocity decreases as the density increases from 45 to 70% relative

density of titanium nitride. Since this system involves a gas, the observation is a consequence of not only the increased heat capacity but also the decrement in porosity which makes gas diffusion difficult.

It was observed in the experiments that samples with initial density lower than 2.0 g/cm^3 give a product broken up into layers as shown clearly in the photograph (a) in Figure 7.7. On the other hand, samples with density higher than 2.0 g/cm^3 produce an integral product cylinder (although slightly expanded) as shown in photograph (b) in Figure 7.7.

7.8 Swelling of the Product:

During the synthesis process, swelling of the samples was observed in every experiment. Solidification of molten product and release of trapped gases are thought to be the causes of this swelling. After each experiment, the volume and the final density ρ_f of the TiC product was determined by measuring the length, diameter and mass of the product. Measurements showed no significant change in diameter, contrary to the reports of Holt [34]; the samples were found to measurably expand only in the longitudinal direction.

The final density ρ_f is presented in Figures 7.8, 7.9, 7.10 and 7.11 as a fraction of the theoretical final density ρ_{th} (= 4.95 g/cm^3). Since the final product structure is

expected to depend on a complex combination of factors involving thermal expansion, outgassing, volume changes due to phase changes, etc., the following explanations of the observed trends of Figures 7.8 to 7.11 are at best qualitative and at worst speculative. A density higher than about 45% of the theoretical final density was not obtainable in these experiments. This is somewhat lower than the density reported by Holt [34].

Figure 7.8 shows that the final density increases from about 35 to 40% of theoretical final density in response to an increase in the initial density from 2.25 to 2.75 g/cm^3; this corresponds to 60 to 75% of the maximum initial density of the mixture. This nonproportional increase is expected since a sample with higher initial density will have less trapped gases to be released during combustion. Figure 7.9 gives the measured final density for various mole ratios of the initial mixture. The percent theoretical density is found to be higher for both titanium-rich and carbon-rich cases than for the stoichiometric case. A compact pressed out of a stoichiometric reactant mixture obviously results in a reaction temperature and net reaction rate near their highest possible values. Outgassing as well as expansion effects are then expected to be more intense than in nonstoichiometric mixtures and to yield correspondingly a product of lowest density. The effect of diluting the

initial mixture with the inert product on the final density is shown in Figure 7.10. The final density increases from about 36 to 46% of theoretical final density in response to diluting the mixture from 0 to 25% by weight with TiC. This again is thought to be a consequence of the reaction temperature and rate which were both lowered with the addition of the diluent, thus reducing outgassing as well as allowing phase transitions conducive to the formation of a dense product. The density of the final product is also found to increase as the sample diameter decreases as shown in Figure 7.11. This is attributed to the smaller quantity of trapped gases in a smaller diameter sample and the ease with which they can elude from the thinner solid.

7.9 Purity of the Product.

In order to confirm the product of reaction, an x-ray diffraction analysis was performed on various samples. Table 7.2 (from Powder Diffraction Files [93]) gives for calibration the largest interplanar spacing for titanium, carbon (graphite) and titanium carbide.

The results of the x-ray diffraction analysis are presented in terms of two-theta spacing. Figure 7.12 gives the analysis for a product made from a sample in stoichiometric proportions. The two strong lines are found at two-theta equal to 36.0 and 41.8, corresponding to

d-spacings of 2.5 and 2.16. In Table 7.2 these are the two strongest lines for TiC, thus confirming the product to be TiC.

Table 7.2 Largest Interplanar spacing for Ti, C and TiC.

Specimen	Interplanar spacing
Ti	2.24, 2.56, 2.34
C	3.36, 1.68, 2.03
TiC	2.16, 2.5, 1.53

7.10 Curve Fitting of the Experimental Data.

In Figures 7.3, 7.4 and 7.6 the best fit curves for the experimental data are provided. Statistical literature [94, 95] suggest that the best fitting method for scattered and replicated data over a field of inputs is that given by the weighted least squares polynomial.

Figure 7.3 shows that at both sides from the middle point (i.e. a=1) sharp gradients occur. Hence, two different correlations for each side (a>1 and a<1) will provide better fitting of the data. The correlation for the rich titanium case side (a>1) is given as:

$$u = 0.41518\ a^2 - 1.6563\ a + 2.1854 \qquad (7.1)$$

with an adjusted coefficient of determination of 0.834. Here, u is the propagation speed in cm/sec and a is number of moles of titanium per mole of carbon in the initial mixture. The correlation for the leaner-titanium side (a<1) is given as:

$$u = -0.8829\ a^2 + 2.6205\ a - 0.80016 \qquad (7.2)$$

with an adjusted coefficient of determination of 0.914.

In Figure 7.4 the regression that fits the data speed versus product dilution is given as:

$$u = -0.00034175\ b\% - 0.018545\ b\% + 0.96745 \qquad (7.3)$$

In this equation b% represents the percent in weight of product present in the reacting mixture. For this least square correlation the adjusted coefficient of determination is 0.835.

In Figure 7.6 the regression for speed versus initial sample density is:

$$u = -1.0623\ \rho_i^2 + 4.56\ \rho_i - 3.8165 \qquad (7.4)$$

with the initial density ρ_i in g/cm^3. This correlation has a .741 coefficient of determination. See Appendix 1 for an analysis of the experimental error.

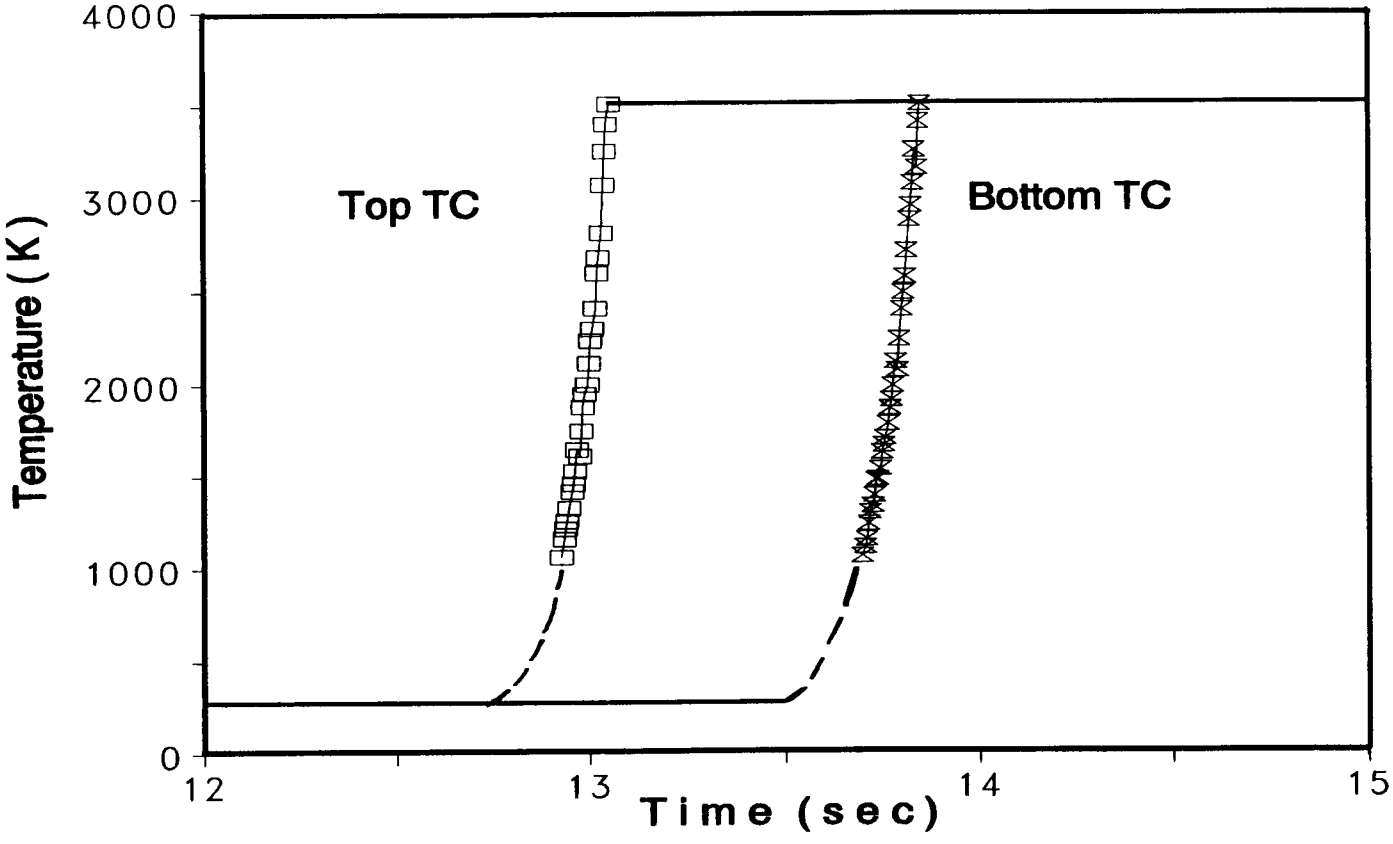

Figure 7.1 Temperature Distribution from Data Acquisition System at Two Near-Axial Locations in the Sample in a Typical Experiment.

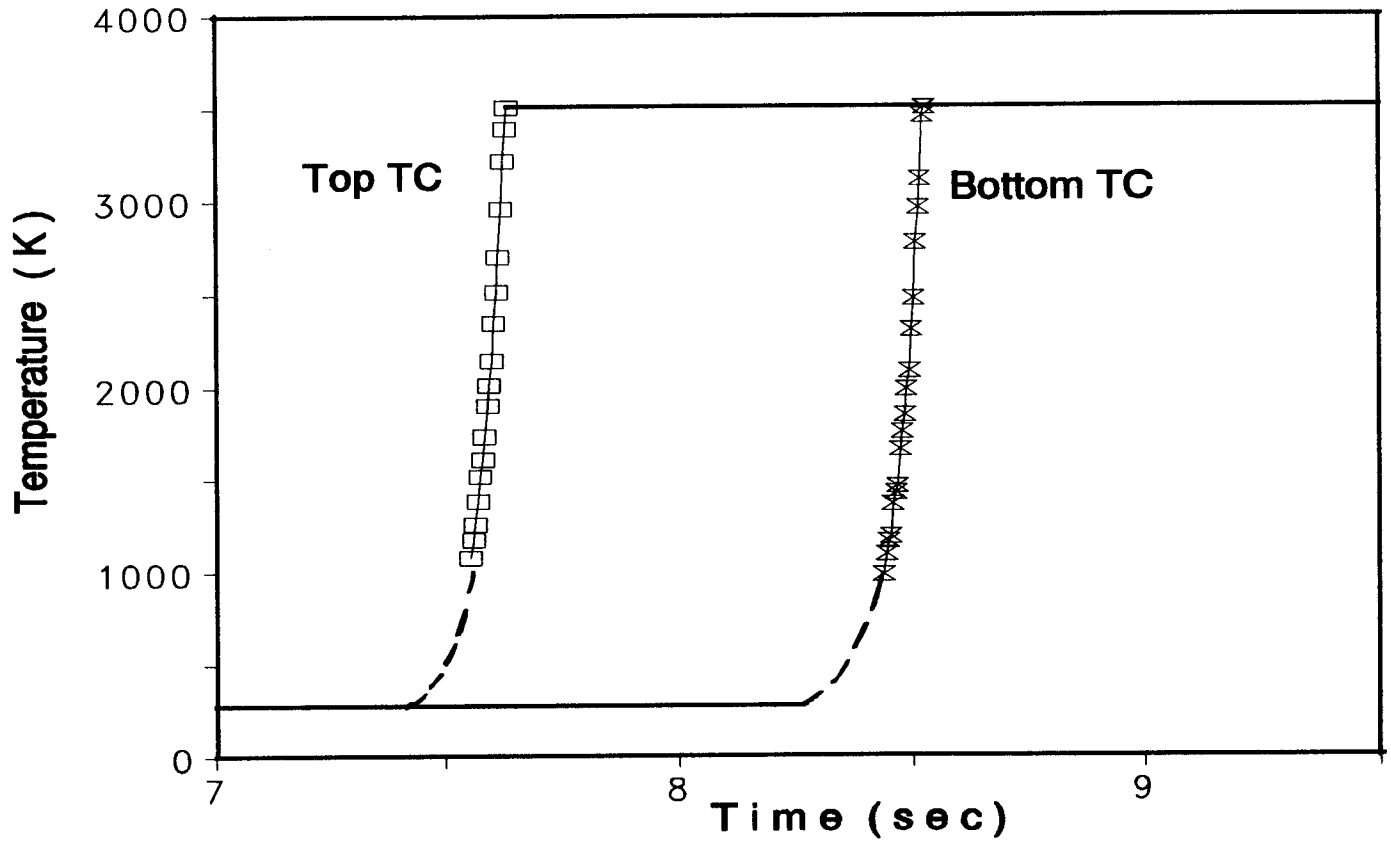

Figure 7.2 Temperature Readout when the Heating Coil is Closer to the Sample (Earlier Ignition).

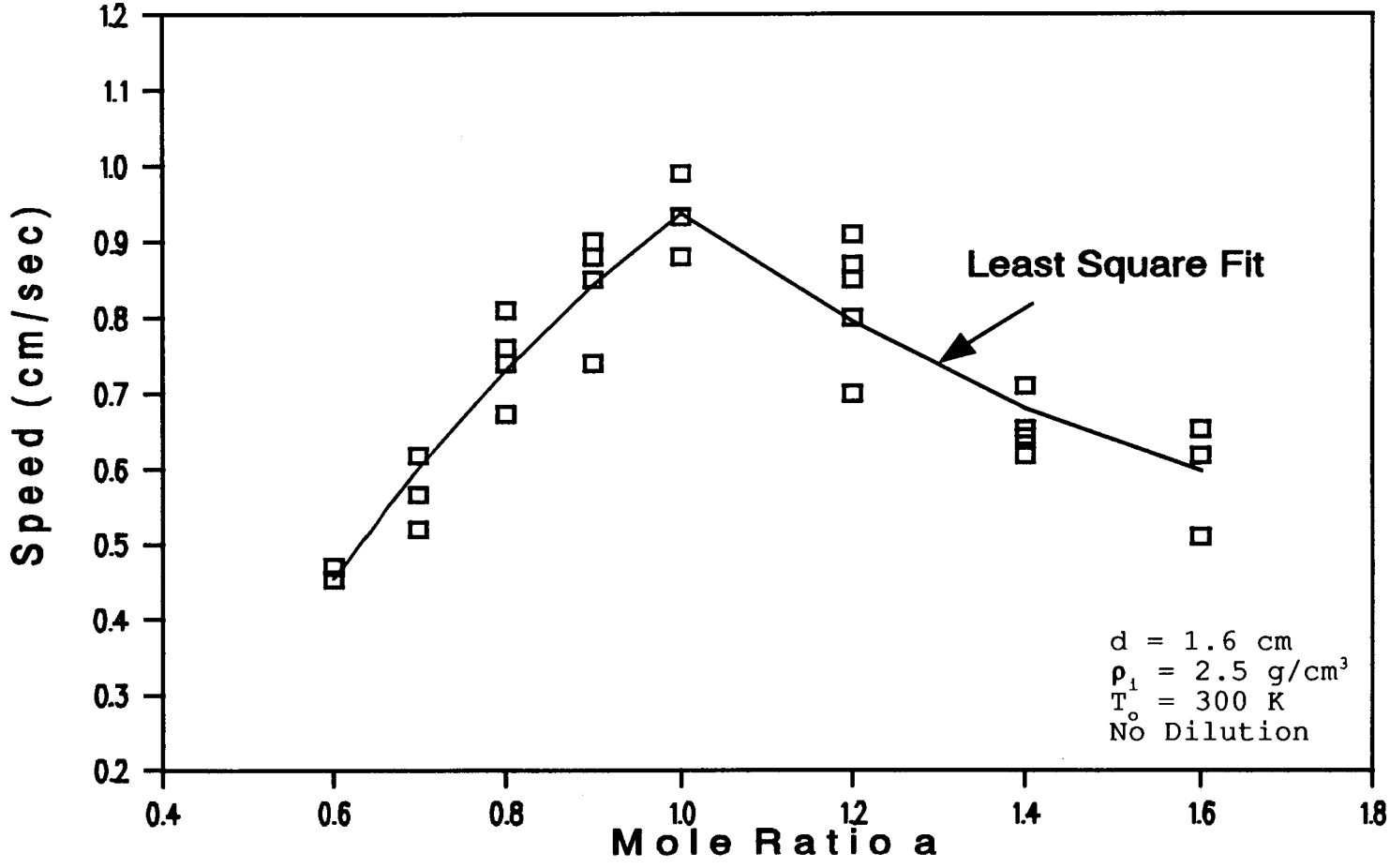

Figure 7.3 Effect of Supply Mixture Composition on the Propagation Speed.

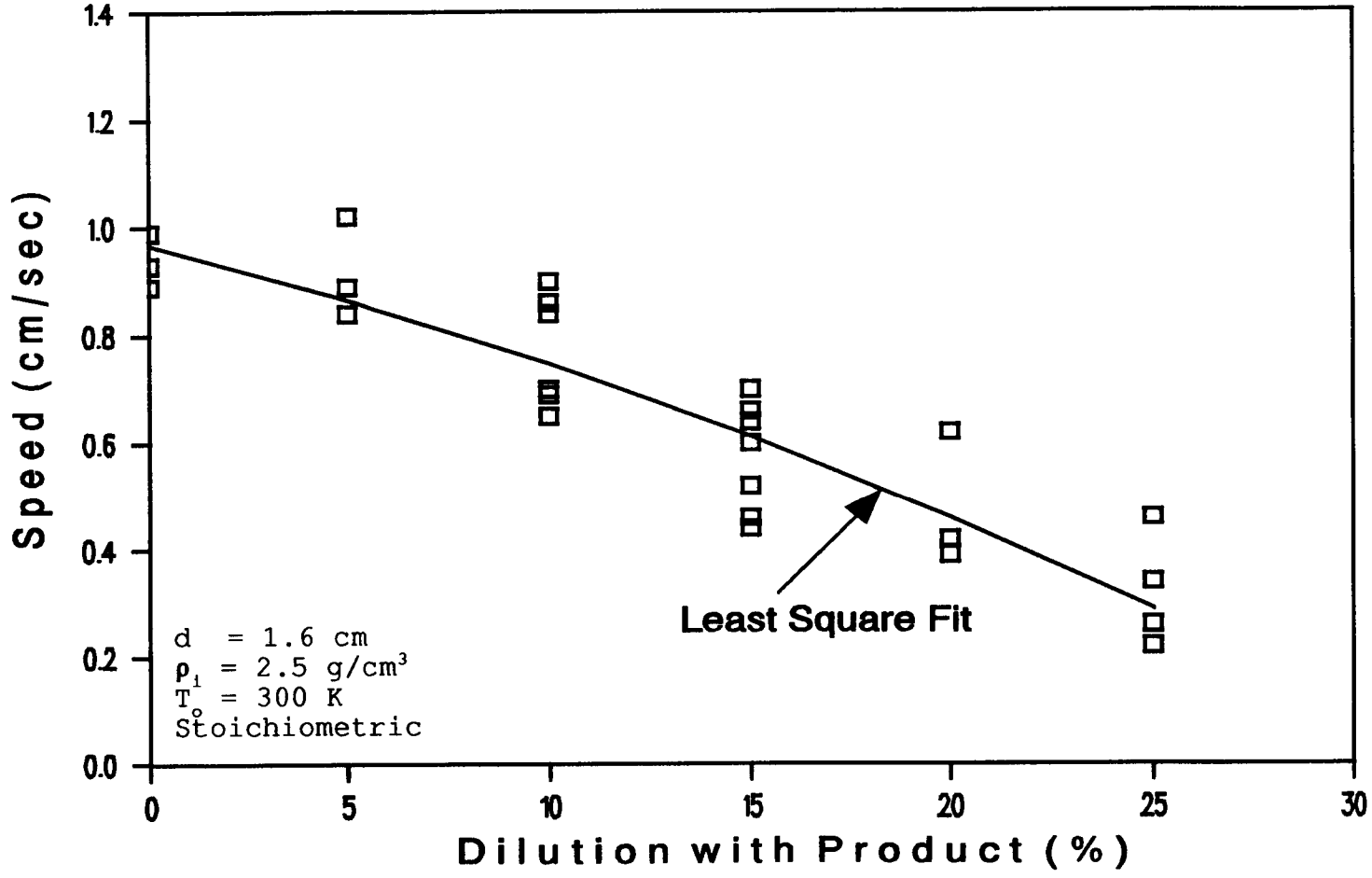

Figure 7.4 Effect of Dilution with the Inert Product on the Propagation Speed.

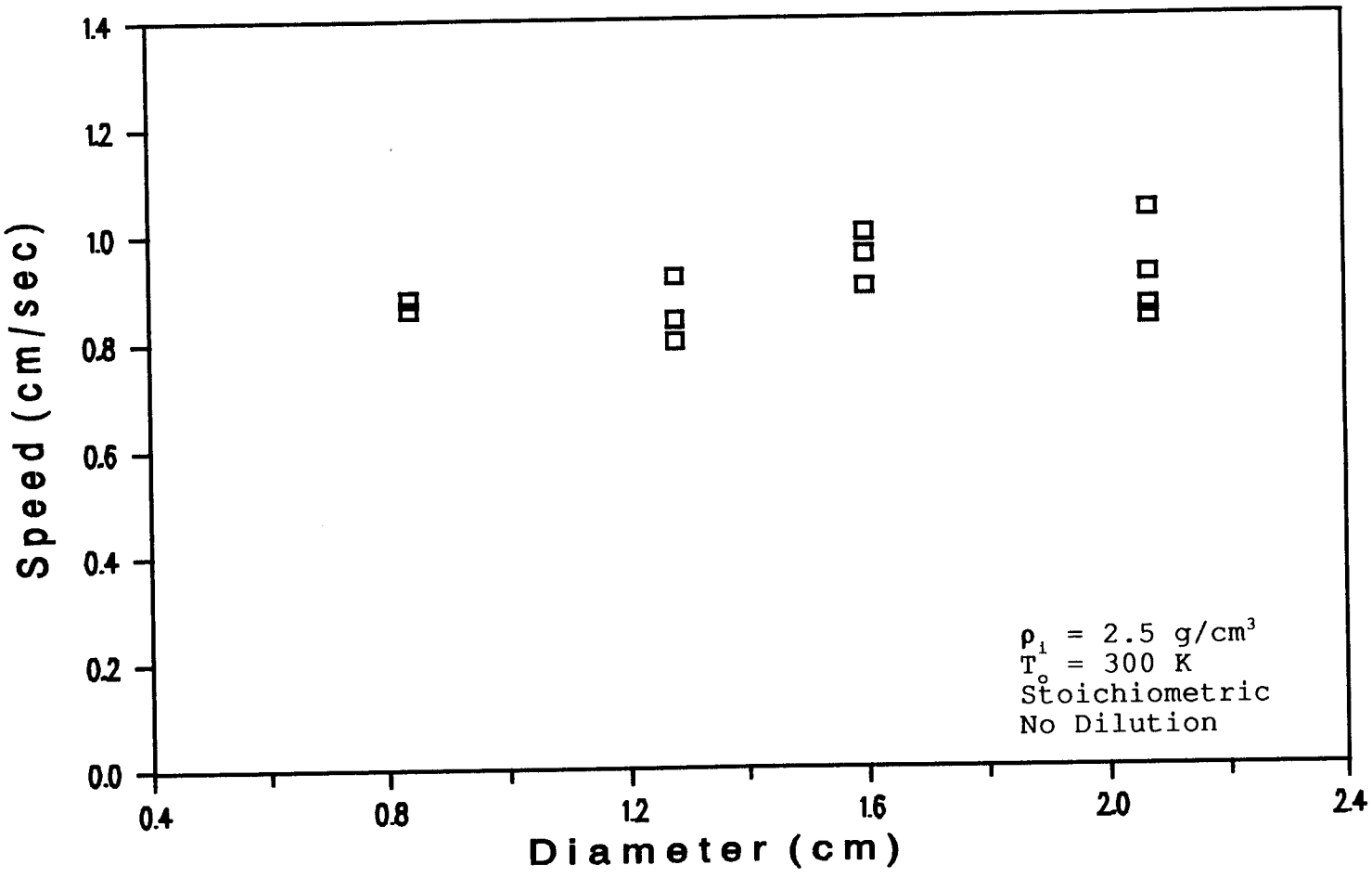

Figure 7.5 Effect of Diameter of the Sample on the Propagation Speed.

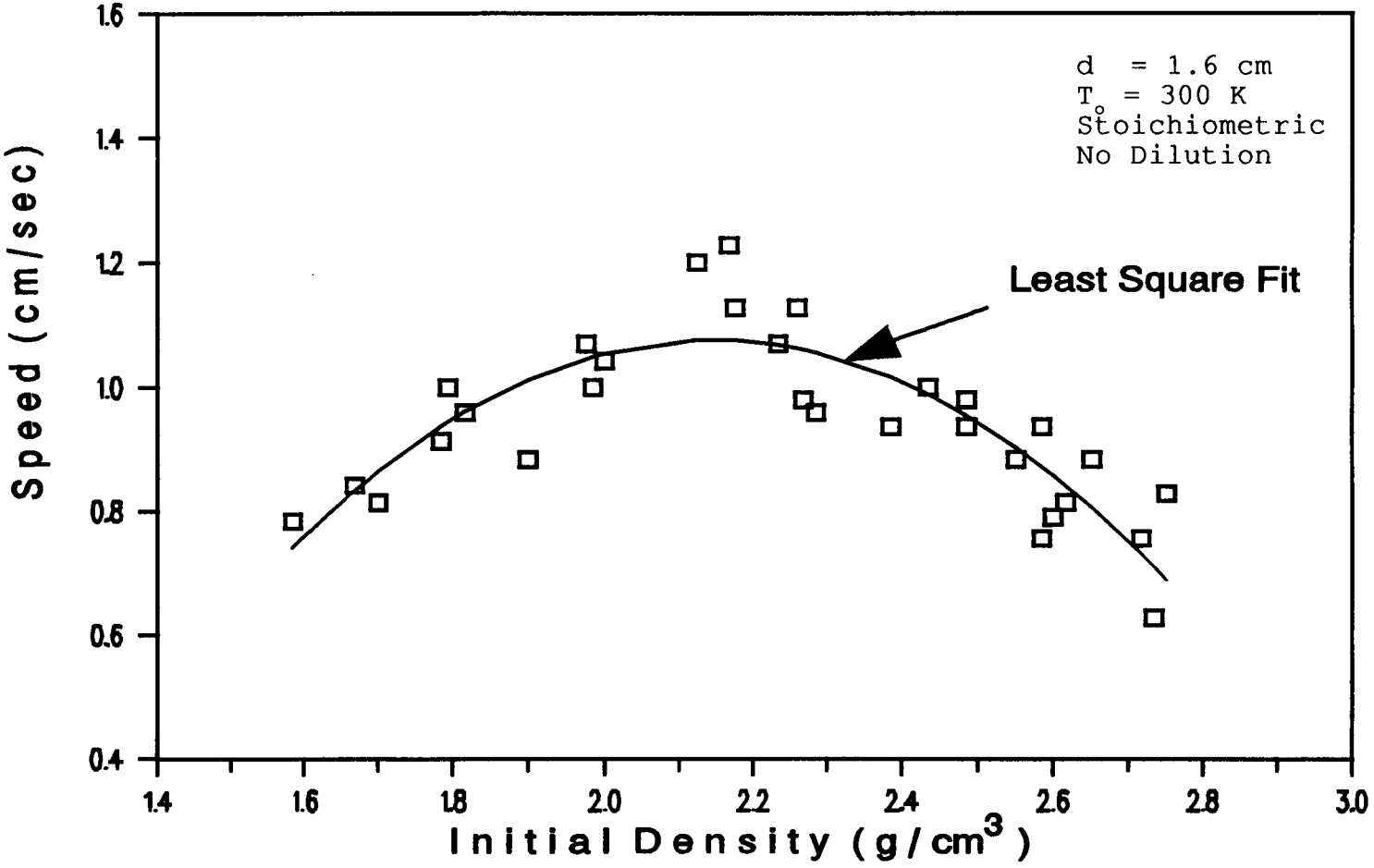

Figure 7.6 Effect of Initial Density of the Compact on the Propagation Speed.

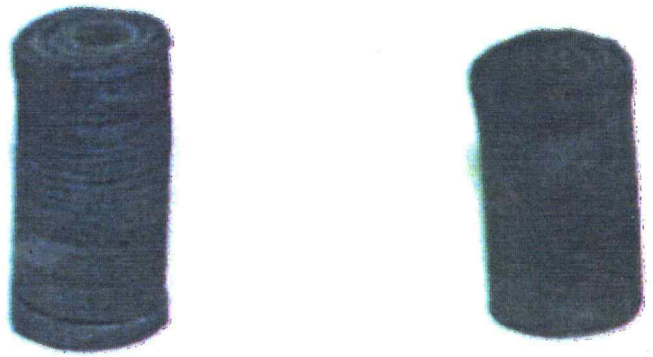

(a) (b)

Figure 7.7 Photographs of Synthesized Products. (a) Low Compact Density, ρ=1.8 g/cm^3. (b) High Compact Density, ρ=2.5 g/cm^3.

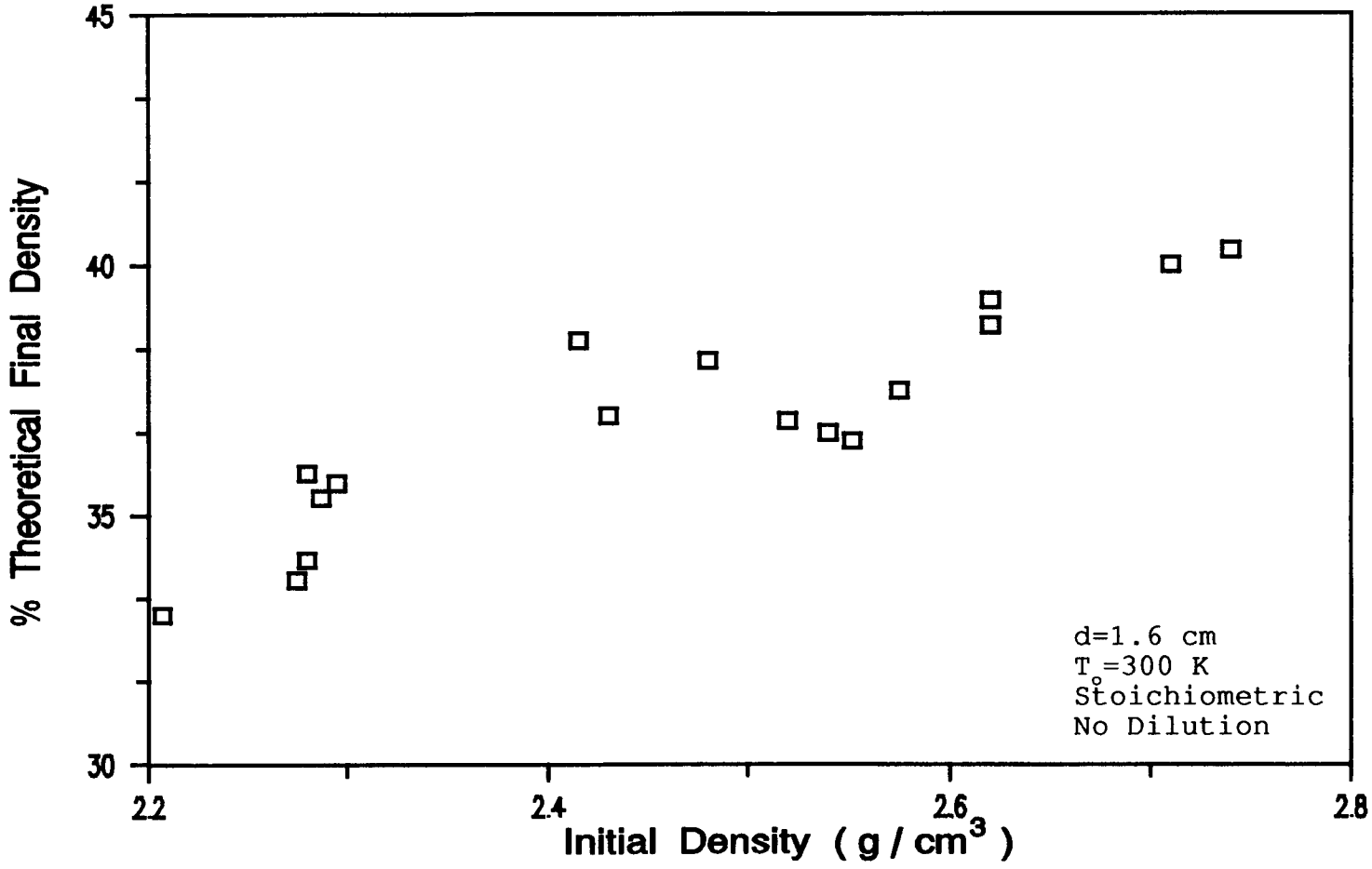

Figure 7.8 Percent Theoretical Final Density as a Function of Initial Sample Density.

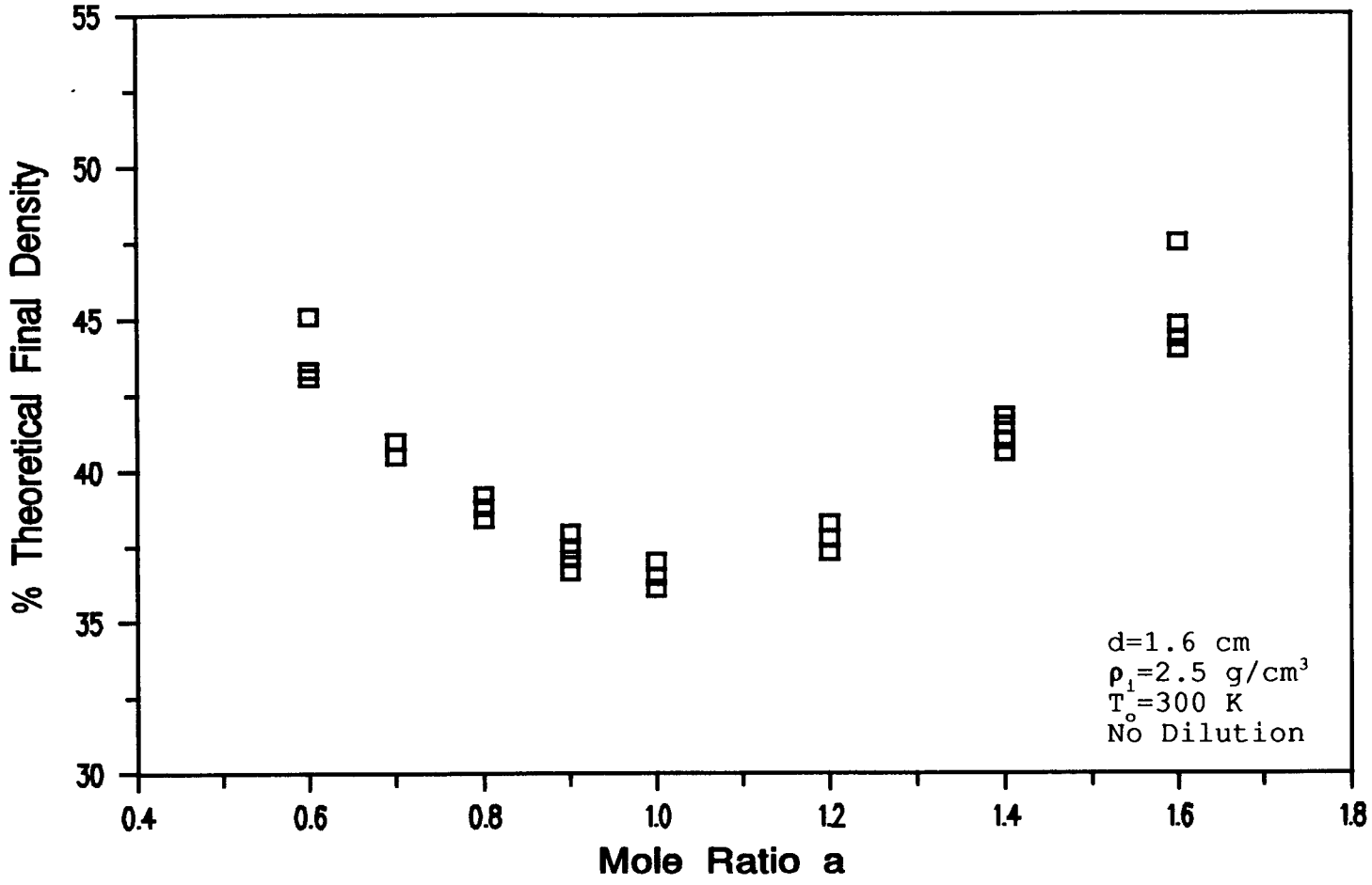

Figure 7.9 Percent Theoretical Final Density as a Function of Mixing Ratio of the Reactants.

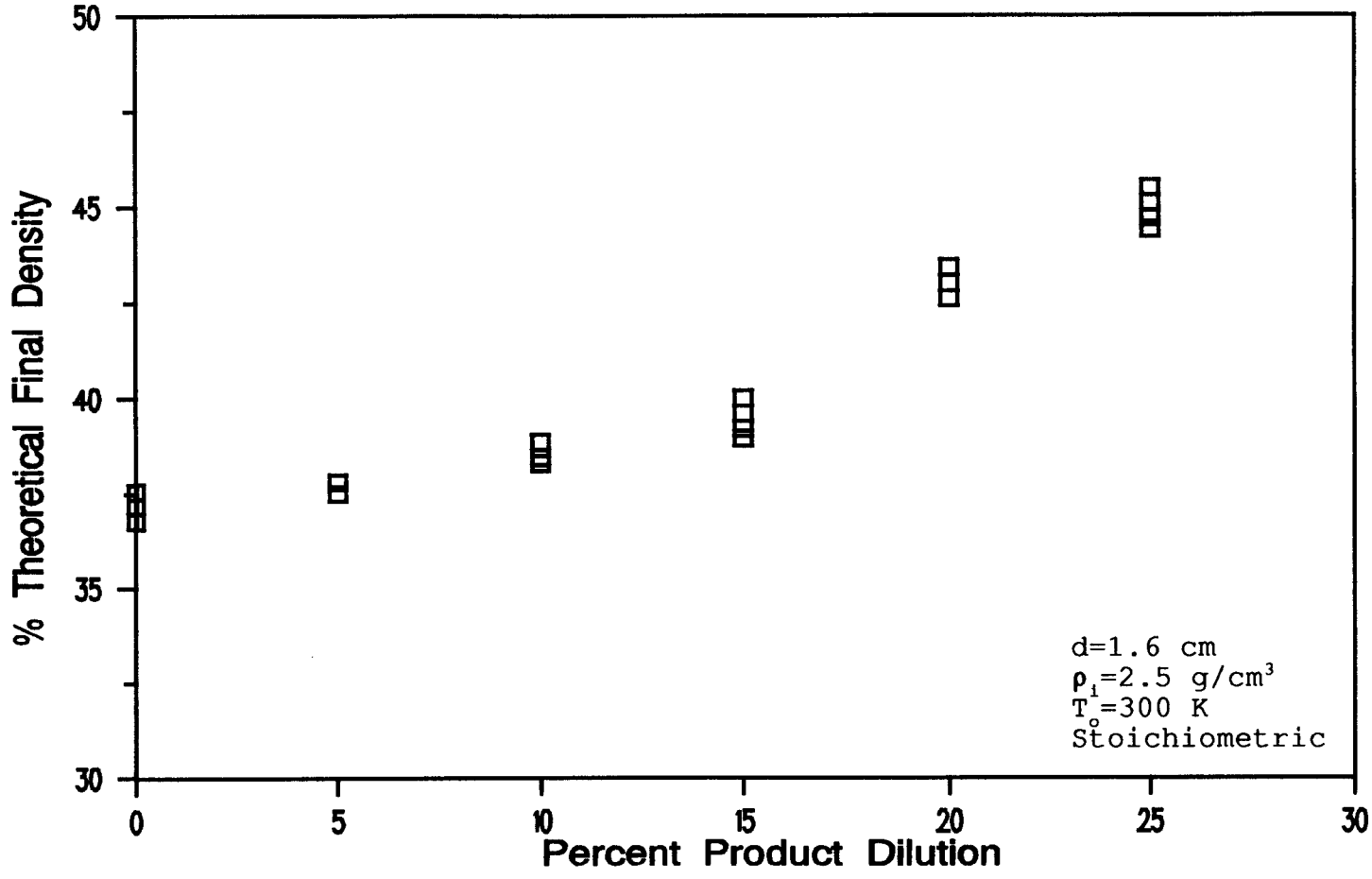

Figure 7.10 Percent Theoretical Final Density as a Function of Dilution with Product.

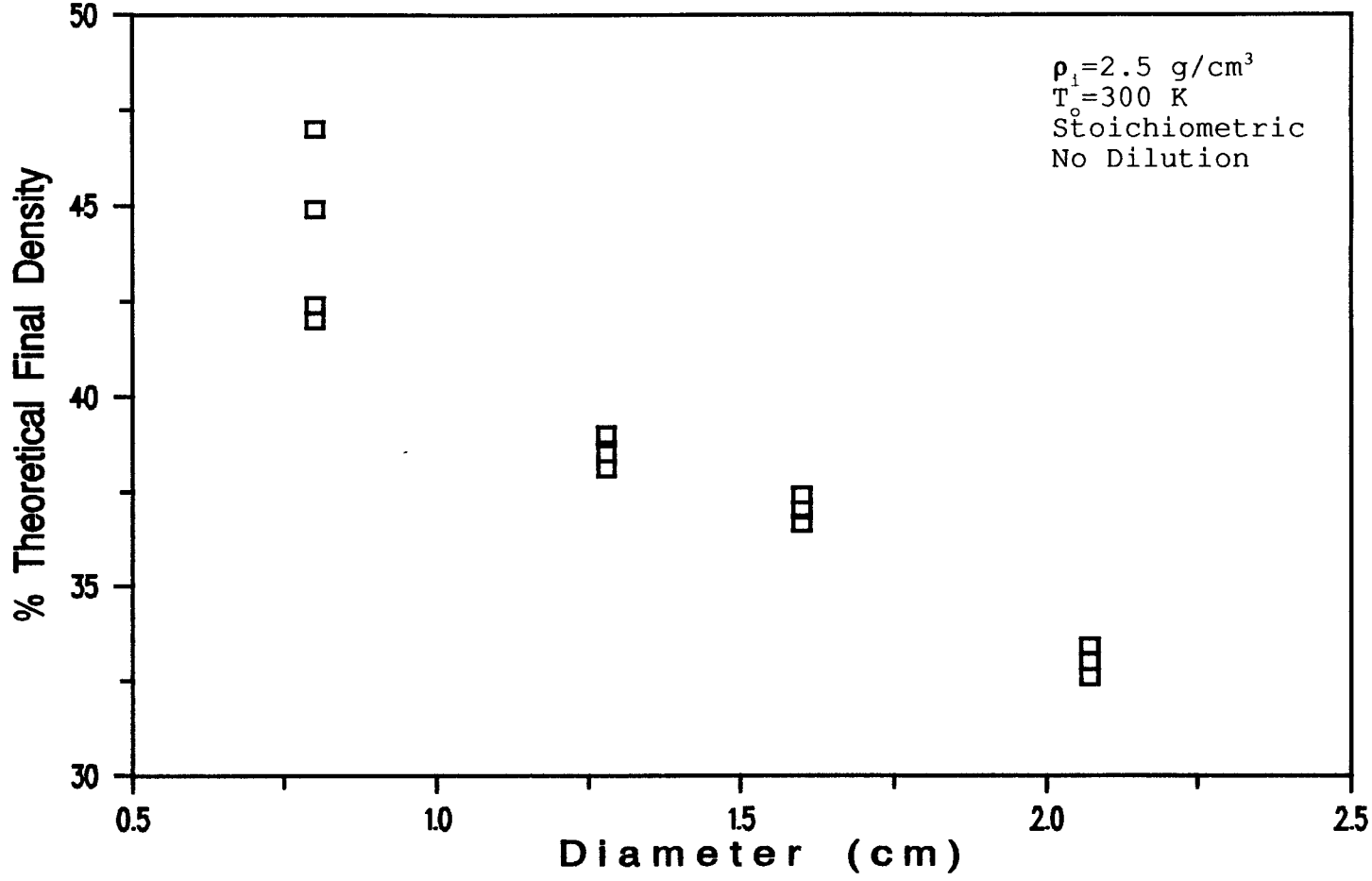

Figure 7.11 Percent Theoretical Final Density as a Function of Sample Diameter.

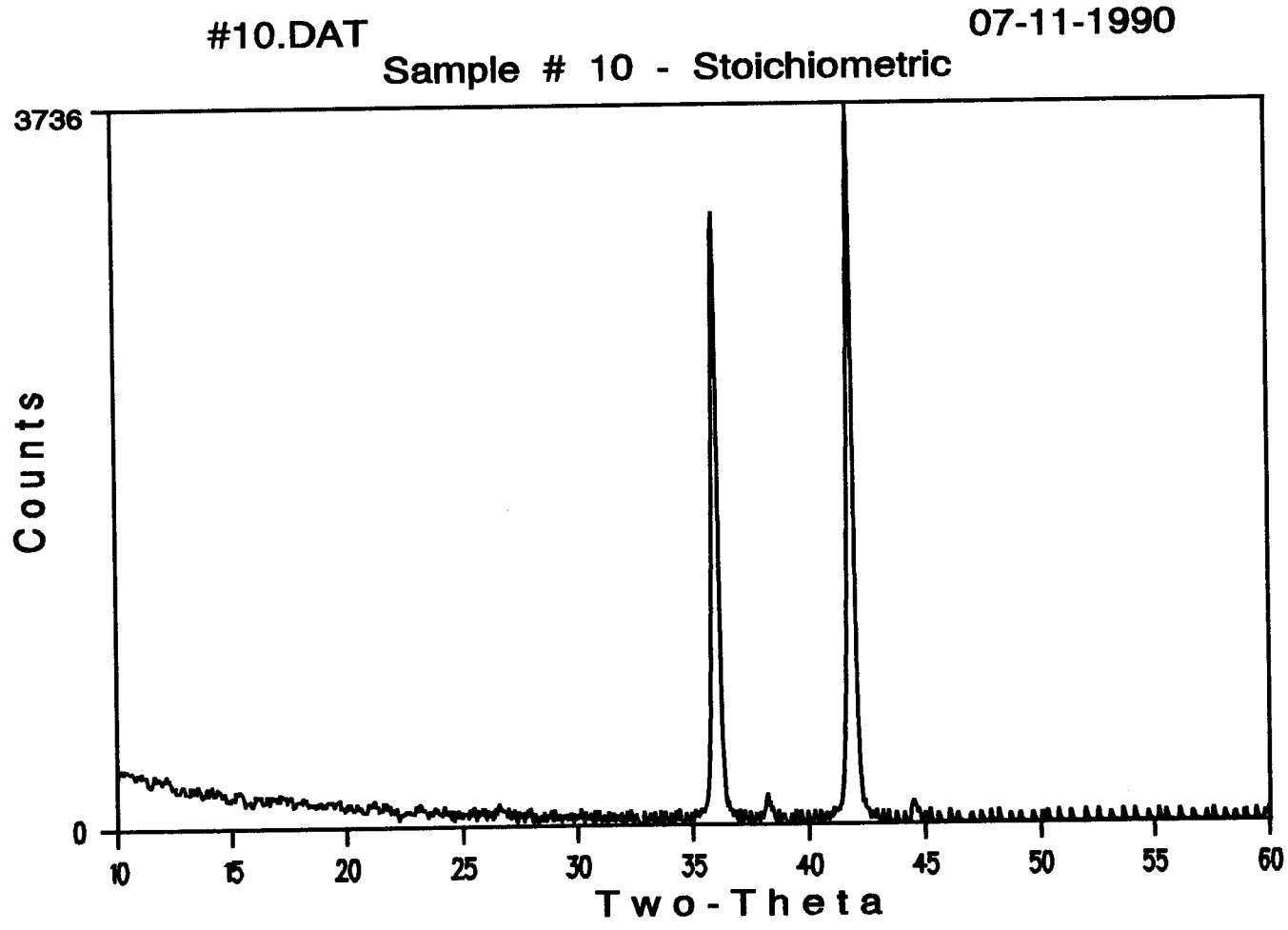

Figure 7.12 X-ray Diffraction Pattern for a Typical Product.

CHAPTER 8

RESULTS OF THE NUMERICAL ANALYSIS OF THE IGNITION PROCESS

8.1 Introduction.

In Chapter 4, Section 4.6, the ignition problem has been discussed. This chapter presents the results of the numerical study of the conditions that will assure that ignition, and subsequent propagation, will occur. The analysis is only for the stoichiometric adiabatic condition, but the same conclusions drawn for this case can apply for non-stoichiometric conditions or for a mixture diluted with TiC product (with a possible shift of curves position). Based on the functionality for the SHS problem described in Chapter 4, the main parameter to vary in the analysis is the Da number. Thus, the main outcome of this ignition analysis is the determination, for a given Da number, of the minimum temperatures of the igniting source needed to ensure that ignition will occur. Below those critical temperatures the mixture will never ignite and above them ignition is always ensured. This determination of critical minimum temperatures permits the delineation of a "range of ignition" plot that

shows, for the whole range of Da number covered in this study, a no-ignition zone and a ignition zone.

8.2 Ignition Study Procedure.

As mentioned in Chapter 4, the ignition criteria to use follows the fact that there is always some temperature at which the rate of heat generation exceeds the loss rate [84]. For modeling our semi-infinite, adiabatic cylinder this heat loss rate implies the conduction of energy from the igniting area to the rest of the cylinder.

In terms of the dimensionless variables defined in Chapter 4, this ignition condition is reached when:

$$\frac{\partial \theta}{\partial y}\Big|_{y=0} = 0 \qquad (8.1)$$

Based on this condition, the computer FORTRAN program listed in appendix 2 was slightly modified to record the time that it will take for the layers adjacent to the igniting source to reach this condition. The long computational runs were done using 5 different computers:

-a VAX 780,

-a Digital Microvax II (VAX Station 5xx Direct Access Memory),

-a SUN Sparc Station 1-Plus (in UNIX system),

-the Mainframe Floating Point System at OSU, a VAX 780

with a FPS-264 attach processor, and

-a 386-20 MHz PC, with floating point math coprocessor.

By far the most time-intensive tasks were accomplished using the mainframe and the SUN Sparc station, while the intermediate and less time-intensive runs were accomplished on the other three computers.

It is expected that the ignition delay will be large if the igniting source temperature is low. Low values of the Da imply that the rate of reaction rate is much smaller than the heat conduction rate. Thus, combining a sample with a small Da number and a low temperature of the igniting source, θ_{hot} , a very large ignition delay will be expected or perhaps no ignition will at all occur. A high thermal conductivity of the sample will cause a large time-of-ignition delay as well.

Ignition processes are characterized by a gradual increase of temperature that is then followed by a rapid increase over a very short time period. Using the criteria for ignition as given in Equation (8.1), it was observed that for $\tau < \tau_{ign}$ the gradual temperature increase took a much larger period than the time to get from the temperature at the ignition condition to the maximum temperature attainable (in this analysis, the adiabatic temperature is θ=0). During most of the time that $\tau < \tau_{ign}$, the mixture

compact experiences only inert heat conduction because the heat-release term is exponentially small. The chemistry of the reaction will remain insignificant everywhere until the temperature reaches somewhere near the ignition condition (this area could be called a transition stage); thereafter, due to the exponential factor in the source term, the chemistry will become dominant and cause a very rapid temperature increase.

Figure 8.1 shows a characteristic temperature behavior near the igniting source as obtained from our numerical calculations. Before the beginning of the process, the mixture compact is everywhere at room temperature. At the start of the process there is an initial stage of inert heat conduction followed by the attainment of the ignition condition. At this condition, the temperature increase occurs quite rapidly until the adiabatic reaction temperature is reached and the reaction wave begins to propagate in a self-supporting manner much as a flame will propagate in a mixture of fuel + oxidant gases.

Once the reacting wave is propagating, it becomes independent of the nature and continued presence of the ignition source.

The ignition study calculations will consist of the following steps:

(1)- select a Da number,

(2)- impose a value for the constant temperature θ_{hot} of the igniting source,

(3)- determine if there is attaintment of the ignition condition given by Equation (8.1)

(4)- if ignition is attained, decrease the value of θ_{hot} until the time delays are suspected to have reached some asymptotic value.

It is important to note that when temperatures of the igniting source become too small, the "semi-infinite" numerical model has to be lengthen by adding more number of nodes. Thus, when the values for θ_{hot} are near the asymptotic minimum values, the computational runs become quite lengthy. This is even more dramatic when the values of Damkohler number are of small magnitude (that is, when the chemical reaction rates are small as compared to the heat conduction rate).

8.3 Results.

Figure 8.2 shows the results for the time to reach the ignition condition for the Da number range under investigation. From the figure one can see that the large Da numbers, as expected, need very short times to reach the condition of ignition. From the numerical runs it is observed that once the condition of ignition was achieved,

there was always propagation of the reacting wave. From Figure 8.2 it is also observed that with large Da numbers ignition occurs even at very low values of temperature of the igniting source. For values of Da number between 100 and 10, the θ_{hot} range above the minimum temperature threshold will produce a relatively fast attaintment of the ignition conditions as compared to the lower range of Da numbers. In Figure 8.2 a spline fitting routine is used so that the curve are shown without the typical sharp straight peaks that mark the numerical values obtained. For values of Da number below 0.1 no attaintment of ignition conditions was obtained, and the number of nodes to simulate the "semi-infinite" length body became too large as did the computational times. The computational times, with the given numerical parameters described in Chapter 5, became extremely high above values of τ of 40-60.

Figure 8.3 show exactly the same curves as Figure 8.2, but asymptotic lines have been added (to guide the eye) to determine the asymptotic minimum values of the temperature of the igniting source θ_{hot}. These asymptotic values are then plotted in Figure 8.4 in a log-Da vs. linear-θ_{hot} fashion; this is very convenient, showing the broad range of Da numbers that are covered. Here the two zones "ignition" and "no ignition" can be separated. To make this separation more clear, Figure 8.5 shows a continuous fitted critical curve.

It is an estimated curve, since only Figure 8.4 shows the values obtained from the asymptotic values found in Figure 8.3.

Thus, for a given value of Da number there exists a critical value of the igniting source above which ignition will always occur. The larger that θ_{hot} is above this critical temperature the easier the mixture compact will ignite. For temperatures lower than the critical value no ignition will occur no matter how long the igniting source is imposed.

Looking again at the plots of θ_{hot} versus τ, Figures 8.2 and 8.3, it is observed that the curves resemble an exponential behavior. The theory of spontaneous ignition delay (see Kanury [84]) predicts this type of exponential behavior. The major advantage of that theory is its ability to predict the following dependencies of the ignition delay: ignition delay is short if the mixture has, (1) a low volumetric heat capacity, (2) a high temperature dependence of the rate of reaction, (3) a high heat of combustion, and (4) a high initial reaction rate. In our solid-solid reaction, all of these conditions are met, with the high temperature dependence clearly substantiating the exponential dependency observed in Figures 8.2 and 8.3.

The actual ignition process of the solid-solid reactions is, in general, too complex to be described by the

simple gas-phase theory. This comment is further corroborated by an exponential fitting of each of the curves shown in Figures 8.2 and 8.3. The individual exponential fittings are plotted in Figures 8.6 to 8.9. Here it is observed that there are discrepancies between the calculated values and the exponential curve. These discrepancies are thought to be due to the physical intrusions of the different parameters that describe the particular kinetics of the solid-solid reactions (also, in the spontaneous ignition theory the reactions are assumed to follow a simple thermal Arrhenius dependency). It is important to mention that the sponta-neous ignition theory neglects the pre-ignition reactant consumption. However, in the solid-solid model there is a depletion of reactants during the ignition period. Nevertheless, the exponential dependency can be considered to be present in our solution of the time delay for ignition; this is better observed in Figure 8.10.

The exponential curve fittings plotted in Figures 8.6 to 8.9 are given by the following correlations:

$Da = 100, \quad \tau = 9.673 \times 10^{-4} \exp(-3.119\ \theta_{hot}), \quad r=0.96$

$Da = 10, \quad \tau = 3.386 \times 10^{-2} \exp(-2.369\ \theta_{hot}), \quad r=0.957$

$Da = 1, \quad \tau = 6.337 \times 10^{-1} \exp(-1.88\ \theta_{hot}), \quad r=0.954$

$Da = 0.1, \quad \tau = 1.729 \times 10^{-1} \exp(-1.136\ \theta_{hot}), \quad r=0.974$

where r is the correlation coefficient.

8.4 Closing Comments.

This chapter presented the results of the numerical study of the ignition process for the SHS solid-solid reaction of the mixture titanium-carbon. The numerical calculations of the onset of ignition showed that the time before the ignition condition is reached is much larger than the time difference between the attainment of the ignition condition and the reaching of the maximum adiabatic temperature. This is clearly the effect of the initial dominance of the conduction rate over the initial slow chemical reaction rate; once the ignition condition is reached, the contrary dominance takes over.

It was observed that reactions with a high Da number need a relatively low time to reach ignition conditions, while for low Da numbers the ignition times become increasingly high. This infers that samples with very high thermal conductivity will take a long time to reach ignition. For low values of the temperature of the igniting source the times to reach ignition become extremely high. From the numerical results it is possible to determine a limiting θ_{hot} vs. Da curve above which ignition will always occur and below which ignition does not occur.

The exponential effect predicted by the theory of spontaneous ignition is only partially observed in the ignition of the solid-solid reaction. However, in an overall

perspective the concepts of spontaneous ignition delay can be extended to the SHS process and probably many of the physical observations for these processes can be quantified on the basis of ignition theory to an extent yet to be determined (while the spontaneous ignition delay theory correlates well with some experimental results of gas-phase reactions, the experimental study of the ignition of SHS processes will be just as complex as the theory.).

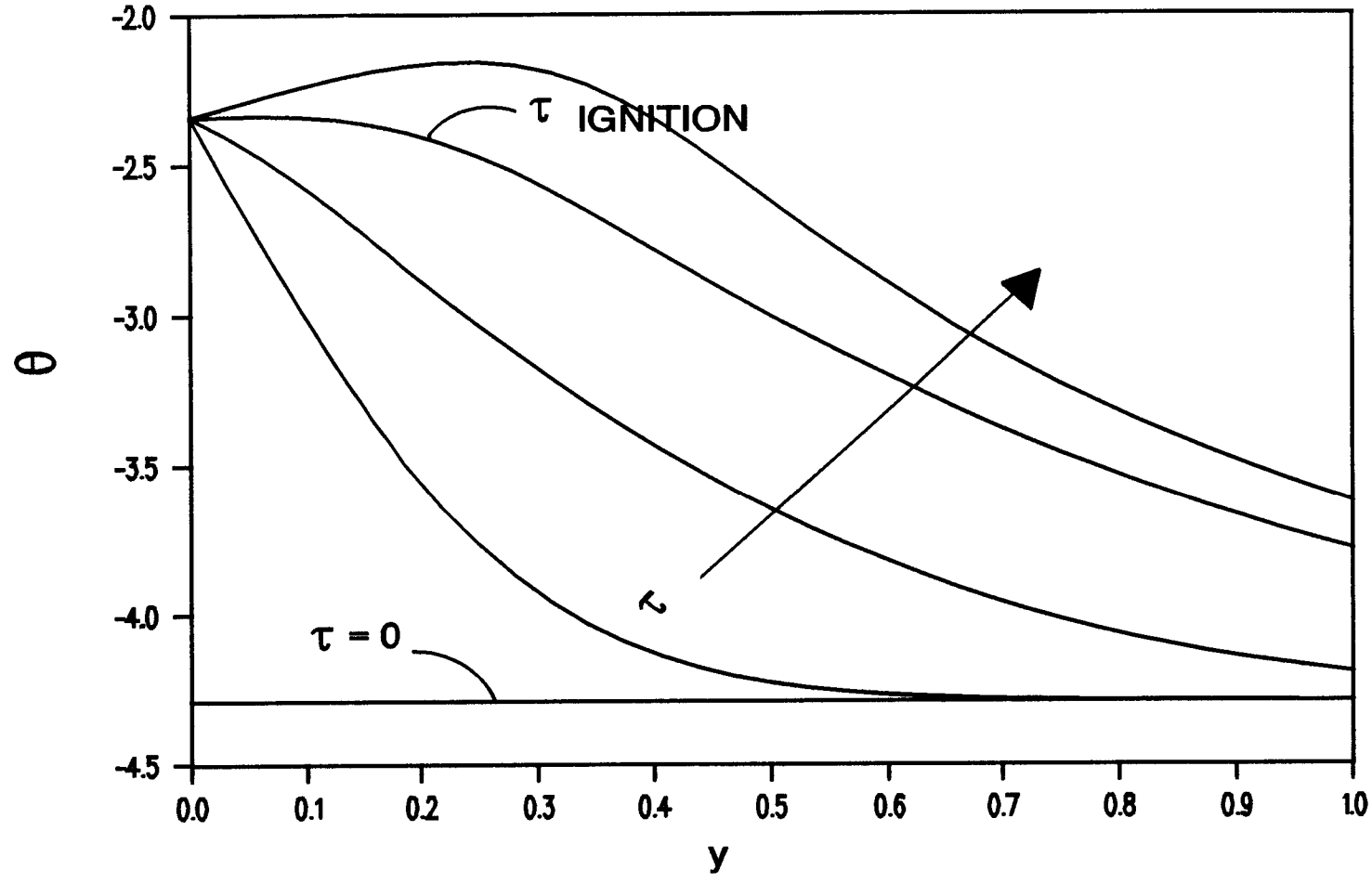

Figure 8.1 Attainment of the Ignition Condition.

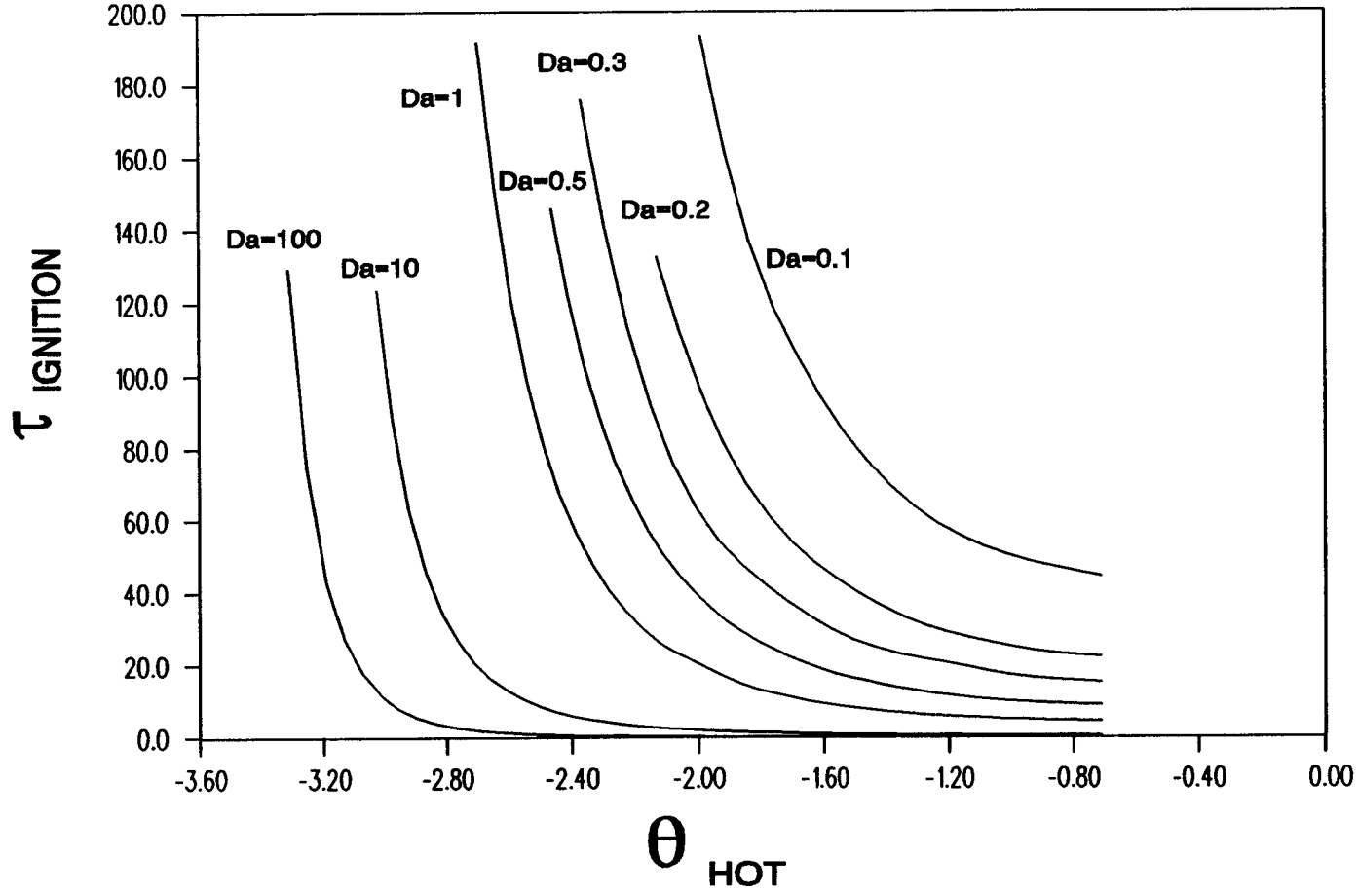

Figure 8.2 Time to Reach the Ignition Condition Versus Temperature of the Igniting Source.

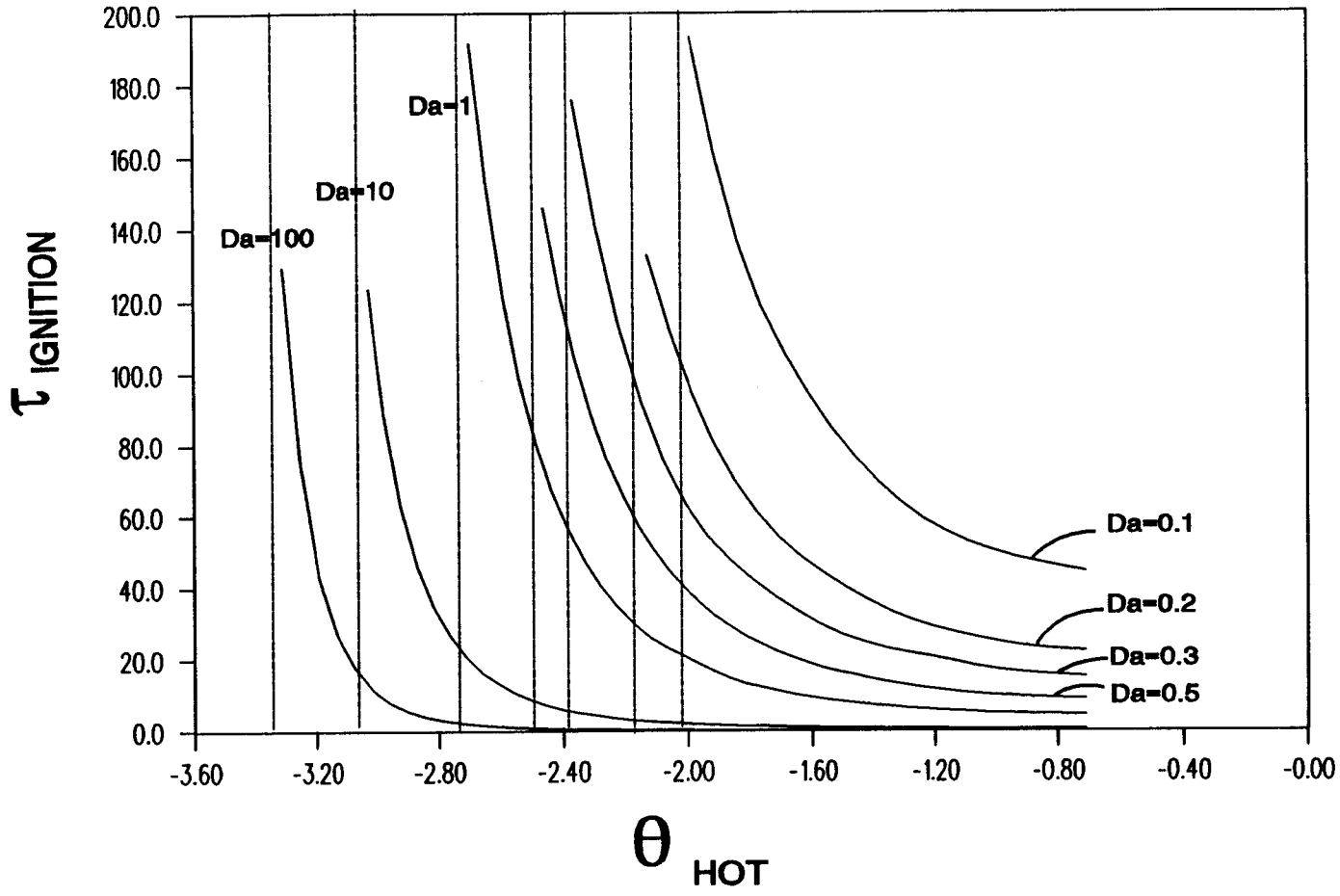

Figure 8.3 Estimated Asymptotic Values for the Minimum Temperature of the Igniting Source.

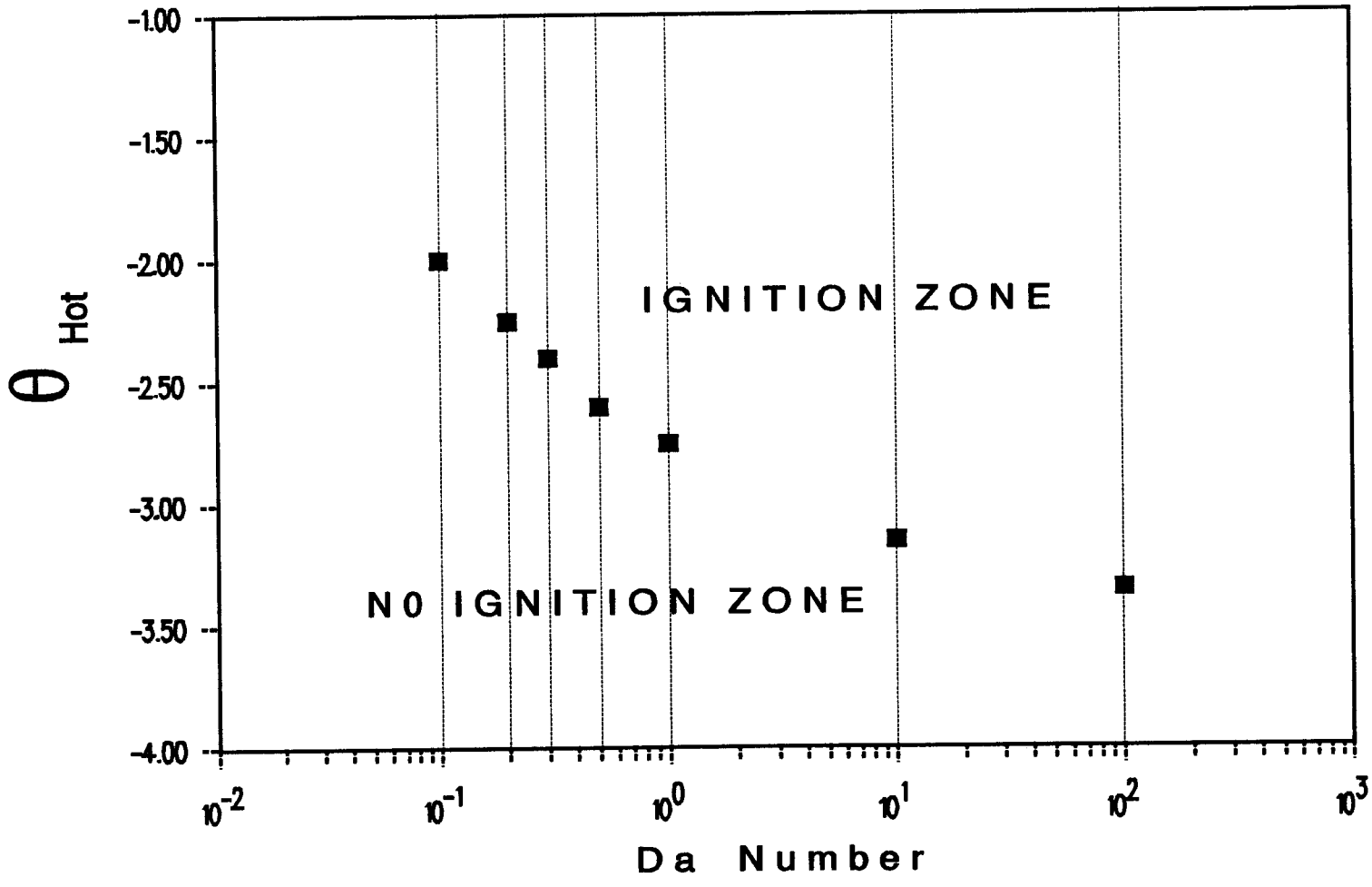

Figure 8.4 Determination of the Ignition and No-Ignition Zones.

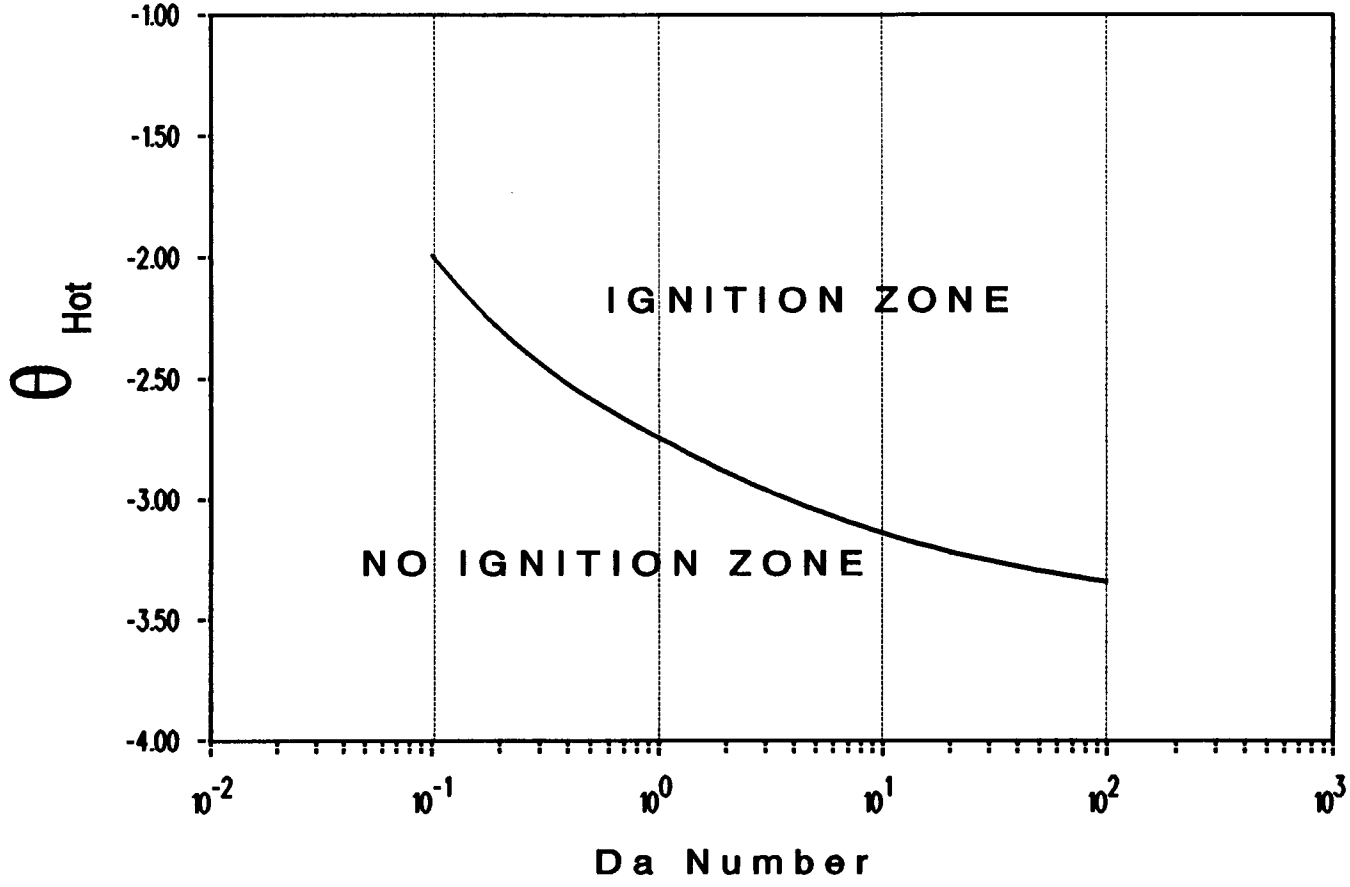

Figure 8.5 Estimated Critical Curve for Separation of the Ignition and No-Ignition Zones.

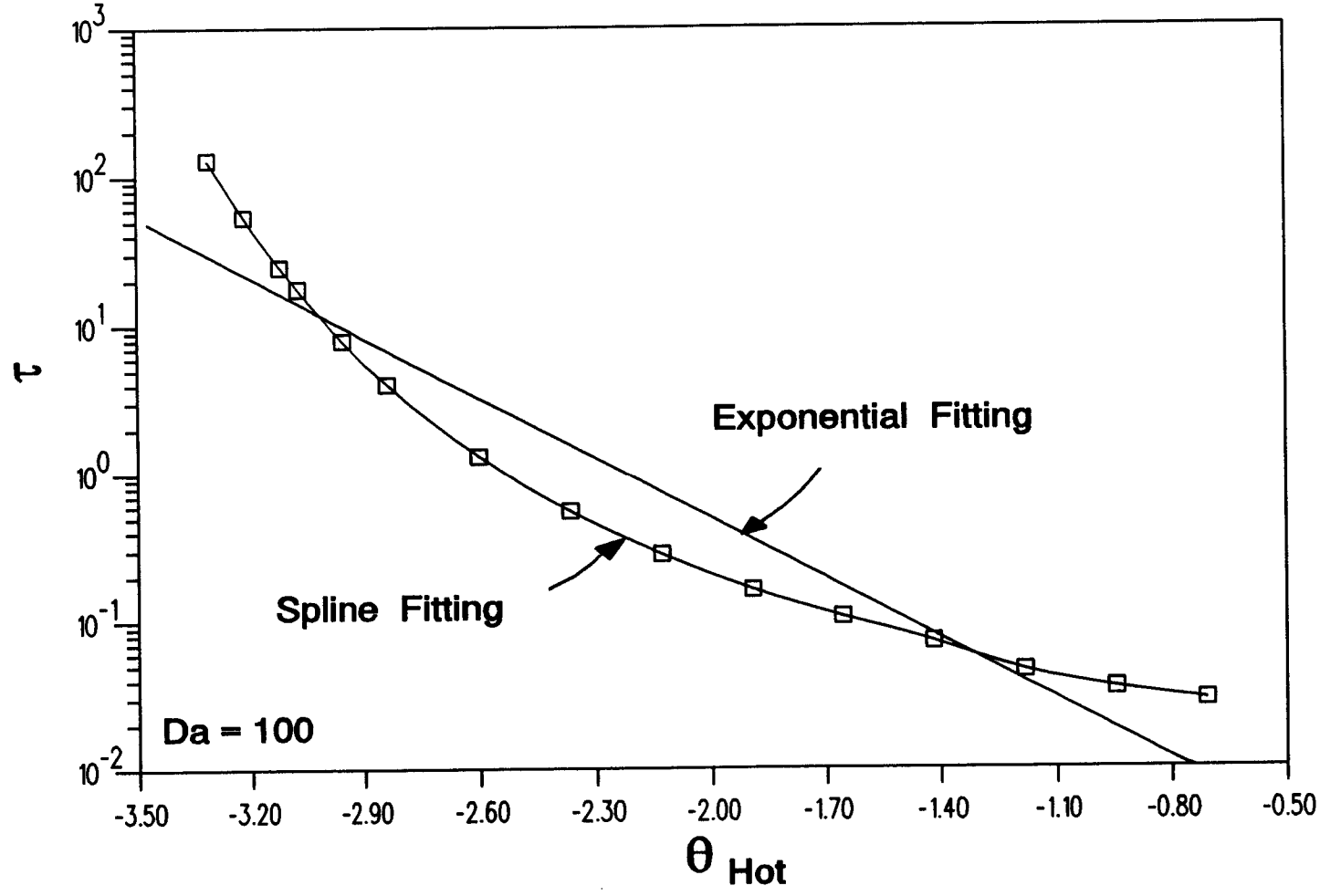

Figure 8.6 Exponential Effect for Da=100.

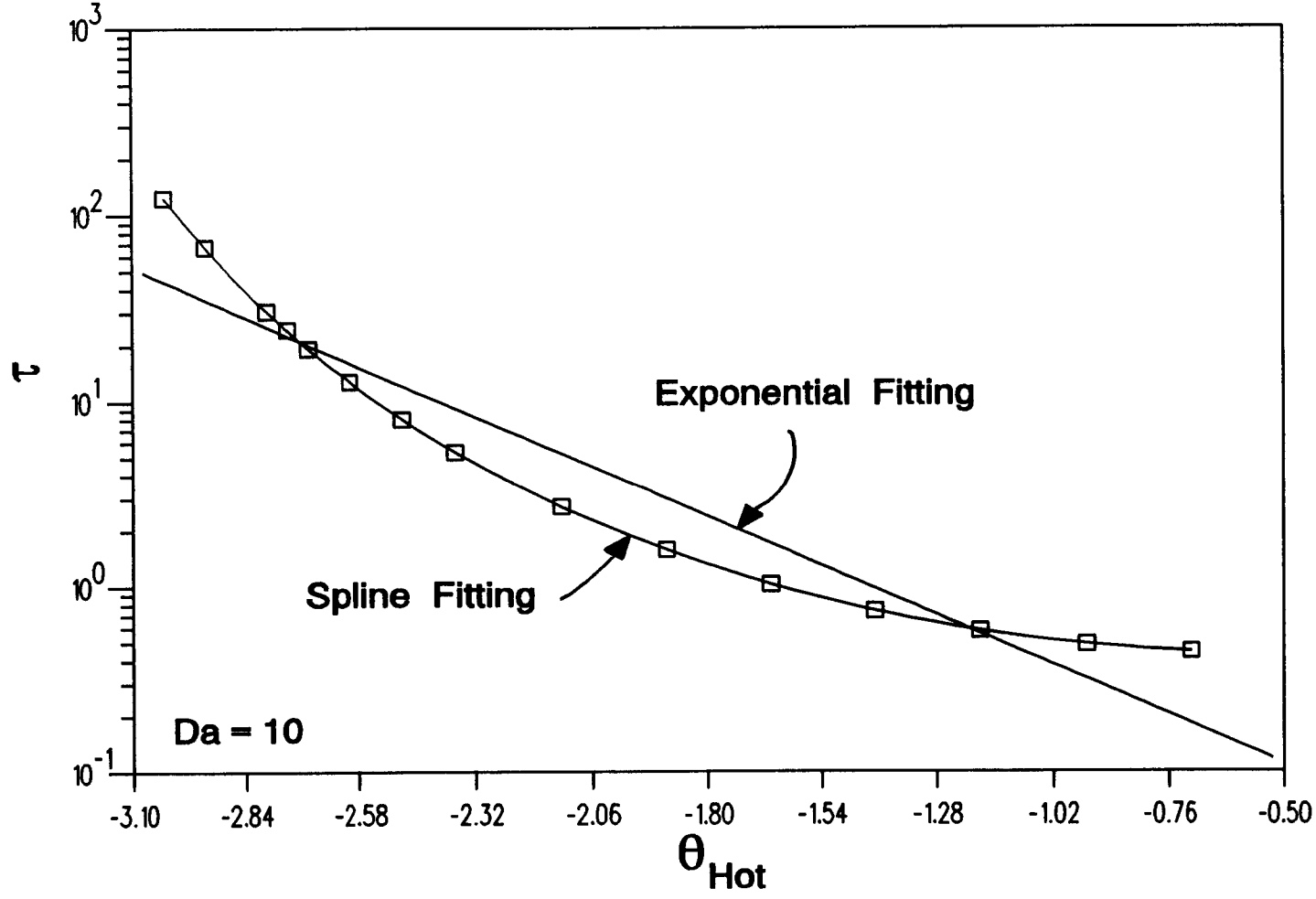

Figure 8.7 Exponential Effect for Da=10.

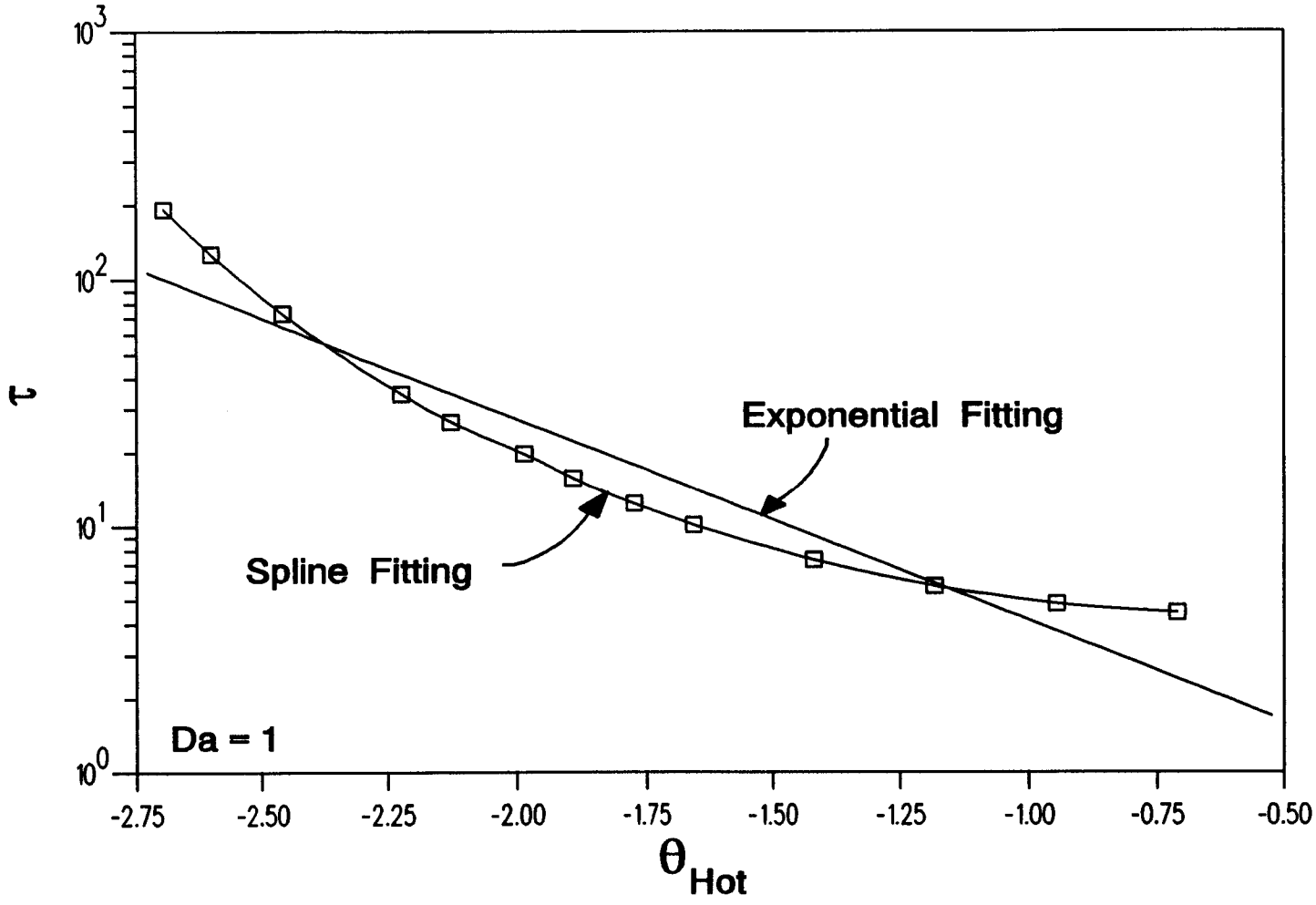

Figure 8.8 Exponential Effect for Da=1.

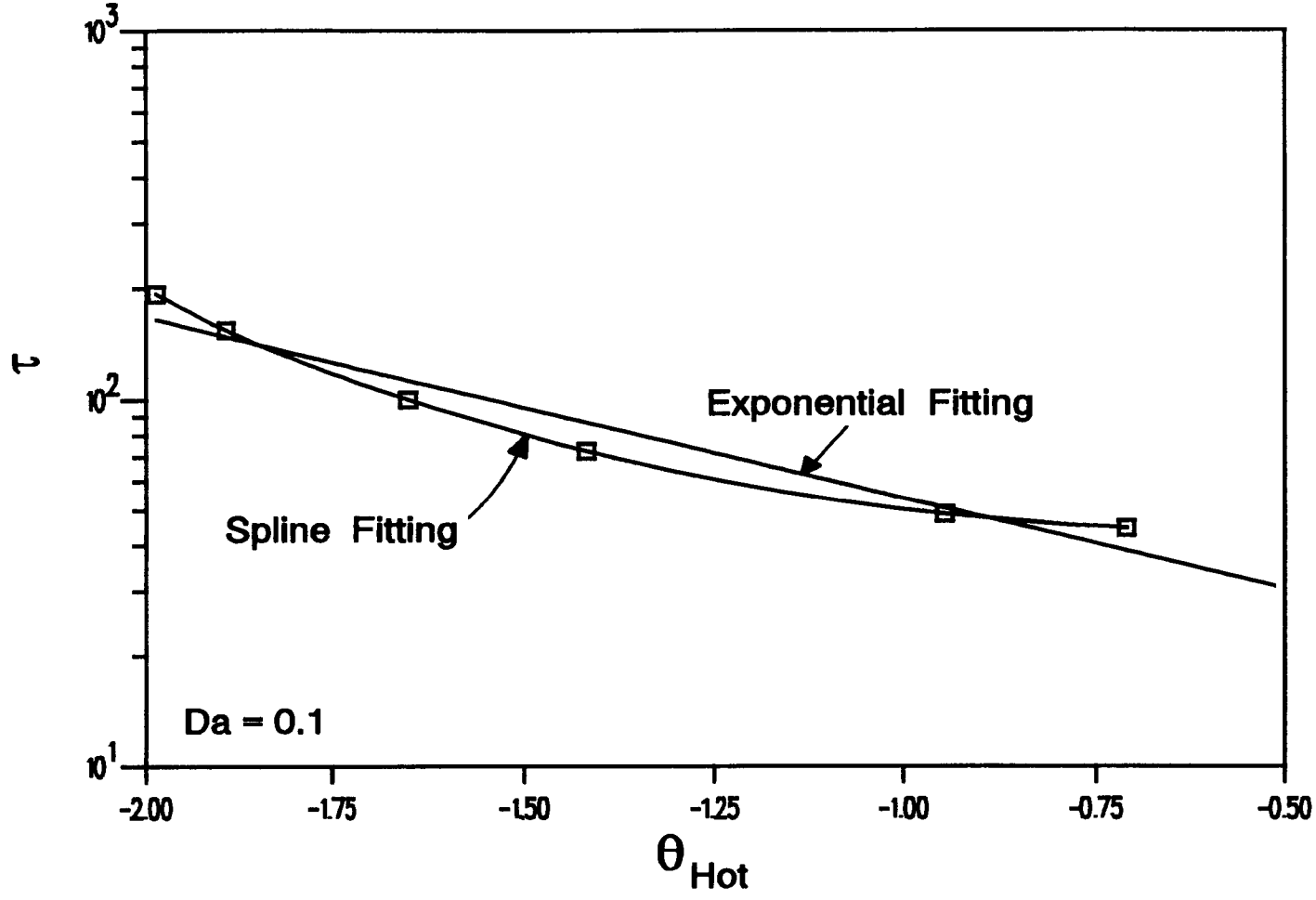

Figure 8.9 Exponential Effect for Da=0.1.

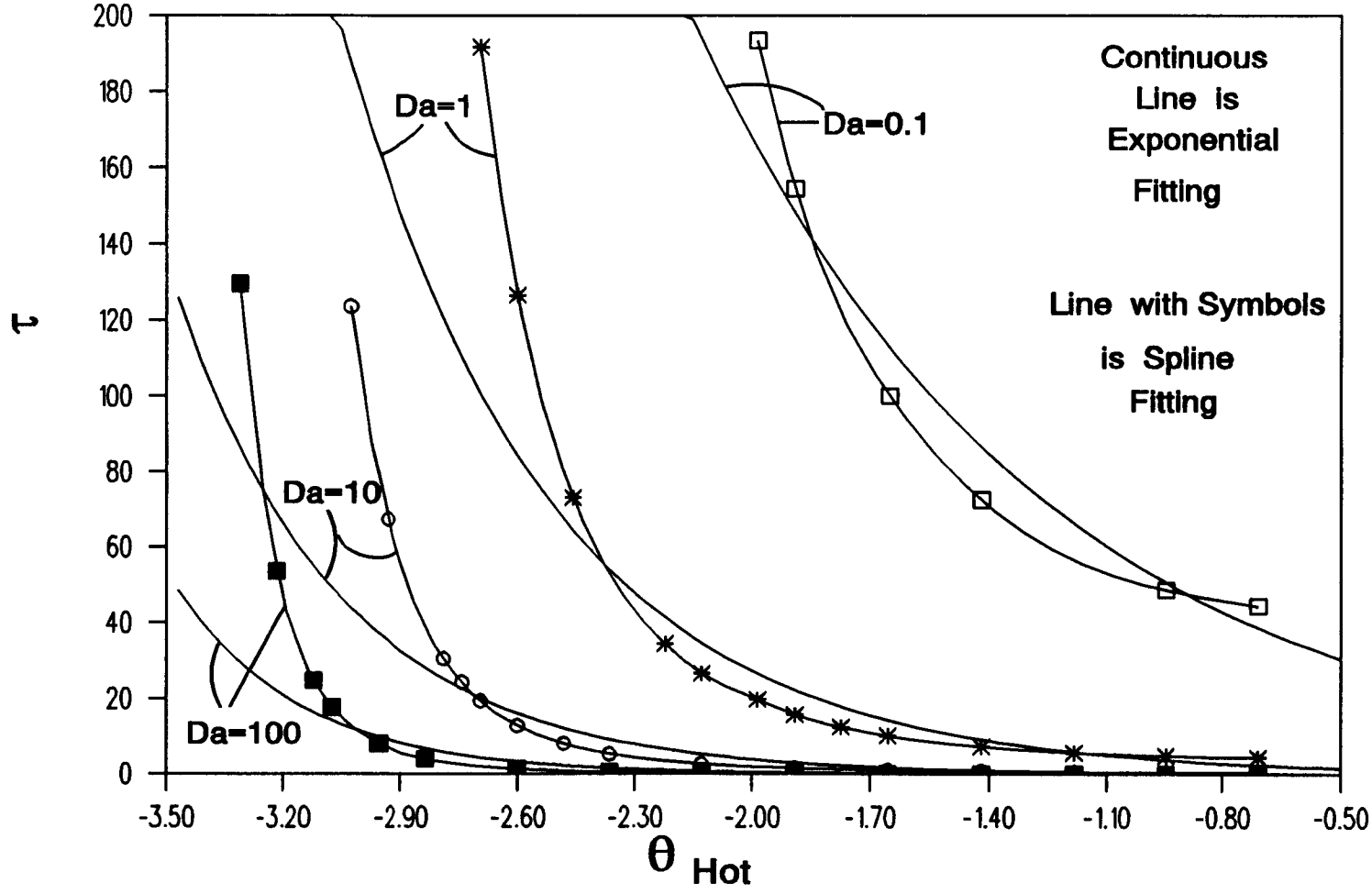

Figure 8.10 Exponential Effect for Various Da Numbers.

CHAPTER 9

NUMERICAL SIMULATION RESULTS FOR PROPAGATION

9.1 Introduction.

Having determined the ignition limits of a stoichiometric SHS titanium-carbon reaction, we will present in this chapter the results of our investigation of the propagation of the reacting wave through the semi-infinite cylindrical body of the mixture. This propagation study is divided in three parts. In the first part, the dimensionless propagation velocity U is determined for different mole ratios of the reactant mixture and for a mixture in stoichiometric proportions diluted with titanium carbide product. A redefined Da number is shown to reduce the calculated propagation speed curves into a single curve that is good for any value of the originally defined Damkohler number. In the second part a comparison is made between the calculated analytical values for dimensionless propagation speed U and the experimental propagation speed u results presented in Chapter 7. The third part presents the results obtained for the characterization of the preheated thickness. Again, by redefining the original Da number, the calculated curves for

this thickness (for all the range of Da numbers covered) are reduced to one single curve that is good for any value of the Damkohler number.

9.2 Numerical Simulation Results for the Dimensionless Propagation Speed U.

As mentioned in Chapter 5, in order to avoid any effect of the boundary conditions, the numerical determination of the propagation speed was done at sufficiently far distances from both ends (the "safe region", as defined in Chapter 5). For slow propagating fronts (small Da numbers) as many as 800 nodes were used to overcome any possible boundary effect.

A calculated typical temperature history for various dimensionless positions along the sample is shown in Figure 9.1. For this figure as well for the next two figures, no value of Da number is shown since these plots represent "typical" curves. Figure 9.1 shows the expected behavior as predicted from combustion knowledge; that is, after the initial sudden temperature rise from the starting room temperature condition (initial condition) the acceleration of the curve begins to diminish near the adiabatic temperature as a consequence of the depletion of reactants. From the numerical results, it is observed that this deceleration effect is more marked when the Da numbers are small.

After many numerical runs it was found that any temperature "peak" (that is no deceleration at all, or overshooting) is only a consequence of inadequate nodal spacing or time increments. Fast-reacting large Da number reactions are a good example when overshooting may be encountered. In order to avoid any sudden increase (peaks above the maximum adiabatic temperature) in these fast reactions, the $\Delta\tau$ or Δy used in the numerical solution must be reduced to the minimum size allowed by the computing equipment available. Figures 9.2 and 9.3 show typical calculated profiles for dimensionless temperature θ and dimensionless titanium concentration ϕ, respectively, for different dimensionless positions along the sample at different times τ. For this case the value of θ_{hot} was purposely taken to be small enough (but above the minimum threshold determined in the previous chapter) in order to see if there were any boundary effects on the temperature profile for the chosen times.

Figure 9.4 shows the numerical results obtained for stoichiometric (a=1) and lean-titanium cases (a<1). The mixtures contain only titanium plus carbon; no product dilution is considered. As expected, stoichiometric cases have faster propagation of the reacting front than non-stoichiometric cases. This figure also shows that large values of the Da number will yield faster propagation

speeds. This is due to the fact that the speed of propagation is directly related to how fast the heat is conducted throughout the sample (the larger the thermal conductivity the larger the speed of propagation). Similar numerical results for the rich titanium case are shown in Figure 9.5. Again, the more the mixture departs from stoichiometry , the smaller the propagation speed. In both Figures 9.4 and 9.5 quenching seem to be approached at the lower end of the Da number range.

The results previously shown in Figures 9.4 and 9.5 are combined in Figure 9.6 to present the variation of dimensionless propagation speed for all the range of mole ratios covered in this study. In this case, the parameter for each curve is the Da number. This figure clearly shows a variation in the order of magnitude by which the propagation speed changes as the Da number changes. To show an even better perspective of this order of magnitude, Figure 9.7 is presented in a semi-log plot. For all Da numbers a monotonical decrease in the magnitude of the dimensionless propagation speed occurs at both the low and upper values of the mole ratio a. Perhaps near these values the reaction fails to propagate, or maybe it will not even ignite. Further investigation is needed to verify this phenomenon. From the ignition study of Chapter 8, it was found that for Da numbers below 0.1 ignition was not possible. This result is

now easier to understand after viewing Figures 9.6 and 9.7; it is observed that for Da=0.1 the curve for propagation speed is very near to the zero value.

The numerical results for the cases where the initial stoichiometric mixture is diluted with product TiC are presented in Figures 9.8, 9.9 and 9.10. For these cases the mixture is considered stoichiometric (a=1), and only b varies. Again, these results confirm the expected trend that any inert in the reacting mixture will produce a reduction in the attained propagation speed as compared to a stoichiometric mixture with no inerts. Large Da numbers produce faster propagation speeds. This can be seen clearly in Figure 9.9. For values of Da number below 0.1, the trend is equivalent to the trend found for undiluted nonstoichiometric cases; as before, when the Da number is below 0.1 there is probably no ignition of the reactant mixture. A sharper resolution of the results of Figure 9.9 are presented in a semi-log plot in Figure 9.10.

The propagation results have been presented showing the propagation speed dependency on the Da number. A major outcome from this study is found by reviewing the predictions of the theory of flame propagation (see Kanury [84]). In flame propagation theory, the fundamental flame speed is defined as the speed at which the flame front travels in a direction normal to itself and with respect to the fresh

reactant mixture. The fundamental flame speed is a thermochemical property of the mixture. The thickness of the adiabatic flame front, being inversely proportional to the flame speed, becomes also an intrinsic thermochemical property of the mixture. If the flame is not adiabatic, then the larger the heat loss, the thicker, cooler and slower the flame front. A high thermal conductivity of the reactant mixture and a high heat of combustion per unit mass of the mixture result in a thinner and faster propagating flame. These effects are better understood with the following equation:

$$u = \frac{1}{\rho_s C_{ps}} \sqrt{\frac{1}{\Lambda} \frac{K \dot{S}'''}{(T_f - T_s)}} \qquad (9.1)$$

where ρ_s, C_{ps} and T_s are values of density, specific heat and temperature evaluated at the supply reactants state; T_f is the flame temperature and Λ is the flame speed eigenvalue. Arranging this equation we obtain

$$u^2 = \frac{1}{\Lambda} \frac{\alpha_s}{\rho_s C_{ps}} \frac{\dot{S}'''}{(T_f - T_s)} \qquad (9.2)$$

Multiplying both sides by L_r^2/α_s^2 and rearranging, we obtain:

$$\frac{L_r^2\, u^2}{\alpha_s^2} = \frac{1}{\Lambda}\, \frac{L_r^2}{\rho_s\, C_{ps}\, \alpha_s}\, \frac{\dot{S}'''}{(T_f - T_s)} \qquad (9.3)$$

Using the dimensionless definitions introduced in Chapter 4, the term located on the left hand side can be easily identified as the square of the dimensionless propagation speed U. Further rearrangement gives:

$$U^2 = \frac{1}{\Lambda}\, \frac{L_r\, \dot{S}'''}{K\, (T_f - T_s)/L_r} \qquad (9.4)$$

The ratio on the right hand side of this equation gives a typical ratio of the chemical reaction rate to the conduction rate; this is the very definition of the Damkohler number. Accordingly,

$$U^2 = \frac{1}{\Lambda}\, Da \qquad (9.5)$$

If the Da number is redefined in such a way that the effects of the reactants composition (i.e. a and b) are separated from it, we obtain a new Da', as given by:

$$Da' = \frac{Da}{\frac{m_C}{m_{mix}}\, C_{Tio}} \qquad (9.6)$$

where the factors in the denominator are the factors of the Da number that introduce the dependency on a and b. Combining Equations (9.5) and (9.6), we obtain

$$\frac{U}{\sqrt{(Da')}} = f(a,b) \quad \text{only} \tag{9.7}$$

i.e. $U/Da'^{1/2}$ is a function of a and b only. This functionality enables us to consolidate all the results presented so far in one single plot which is valid for any Da number. Figures 9.11 and 9.12 present the results of dividing all of the propagation speeds calculated by the square root of their corresponding Da'. Both general cases are considered, one for the variation with mole ratio a with no product dilution (a varies, b=0) and one for stoichiometric mixture with product dilution (a=1, b varies). The small discrepancies shown in the curves are of such numerically small values that these discrepancies can be considered neglectable. This new functionality can be considered very relevant, since any possible case (and Da number) can be determined simply from this curve. The kinetic model of Kanury apparently leads to the sought unified model for simulating the SHS process (see the Closing Comments section in Chapter 2).

9.3 Comparison of the Numerically Evaluated Propagation Speed U with Experimental Results.

From the dimensionless definitions introduced in Chapter 4, it is easy to show that the relation between the dimensionless propagation speed U and the measured propagation speed u is:

$$U = \frac{L_r}{\alpha_r} u \qquad (9.8)$$

where α_r is the reference thermal diffusivity and L_r is a reference length. From the numerical evaluation of parameters (Chapter 5), the value for the reference thermal diffusivity was evaluated from the values of ρ_r, Cp_r and K_r of the mixture. However a value for L_r has not been really defined. It is thought that the best choice would be a non trivial reference length related to the process under study, such as is the preheated length. Due to the obvious physical limitations to measure such a length experimentally, we made use of the theory of flame propagation that shows that

$$\delta_f \approx \frac{\alpha}{u} \qquad (9.9)$$

in the evaluation of parameters in Chapter 5. By making an analogy of the flame thickness δ_f to the preheated length L_r in the SHS process we may be able to determine an

approximate value of the ratio L_r/α_r. The propagation velocity u chosen for the evaluation is that obtained experimentally for stoichiometric conditions with no product dilution (a=1, b=0); thus,

$$\frac{L_r}{\alpha_r} \approx \frac{1}{u} = \frac{1}{0.94} \qquad (9.10)$$

Based on this ratio and Equation (9.8), the numerical results for propagation velocity U are transformed to propagation velocity u (in cm/sec). Figures 9.13 and 9.14 show the results of this comparison, the first for the cases of variation of the mole ratio a and the second for the cases that there is titanium carbide product diluted with the stoichiometric titanium plus carbon mixture. The numerical data is in good agreement with the experimentally measured data. The assumptions made in developing the model could account for the slight differences observed in the comparison.

9.4 Numerical Determination of the Preheated Length.

While the measurement of the preheated length experimentally is a very difficult task, it is possible to obtain an estimate of this distance by a numerical analysis. The preheated length is not always a constant value but it is different from one given condition to another. To help

visualize this fact, Figure 9.15 shows how the dimensionless temperature profile changes as the Da number changes. Fast-propagating high Da number cases show a very sharp profile decrease near the reaction zone, while slow-propagating low Da number cases show a more gradual decrease of temperature.

The estimation of the value of the preheated length can become ambiguous if an arbitrary criteria is selected. One could choose, for example, the distance from where the temperature starts to decrease to where the temperature reaches the initial room temperature condition. This selection will give very large preheated lengths. Another selection could be the distance from where the temperature starts to decrease to where the temperature is within a certain percent of the initial temperature condition. This selection for evaluating the preheated length would be really ambiguous. To avoid the selection of such criteria, we again make use of the existing combustion knowledge. The theory of flame propagation (see Kanury [84]) defines the flame front thickness δ as the ratio of the maximum temperature difference $(T_f - T_s)$ to the maximum temperature gradient dT/dx which occurs at the point of inflexion of the profile, that is:

$$\delta = \frac{T_f - T_s}{\left.\frac{dT}{dx}\right|_{max}} \qquad (9.11)$$

where T_f is the flame temperature and T_s is the temperature of the supply reactants. Borrowing this concept from the theory of flame propagation and taking the likeness of this flame thickness to the preheated thermal length of our problem, we can adjust Equation (9.11) in terms of the dimensionless variables used in this study, to obtain:

$$\Delta y_{ph} = \frac{\theta_{ad} - \theta_o}{\left.\frac{d\theta}{dy}\right|_{max}} \qquad (9.12)$$

where Δy_{ph} represents the preheated length, and as before, θ_{ad} is the adiabatic temperature and θ_o is the initial temperature. Figure 9.16 presents this equation in a graphic form. This sketch shows how the dimensionless preheated length can be measured graphically. All the calculated numerical profiles of temperature were plotted and, by using this graphical technique, the preheated length was measured for each case. To make better use of the determination of this preheated length, we recall from the dimensionless definition of time that $L_r^2 \tau = \alpha t$. Thus, we are making a resemblance of the analogy between the measured preheated length and the calculated preheated length and by plotting the square of the calculated preheated length, we will be showing a proportionality to the reaction times. The larger the value of L_r the slower the propagation; thus when $L_r \to \infty$

the propagation speed goes to zero (quenching occurs). Figures 9.17 to 9.21 show the results of determining graphically the length of the preheated length (and its square) as a function of mole ratio for different Da numbers. These figures show that near the limits of the mole ratio covered in this study, the values of the square of the preheated length are close to reaching asymptotic values. This may be an indication that these values of mole ratio are close to the quenching conditions. Figure 9.22 shows the combination of the results of Figures 9.17 and 9.17 in a semi-log plot to observe the different orders of magnitude that are covered by the square of the preheated length. As expected, a fast moving reaction front, which is due to a high Da number reaction, has a thin preheated length, while the slow pace, low Da numbers reactions, have large preheated lengths. The smallest preheated length, of course, results for the stoichiometric case. Figure 9.23 to 9.25 show the results of the graphical determination of the preheated length (and its square) as a function of the product dilution for different Da numbers. As in Figure 9.22, Figure 9.26 combines these results into a single graph to show the orders of magnitude covered by the preheated length. An asymptotic behavior near the edge of the range studied for the moles of product dilution b is not observed, as it was for the case of variation of the mole ratio a.

The geometrically calculated results for preheated length have been presented in these figures as dependent on the Da number. As previously done for the results of propagation speed, it is desirable to obtain a single plot that will provide the preheated length without the Da number as a parameter. This way all the curves presented in Figures 9.17 to 9.21 for various mole ratios will collapse into a single representative curve for all of those cases. The same result will occur to the curves of Figure 9.23 to 9.25 for the cases of dilution with product. This is accomplished by again making use of the theory of flame propagation that estimates the flame thickness as the ratio of α/u. Using this concept and the relationship between the dimensionless velocity of propagation U and the measured speed u, we obtain:

$$\delta \approx \frac{\alpha}{u} \quad \frac{\frac{L_r}{\alpha} u}{U} \tag{9.13}$$

This reduces to:

$$\frac{\delta}{L_r} = \Delta Y_{ph} \approx \frac{1}{U} \tag{9.14}$$

Here, Δy_{ph} is the preheated length. If we multiply both sides by $Da'^{1/2}$ {Da' was defined in Equation (9.6)}, we obtain:

$$\Delta y_{ph} \sqrt{Da'} = \frac{\sqrt{Da'}}{U} \qquad (9.15)$$

where the right hand side was previously determined to be only a function of a and b. Thus,

$$\Delta y_{ph} \sqrt{Da'} = f(a,b) \quad \text{only} \qquad (9.16)$$

Figure 9.27 shows the results of multiplying by all the results presented in Figures 9.17 to 9.21 by $Da'^{1/2}$. Clearly the differences obtained are nothing but a signal of graphical errors made while geometrically determining the thickness of the preheated length. To present the results of the reduction into a single curve, the curves in Figure 9.27 are averaged and presented in Figure 9.28.

Figure 9.29 presents the curves that result from multiplying the dimensionless preheated length by $Da'^{1/2}$ as a function of the dilution with product. Again, differences are observed due to errors incurred while geometrically determining the preheat length Δy_{ph}. The average of these curves is presented in a single curve in Figure 9.30.

9.5 Concluding Remarks.

In this chapter the results of the numerical study of the propagation speed for the SHS solid-solid reaction of titanium-carbon have been presented. The calculations verify

that large Da numbers reactions are equivalent to fast propagations. As expected, nonstoichiometric cases show smaller propagation speeds as compared to the stoichiometric case. The farther the mole ratio is from stoichiometric conditions, the smaller the propagation speed. For values of Da number less than 0.1, no propagation could be determined. Low values of Da number are synonym of long computational times and large number of nodes to simulate a semi-infinite length.

The theory of flame propagation proves very valuable in reducing the propagation speed results to a single curve that is useful for any value of the Da number. This result can be considered very relevant and perhaps substantiates that the Kanury kinetic model could be the unified model sought for simulating the SHS process. Again, by invoking combustion knowledge results, the numerical data obtained for dimensionless propagation speed has been compared to the experimental values. The comparison can be considered to be in very good agreement if it is observed that some assumptions of the model (like the constant properties assumption) might produce a considerable effect on the calculated values.The combustion concept of flame thickness also proves very useful to determine a parametric curve for the dimensionless preheated length that does not depend on the Da number, but only on the stoichiometry of the problem.

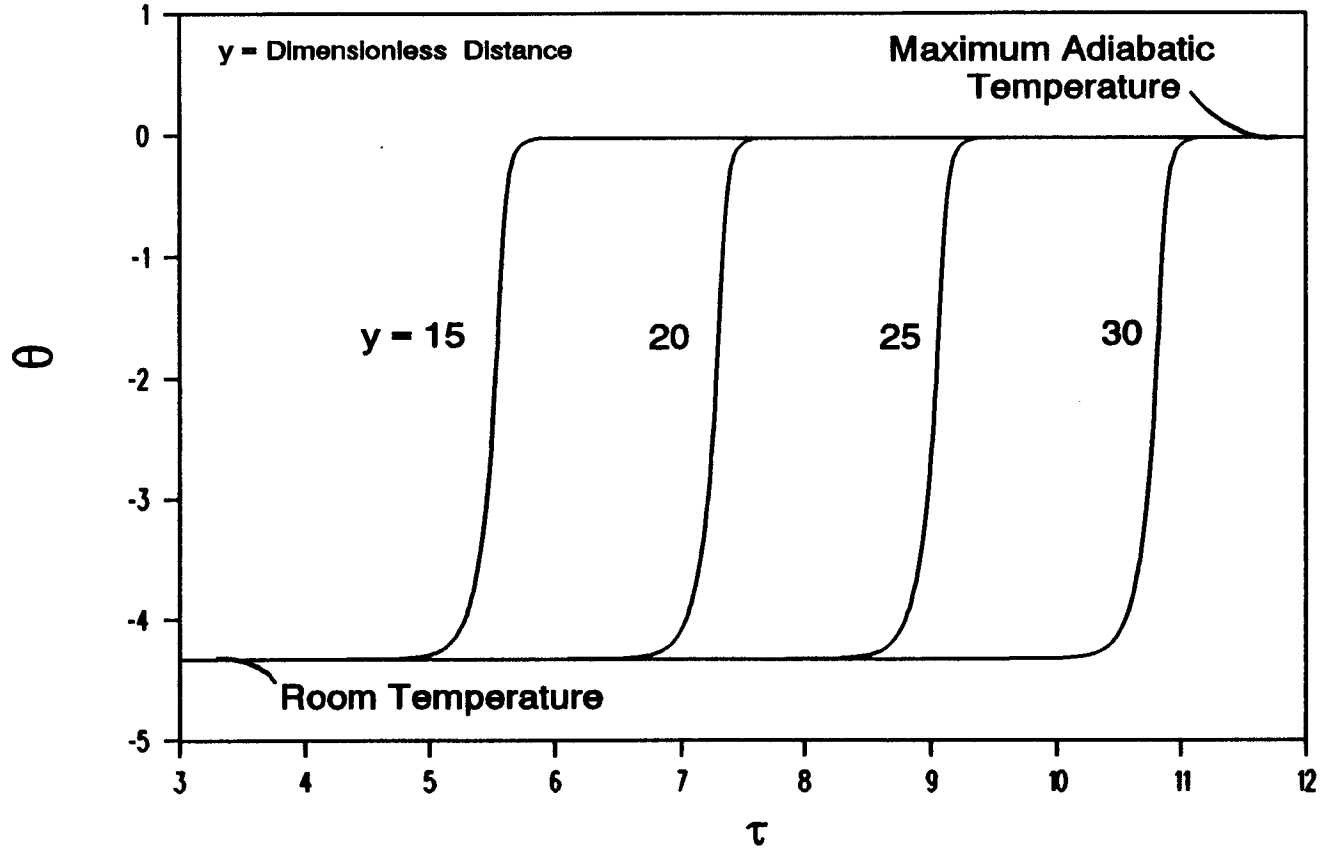

Figure 9.1 Typical Temperature History at Different Dimensionless Positions Along the Sample.

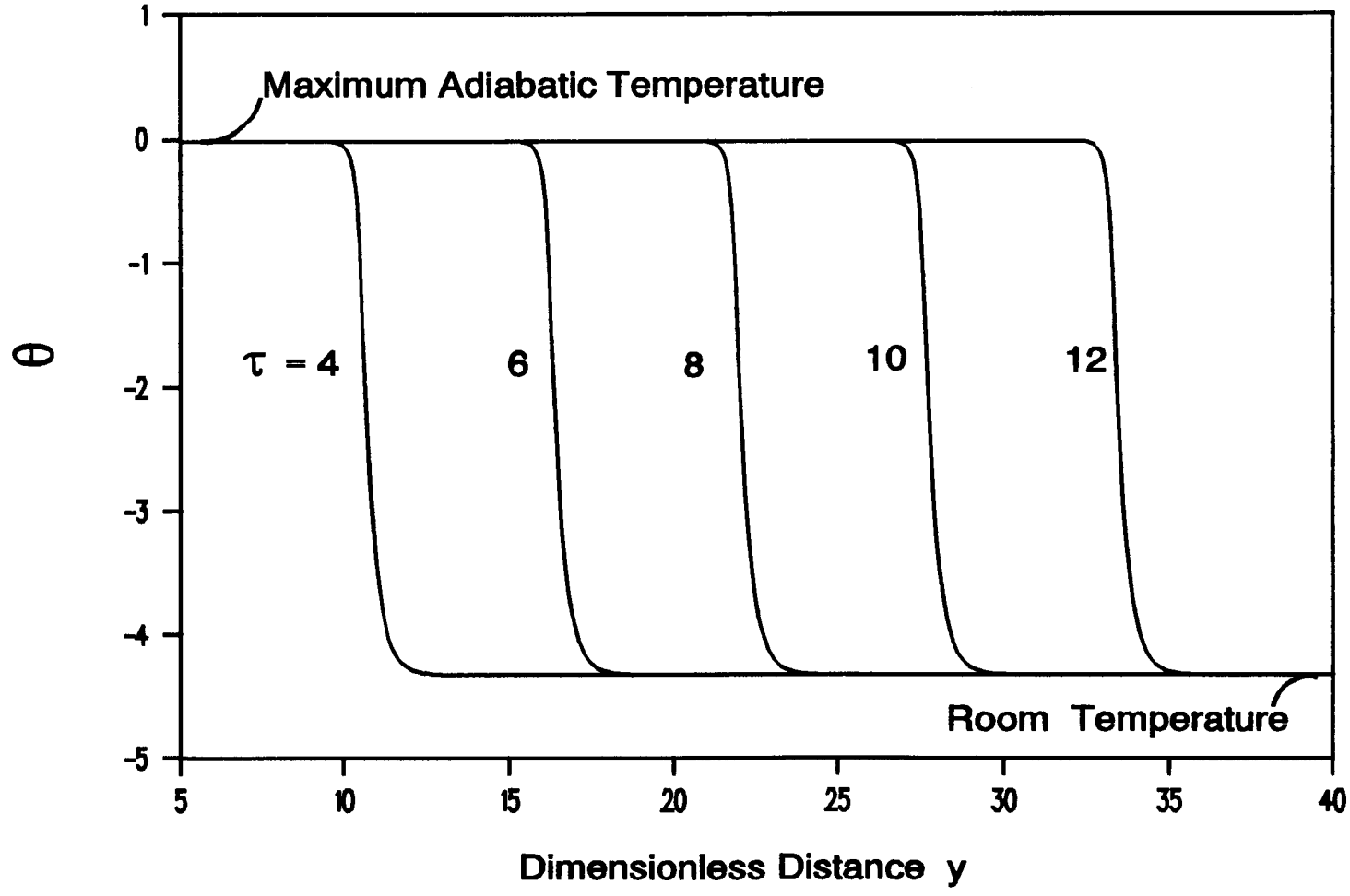

Figure 9.2 Typical Temperature Profile at Different Times.

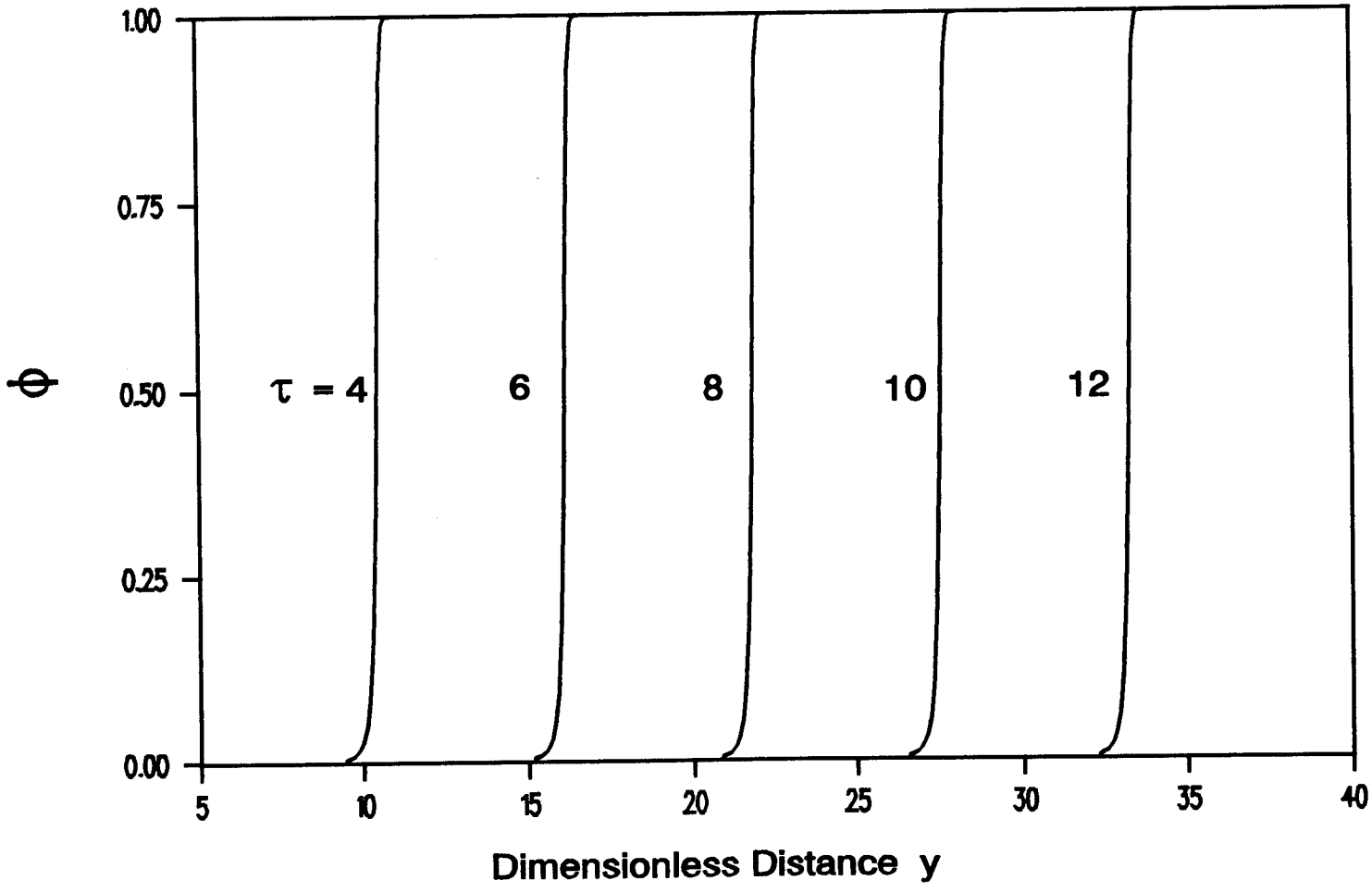

Figure 9.3 Typical Profile of Dimensionless Concentration Depletion Along the Sample at Different Times.

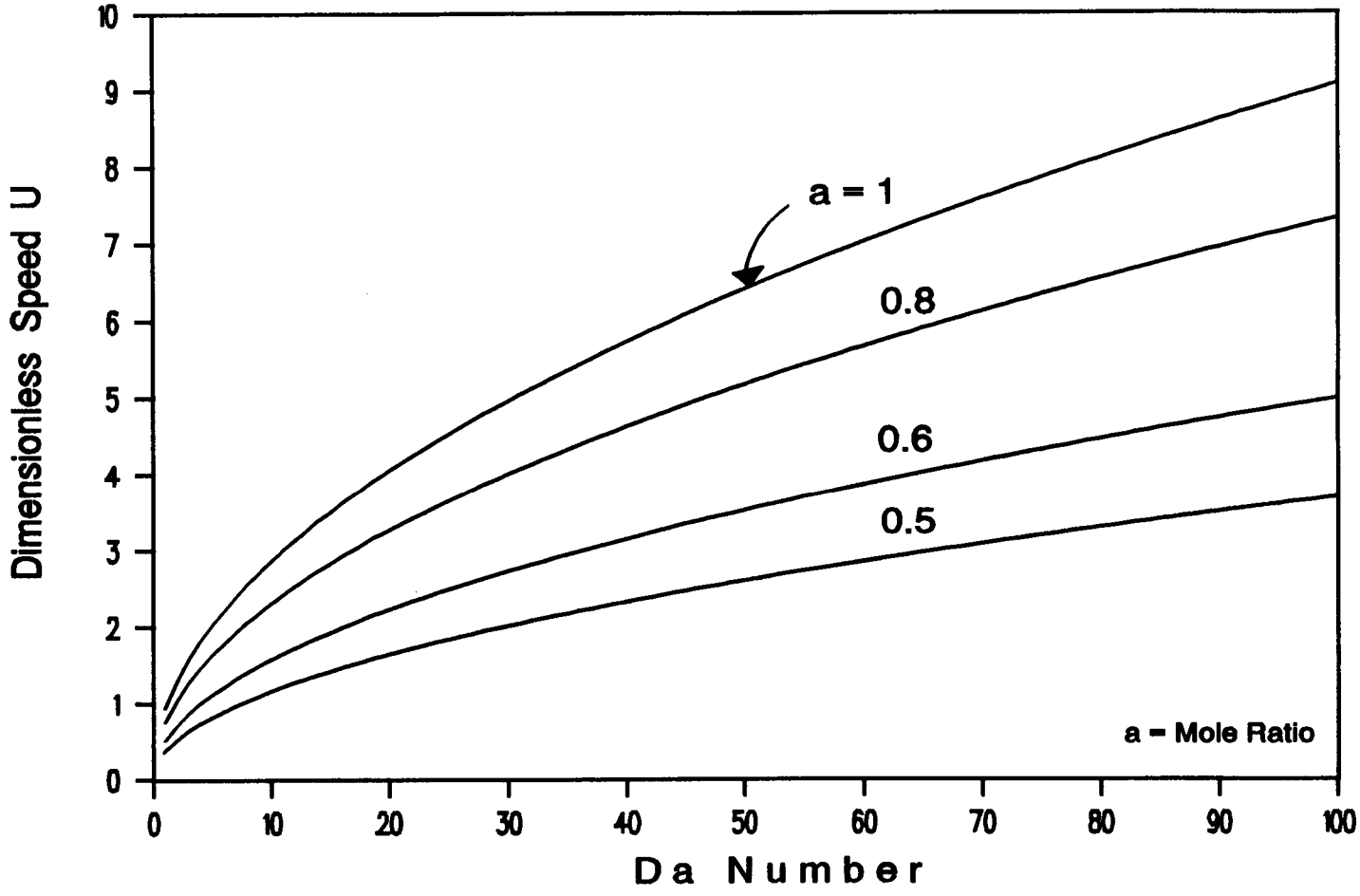

Figure 9.4 Calculated Propagation Speeds for Stoichiometric and Lean-Titanium Cases ($a \leq 1$).

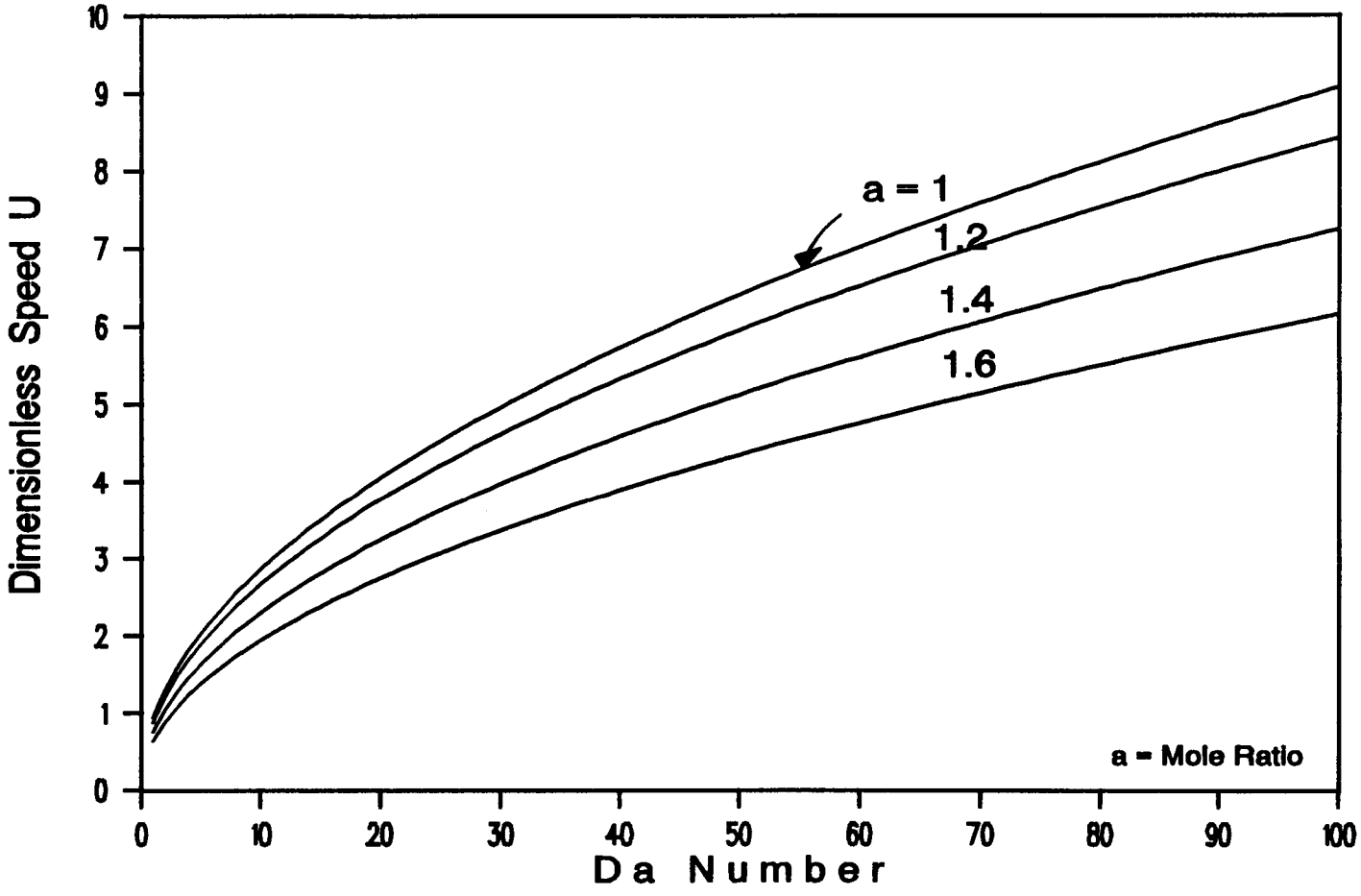

Figure 9.5 Calculated Propagation Speeds for Stoichiometric and Rich-Titanium Cases (a≥1).

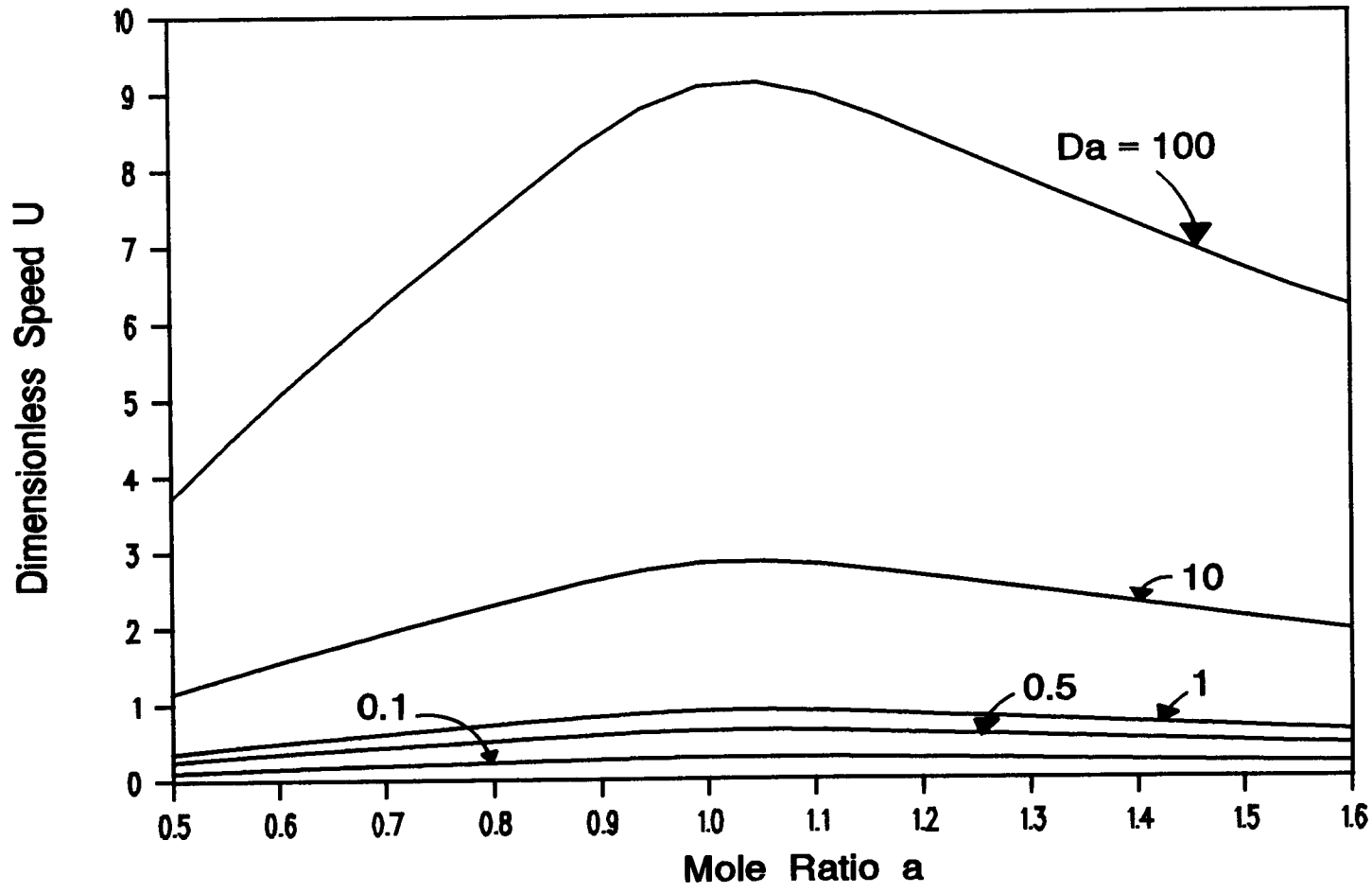

Figure 9.6 Propagation Speed U as a Function of the Mole Ratio for Various Da Numbers.

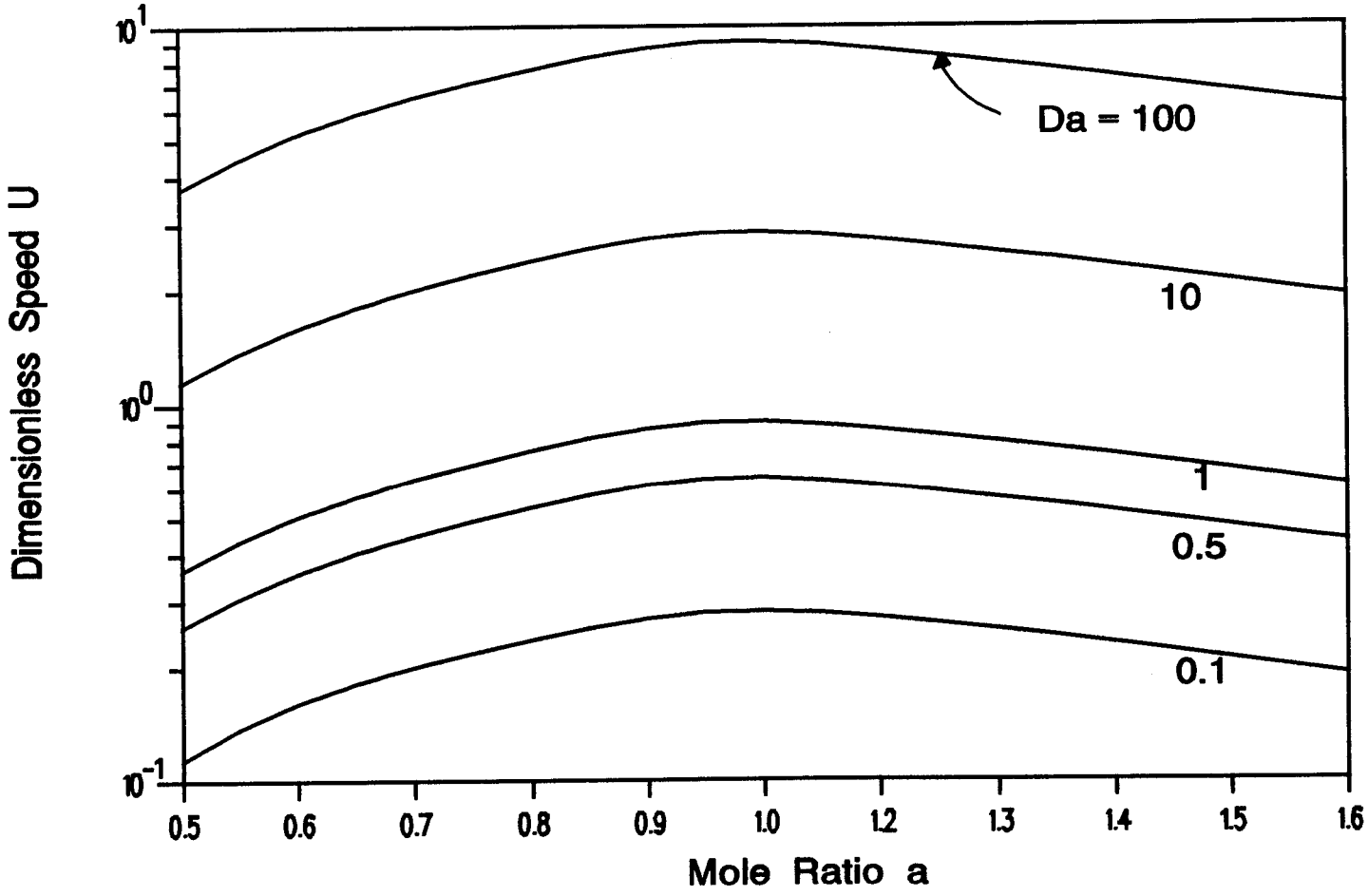

Figure 9.7 Logarithmic Propagation Speed U as a Function of the Mole Ratio for Various Da Numbers.

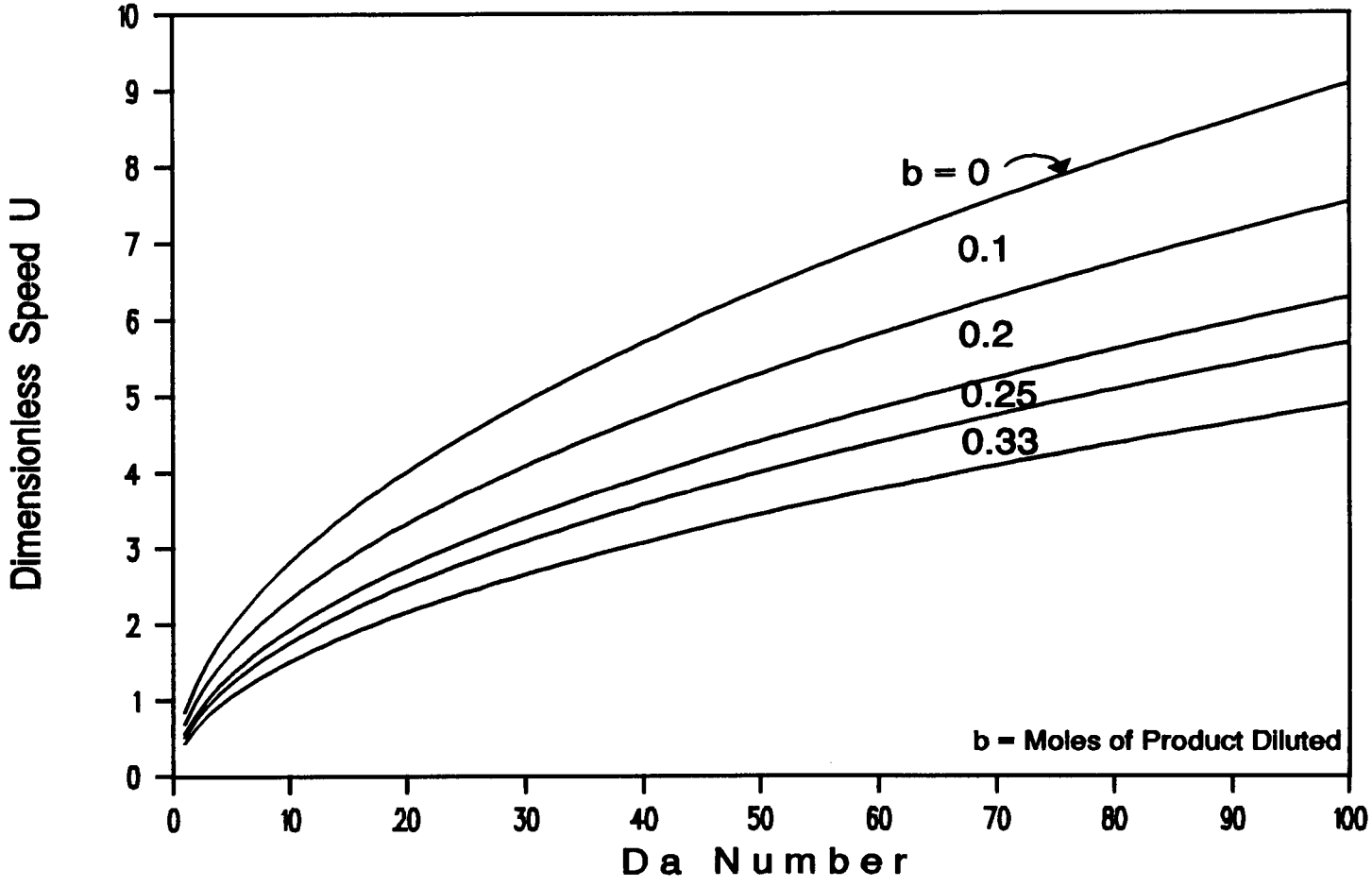

Figure 9.8 Calculated Propagation Speed U as Function of the Da Number for Different Degrees of Dilution with Product.

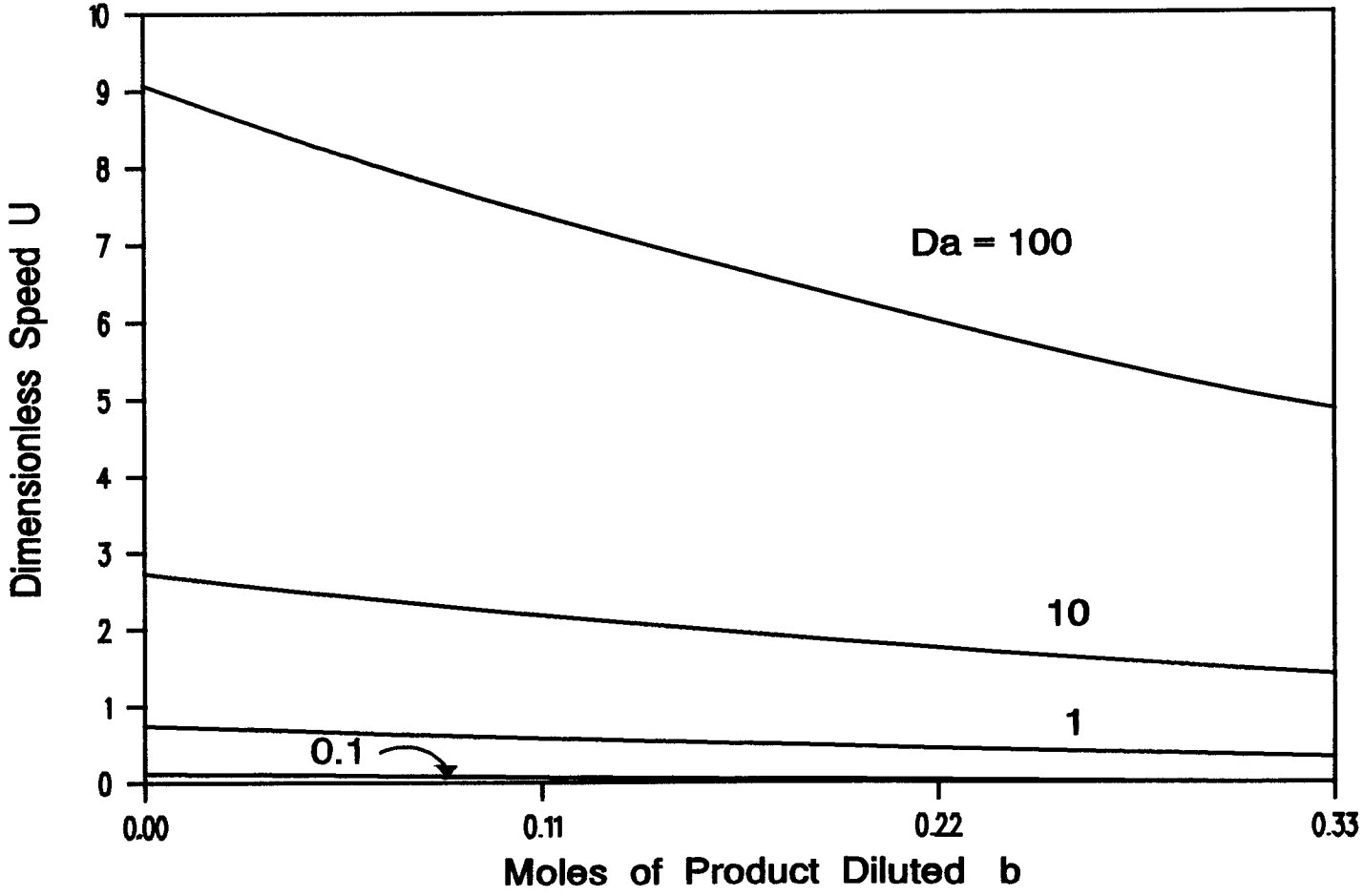

Figure 9.9 Propagation Speed U as a Function of Dilution with Product for Different Da Numbers.

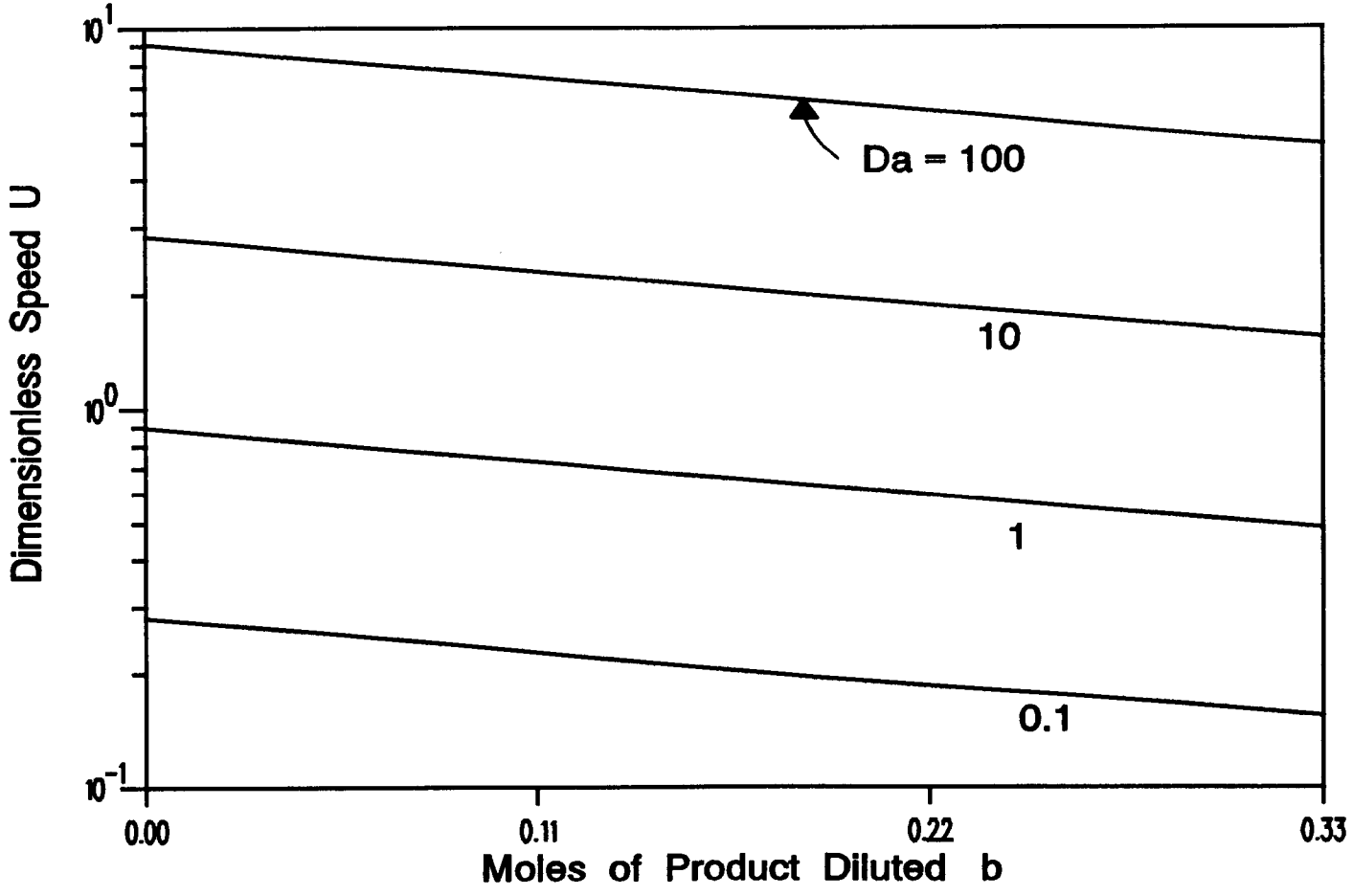

Figure 9.10 Logarithmic Propagation Speed U as a Function of Dilution with Product for Different Da Numbers.

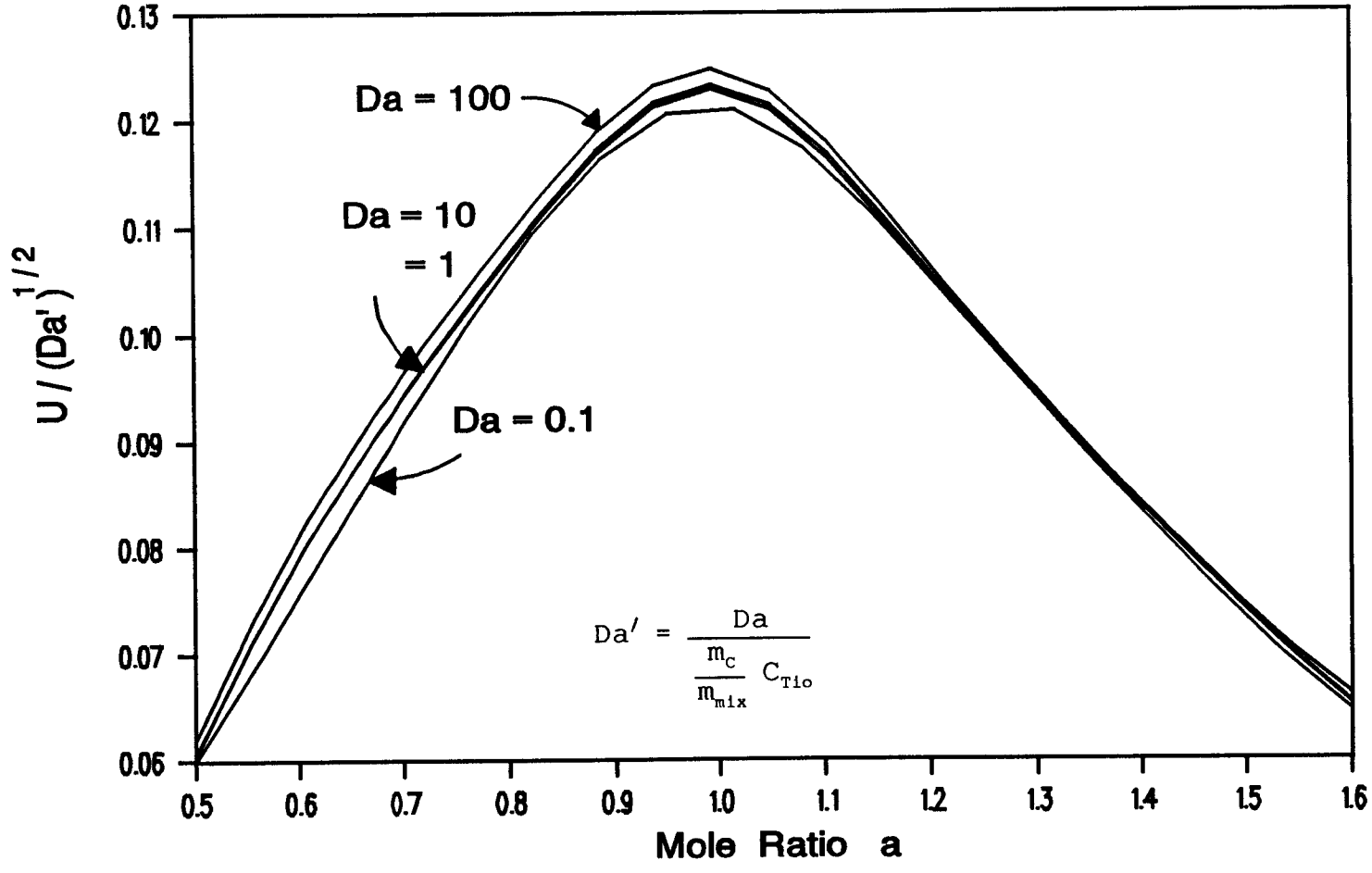

Figure 9.11 Reduced Propagation Speed as a Function of the Mole Ratio a.

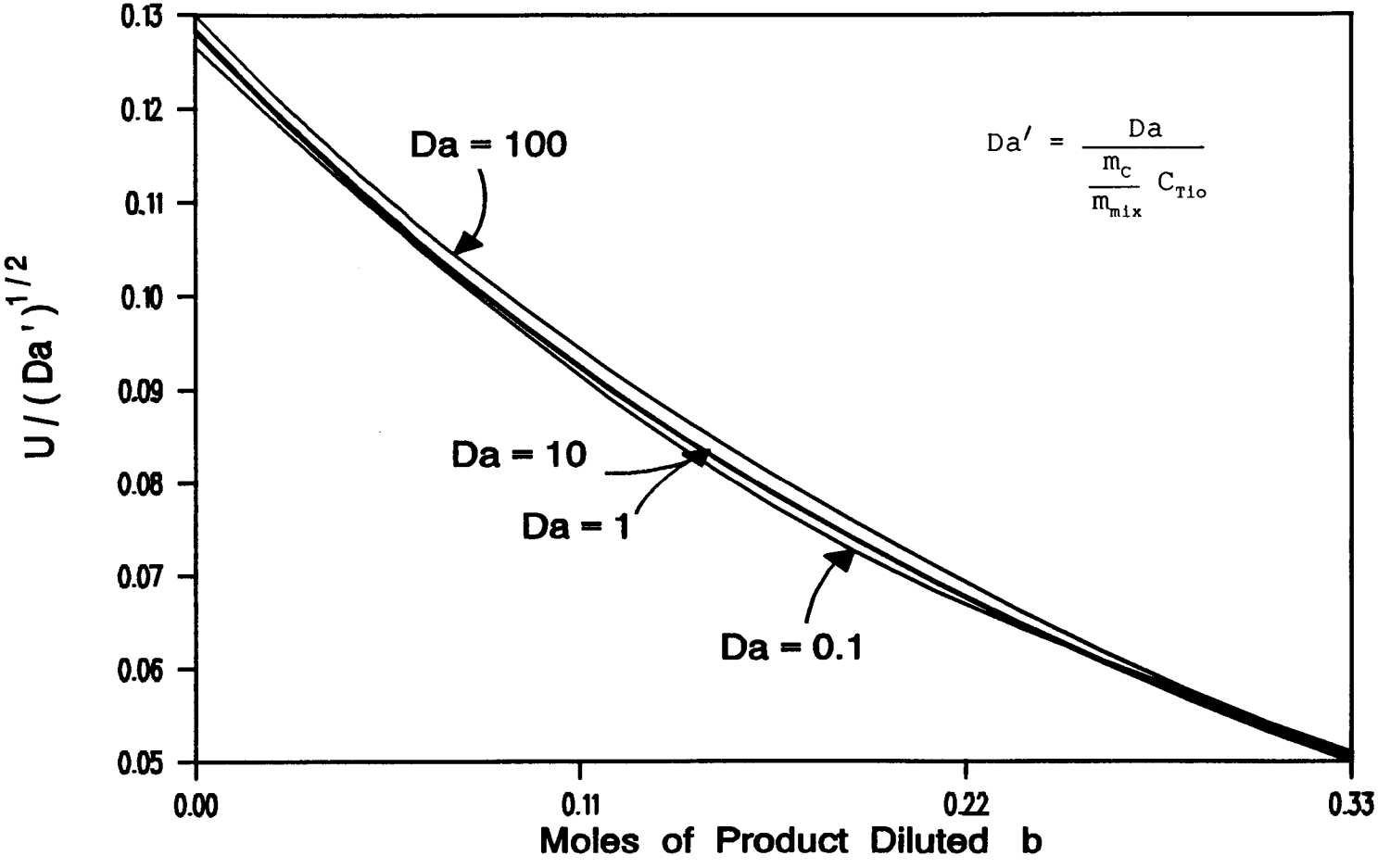

Figure 9.12 Reduced Propagation Speed as a Function of Product Dilution.

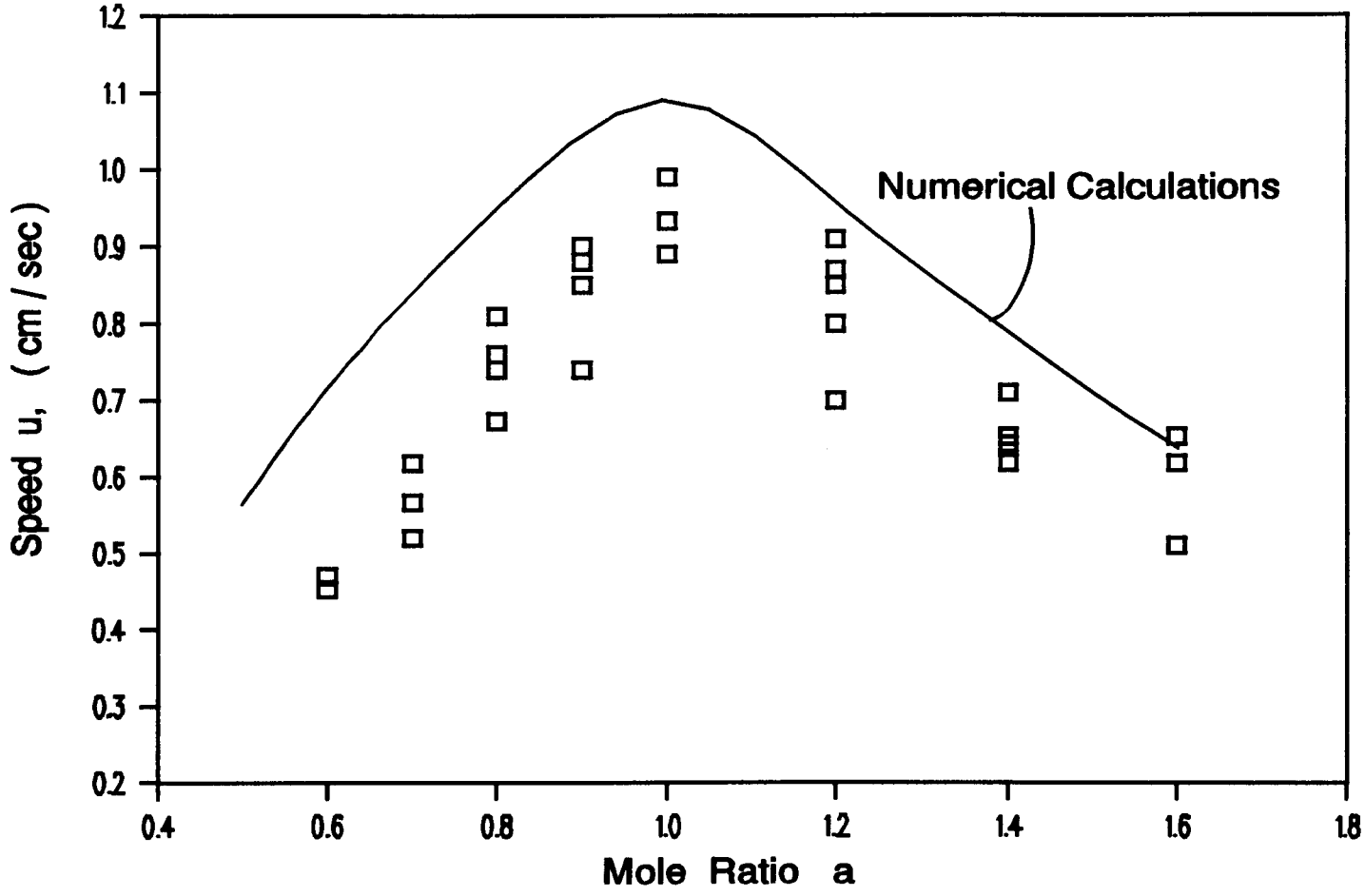

Figure 9.13 Comparison Between the Calculated Propagation Velocity and the Experimental Values, as a Function of the Mole Ratio.

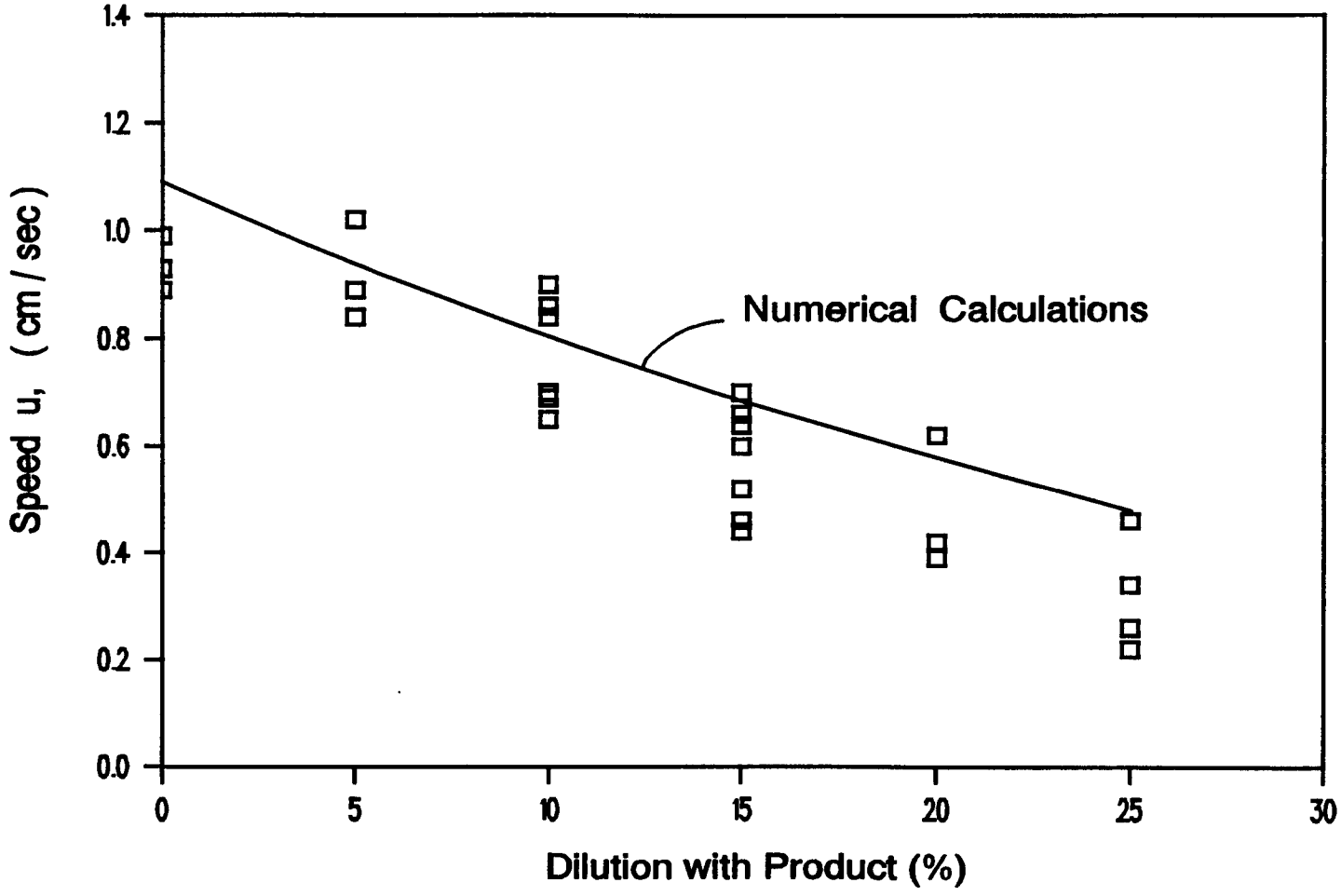

Figure 9.14 Comparison Between the Calculated Propagation Velocity and the Experimental Values, as a Function of Dilution with Product.

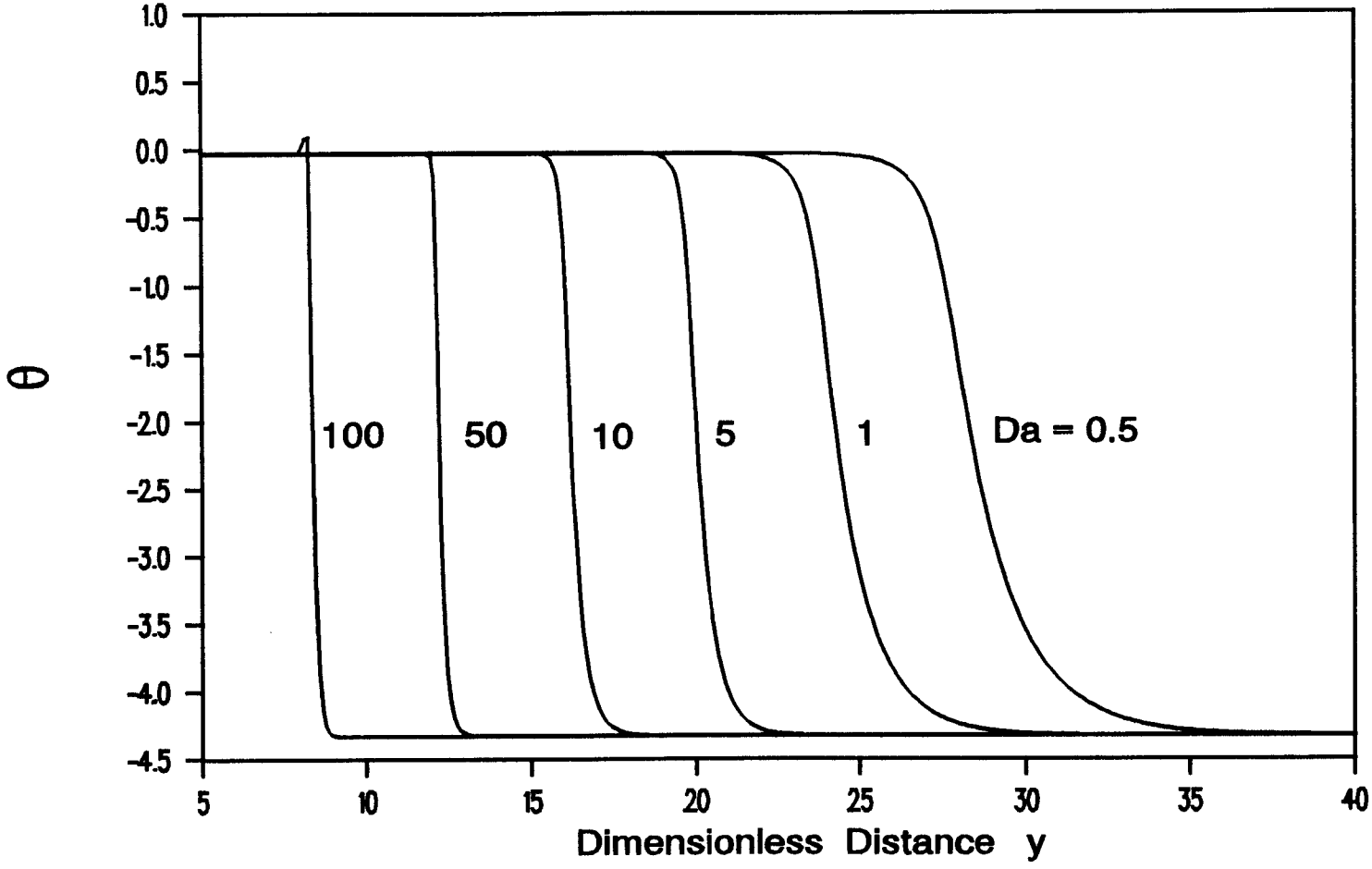

Figure 9.15 Variation of the Dimensionless Temperature Profile as Da Number Changes.

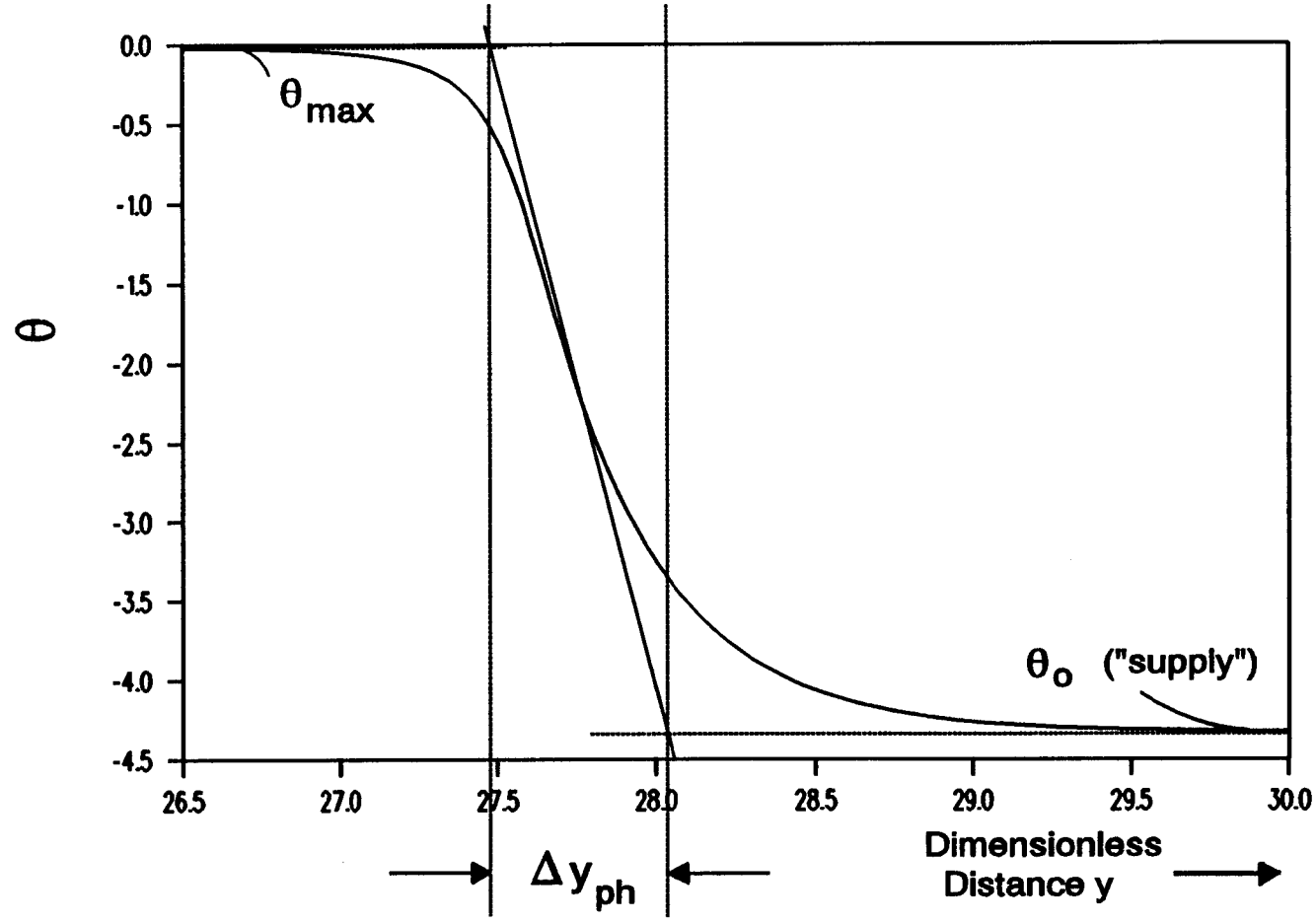

Figure 9.16 Scheme of the Preheated Length. Physical Meaning of Variables in Equation (9.12).

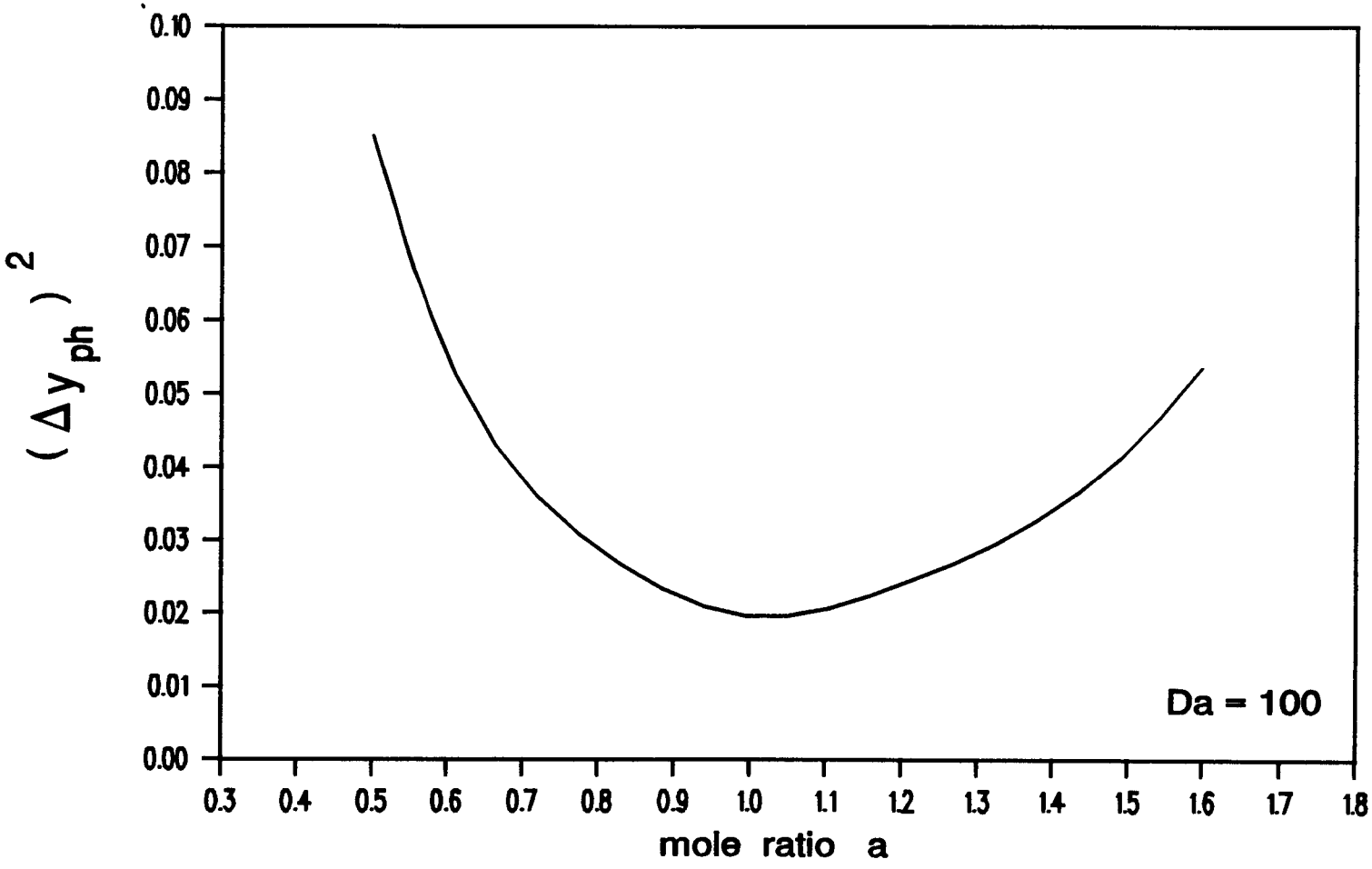

Figure 9.17 Square of the Preheated Length as a Function of the Mole Ratio for Da=100.

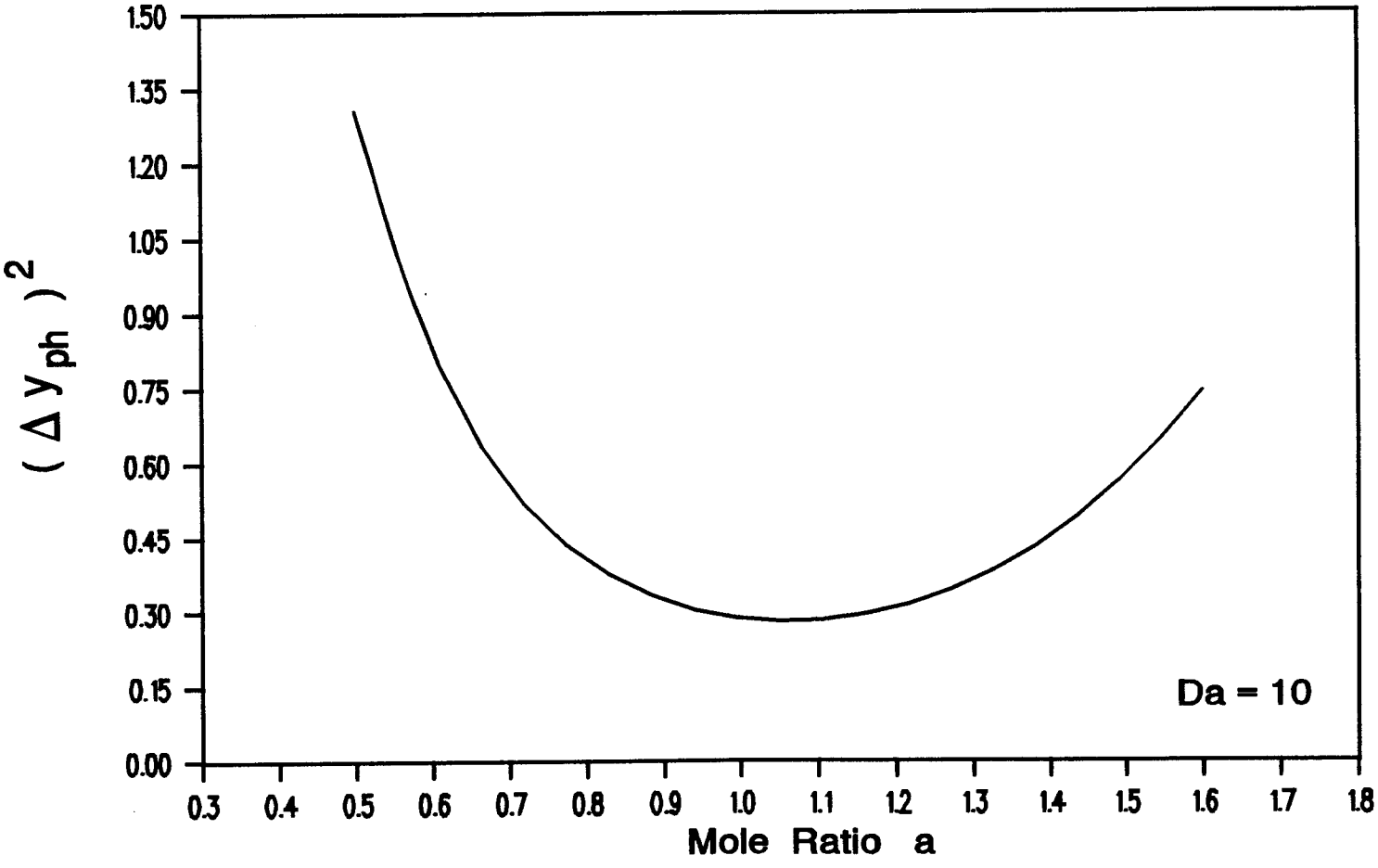

Figure 9.18 Square of the Preheated Length as a Function of Mole Ratio for Da=10.

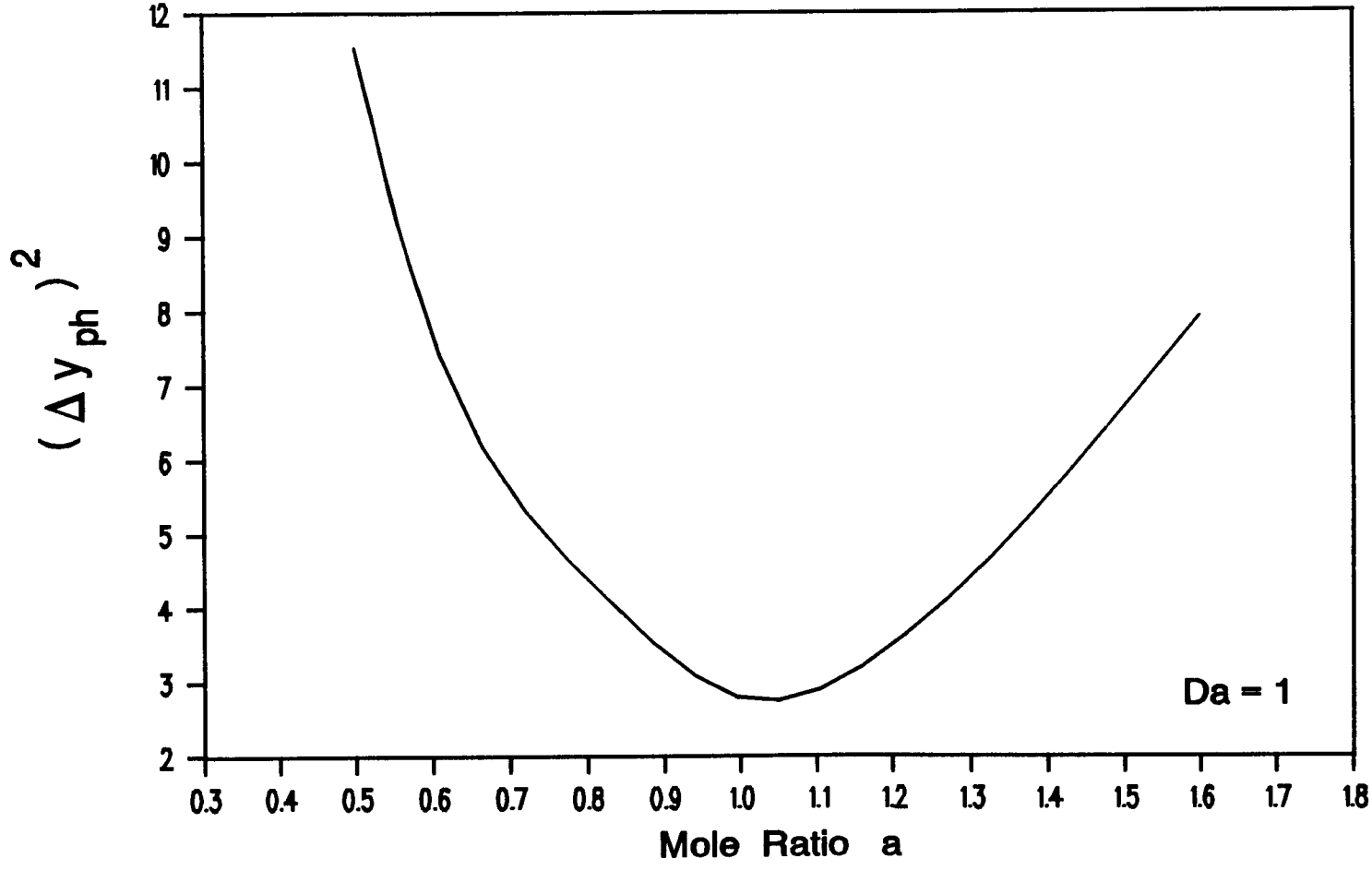

Figure 9.19 Square of the Preheated Length as a Function of Mole Ratio for Da=1.

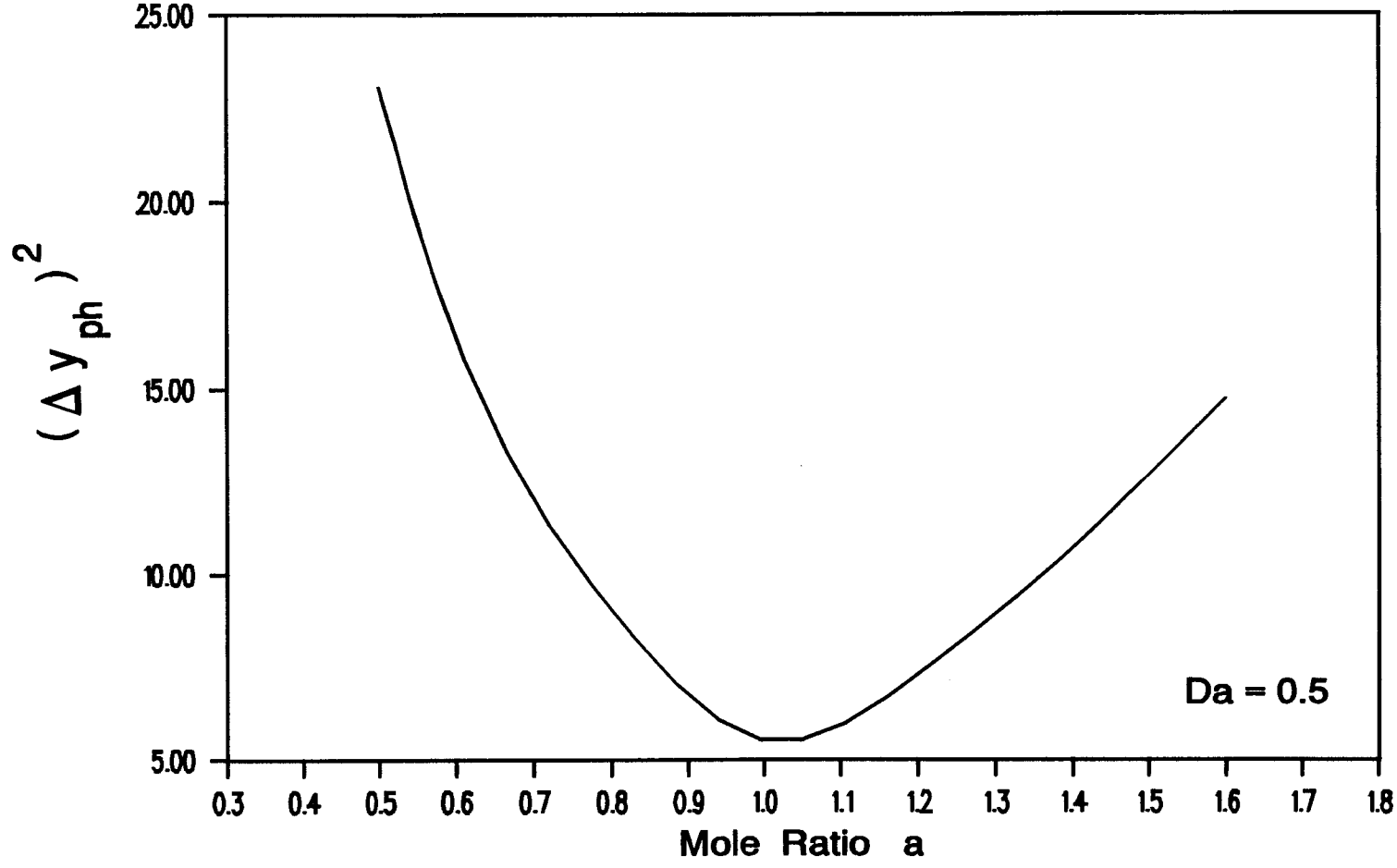

Figure 9.20 Square of the Preheated Length as a Function of Mole Ratio for Da=0.5.

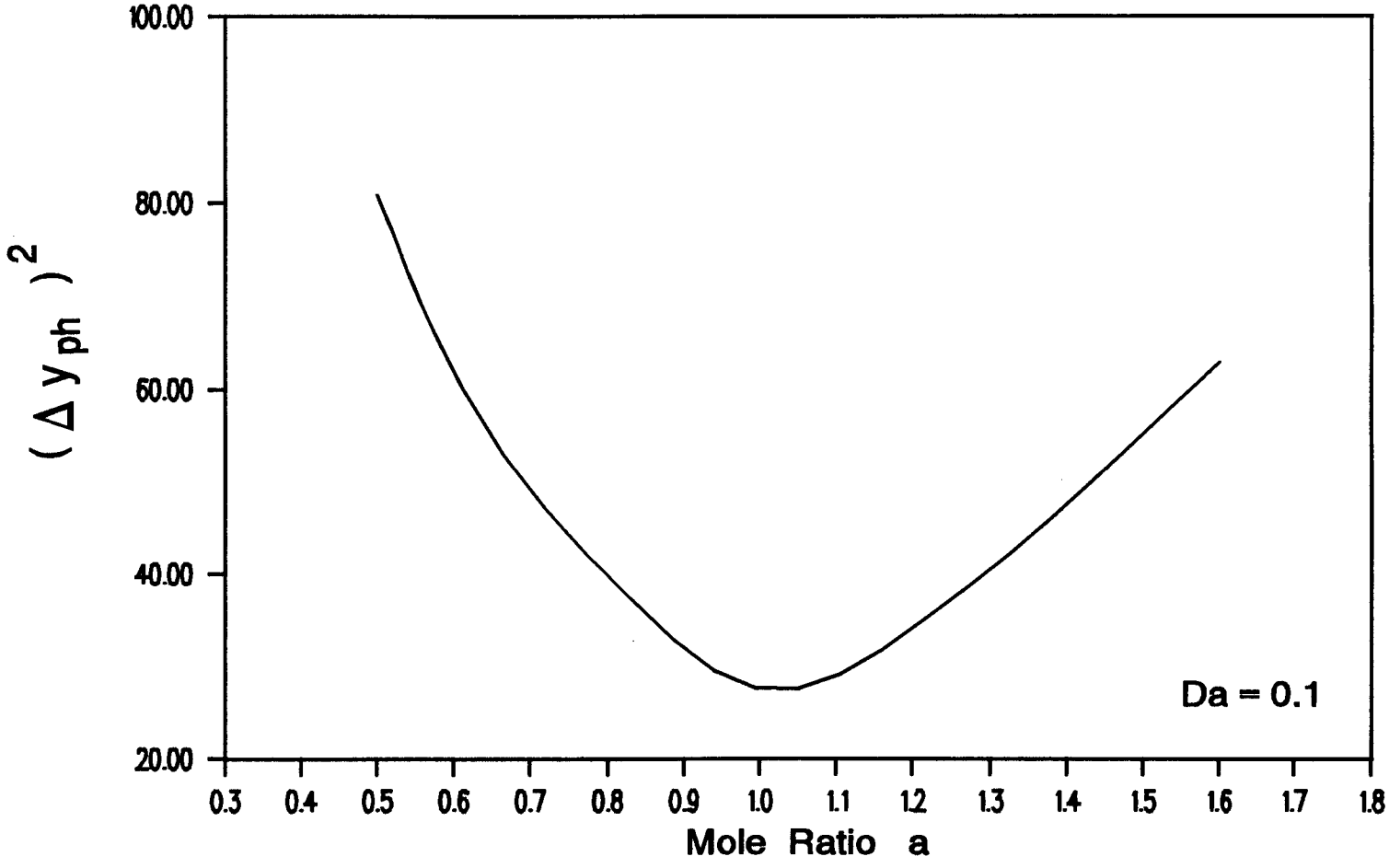

Figure 9.21 Square of the Preheated Length as a Function of Mole Ratio for Da=0.1.

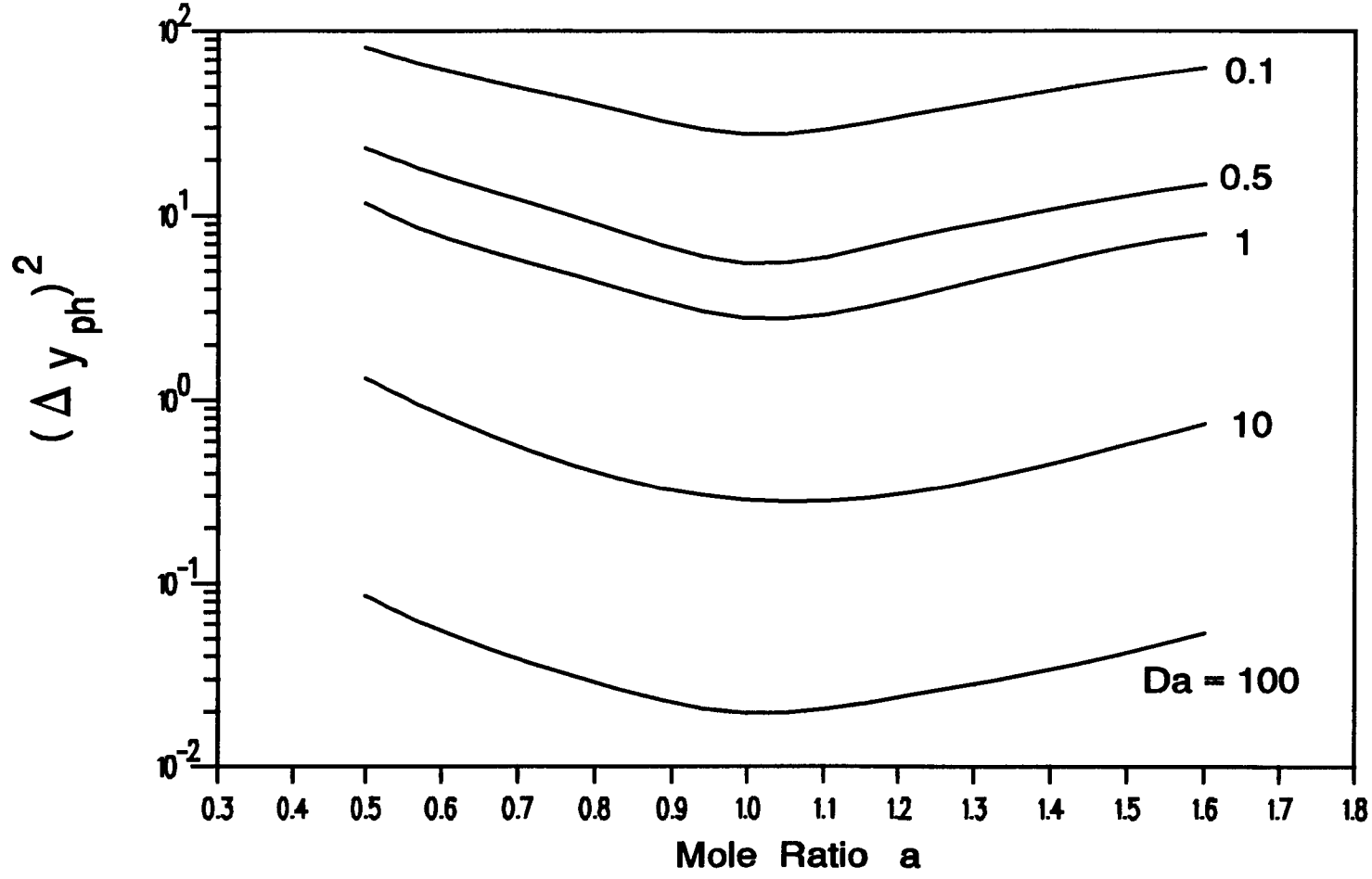

Figure 9.22 Square of the Preheated Length as a Function of Mole Ratio with the Da Number as a Parameter.

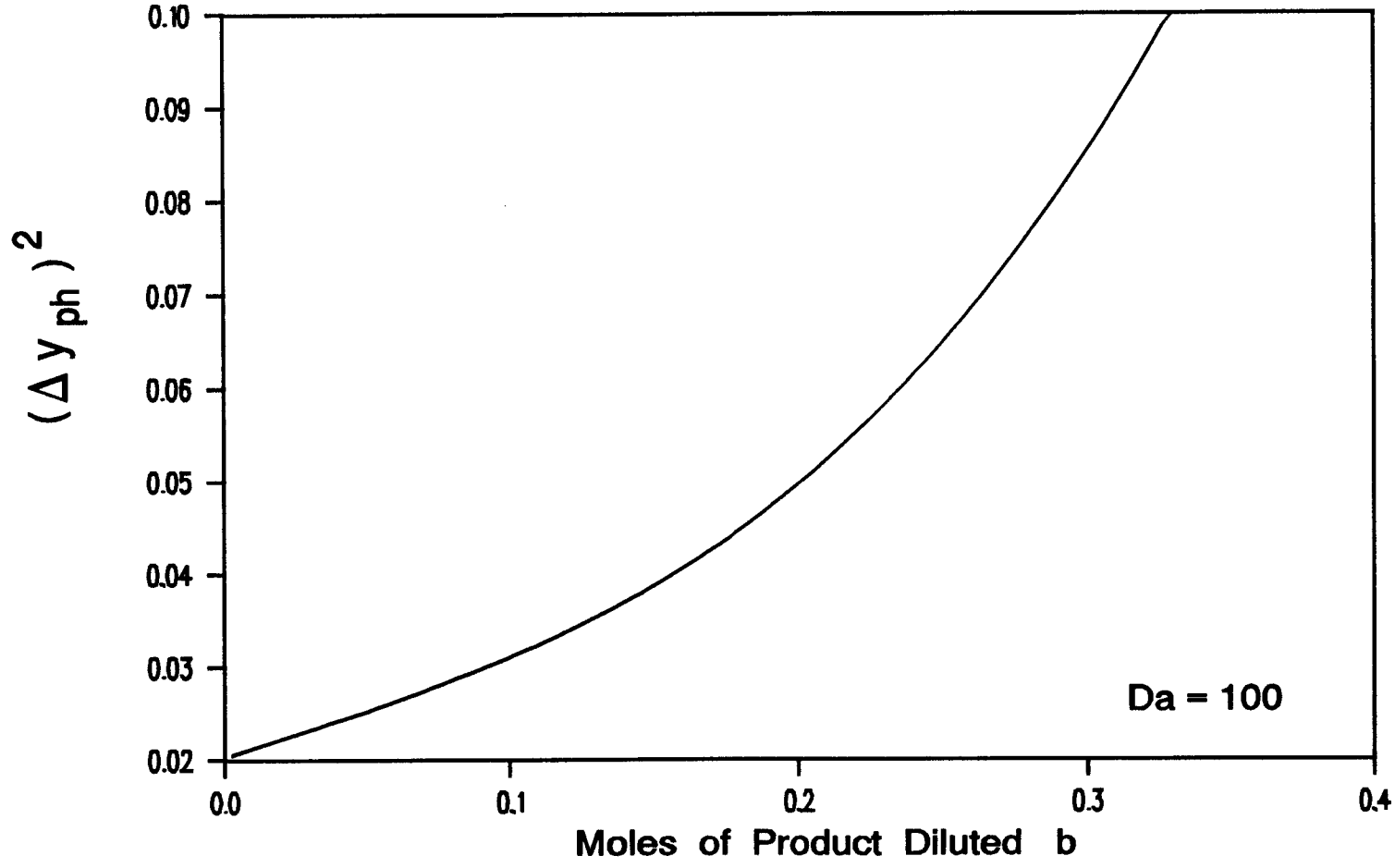

Figure 9.23 Square of the Preheated Length as a Function of Product Dilution for Da=100.

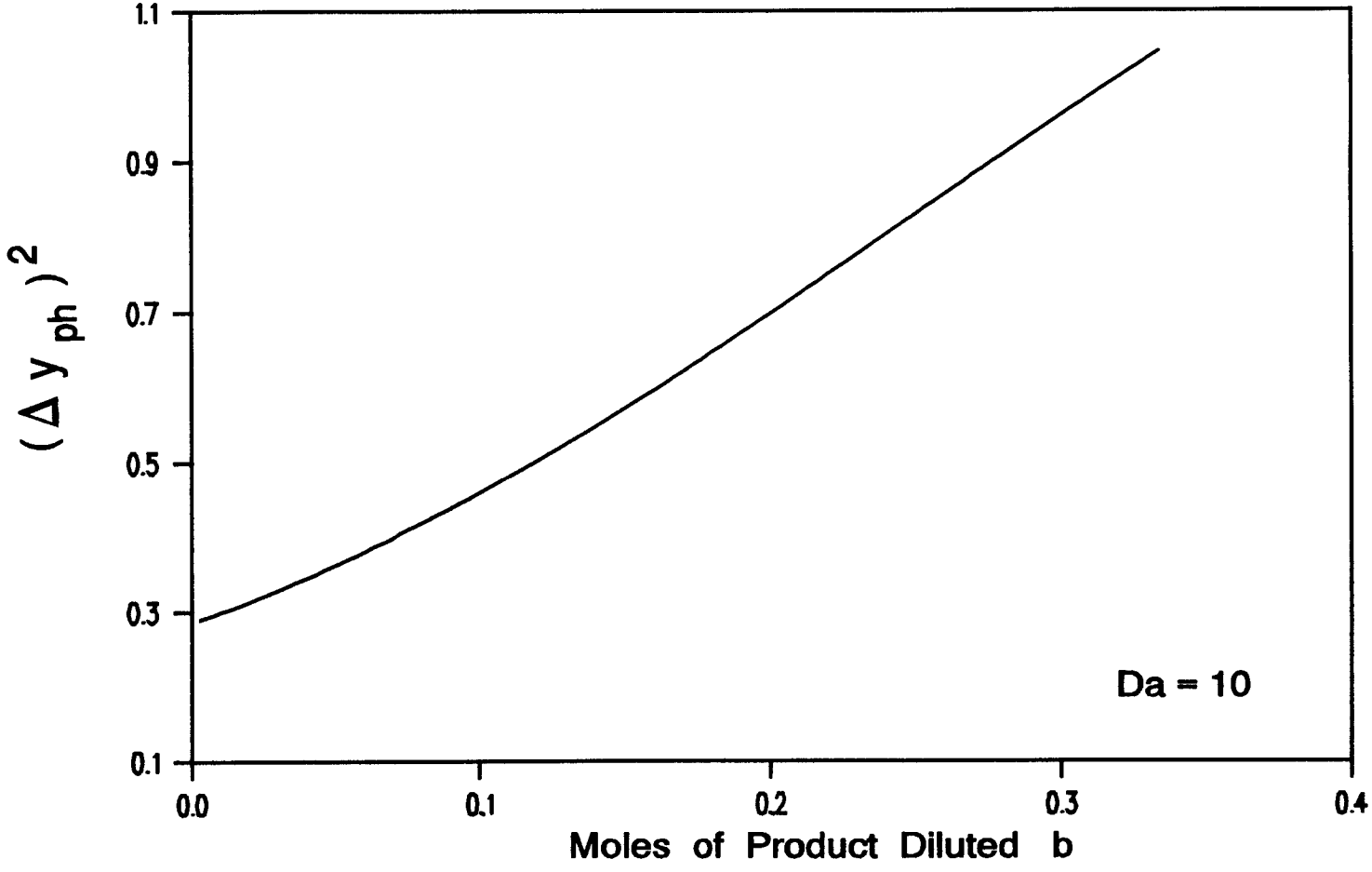

Figure 9.24 Square of the Preheated Length as a Function of Product Dilution for Da=10.

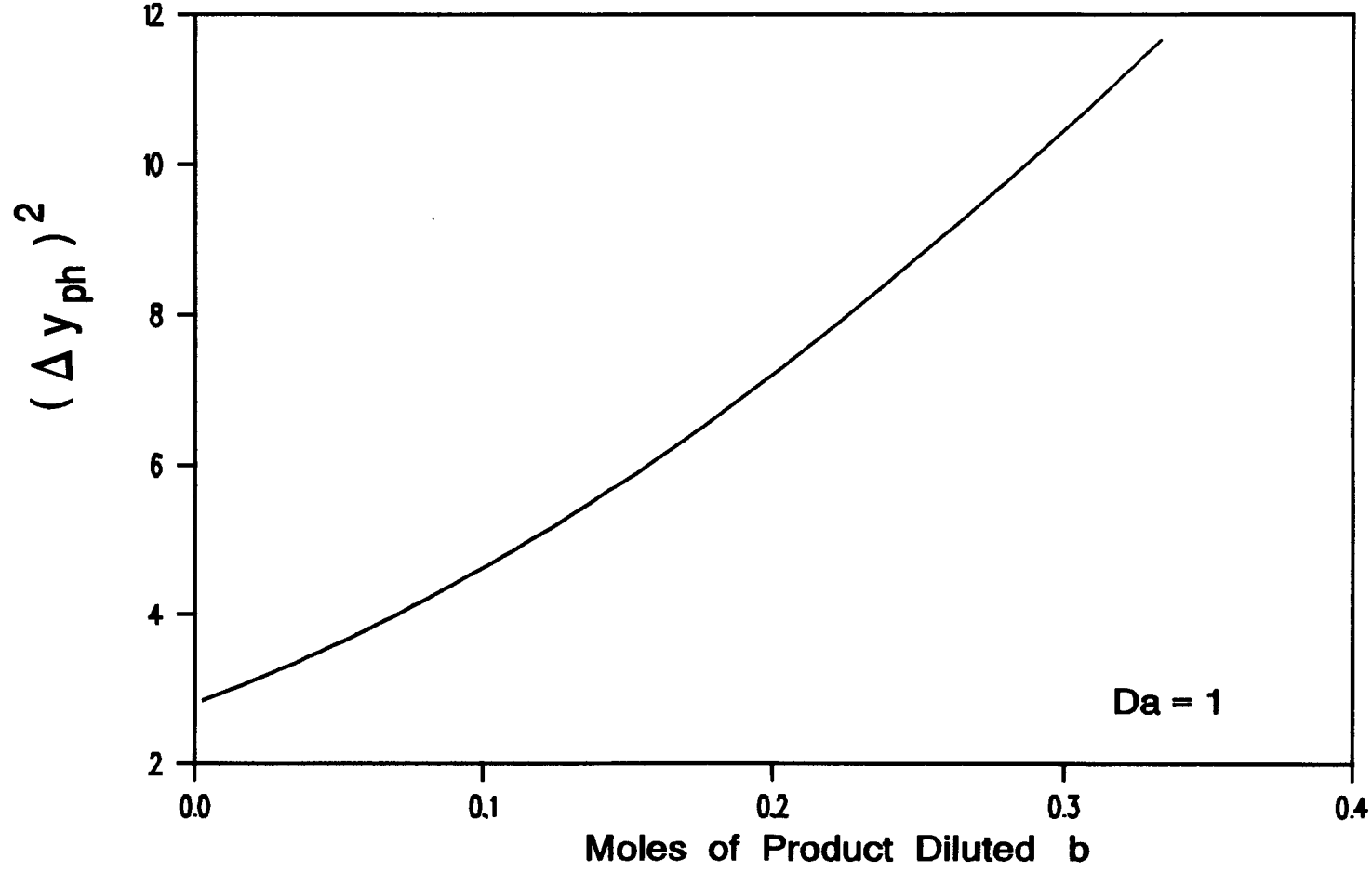

Figure 9.25 Square of the Preheated Length as a Function of Product Dilution for Da=1.

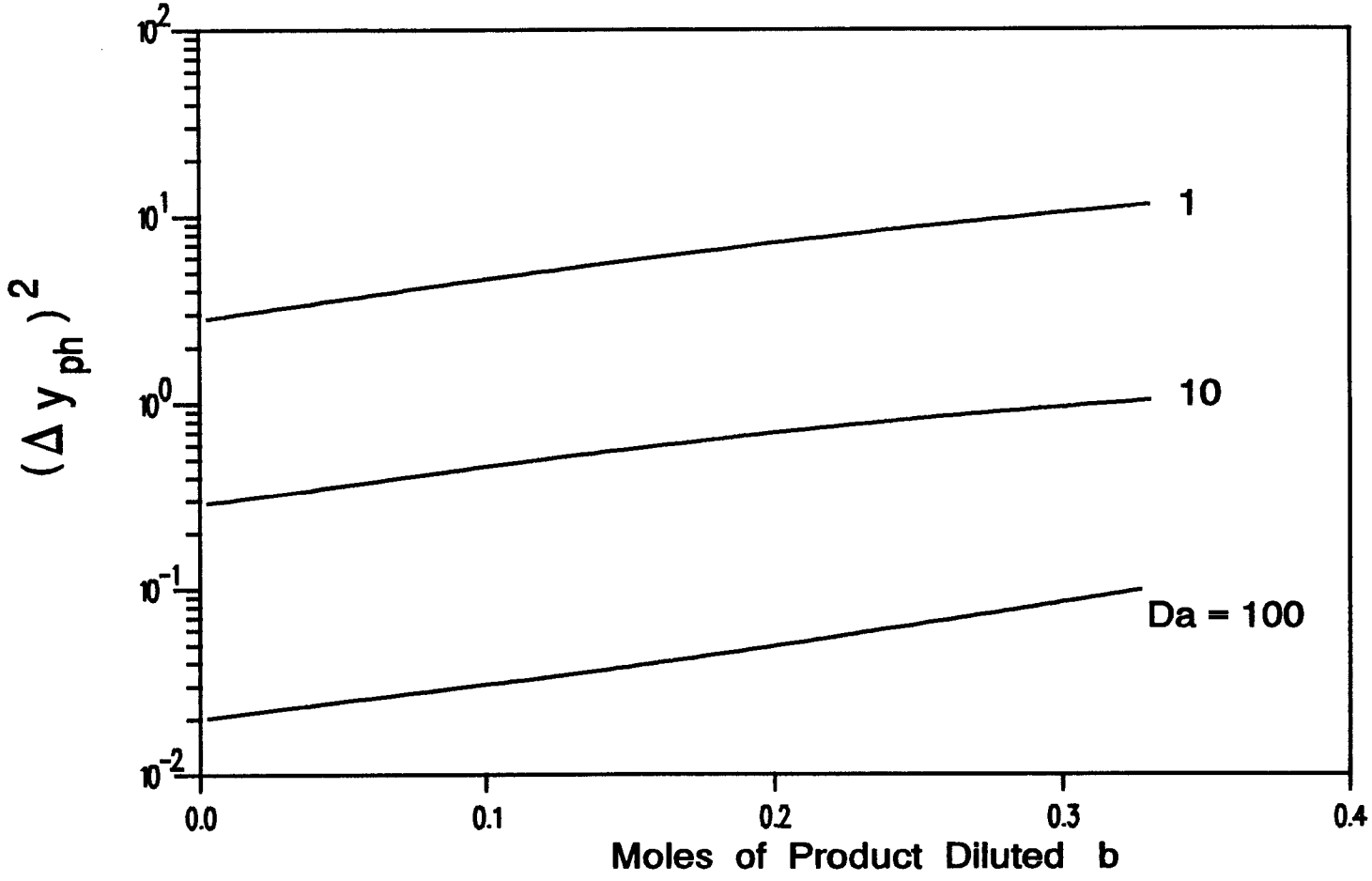

Figure 9.26 Square of the Preheated Length as a Function of Product Dilution with the Da Number as a Parameter.

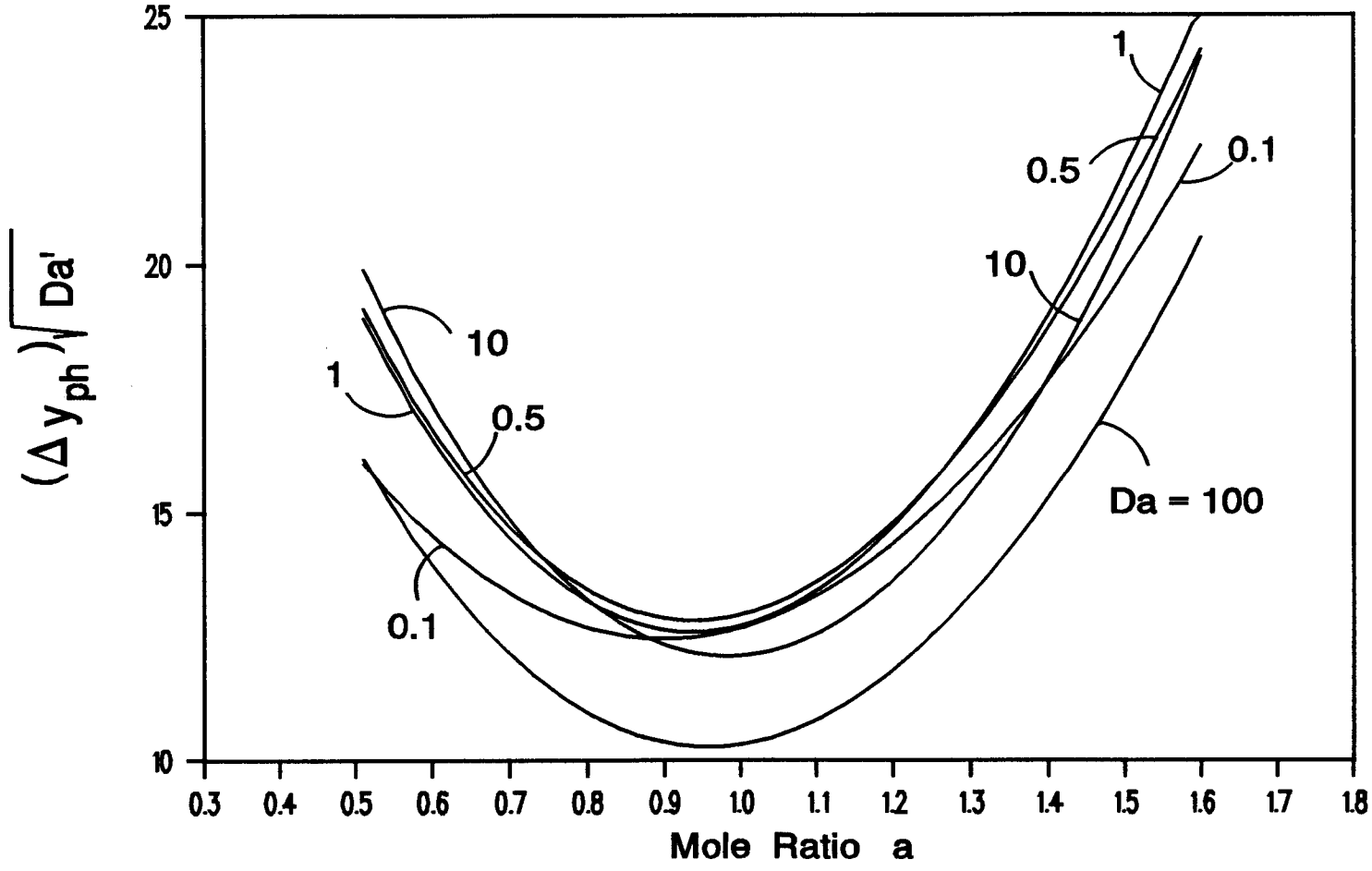

Figure 9.27 The Preheated Length as a Function of the Mole Ratio.

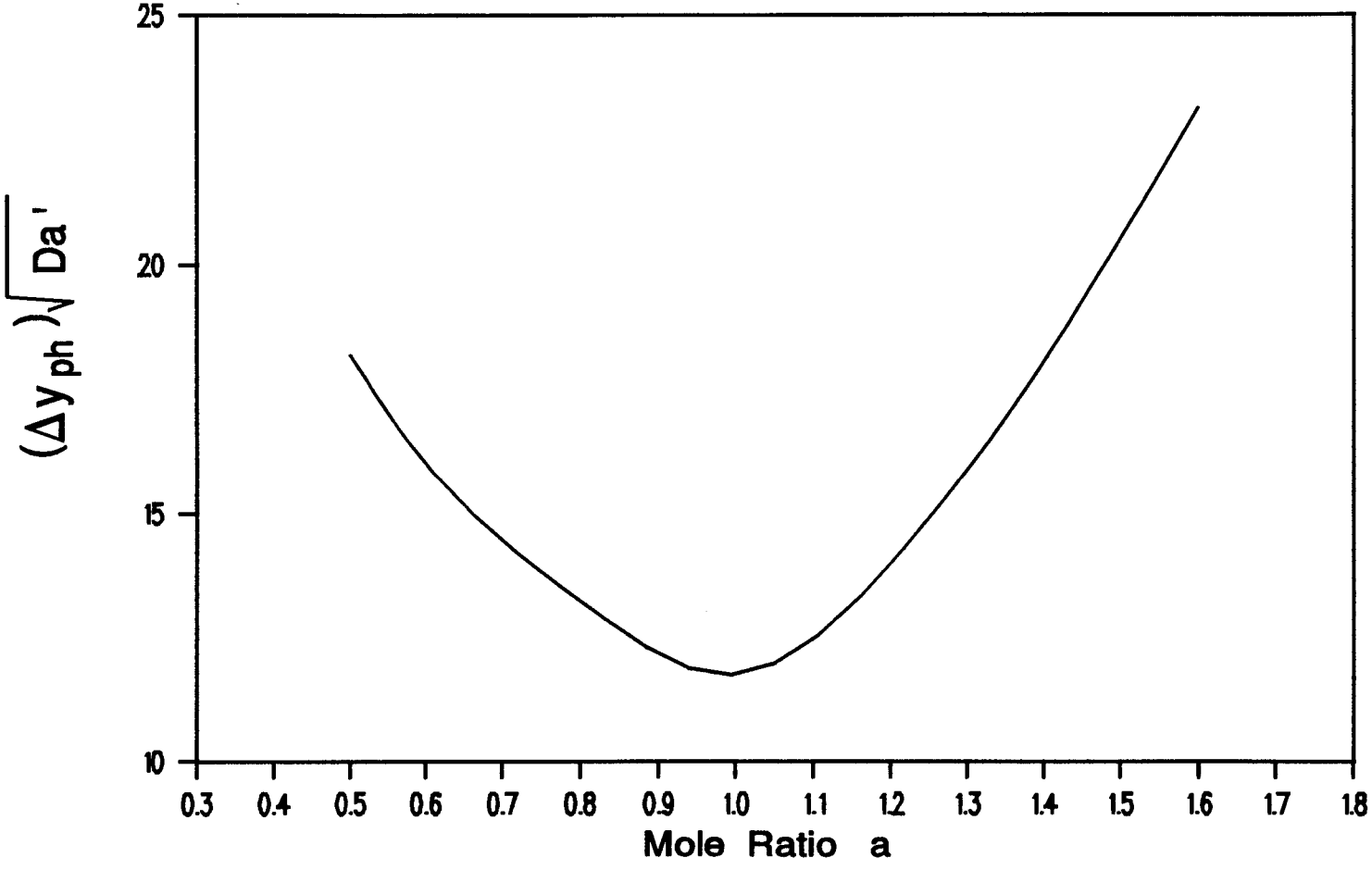

Figure 9.28 Averaged Preheated Length as a Function of the Mole Ratio.

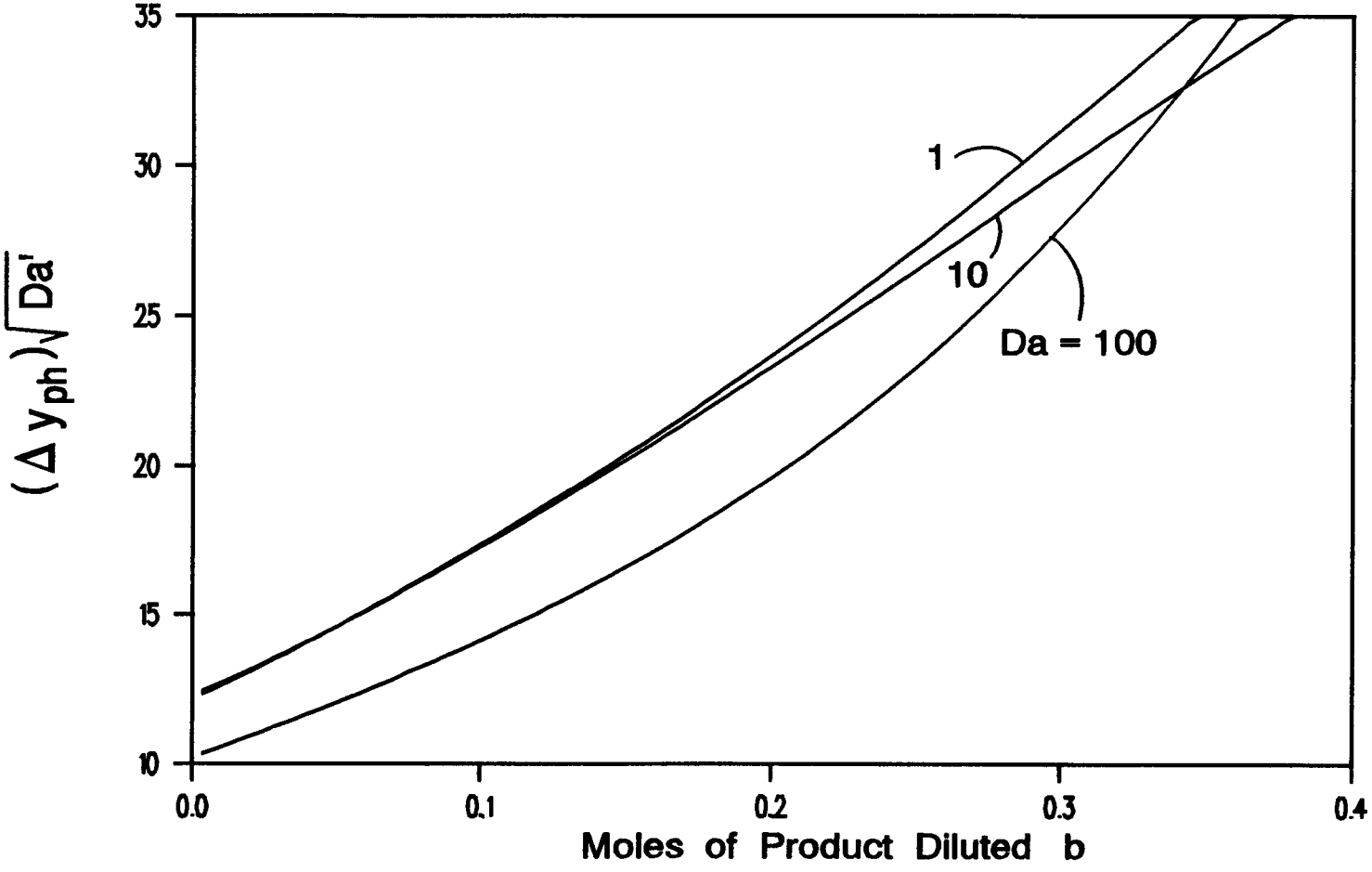

Figure 9.29 The Preheated Length as a Function of the Dilution with Product.

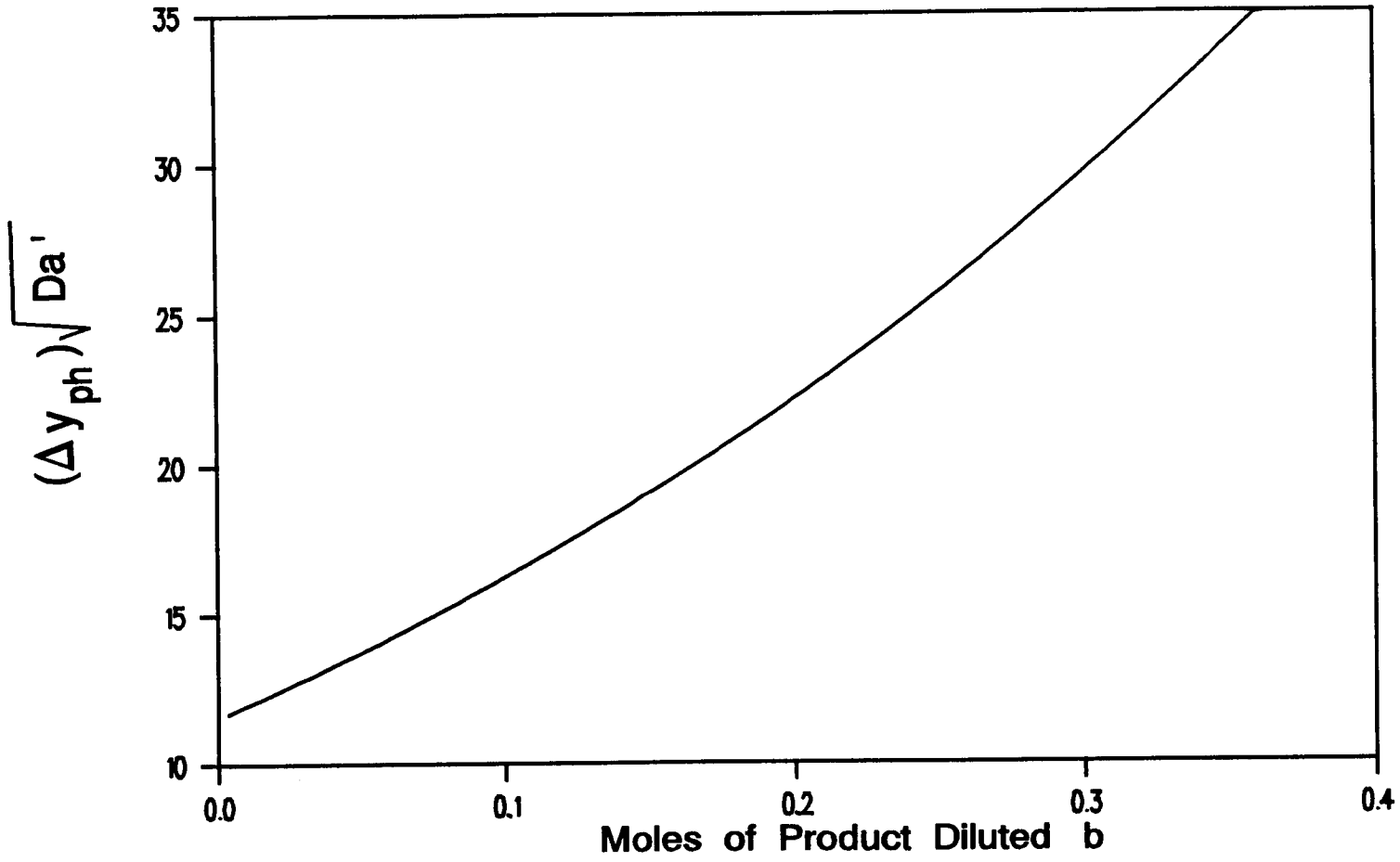

Figure 9.30 Averaged Preheated Length as a Function of the Dilution with Product.

CHAPTER 10

CONCLUSIONS AND RECOMMENDATIONS FOR FUTURE WORK

10.1 Conclusions.

In this thesis, we have presented an experimental and numerical (dimensionless) evaluation of the propagation velocity for the SHS solid-solid reaction of titanium and carbon, as well as a study of the ignition process for the reaction. The thesis includes an introduction and literature of the SHS problem, a review of the current kinetic models used to study the process and mainly a description of the kinetic model for solid-solid reactions developed by Kanury. This kinetic model is implemented in the governing equations to analytically describe the process. The introduction of some suitable dimensionless variables permits the generalization of the analysis and permits the main factors affecting the process to be embedded in a single key parameter, the Da number. This parameter includes the overall effects of thermal properties (density ρ, thermal conductivity K, and specific heat C_p), stoichiometry of the reaction, carbon particle size , a process constant, a compression effect and the diffusion of titanium through an

intermediate complex. This section summarizes the main results obtained in both analytical and experimental studies.

The experimental results included the propagation speed variations for the following cases: (i) different mole ratio of the reactants with no dilution with product, (ii) stoichiometric mixtures with some % product dilution, (iii) density changes, and (iv) change in diameter of the mixture compact. For the first case, it was found that the reaction quenches for mole ratios smaller than 0.6 and larger than 1.6. For the second case, the quenching occurred for mixtures containing more than 27.5 weight % of inert titanium carbide. For the third case, the results of propagation speed included a density range from 1.59 to 2.75 g/cm^3, which were the densities at which it was possible to practically compress the mixtures. The fourth case showed that for diameters above 8 mm (our practical limit) there are no perceivable speed of propagation differences between compacts of different diameter. The propagation range varied from about 0.94 cm/sec at stoichiometric conditions to about 0.25 cm/sec near the quenching conditions.

The synthesis samples are found to expand mainly in the longitudinal direction producing a highly porous final product. This porosity varied with the alteration of different system parameters, but the final density was never

found to exceed 50% of the theoretical final density of titanium carbide. A x-ray diffraction analysis enabled the confirmation of the purity of the products.

Initial mixture compacts were required to be vacuum-heat-treated at above 500 °C in order to volatilize impurities embedded in the mixture. Without the heat-treatment the reaction wave did not propagate or once the sample started reacting, the sample would break apart due to the sudden evolution of the impurities.

The analytical study included an examination of ignition and the determination of the propagation velocity and of the dimensionless preheated length. The ignition study examined the effect of Da number and of the constant-temperature igniter on the times to reach ignition. Only the stoichiometric case with no dilution was analyzed for ignition. A criterion was selected to determine the attainment of the ignition. From the numerical runs, it was observed that every time the ignition condition was reached, a propagation would always occur, thus confirming that the selection of the ignition condition was correct. Large values of Da numbers produced a relatively fast ignition while cases where $Da<0.1$ did not show the attainment of ignition and needed very long "semi-infinite" sizes (i.e. a large number of nodes). By estimating asymptotical values for the minimum temperatures of the igniting source that

would ignite a compact of a given Da number, it was possible to define two zones in a plot of temperature of the igniter versus Da number. The upper zone is a zone where any combination of θ_{hot} and Da number will always lead to ignition and the lower one is a zone where no ignition is possible. All the known characteristics of ignition are observed in the numerical simulation, such as large pre-ignition times and very short (especially for large Da numbers) times between the attainment of ignition condition and the attainment of the maximum reaction temperature.

The numerical results for propagation speed showed that mixtures with large Da numbers will have fast reactions. Low Da numbers,as in ignition, need large lengths to ensure that no end-effects influence the calculated value of propagation speed. As in any numerical treatment, long samples and low time increments combined for very time consuming computational tasks.

As expected, the farther away from stoichiometric conditions, the slower the propagation speeds. This was also observed for the cases where the product was diluted in the original stoichiometric mixture. By invoking the theory of flame propagation and by separating the composition effects (i.e. a and b) from the originally defined Da number, it was possible to reduce all the calculated results for propagation speed into a single curve. This curve is independent

of the Da number and depends only on the stoichiometry of the reaction. This result is relevant since a mixture with its particular Da number could be correlated by means of this single curve, an extended and powerful result. This proves how appropriate the kinetic model of Kanury can be to analyze the SHS processes.

The numerical results for propagation speed U are compared against the experimentally measured speeds of propagation u by using a relation drawn from the theory of flame propagation. The results are in good agreement realizing that in the numerical simulation there were assumptions that could influence the calculated results.

For the final part of the numerical analysis, the preheated length is measured graphically (from recorded temperature profiles) for all the cases covered in the propagation study. Fast moving reaction fronts show to be reactions of very thin preheated lengths, as expected from basic combustion knowledge. The concept of flame thickness proves very useful to determine a parametric curve for the dimensionless preheated length that does not depend on the Da number, but only on the stoichiometry of the problem. This is again an important conclusion resulting from combining combustion concepts to the SHS analysis.

10.2 Recommendations for Future Work.

There are several tasks that should be improved both experimentally and analytically to fully cover the study the SHS solid-solid reaction between titanium and carbon.

First, experimentally, the temperature measuring technique should use an alternate method that avoids the need to drill the samples for inserting thermocouples. The technique used in the present experiments has many drawbacks to be recommended. First, the method is extremely time-consuming especially if the sample breaks during the drilling and the preparation of the sample has to start over. Secondly, the positioning of thermocouples is dependent on the length of samples fabricated. For every experiment, distances between thermocouples and the distance the thermocouples are from the ends of the sample have to be adjusted accordingly. Thirdly, in every experiment the thermocouples melt since the temperatures of reaction were generally over the limit of the tungsten-rhenium thermocouples. Accordingly, the maximum reaction temperatures were not recorded. Optical techniques might be used, but they will have the disadvantage that gases evolving from the reacting sample could "obscure" the true temperature readouts.

If drilling for thermocouples can be avoided, then it is probable that smaller density ranges could be tested to reach the point of quenching. Good quality cylinder-ram sets

are needed to allow for higher compression. The quality of the sets used in this experiment were not necessarily the best option, but were within the low-budget of the experiments.

The experimental setup could be improved to allow the determination of propagation speeds for different initial temperature conditions. This could include an on-site heat treatment of the samples, so that they do not have to be exposed to the oxygen-bearing atmosphere before reaction.

Perhaps a better option to ignite the compact could be some sort of centered radiant flux (like a laser) which could reveal experimental ignition times and minimum energy inputs. In these experiments the igniting coil had to be re-positioned in every single experiment due to twisting of the coil or to allow for the expansion of the sample; this technique did not allow a controlled method for deriving ignition times.

The effect of particle size needs to be investigated as well. However, due to the melting of the titanium particle, only the carbon particle variation may need to be investigated.

The mixing of the reactants definitely needs improvement. The low budget of the present experiments did not allow for a better method as the one described in Chapter 6. If additional experiments are to be tried, a ball-mill with

an inert atmosphere should be the best option.

Analytically, the model can be improved to account for the melting of the titanium and for elongation of the sample as the reaction progresses. Appropriate values for physical properties of the porous mixture are necessary in order to obtain reliable analytical results. These properties need to be known for the different cases under investigation,that is, for stoichiometric and nonstoichiometric mixtures, for different densities, etc. The effect that larger compaction (i.e. larger ρ_{mix}) has on the thermal conductivity needs to be clearly determined to appropriately model the reaction. This will permit the analytical verification of the behavior of propagation speed versus density, shown in Figure 7.6. Most importantly, the determination of the variation of this physical properties with temperature will yield an important contribution to the analysis of SHS processes, given the high range of reaction temperatures reached.

This study used constant values for the Zeldovich and Stefan numbers; it needs to be verified if changes in the stoichiometry of the reaction produce a different value of these parameters and how drastic are those changes to require further propagation calculations.

With respect to the ignition problem studied here, it is important to note that this examination was performed for a stoichiometric mixture with a prescribed surface tempera-

ture boundary condition. Further calculations for conditions other than the stoichiometric (and with product dilution) are required, as well as a prescribed surface heat flux boundary condition.

The implementation of the Kanury kinetic model has proved to be a powerful tool in studying the SHS solid-solid reaction of titanium and carbon, hence it will be advisable to extend his model to other SHS reactions that follow the same mechanism of reaction as the titanium and carbon mixtures.

BIBLIOGRAPHY

1. Merzhanov, A. G. and Dubovitskii, F. I., "The Theory of Stationary Combustion in Powders," Institute of Chemical Physics of the Academy of Sciences USSR, pp. 917-920, June 13, 1959.

2. Manelis, G. B., Merzhanov, A. G., Dubovitskii, F. I., "The Mechanism of the Combustion of Powders," Doklady Akademii Nauk SSSR, Vol. 133, No. 2, pp. 399-400, July, 1960.

3. Merzhanov, A. G., "The Theory of Stable Homogeneous Combustion of Condensed Substances," Combustion and Flame, Vol. 13, April 1969.

4. Puszynski, J. D., Degreve, J., Hlavacek, V., "Modeling of Exothermic Solid-Solid Noncatalytic Reactions," Ind. Eng. Chem. Res., 26, 1424-1434, 1987.

5. Kumar, S., Puszynski, J. A., Hlavacek, V, "Combustion Characteristics of Solid-Solid Systems Experiment and Modeling," Combustion and Plasma Synthesis of High Temperature Materials, VCH. Publishers NY, in press 1990.

6. Hlavacek, V., Puszynski, J. A., Degreve, J., Kumar, S., "Propagation of Reaction Fronts in Exothermic Heterogeneous Noncatalytic Systems Solid-Solid and Solid-Gas," Chemical Engineering Science, Vol. 41, No. 4, pp. 877-882, 1986.

7. Boddington, T., Cottrell, A., Laye, P. G., "A Numerical Model of Combustion in Gasless Pyrotechnic Systems," Combustion and Flame, 76:63-69, 1989.

8. Rice, R. W., McDonough, W. J., "Intrinsic Volume Changes of Self-Propagating Synthesis," Communicacions of the Am. Ceram. Society, J. Am. Ceram. Soc., 68[5] C-122-C-123, 1985.

9. Hansen, G. P., Fredin, L. and Margrave, J. L., "Characterization of Vapors Evolved During High-Temperature Synthesis," Goverment Report #LA-UR--86-382, DE86 006042 for Los Alamos National Laboratory, Proceedings DARPA/Army Symposium on Self-Propagating High-Temperature Synthesis (SHS), October, 1985.

10. Kecskes, L. J. and Niiler, A., "Impurities in the Combustion Synthesis of Titanium Carbide," J. Am. Ceram. Soc., 72[4] 655-61, 1989, U.S. Army Ballistic Research Lab.

11. Munir, Z. A. and Anselmi-Tamburini, U., "Self-Propagating Exothermic Reactions: The Synthesis of High-Temperature Materials by Combustion," Materials Science Reports, 3, 277-365, 1989.

12. Munir, Z. A., "Synthesis of High-Temperature Materials by Self-Propagating Combustion Methods," Ceramic Bulletin, Vol. 67, No. 2, 1988.

13. Ristic, M. M. and Dragojevic-Nesic, M., "Densification Kinetics During Sintering of Materials by a Flow Mechanism," Journal of Materials Science Letters, 6, 1091-1092, 1987.

14. Mullins, M. E. and Riley, E., "The Effect of Carbon Morphology on the Combustion Synthesis of Titanium Carbide," Journal of Mater. Res., Vol. 4, No. 2, Mar/Apr, 1989.

15. Hardt, A. P. and Phung, P. V., "Propagation of Gasless Reactions in Solids-I. Analytical Study of Exothermic Intermetallic Reaction Rates," Combustion and Flame, 21, 77-89, 1973.

16. Williams, L. S., "Method of Producing Compacts by Reacting Particulate Ingredients," US Patent 3,353,954. Nov. 21, 1967.

17. McKenna, P. M., "Process for Preparing Tungsten Monocarbide," US Patent 3,379,503. April 23, 1968.

18. Lowndes, J. C., "DARPA, USAF Develop Advanced Materials Processing Technology," Aviation Week & Space Technology, July 7, 1986.

19. Kottke, T. and Niiler, A., "Thermal Conductivity Effects on SHS Reactions," Technical Report #BRL-TR-2889 (ADA 1946920 XSP), Ballistic Research Laboratory, March 1988.

20. Kanury, A. M. and Huque, Z., "Chemical Kinetics of Reactions of the Type: Solids --> Solids," WSS/CI 89-2, The Combustion Institute/ Western States Section Preprint, Spring Meeting, Washington State University, Pullman, WA, March 1989.

21. Kanury, A. M., "Self-Propagating High-Temperature Synthesis of Materials Employing Combustion Reactions of the Type: Solid --> Solid," Paper presented at the 25th ASME/AIChE National Heat Transfer Conference, Houston, TX, July 1988. Published in Heat Transfer Houston, 1988, Conference Proceedings, AIChE Symposium Series 84, No. 263, pp. 44-49, 1988.

22. Huque, Z., Kanury, A. M. and Hernandez-Guerrero, A., "Theoretical Analysis of Combustive Synthesis of Titanium Carbide," Paper presented in a session entitled: Reaction Engineering of the Manufacture of High Performance Ceramics II. Self-Propagating High-Temperature Synthesis, at the 1989 Annual AIChE Meeting, Nov. 5-10, 1989. In press in the Conference Proceedings.

23. Munir, Z. A. and Holt, J. B., Editors, Combustion and Plasma Synthesis of High Temperature Materials, from papers of the International Symposium on Combustion and Plasma Synthesis of High Temperature Materials, held in October, 1988 in San Francisco, Calif., 1990, VCH Publishers.

24. Sheppard, L. M., "Powders that Explode into Materials," Advanced Materials and Processes, 2(2), pp.25-32, Feb. 1986.

25. Crider, J. F., "Self-Propagating High Temperature Synthesis -A Soviet Method for Producing Ceramic Materials," Ceram. Eng. Sci. Proc., Vol.3 [9-10], pp. 519-528, 1982.

26. Hardt, A. P., "Low-Pressure Self-Propagating High-Temperature Synthesis," Final Report, Government Report No. LMSC-F145665, February, 1987.

27. Merzhanov, A. G., Borovinskaya, I. P., Karjuk, G. G., Dubovitsky, F. I., Prokudina, V. K., Ratnikov, V. I., Bochko, A. V., Moshkovsky, E. I., Sharivker, S. J. and Krizhanovsky, S. S., "Process for Preparing Titanium Carbide," U.S. Patent 4,161,512, July 17, 1979.

28. Kanury, A. M., Hernandez-Guerrero, A. and Huque, Z., "A Model for the Chemical Kinetics of Reactions of the Type Solids --> Solids," AIChE Annual Meeting, Chicago, IL, November 11-16, 1990.

29. Aleksandrov, V. V. and Korchagin, M. A., "Mechanism and Macrokinetics of Reactions Accompanying the Combustion of SHS Systems," Fizika Goreniya i Vzryva, Vol. 23, N0. 5, pp. 55-63, 1987. (Translation pp. 557-564, Combustion, Explosion and Shockwaves, 23(5), 1987.)

30. Aleksandrov, V.V.; Korchagin, M. A.; Boldyrev, V. V. "Mechanism and Macrokinetics of a Reaction of Components in a Powder Mixture," Doklady Akademi Nauk SSSR, Vol. 292, No. 4, pp. 879-881, February, 1987. (Translated by the Plenum Publishing Corp. 0012-5016/87/0002-0114.)

31. Merzhanov, A. G., "New problems in the Theory and Practice of Combustion Processes," pp.74-85 in Problems in

Chemical Kinetics, (N. M. Emanuel, Editor), MIR Publishers, Moscow, 1981.

32. Merzhanov, A. G., Shkiro, V. M. and Borovinskaya, I. P., "Method of Producing Refractory Carbides, Borides, Silicides, Sulfides, and Nitrides of Metals of Groups IV, V, and VI of the Periodic System," U.S. Patent 3,726,643, April 10, 1973.

33. Corbin, N. D. and McCauley, J. W., "Self-Propagating High Temperature Synthesis (SHS): Current Status and Future Prospects," Gov. Report # AD-A169 588 (RN MTLMS861), U.S. Army Materials Technology Laboratory, 12 pp., May 1986.

34. Holt, J. B., "Combustion Synthesis of Refractory Materials," UCRL-53258, Report of Lawrence Livermoore National Laboratory, Livermoore, Cal., 1982.

35. Kanury, A. M., "A Kinetic Model for Metal + Nonmetal Reactions," submitted for review to Metallurgical Transactions, 1991.

36. Hernandez-Guerrero, A., Huque, Z. and Kanury, A. M., "An Experimental Investigation of Combustive Synthesis of Titanium Carbide," accepted for publication in Combustion, Science and Technology, 1991.

37. Hardt, A. P. and Holsinger, R. W., "Propagation of Gasless Reactions in Solids-II. Experimental Study of Exothermic Intermetallic Reaction Rates," Combustion and Flame, 21, pp. 91-97, 1973.

38. Holt, J. B. and Munir, Z. A., "Combustion Synthesis of Titanium Carbide: Theory and Experiment," Journal of Material Science, Vol. 21., pp. 251-259, 1986.

39. Shkiro, V. M., Nersisyan, G. A., Borovinskaya, I. P., "Principles of Combustion of Tantalum-Carbon Mixtures," Fizika Goreniya i Vzryva, Vol. 14, No. 4, pp. 58-64, July-Aug 1978. Translated by Plenum Publishing Corp. 0010-5082/78/1404-0455.

40. Shkiro, V. M., Nersisyan, G. A., Borovinskaya, I. P., Merzhanov, A. G. and Shektman, V. S., "Preparation of Tantalum Carbides by Self-Propagating High-Temperature Synthesis (SHS)," Poroshkovaya Metallurgiya, No. 4(196), pp. 14-17, April 1979. Translated by Plenum Publishing Corp. 0038-5735/79/1804-0227.

41. Henshaw, W. F., Niiler, A. and Leete, T., "Self-Propagating High-Temperature Synthesis of Ceramics in Vacuum," Goverment Memorandum Report ARBRL-MR-03354 (Govt Accession Number ADA142506), US Army Ballistic Research Laboratory, 31 pps., April 1984.

42. Rogachev, A. S., Mukas'yan, A. S. and Merzhanov, A. G., "Structural Transition in the Gasless Combustion of Titanium-Carbon and Titanium-Boron Systems," Doklady Akademii Nauk SSSR, Vol. 297, No. 6, pp. 1425-1428, December, 1987. Translated by Plenum Publishing Corp. 0012-5016/87/0012-1240.

43. Maksimov, Y. M., Lepakova, O. K. and Raskolenko, L. G., "Combustion Mechanism of a Titanium-Boron System with the Use of Quenching of the Reaction Front," Combustion, Explosion and Shock Waves, translated from Fizika Goreniya i Vzryva, Vol. 24, No. 1, pp. 48-53, Jan-Feb 1988.

44. Riley, M. A. and Niiler A., "Low Pressure Compaction of SHS Prepared Ceramics," Memorandum Report BRL-MR-3574, US Army Ballistic Research Laboratory, March 1987.

45. Kushid, B. M. and Merzhanov, A. G., "Structural Conversion in Gasless Combustion of Heterogeneous Systems with a Melting Metallic Reagent," Doklady Akademii Nauk SSSR, Vol. 298, No. 2, pp. 414-417, January, 1988. Translated by Plenum Publishing Corp.

46. Vadchenko, S. G., Grigoriev, Y. M. and Merzhanov, A. G., "Investigation of the Mechanism of the Ignition and Combustion of the Systems Ti + C, Zr + C, by an Electrothermographic Method," Fizika Goreniya i Vzryva, Vol. 12, No. 5, pp. 676-682, Sept-Oct, 1976. Translated by Plenum Publishing Corp.

47. Knyazik, V. A., Merzhanov, A. G., Solomonov, V. B. and Shteinberg, A. S., "Macrokinetics of High-Temperature Titanium Interaction with Carbon Under Electrothermal Explosion Conditions," Fizika Goreniya i Vzryva, Vol. 21, No. 3, pp. 69-73, 1985. Translated by Plenum Publishing Corp. 0010-5082/85/2103-0333.

48. Azatyan, T. S., Mals'tsev, V. M., Merzhanov, A. G. and Seleznev, V. A., "Some Principles of Combustion of Titanium-Silicon Mixtures," Fizika Goreniya i Vzryva, Vol. 15, No. 1, pp. 43-49, January-February, 1979. Translated by Plenum Publishing Corp. 0010-5082/79/1501-0035.

49. Maksimov, Y. M., Pak, A. T., Lavrenchuk, G. B., Naiborodenko, Y. S. and Merzhanov, A. G., "Combustion of Gasless Systems," Fizika Goreniya i Vzryva, Vol. 15, No. 4, pp. 156-159, May-June, 1979. Translated by Plenum Publishing Corp. 0010-5082/79/1503-0415.

50. Merzhanov, A. G., Filonenko, A. K., Borovinskaya, I.P., "New Phenomena in Combustion of Condensed Systems," Doklady Akademii Nauk SSSR, Vol. 208, No. 4, 00.892-894, Feb. 1973. Translated by Plenum Publishing Corporation UDC 546.

51. Merzhanov, A. G. and Borovinskaya, I. P., "A New Class of Combustion Process," Combustion Science and Technology, Vol. 10, pp. 195-201, 1975.

52. Strunina, A. G., Butakova, E. A., Demidova, L. K. and Barzykin, V. V., "Combustion of Gasless Systems at Cryogenic Temperatures," Combustion, Explosion and Shock Waves, translated from Fizika Goreniya i Vzryva, Vol. 24, No. 2, pp. 99-102, March-April, 1988.

53. Miyamoto, Y., Nakamoto, T. and Koizumi, M., "Ceramic-to-Metal Welding by a Presurized Combustion Reaction," J. Mater. Res. 1 (1), Jan/Feb, 1986.

54. Yamada, O., Miyamoto, Y. and Koizumi, M., "Self-Propagating High-Temperature Synthesis of the SiC," J. Mater. Res., 1 (2), Mar/Apr 1986.

55. Yamada, O., Miyamoto, Y. and Koizumi, M., "High-Pressure Self-Combustion Sintering of Titanium Carbide," J. Am. Ceram. Soc., 70[9] C-206-C-208, 1987.

56. Quabdesselam, M. and Munir, Z. A., "The Sintering of Combustion-Synthesized Titanium Diboride," Journal of Materials Science, Vol. 22, pp. 1799-1807, 1987.

57. Manley, B., Holt, J. B. and Munir, Z. A., "Sintering of Combustion-Syntesized Titanium Carbide," Sintering and Heterogeneous Catalysis, Materials Science Research, Vol.16, Edited by G. C. Kuczynski, A. E. Miller, and G. A. Sargent, 1984.

58. Butakova, E. A. and Strunina, A. G., "Thermophysical Properties of Some Thermite and Intermetallic Systems," Fizika Goreniya i Vzryva, Vol. 21, No. 1, pp. 71-73, January-February, 1985. Translated by Plenum Publishing Corp. 0010-5082/85/2101-0067.

59. Maslov, V. M., Borovinskaya, I. P. and Ziatdinov, M. Z., "Combustion of the Systems Niobium-Aluminum and Niobium-Germanium," Fizika Goreniya i Vzryva, Vol. 15, No. 1, pp. 49-57, Jan-Feb 1979. Translated by the Plenum Publishing Corp. 0010-5082/79/1501-0041.

60. Rice, R. W., Richardson, G. Y., Kunetz, J. M. Schroeder, T. and McDonough, W. J., "Effects of Self-Propagating Synthesis Reactant Compact Character on Ignition, Propagation and Resultant Microstructure," Ceramics Engineering and Science Proceedings, Vol. 7, N0.7-8, pp. 737, 1986.

61. Aldushin, A. P., Merzhanov, A. G. and Khaikin, B. I., "Some Features of Combustion of Condensed Systems with High-Melting-Point Reaction Products," Doklady Akademii Nauk SSSR, Vol. 204, No. 5, pp. 1139-1142, June, 1972. Translated by Plenum Publishing Corp., UDC 536.46.

62. Kovalenko, Y. A., "Limiting Conditions for Steady Gasless Combustion with Heat Transfer at a Wall," Fizika Goreniya i Vzryva, Vol. 23, No. 6, pp. 61-65, Nov-Dec 1987. Translated by Plenum Publishing Corp. 0010-5082/87/2306-0720.

63. Strunina, A. G., Ermakov, V. I. and Barzykin, V. V., "Influence of Heat Losses and Thermophysical Parameters on the Ignition Process of Gasless Systems of Wave Combustion," Fizika Goreniya i Vzryva, Vol. 14, No. 4, pp. 42-50, July-August 1978. Translated by Plenum Publishing Corp. 0010-5082/78/1404-0441.

64. Strunina, A. G., Ermakov, V. I. and Averson, E. A., "Limiting Conditions of Ignition of Gasless Systems by a Combustion Wave," Fizika Goreniya i Vzryva, Vol. 15, No. 4, pp. 77-84, July-Aug 1979. Translated by the Plenum Publishing Corp. 0010-5082/79/1504-0484.

65. Strunina, A. G., Demikova, L. K., Firsov, A. N. and Merzhanov, A. G., "Stability of Gasless System Combustion in the Presence of Heat Losses," Fizika Goreniya i Vzryva, Vol. 23, No. 3, pp. 52-58, May-June 1987. Translated by Plenum Publishing Corp. 0010-5082/87/2303-0294.

66. Dvoryankin, A. V., Strunina, A. G. and Ivleva, T. P., "Temperature Fields and Combustion Stability in Gasless Systems," Combustion, Explosion and Shock Waves, translated from Fizika Goreniya i Vzryva, Vol. 24, No. 4, pp. 93-98, July-April, 1988.

67. Lyubchenko, V. I. and Marchenko, G. N., "Non-Adiabatic Regimes of Gasless Combustion of Reacting Condensed Substances," Doklady Akademii Nauk SSSR, Vol. 298, No. 3, pp. 645-650, January, 1988. Translated by Plenum Publishing Corp. 0012-5016/88/0001-0081.

68. Aldushin, A. P., Lugovoi, V. D., Merzhanov, A. G. and Khaikin, B. I., "Conditions for Degeneration of a Steady Combustion Wave," Sov. Phys. Dokl., 23(12), December,1978; Translated by American Institute of Physics, 1979, 0038-5689/78/12 0914-03.

69. Aleksandrov, V. V., Davydenko, A. A., Kovalenko, Y. A. and Poddubnyi, N. P., "Influence of Two-Dimensionality of the Front with Heat Losses on the Limits of Stationary Gasless Combustion," Fizika Goreniya i Vzryva, Vol. 23, No. 2, pp. 70-80, March-April, 1987. Translated by the Plenum Publishing Corporation 0010-5082/87/2302-0182.

70. Varma, A., Cao, G. and Morbidelli, M.; "Self-Propagating Solid-Solid Noncatalytic Reactions in Finite Pellets," AIChE Journal, Vol. 36, No. 7, pp. 1032-1038, July 1990.

71. Grosshandler, W. L., Editor, "Research Needs in Direct Combustion Synthesis," Summary of a National Science Foundation Workshop in February 21-22, 1990, Division of Chemical and and Thermal Systems, NSF, Washington, D.C. July. 1990.

72. Doraiswamy, L. K. and Sharma, M. M., Heterogeneous Reactions, Analysis, Examples and Reactor Design, Vol. 1 Gas Solid and Solid-Solid Reactions, 1984, John Wiley and Sons.

73. Harrison, L. G., "The Theory of Solid Phase Kinetics," Chapter 5, pp. 377-462 in Comprenhensive Chemical Kinetics, Vol. 2: The Theory of Kinetics, (C. H. Bamford and C. F. H. Tipper, Editors), Elsevier, Amsterdam, 1969.

74. Jost, W., Diffusion in Solids, Liquids and Gases, Academic Press, New York, NY, 1952.

75. Glasstone, S., Laidler, S. J. and Eyring, H., The Theory of Rate Processes, McGraw-Hill, New York, NY, 1941.

76. Hauffe, K., Oxidation in Metals, Plenum Press, New York, NY, 1965.

77. Kofstad, P., High-Temperature Oxidation of Metals, John Wiley, New York, NY, 1966.

78. Haasen, P., Physical Metallurgy, Cambridge University Press, London, England, 1978.

79. Carter, R. E., "Kinetic Model for Solid State Reactions," The J. of Chemical Physics, 34(6), pp. 2010-2015, 1961.

80. Sarian, S., Journal of Applied Physics, Vol. 40, pp. 3515, 1969.

81. Kulkarni, A. K., Kumar, M. and Kuo, K. K., "Review of Solid-Propellant Ignition Studies," AIAA Journal, Vol. 20, No. 2, Febrero 1982.

82. Kuo, K. K., Principles of Combustion, John Wiley and Sons, 1986.

83. Kuo, K. K. and Summerfield, M., "Fundamentals of Solid-Propellant Combustion," Progress in Astronautics and Aeronautics Series, Vol. 90, 1984.

84. Kanury, M. A., Introduction to Combustion Phenomena, Gordon and Breach Science Publishers, Combustion Science and Technology, V. 2, 1984.

85. Glassman, I., Combustion, Academic Press, 2nd. Ed. 1987.

86. Anderson, D. A., Tannehil, J. C. and Pletcher, R. H., Computational Fluid Mechanics and Heat Transfer, Mc Graw-Hill, 1984.

87. Thermophysical Properties of Matter, The TPRC Data Series, V.4-5, "Specific Heat of Metallic and Non-metallic Elements and Alloys," Y.S Touloukian and E. H. Buyco, Editors, IFI/Plenum, New York-Washington, 1970.

88. User Manual for DT2801 Series, Document UM-0066-D-1855, Data Translation , Inc., January 1981.

89. User Manual for PCLab, Document UM-02899-A, Data Translation, Inc., January, 1982.

90. Hot Spot Application Manual, DCC Corporation, Pennsauken NJ, January 1986.

91. Maslov, V. M., Borovinskaya, I. P. and Merzhanov, A. G., "Problem of the Mechanism of Gasless Combustion," Fizika Goreniya i Vzryva, Vol. 12, No. 5, pp. 703-709, Sept-Oct, 1976. Translated by the Plenum Publishing Corp.

92. Eslamloo-Grami, M. and Munir, Z. A., "Effect of Porosity on the Combustion Synthesis of Titanium Nitride," Journal of American Ceramic Society, 73, [5], pp. 1235-1239, 1990.

93. Powder Diffraction File, International Centre for Diffraction Data, JCPDS, Swarthmore, Pennsylvania, 1987.

94. Petersen, R. G., Design and Analysis of Experiments, Marcel Dekker, Inc., New York and Basel, 1985.

95. Benedict, R. P., "Engineering Analysis of Experimental Data," Journal of Engineering for Power, Transaction of the ASME, pp. 21-30, January, 1969.

APPENDICES

APPENDIX 1

EXPERIMENTAL ERROR ANALYSIS

From mathematical analysis, for the case when the dependent variable Y is a given function of independent variables X_1, X_2, X_3,...,X_n, W_Y is the uncertainty interval for the quantity Y, and W_1, W_2, W_3,...,W_n are the uncertainty intervals for the independent variables, W_Y is given as:

$$W_Y^2 = \left(\frac{\partial Y}{\partial X_1}W_1\right)^2 + \left(\frac{\partial Y}{\partial X_2}W_2\right)^2 + \ldots\ldots + \left(\frac{\partial Y}{\partial X_n}W_n\right)^2 \qquad (A.1)$$

if the uncertainties in the independent variables are all given with the same odds. In Equation (A.1), $Y = f(X_1, X_2, \ldots, X_n)$ and the independent variables X_1, X_2, ..., X_n are measured quantities. If Y is comprised of products and quotients of the measured variables, then the following equation can be obtained from equation (A.1):

$$\frac{W_Y^2}{Y^2} = \frac{W_{X1}^2}{X_1^2} + \frac{W_{X2}^2}{X_2^2} + \ldots\ldots + \frac{W_{Xn}^2}{X_n^2} \qquad (A.2)$$

In our experiments the speed of propagation, u, was

determined simply by dividing the distance by the time. The distance, x, was the gap between the thermocouples beads, typically 7 mm, and the time, t, was measured as the time difference for the thermocouples on each side of the gap to reach some established temperatures. The time differences were typically from about 0.5 to 0.8 seconds. The smallest distance that could be read from the scale used to measure the gap between thermocouples was 1 mm and the voltage readouts from the thermocouples were taken every 1/400 sec. Thus, if we apply Equation (A.2) to the definition of velocity u=x/t, we obtain the square of the relative error in the speed measurement:

$$\frac{W_u^2}{u^2} = \frac{W_x^2}{x^2} + \frac{W_t^2}{t^2} \qquad (A.3)$$

For the typical values used in the experiments, we obtain:

$$\frac{W_u^2}{u^2} = \left(\frac{1\ \text{mm}}{7\ \text{mm}}\right)^2 + \left(\frac{1/400}{.5\ \text{---}\ .8}\right)^2 \qquad (A.4)$$

$$\frac{W_u^2}{u^2} = (.1428)^2 + (.005\ \text{---}\ .003)^2 \qquad (A.5)$$

From the relative values of each term in this equation, we see that by far the single most important factor that will

affect the speed measurement is the gap between thermocouples. The second term can be considered negligible as compared to the first term.

There is not too much that can be done about reducing this relative error, since the dimensions of the samples are a constrain in the size of the gap between thermocouples (see Chapters 6 and 7). Only when the samples were much larger than the typical 20-23 mm lengths used, could a larger gap be set, thus reducing the relative error in the measurement.

The results from our experiments depend on various other factors that could be of larger impact than the one given by the relative error in the gap measurement. For instance, the mixing process described in Chapter 6, could possibly be a parameter of the SHS problem, since too short of a mixing process may fail to ensure uniformity in the mixture while too long a mixing process would allow oxidation of the reactants. The process of thermal treatment also affects the experimental output. When no heat-treatment was performed, there was not a propagation of the reacting wave and for low range heat-treatment (around 350 °C) there was a mixed set of results, some samples would react while some other samples would only partially react. Errors introduced by the experimenter could also be of some effect, some probably unidentified .

The important task of measuring significant errors (independently of any assumed curve fit of the data), was approached by performing a number of experiments at every condition (mole ratio, diameter, dilution, etc.) to determine the replicability of the output data. Some scatter in the data is observed (see Chapter 7). Previous investigations have noted that even in experiments conducted by the same investigator, scatter of data is unavoidable [94, 95]. In our experiments, this scatter is believed to be mainly due to the unavoidable nonuniformity in the mixing of the reactant powders and in the compaction density.

From the experimental replications it is possible to determine the best values of the speed, within some confidence intervals, for each point. By using this best values a curve fit can be found (given in Chapter 7). Benedict [95] establishes that "the best estimate of the value of the population mean at a given input is the average of the available measurements." Thus, we are left with determining the confidence intervals of the replications, which in our case, will be considered as a "small size" data. For small number of replications N, the standard deviation σ is given by:

$$\sigma = \left[\frac{1}{N-1}\sum_{i=1}^{N}(X_i-\overline{X})^2\right]^{1/2} \qquad (A.6)$$

where X_i is the value of the i-th observation and $\bar{X}$ is the mean value of the observation. By using this standard deviation for small number of replications N, an estimate of the true value $\bar{X}'$ of X can be found from:

$$\bar{X}' = \bar{X} \pm \frac{t_{N-1,p}\sigma}{\sqrt{N}} \qquad (A.7)$$

where the ± quantity indicates the desired confidence interval. This quantity can be determined form tabulated data found in any statistical text [94, 95], under the name Student t-distribution. With a 90% confidence interval, Table A.1 provides the best estimates of propagation velocity from the experimental data. These values are plotted in an error-bar fashion in Figures A1, A2 and A3. Based on these best estimates, the data is curve fitted and the corresponding equations are provided in Chapter 7.

Table A.1 Estimation of the Best Propagation Speed Value Using a 90% Confidence Interval.

Sample Diameter (cm)	Propagation Speed (cm/sec)
0.84	0.87 ± 0.06
1.28	0.84 ± 0.08
1.60	0.94 ± 0.05
2.08	0.87 ± 0.08
Mole Ratio a	
0.6	0.47 ± 0.06
0.7	0.57 ± 0.08
0.8	0.75 ± 0.07
0.9	0.84 ± 0.09
1.0	0.94 ± 0.05
1.2	0.82 ± 0.08
1.4	0.65 ± 0.05
1.6	0.61 ± 0.07
% of Dilution with Product	
0	0.94 ± 0.05
5	0.86 ± 0.09
10	0.77 ± 0.08
15	0.53 ± 0.08
20	0.38 ± 0.04
25	0.27 ± 0.10

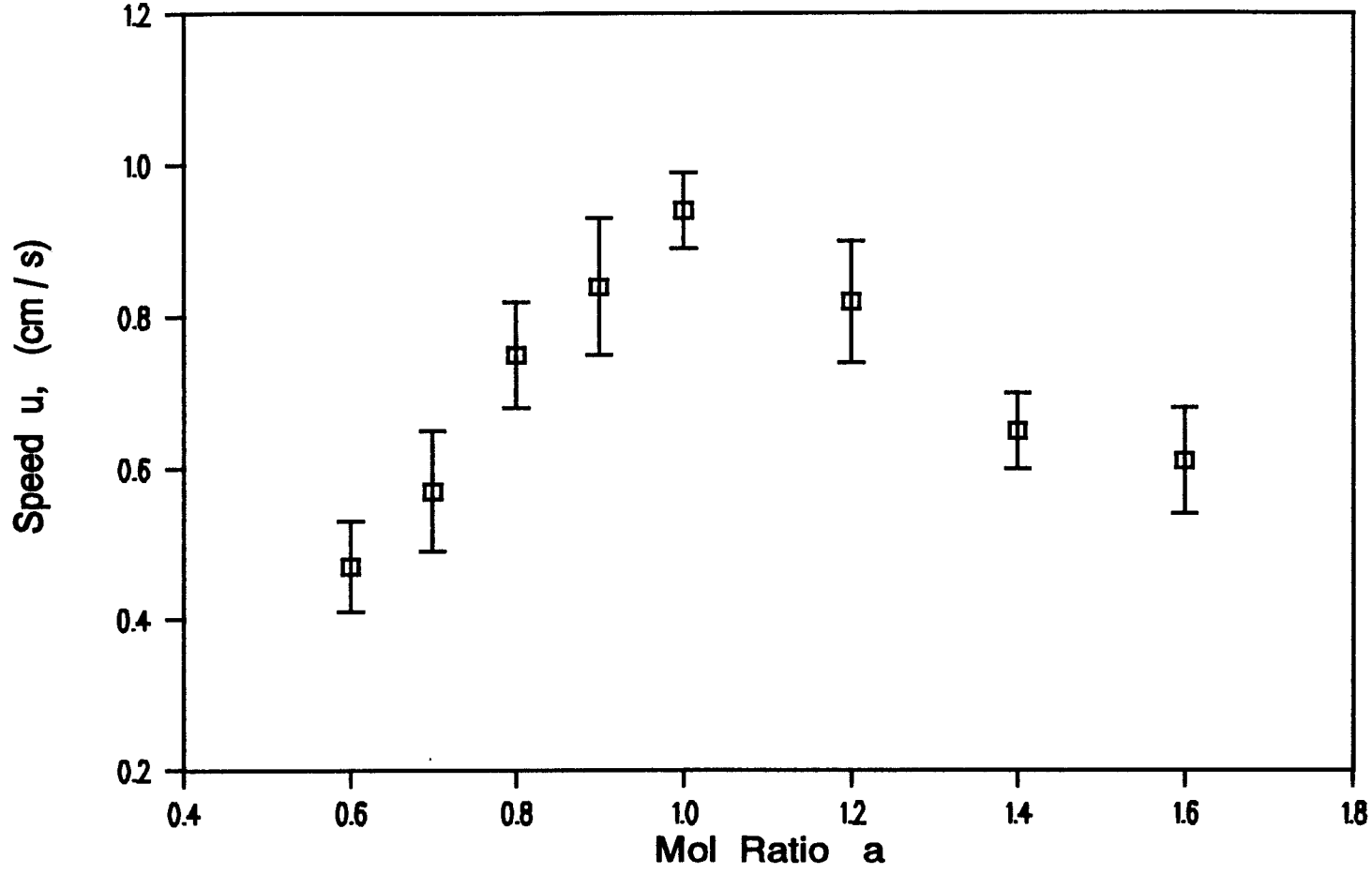

Figure A.1 Best Estimate of the Propagation Velocity as a Function of Mole Ratio.

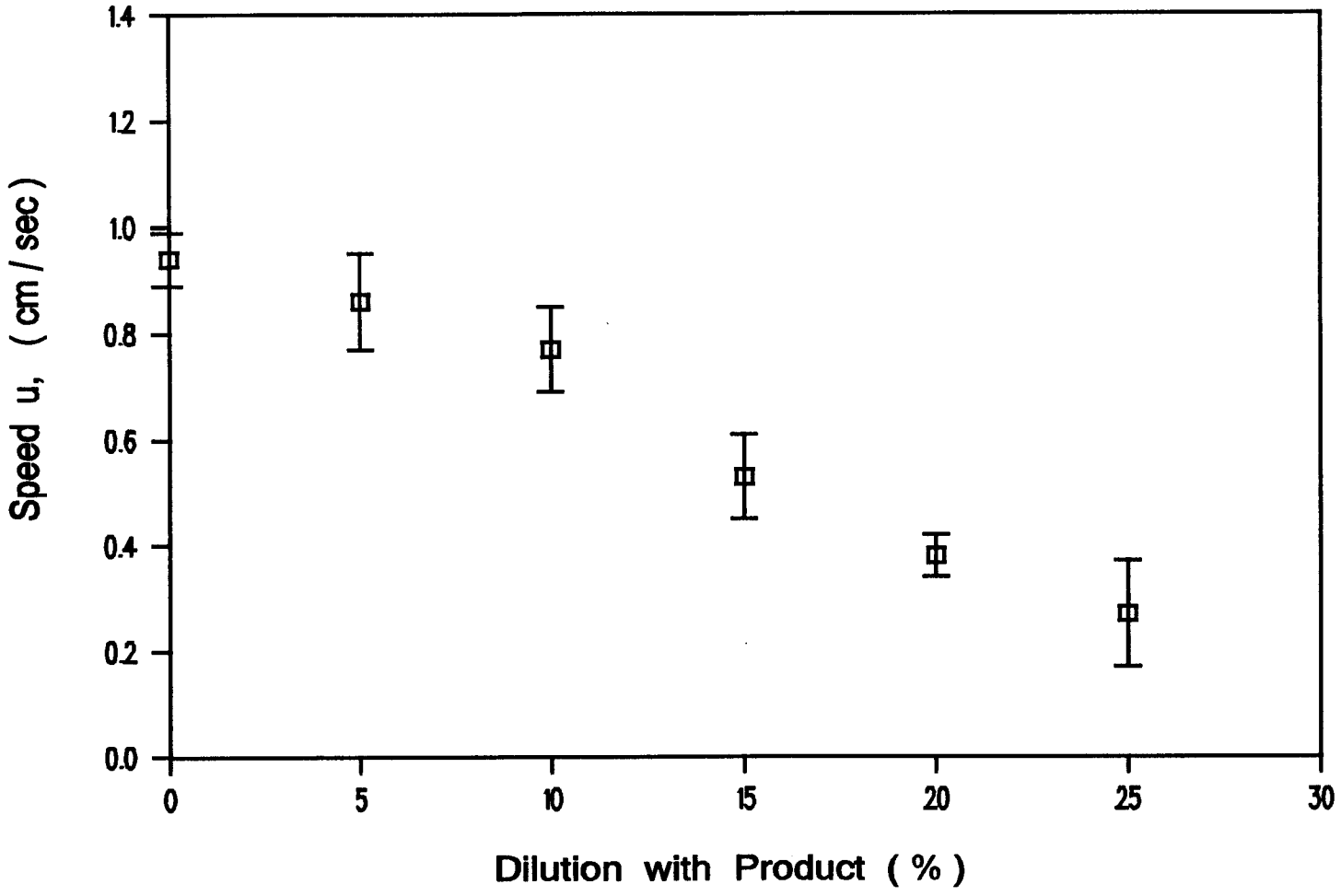

Figure A.2 Best Estimate of the Propagation Velocity as a Function of Dilution with Product.

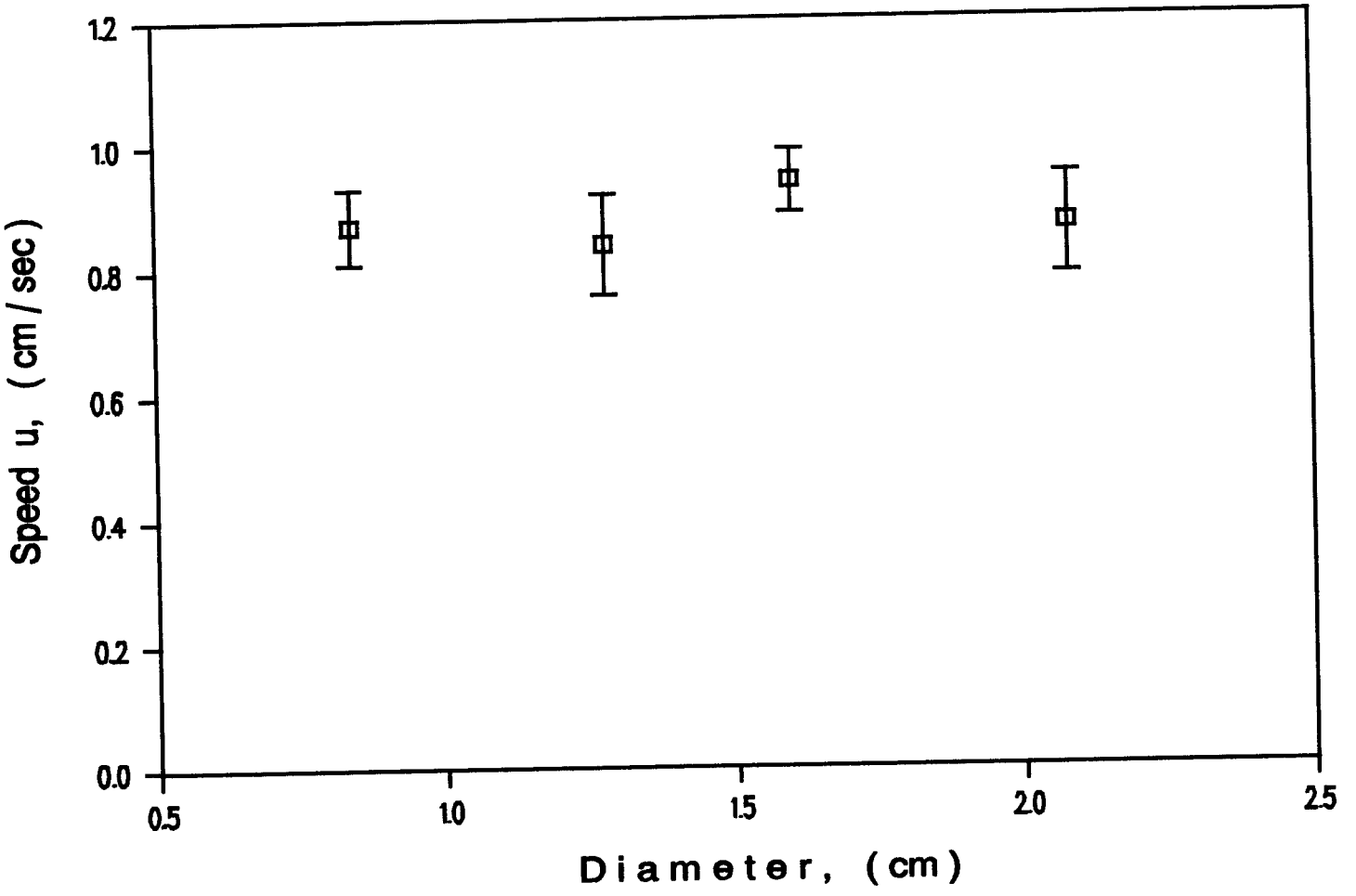

Figure A.3 Best Estimate of the Propagation Velocity as a Function of the Diameter of the Sample.

APPENDIX 2

FORTRAN CODE USED IN THE STUDY

```
C          SELF-PROPAGATING HIGH-TEMPERATURE SYNTHESIS
C          THIS CODE IS WRITTEN FOR A DIMENSIONLESS
C                    MODEL IN A 1-D FORMAT
C          THE PROGRAM WILL DETERMINE THE CONDITIONS UNDER
C          WHICH IGNITION WILL OCCUR AND IT WILL ALSO
C          CALCULATE THE SPEED OF PROPAGATION OF A SHS
C          REACTION WAVE ALONG A VERTICAL CYLINDRICAL
C          REACTANT COMPACT MIXTURE OF TITANIUM AND CARBON
C               THE CHEMICAL REACTION IS OF THE KIND:
C
C                        C + a Ti + b TiC  -->
C
C          WHERE a INDICATES IF THE REACTION IS RICH-Ti OR
C          LEAN-Ti CASE. a=1 INDICATES A STOICHIOMETRIC
C          REACTION, a>1 IS RICH-Ti AND A<1 IS LEAN-Ti.
C          INDICATES DILUTION OF THE INITIAL MIXTURE WITH
C                          PRODUCT TiC        .
C
C          DESCRIPTION OF THE NAMES USED IN THIS CODE
C          N=NUMBER OF AXIAL NODES
C          THETANEW(I)=MOST CURRENT VALUE OF THETA
C          THETAOLD(I)=OLD VALUE OF THETA
C          THETAIT(I)="DUMMY" OR THETA OF ITERATION
C          THE SAME APPLIES TO THE VARIABLES FOR PHI AND
C          DELTA
C          UPPER(I), XLOWER(I), ALPHA(I), GAMMA(I), Z(I)
C          AND DIAG(I) ARE VARIABLES USED IN THE SOLUTION
C          OF THE TRIDIAGONAL ROUTINES
C          ZETA= ZELDOVICH NUMBER
C          H= STEFAN NUMBER
C          THETAO=INITIAL (OR ROOM) TEMPERATURE
C          TR=REFERENCE TEMPERATURE
C          TADIAB=ADIABATIC TEMPERATURE
C          THOT=TEMPERATURE AT THE TOP SURFACE
C          THETAHOT=DIMENSIONLESS TEMPERATURE AT TOP SURFACE
C          THETAO=DIMENSIONLESS INITIAL TEMPERATURE
C          CTIO=INITIAL CONCENTRATION OF TITANIUM
C          ALPHAR=REFERENCE THERMAL CONDUCTIVITY
```

```
C          POWER, HZDA, DASTAR, C1, C2, A1, AMINUS1,BPLUS1
C          XMRHOTI, XMROTIC, SOURCE,DELTA3, ETC. ARE
C          VARIABLES USED TO MAKE THE PROGRAM MORE EFFICIENT
C          SO REPETITIVE CALCULATIONS ARE DONE ONLY ONCE
C          SOME OTHER VARIABLES ARE STRAIGHT FORWARD TO
C          UNDERSTAND FROM THE ANALYSIS
C          IMPRIMIR=SETS THE NUMBER OF INTERVALS OF DELTA
C                   TIME THAT WILL PASS BEFORE DATA IS SENT
C                   TO FILE IN UNIT 2 (USUALLY NAMED *1.PRN)
C          ICOUNTER= COUNTER FOR VARIABLE IMPRIMIR
C          IFILE2= SETS THE NUMBER OF INTERVALS OF DELTA TIME
C                   THAT WILL PASS BEFORE DATA IS SENT TO
C                   FILE IN UNIT 6 (USUALLY NAMED *2.PRN)
C          ICUENTA=COUNTER FOR VARIABLES IFILE2 AND DE2A3
C          DE2A3= SETS THE MAXIMUM TIME TAU THAT WILL BE
C                 STORED IN UNIT 6. AFTER THIS TIME DATA WILL
C                 BE SENT TO UNIT 7 (NAMED USUALLY *3.PRN.
C                 THIS ALLEVIATES THE DATA LOAD FOR *2.PRN.
C          UNIT 11 IS LEFT READY IN CASE SOME MORE DATA IS
C          NEEDED
C          TAUMAX=SETS AN UPPER LIMIT TO CALCULATIONS.
C          HOWEVER THE MAIN CRITERION USED TO STOP THE RUN IS
C          WHEN A GIVEN NODE HAS FULLY BURNED (I.E. PHI OR
C          DELTA ARE 0)
C          DY=DIMENSIONLESS NODAL DISTANCE
C          DYN="SEMI-INFINITE" TOTAL DIMENSIONLESS DISTANCE
C          DTIME=DIMENSIONLESS TIME STEP
C          TIEMPO=CURRENT TOTAL TIME TAU
C          PERCENT=PERCENT FROM THE SCALE THETAO TO THETADIAB
C          THAT WILL BE APLIED TO THE UPPER SURFACE
C          RHS(I)=RIGHT HAND SIDE OF EQUATION I
C          ICHECK= VARIABLE USED TO CHECK IF CONVERGENCE IN
C          THE MOST CURRENT ITERATION HAS BEEN ACHIEVED
C
        PROGRAM SHS
C     ******************************************************
        PARAMETER (N=600)
        REAL*8 THETANEW(N+1),THETAOLD(N+1), THETAIT(N+1),
     & PHINEW(N)
        REAL*8 PHIOLD(N+1),DELTANEW(N+1),DELTAOLD(N+1),
     & DIAG(N)
        REAL*8 UPPER(N), XLOWER(N), ALPHA(N), GAMMA(N),
     & Z(N),RHS(N)
        REAL*8 ZETA,POWER, THETAHOT, THETAO, SOURCE, TR
     & TADIABAT, CTIO, HZDA
        REAL*8 ALPHAR, RHOMIX, CPMIX, XKMIX, THOT, XMCMMIX,
     & H, RHOHAT, DASTAR
        REAL*8 C1, C2, A1, AMINUS1, BPLUS1, XMRHOTI, XMROTIC,
     & DYN, XALPHAR
        REAL*8 TIEMPO, DELTA3, A, B, DA, PERCENT, CPHAT,
```

```
     & TEMPAD, DE2A3
C
       OPEN(UNIT=2,FILE='91.prn',STATUS='unknown')
       OPEN(UNIT=6,FILE='92.prn',STATUS='unknown')
       OPEN(UNIT=7,FILE='93.prn',STATUS='unknown')
       WRITE (2,*) '5e5dy1'
       WRITE (6,*) '5e5dy1'
       WRITE (7,*) '5e5dy1'
C
C      OPEN(UNIT=11,FILE='a14d100.prn',STATUS='unknown')
C      WRITE (11,*) 'sa14d100'
C     ****************************************************
C                  SPECIFIC DATA FOR THIS RUN
C      INDICATE IF THERE IS LACK OR EXCESS OF Ti
                          A=1.D0
C      INDICATE IF THERE IS PRODUCT DILUTION IN INITIAL
C      MIXTURE
                          B=0.D0
C      ENTER THE DAMKOHLER NUMBER
                         DA=.1D0
C      ENTER THE PERCENT OF TADIABAT TO BE APPLIED TO THE
C      TOP SURFACE
                  PERCENT=1.0D0
C
C     ****************************************************
C         NOW WE SET THE PRINTING PARAMETERS. IMPRIMIR SETS
C
       IMPRIMIR=100
       IFILE2=20000
       TAUMAX=250.D0
       DY=.1D0
       DTIME=.00005D0
       DE2A3=150.D0
C
C     ****************************************************
C                               CONSTANTS
C      FIRST THE MOLECULAR WEIGHTS
         XMCARBON=12.D0
         XMTI=48.D0
         XMTIC=60.D0
C      THEN DENSITIES
         DTI=4.54D0
         DTIC=4.95D0
C      GAS CONSTANT IN cal/(mol K)
         RGASES=1.987D0
C      BOTZMANN CONSTANT IN W/(m2 K4)
C         SIGMAR=5.676D-08
C      THE RELATIVE VALUES FOR DENSITY, CP AND K
         RHOR=2200.D0
         CPR=950.D0
```

```
          XKR=1.67D0
          ALPHAR=XKR/(RHOR*CPR)
C       NOW THE MIXTURE DENSITY, CP AND K
C       HOWEVER, THE VALUES FOR CP ARE FUNCTIONS OF a AND b
C       THUS, TO EVALUATE CPMIX WE NEED TO ENTER THE VALUES
C       FOR CPc,CPti AND CPtic EVALUATED AT 1400 K.
          RHOMIX=RHOR
          XKMIX=XKR
C       NOW THE CP'S IN J/kg K
        CPC=1964.D0
        CPTI=698.D0
        CPTIC=890.D0
C
           CPMIX=(12.*CPC+48.*A*CPTI+60.*B*CPTIC)/ (12.+
     &           48.*A+ 60.*B)
C       NOW THE REST OF PARAMETERS USED IN ENERGY EQUATION
C       ENTHALPY OF COMBUSTION IN J/(kg OF C)
          HC=1.5257D+07
C       NOW IN J/(kg OF TiC)
          HCTIC=3051400.D0
C       ACTIVATION ENERGY
          E=33000.D0
C       EMMISIVITY OF THE MIXTURE
C         EPSILON=.8D0
C       INITIAL TEMPERATURE OF SAMPLE AND SURROUNDINGS
          To=300.D0
C
C     ***************************************************
C               REFERENCE TEMPERATURE, TEMP TOP SURFACE
C
        TADIABAT= To + HCTIC / CPR
             TR = TADIABAT
           THOT= TADIABAT * PERCENT
C
C       THE ADIABATIC TEMPERATURE IF NONSTOICHIOMETRIC IS
        IF (A.GT.1.) THEN
               TEMPAD=To + HCTIC/((A-1)*CPTI +(1+B)*CPTIC)
                     ELSE
               TEMPAD=To + A*HCTIC/((1-A)*CPC +(A+B)*CPTIC)
        ENDIF
C
C     ***************************************************
C                DETERMINE VALUE OF PARAMETERS
C
               XMCMMIX=XMCARBON/(XMCARBON + XMTI*A + XMTIC*B)
C
                 CTIO = A/(A*XMTI/DTI + B*XMTIC/DTIC)
C
                     H=HC/(CPR*TR)
                  ZETA=E/(RGASES*TR)
```

```
                RHOHAT=RHOMIX / RHOR
                 CPHAT=CPMIX/CPR
            IF (A.EQ.1.D0 .AND. B.EQ.0.D0) THEN
                 CPHAT=1.D0
            ENDIF
C        WRITE (*,*) CPMIX,CPR,CPHAT
C       STOP
C
C      NEXT FACTORS WILL APPEAR IN THE NUMERICAL ITERATIONS
C        THEY ARE CALCULATED HERE FOR EFFICIENCY
C
                  HZDA=H*ZETA*DA
                DASTAR=DA/(RHOHAT*XMCMMIX)
                    C1=DTIME/RHOHAT/CPHAT
                    C2=C1*HZDA
                    A1= DTIME/RHOHAT/CPHAT/DY**2.
              AMINUS1=A-1.D0
               BPLUS1=B+1.D0
              XMRHOTI=XMTI/DTI
             XMROTIC=XMTIC/DTIC
C
C     ****************************************************
C         THE DIMENSIONLESS TEMPERATURES ARE EVALUATED NOW
C
C       TEMPERATURE AT THE TOP SURFACE
              THETAHOT=ZETA*(THOT/TR-1.D0)
C       TEMPERATURE EVERYWHERE AT TAU<0
               THETAO=ZETA*(To/TR-1.D0)
C       TEMPERATURE OF SURROUNDINGS
C             TETAINF=ZETA*(300./TR-1.D0)
C     ****************************************************
C           NOW LOTS OF WRITING TO FILES
C
          WRITE(2,700) A,B,DA
 700      FORMAT(F7.2,F7.2,F7.2)
C
          WRITE(2,710) THOT,PERCENT,TADIABAT
 710      FORMAT(F10.4,F10.4,F8.2)
C
          WRITE(2,720) THETAO,THETAHOT
 720      FORMAT(F10.6,F10.6)
C
          WRITE(2,730) N
 730      FORMAT(I3)
C
          WRITE(2,740) CTIO,XMCMMIX
 740      FORMAT(F10.6,F8.4)
C
           WRITE(2,750) RHOR,RHOMIX,RHOHAT
 750      FORMAT(F10.3,F10.3,F7.3)
```

```
C
      WRITE(2,760) XKR,XKMIX,CPR,CPMIX
 760  FORMAT(F10.4,F10.4,F10.3,F10.3)
C
      XALPHAR=ALPHAR*1E7
      WRITE(2,770) XALPHAR
 770  FORMAT(F12.7)
C
C      WRITE(2,780)
C 780  FORMAT(/,'DIMENSIONLESS')
C
      DYN=DY*N
      WRITE(2,790) DY,DYN
 790  FORMAT(F8.4,F8.3)
C
      WRITE(2,800) DTIME,TAUMAX
 800  FORMAT(F10.6,F8.2)
C
      WRITE(2,810) H,ZETA
 810  FORMAT(F10.5,F10.5)
C
      WRITE (2,815) HZDA
 815  FORMAT(F8.2)
C
      WRITE(2,820) C1, C2
 820  FORMAT(F10.6,F10.6)
      WRITE (2,821) TEMPAD
 821  FORMAT(F8.2)
C
C     ****************************************************
C          INITIALIZE THE THETA, DELTA AND PHI FIELDS
C
C            THETANEW(0)=THETAHOT
C            THETAOLD(0)=THETAHOT
      DO 20 I=1,N
            THETANEW(I)=THETAO
            THETAOLD(I)=THETAO
             THETAIT(I)=THETAOLD(I)
              PHINEW(I)=1.D0
              PHIOLD(I)=1.D0
            DELTANEW(I)=1.D0
            DELTAOLD(I)=1.D0
 20   CONTINUE
C
C     WRITE THIS INITIAL PROFILE IN FILES
C      WRITE (6,*) THETAHOT
      DO 30, I=1,10
         WRITE(6,31) I,THETANEW(I),DELTANEW(I),PHINEW(I)
 30   CONTINUE
 31   FORMAT(I3,F10.5,F10.5,F10.5)
```

```
C
      WRITE(2,*) 'TIME',1,10,100,150,200
C
      WRITE (2,32) TIEMPO, THETANEW(1), THETANEW(10),
     & THETANEW(100), THETANEW(150),THETANEW(200)
 32   FORMAT(F8.2,F8.4,F8.4,F8.4,F8.4,F8.4)
C      STOP
C     ****************************************************
C        NOW WE SET UP THE LHS MATRIX AND FACTORIZE IT
C
           DIAG(1)=1.D0+2.D0*A1
         UPPER(1)=-A1
       XLOWER(N-1)=-A1
         DIAG(N-1)=1.D0+2.D0*A1
C
      DO 500 I=2, N-2
            XLOWER(I)=-A1
              DIAG(I)=1.D0+2.D0*A1
             UPPER(I)=-A1
 500  CONTINUE
C
      ALPHA(1)=DIAG(1)
      GAMMA(1)=UPPER(1)/ALPHA(1)
      DO 520 J=2, N-2
      ALPHA(J)=DIAG(J)-XLOWER(J)*GAMMA(J-1)
      GAMMA(J)=UPPER(J)/ALPHA(J)
 520  CONTINUE
C
      ALPHA(N-1)=DIAG(N-1)-XLOWER(N-1)*GAMMA(N-2)
C     ****************************************************
        WRITE (*,*) 'PROGRAM IS RUNNING'
C     !!!!!!!!!!!!!!!!!!!!!!!!!!!!!!!!!!!!!!!!!!!!!!!!!!!
C                  NOW COMPUTATIONS START
C
 100                TIEMPO=TIEMPO+DTIME
C
C      NEXT COUNTER KEEPS TRACK OF PRINTING
       ICOUNTER=ICOUNTER+1
       ICUENTA=ICUENTA+1
C
C      MATRIX SOLUTION STARTS HERE. WE FIRST SET UP THE RHS
C      FIRST NODE i=1
 120           POWER=(ZETA* THETAIT(1))/(ZETA+THETAIT(1))
               SOURCE=C2*PHIOLD(1)*DELTAOLD(1)*DEXP(POWER)
               RHS(1)=A1*THETAHOT + THETAOLD(1) + SOURCE
C
C      THEN THE REST OF NODES UPTO N-2
       DO 150 I=2,N-2
                POWER=(ZETA*THETAIT(I))/(ZETA+THETAIT(I))
               SOURCE=C2*PHIOLD(I)*DELTAOLD(I)*DEXP(POWER)
```

```
                RHS(I)=THETAOLD(I) + SOURCE
 150    CONTINUE
C
C       THEN LAST NODE i=N-1
                POWER=(ZETA*THETAIT(N-1))/(ZETA +
     &                THETAIT(N-1))
              SOURCE=C2*PHIOLD(N-1)*DELTAOLD(N-1)
     &                    *DEXP(POWER)
            RHS(N-1)=A1*THETAOLD(N)+THETAOLD(N-1)+SOURCE
C
C               NOW WE SOLVE THE TRIDIAGONAL MATRIX
C                     FIRST FORWARD SOLUTION
              Z(1)=RHS(1)/ALPHA(1)
        DO 180 J=2,N-1
              Z(J)=(RHS(J)-XLOWER(J)*Z(J-1))/ALPHA(J)
 180    CONTINUE
C                     THEN BACKWARD SOLUTION
             THETANEW(N-1)=Z(N-1)
        DO 200 J=N-2,1,-1
              THETANEW(J)=Z(J)-GAMMA(J)*THETANEW(J+1)
 200    CONTINUE
C
C            NOW WE CHECK FOR CONVERGENCE OF THETA SOLUTION
                   ICHECK=1
        DO 250 I=1,N-1
             IF (DABS(THETANEW(I)-THETAIT(I)).GT. .01D0) THEN
                   ICHECK=0
             ENDIF
 250    CONTINUE
C
             IF (ICHECK.EQ.0) THEN
                   DO 270 I=1,N-1
                     THETAIT(I)=THETANEW(I)
 270                 CONTINUE
                   GOTO 120
             ENDIF
C
C      NOW WE KNOW THE TEMPERATURE FIELD. DETERMINE PHI AND
C                    DELTA FOR EACH NODE
C
        DO 320 I=1,N-1
          IF (PHINEW(I).LT. .005D0 .OR. DELTANEW(I).LT.
     &                                      .005D0) THEN
                GOTO 320
          ENDIF
C
              POWER=(ZETA*THETAOLD(I))/(ZETA+THETAOLD(I))
            SOURCE=PHIOLD(I)*DELTAOLD(I)*DEXP(POWER)
            DELTA3=(DELTAOLD(I))**3. - DTIME*DASTAR*SOURCE
C       NOW WE AVOID TO RAISE A NEGATIVE NUMBER TO A POWER
```

```
                IF (DELTA3.LT. 0.D0) THEN
                                DELTA3=0.D0
                ENDIF
          DELTANEW(I)=DELTA3**(1./3.)
C
C          WRITE(*,*) DELTA3,DELTANEW(I)
          PHINEW(I)=(AMINUS1+(DELTAOLD(I))**3.)/((AMINUS1 +
     & (DELTAOLD(I))**3. )*XMRHOTI + (BPLUS1- (DELTAOLD(I)
     &                                    )**3.) *XMROTIC)
C
          PHINEW(I)=PHINEW(I)/CTIO

C       GOES TO ANOTHER NODE i+1 EVALUATION OF PHI AND DELTA:
 320    CONTINUE
C
C       ***************************************************
C             ANOTHER SCANNING OF THE SAMPLE IS FINISHED
C                 LETS CHECK IF IT IS TIME TO PRINT
          IF (ICUENTA.EQ.IFILE2) THEN
C
                    IF (TIEMPO.LT.DE2A3) THEN
                                      NUMBER=6
                                    ELSE
                                      NUMBER=7
                    ENDIF
C
                  WRITE (NUMBER,600) TIEMPO
 600                FORMAT(F8.3)
C
                    DO 610 I=1,N
          WRITE (NUMBER,620) I, THETANEW(I), DELTANEW(I),
     &      PHINEW(I)
 610                CONTINUE
 620                FORMAT(I3,F10.5,F10.5,F10.5)
C
                    ICUENTA=0
          ENDIF
C
          IF (ICOUNTER.EQ.IMPRIMIR) THEN
        WRITE(2,630)   TIEMPO,   THETANEW(1),   THETANEW(10),
     &     THETANEW(100),
     & THETANEW(150),THETANEW(200)
 630    FORMAT(F8.3,F9.5,F9.5,F9.5,F9.5,F9.5,F9.5)
C
                    ICOUNTER=0
C
          ENDIF
C     ***************************************************

C       NOW WE UPDATE THE VARIABLES
```

```
          DO 350 J=1,N-1
               THETAOLD(J)=THETANEW(J)
                THETAIT(J)=THETANEW(J)
               DELTAOLD(J)=DELTANEW(J)
                 PHIOLD(J)=PHINEW(J)
C
               IF (PHINEW(J). LT. .005D0) THEN
                  PHINEW(J)=0.D0
                  PHIOLD(J)=0.D0
               ENDIF

               IF (DELTANEW(J).LT. .005D0) THEN
                  DELTANEW(J)=0.D0
                  DELTAOLD(J)=0.D0
               ENDIF
 350     CONTINUE
C
C     ******************************************************
C                        CRITERIA TO STOP
C       NOW WE WILL CHECK IF THE LAST LAYER HAS ALREADY
C       IGNITED
          IF (PHINEW(210).LT. .005D0 .OR. DELTANEW(210).LT.
     &                                          .005D0) THEN
                    GOTO 7000
          ENDIF
C
C       OR IF WE HAVE EXCEEDED THE MAXIMUM COMPUTING TIME
          IF (TIEMPO.GT.TAUMAX .OR. DELTANEW(1).gt. 10.D0)
     &                                                THEN
             GOTO 7000
          ENDIF
C
C       IF NEITHER OF THESE CONDITIONS HAVE BEEN REACHED,
C         THEN IT IS TIME TO STEP FORWARD IN TIME AND DO
C               ANOTHER WHOLE SCANNING
C
                       GOTO 100
C     ******************************************************
C                         END END END END END
C       HERE WE WILL STORE THE LAST VALUES OF THETA, DELTA &
C                       PHI FIELDS
C
C 7000   IF (TIEMPO.LT.DE2A3) THEN
C                             NUMBER=6
C                           ELSE
C                             NUMBER=7
C        ENDIF
C
 7000   WRITE (NUMBER,7010) TIEMPO
 7010   FORMAT(F8.3)
```

```
C
C       write (number,*) 0,thetahot
        DO 7020 I=1,N
          WRITE(NUMBER,7025) I, THETANEW(I), DELTANEW(I),
     &                                          PHINEW(I)
 7020   CONTINUE
 7025     FORMAT(I3,F10.6,F10.6,F10.6)
C
        WRITE(2,7028) TIEMPO, THETANEW(1), THETANEW(10),
     & THETANEW(100), THETANEW(150),THETANEW(200)
 7028   FORMAT(F8.3,F9.5,F9.5,F9.5,F9.5,F9.5,F9.5)

        IF (PHINEW(N-1).LT .001D0 .OR. DELTANEW(N-1).LT.
     &                                    .001D0) THEN
            WRITE(11,*) 'sample burned all the way to n'
        ENDIF
C 7030  FORMAT(/,'SAMPLE BURNED ALL THE WAY TO N')
C
        IF (TIEMPO.GT.TAUMAX) THEN
        WRITE(11,*) 'TAUMAX IS SMALLER THAN TIME NEEDED TO
     &                                          BURN SAMPLE'
        ENDIF
C
C        TOTALCPU=CPU()
C        TOTALCPU=TOTALCPU/3600.D0
C        WRITE (2,7050) TOTALCPU
C 7050  FORMAT(/,'CPUTIME=',F10.6,'REAL COMPUTATION TIME IN
c     &  HOURS')
C        WRITE (2,*) 'TIME IS',TIME$
C        WRITE (2,*) 'DATE IS',DATE$
C        WRITE (2,*) 'STARTED',FECHA1$
C        WRITE (2,*) '   AT',TIEMPO1$
C
        END
```

APPENDIX 3

PC-LAB CODE FOR DATA ACQUISITION

```
1   '   THIS PROGRAM IS WRITTEN TO CONVERT THE VOLTAGES
2   '  OBTAINED THROUGH THE DATA ACQUISITION BOARD DIRECTLY
3   '            TO DEGREES KELVIN
3   '
4   '  WRITTEN BY:   ABEL HERNANDEZ-GUERRERO        JULY 1989
5   '
6   ' THE CONVERSION TABLES FOR THE PARTICULAR TYPE OF
7   ' THERMOCOUPLES USED IN THE EXPERIMENT (FROM THE OMEGA
8   ' COMPANY) HAVE BEEN FIT INTO CORRELATIONS, THEREFORE
9   ' THIS PROGRAM WILL NOT WORK WITH A DIFFERENT TYPE OF
10  '                  THERMOCOUPLES
11  ' THE PROGRAM IS SET SO THAT IT WILL SCAN BOTH
12  ' THERMOCOUPLES FOR THE WHOLE DURATION OF THE EXPERIMENT,
13  ' BUT IT WILL ASK THE OPERATOR HOW MANY SECONDS ARE TO BE
14  ' STORED IN THE HARD DISK. IN THIS WAY, IF A EXPERIMENT
15  ' TOOK 25 SECONDS BUT IT WAS OBSERVED THAT THE
16  ' PROPAGATION FINISHED IN ONLY 18 SECONDS ALL THE WAY
17  ' DOWN TO THE BOTTOM OF THE SAMPLE THEN ONLY 18 SECONDS
18  ' NEED TO BE STORED. IF IT IS JUDGED THAT DATA BELOW 1000
19  ' K ARE NOT NEEDED THEN THE OPERATOR CAN INSTRUCT TO DO
20  ' SO. THE DATA WILL BE STORED IN TWO FILES NAMED "two"
21  '                  AND "three"
21  '
25  ' PCLAB BASIC definition file (long names)
30  ' This file may be MERGEd with a user program
35  ' to define routine offsets and establish the PCLAB
40  ' segment.
50  ADC.VALUE=3                    : ADC.ON.TRIGGER=6
60  SETUP.ADC=9                     : ADC.SERIES=12
70  BEGIN.ADC.DMA=15                : TEST.ADC.DMA=18
80  WAIT.ADC.DMA=21                 : DAC.VALUE=24
90  DAC.ON.TRIGGER=27               : SETUP.DAC=30
100 DAC.SERIES=33                    : BEGIN.DAC.DMA=36
110 TEST.DAC.DMA=39                  : WAIT.DAC.DMA=42
120 SET.CLOCK.DIVIDER=45             : SET.SLOW.CLOCK=48
130 SET.CLOCK.FREQUENCY=51           : SET.CLOCK.PERIOD=54
140 ENABLE.FOR.INPUT=57              : ENABLE.FOR.OUTPUT=60
150 INPUT.DIGITAL.VALUE=63           : OUTPUT.DIGITAL.VALUE=66
```

```
160   INPUT.DIGITAL.ON.TRIGGER=69    :
OUTPUT.DIGITAL.ON.TRIGGER=72
170 SET.ERROR.CONTROL.WORD=75    : GET.ERROR.CODE=78
180 SELECT.BOARD=81              : SET.BASE.ADDRESS=84
190 SET.DMA.CHANNEL=87           : SET.ADC.RANGE=90
200 SET.ADC.CHANNELS=93          : SET.DAC.RANGE=96
210 SET.LINE.FREQUENCY=99        : SET.TOP.GAIN=102
220 SET.TIMEOUT=105              : GET.DT.ERROR=108
230 RESET.DT=111                 : GET.DT.STATUS=114
240 CALL.WFC=117                 : CALL.WFO=120
250 CALL.WFI=123                 : STOP.ADC.DMA=126
260 STOP.DAC.DMA=129             : CONTINUOUS.ADC.DMA=132
270 CONTINUOUS.DAC.DMA=135       : MEASURE.VOLTS=138
280 MEASURE.THERMOCOUPLE=141     : MEASURE.COMPENSATION=144
290 ANALOG.TO.VOLTS=147          : VOLTS.TO.DEGREES=150
300 DEGREES.TO.VOLTS=153         : DELAY=156
310 STROBE=159                   : WAIT.ON.DELAY=162
320 GENERATE.CLOCK=165           : COUNT.EVENTS=168
330 READ.EVENTS=171              : GET.FREQUENCY=174
340 STOP.CLOCK=177               : INITIALIZE=180
350 TERMINATE=183                : ISBX.READ=186
360 ISBX.WRITE=189               : FIND.DMA.LENGTH=192
370 ENABLE.SYSTEM.CLOCK=195      : DISABLE.SYSTEM.CLOCK=198
380 '
390 DEF SEG=&H0       ' get the PCLAB segment
400 PCLSEG = PEEK ( &H4FE ) + 256*PEEK ( &H4FF )
410 DEF SEG=PCLSEG    ' address the PCLAB segment
420 '
430 ' Copyright (C) 1983, 1987.    Data Translation, Inc.
100  Locke  Drive,
440 ' Marlboro Massachusetts 01752-1192.
450 '
460 ' General permission to copy or modify, but not for
461 ' profit, is hereby granted,  provided  that  the  above
462 ' copyright notice is included and reference made to the
463 ' fact that reproduction privileges  were  granted by
464 ' Data Translation, Inc.
500 '
510 PRINT " A/D CONVERSION SERIES"
520 PRINT
530 PRINT "This PCLAB program performs a series of A/D"
540  PRINT "conversions  on  an  operator-specified  channel
scan."
550 PRINT "This uses the Programmed I/O routine: ADC.SERIES"
560 PRINT
570 '       Tested: 28 Nov 83
580 '       Modified: 18 Jan 85 for PCLAB V2.0
590 '       Tested: 24 Nov 86 for PCLAB V3.0
600 '
610 '   All variables should be given initial values
```

```
620 '   before being used in PCLAB calls.
630 '
640 INPUT " TOTAL NUMBER OF SCANS : ", NUMBER.OF.VALUES%
650 DIM ANALOG.DATA.ARRAY%(NUMBER.OF.VALUES%)
660 ERROR.VALUE% = 0
670 '
680 CALL INITIALIZE
710 '
720 CALL SET.ERROR.CONTROL.WORD(ERROR.VALUE%)
730 '
740 HIGH.V! = .045                'Highest voltage in range
750 LOW.V! = -.045                 'Lowest voltage in range
760 RANGE! = HIGH.V! - LOW.V!        'Total voltage range.
770 '
780 NOC! = 4096!
790 '
800 LSB! = RANGE! / NOC!     'Voltage of least Significant
Bit.
810 '  The following section sets up the A/D.
820 '
830 TIMING.SOURCE% = 0         ' Software trigger, internal
clock.
840 '
850 'Select the proper board here.
860 BOARD% = 3
870 CALL SELECT.BOARD(BOARD%)
880 ' Define channel scan.
890 '
920 '
940  INPUT  "  Enter  the  first  channel  in  the  scan  ",
START.CHAN%
950 INPUT " Enter the last channel in the scan ", END.CHAN%
960 '
970 IF (START.CHAN% <= END.CHAN%) GOTO 1020
980 PRINT " The starting channel number";
990  PRINT  "cannot  be  greater  than  the  ending  channel
number."
1000 GOTO 940
1010 '
1020 SCAN.LENGTH% = (END.CHAN% + 1) - START.CHAN%
1030 NUMBER.OF.SCANS% = (NUMBER.OF.VALUES% / SCAN.LENGTH%)
- 1
1040  PRINT  "  This  will  perform  "; NUMBER.OF.SCANS%;  "
complete scans."
1050 '
1055 INPUT "MINIMUM TEMPERATURE TO WRITE";LIMIT
1060 INPUT " Enter the desired Gain (1,2,4,8) ", GAIN%
1070 '
1080 CALL SETUP.ADC(TIMING.SOURCE%, START.CHAN%, END.CHAN%,
GAIN%)
```

```
1090 CALL GET.ERROR.CODE(ERROR.VALUE%)
1091 PRINT "error= ";ERROR.VALUE%
1100 IF ERROR.VALUE% = 0 GOTO 1130
1110 PRINT "*** Illegal channels or gain specified.": GOTO
940
1120 '
1130 'SCALED.LSB! = LSB! / GAIN%          'Calculate scaled
LSB
1140 'SCALED.LOW! = LOW.V! / GAIN%        'Calculate scaled
LOW voltage.
1145 '
1150 CJCHAN% = 0
1151 TYPE%=116
1153 'CALL MEASURE.VOLTS(CJCHAN%,VOLTS!)
1154 '
1155 PRINT "GAIN =";GAIN%,"VOLTS =";VOLTS!
1160 CALL ADC.VALUE(CJCHAN%, GAIN%, CJADATA%)
1170 CJTEMP = (((CJADATA% * .04) / 4096) - .02) * 2000
1171 CALL DEGREES.TO.VOLTS(TYPE%,CJTEMP,CJVOLTS)
1172 PRINT "CJVOLTS=";CJVOLTS
1175 PRINT "CJADATA =";CJADATA%,"CJTEMP =";CJTEMP
1180 ' Next set up the internal clock.
1190 '
1200  INPUT " Enter the sampling frequency in Hz (13. -
12000.) ",REQUESTED.FREQ
1210 CLOCK.DIVIDER% = (800000! / REQUESTED.FREQ) - .5
1220 ACTUAL.FREQ = 800000! / CLOCK.DIVIDER%
1230 PRINT "Actual frequency is ";ACTUAL.FREQ;" Hertz"
1240 PRINT "Please wait ..... I'm working."
1250 'PRINT " Requested frequency is "; REQUESTED.FREQ; "
Hertz"
1260 'PRINT " "
1270 'PRINT " Please wait.... I'm working."
1280 '
1290 'CALL ADC.VALUE(CJCHAN%, GAIN%, CJADATA%)
1300 'CJTEMP = (((CJADATA% * .04) / 4096) - .02) * 2000
1310 'CALL SET.CLOCK.FREQUENCY(REQUESTED.FREQ)
1320 CALL SET.CLOCK.DIVIDER (CLOCK.DIVIDER%)
1330 '
1340 ' This performs the actual data collection.
1350 '
1360 CALL DISABLE.SYSTEM.CLOCK      ' Turn off PC's time of
day clock.
1370    CALL    ADC.SERIES(NUMBER.OF.VALUES%,
ANALOG.DATA.ARRAY%(1))
1380 CALL ENABLE.SYSTEM.CLOCK       ' Turn on PC's time of
day clock.
1390 CALL GET.ERROR.CODE(ERROR.VALUE%) ' Clear any error
status
1400  IF  ERROR.VALUE%  <>  0  THEN  PRINT  "Error  during
```

```
acquisition. ", ERROR.VALUE%
1410 '
1420 ' Now ask for scan number to translate and display.
1430 '
1440 PRINT
1450  'INPUT "  Do you want to save the data on your
diskette?(Y or N)"; ANS$
1455 ANS$="Y"
1460 IF ANS$ = "N" OR ANS$ = "n" THEN END
1470 'INPUT " TYPE THE FILE NAME: "; FL$
1475 FL$="Three"
1480 OPEN FL$ FOR OUTPUT AS #1 : OPEN "two" FOR OUTPUT AS #2
: CHANNEL$="THREE":TIME=0
1490 PRINT "Wait... I'm writing."
1740 FOR SCAN% = 1 TO NUMBER.OF.SCANS%
1750 SP% = SCAN% * SCAN.LENGTH%
1760 FOR C.PNT% = 0 TO SCAN.LENGTH% - 1
1770 CHANNEL% = C.PNT% + START.CHAN%
1780 '
1790 'Convert analog data value into a voltage in volts
1800  'CALL  ANALOG.TO.VOLTS(ANALOG.ARRAY%(SP%  +  C.PNT%),
GAIN%, VOLTAGE!)
1810    VOLTAGE!=    (((ANALOG.DATA.ARRAY%(SP%+C.PNT%)    *
9.000001E-02) /4096) - .045)
1815    'LPRINT    "scan%=";SCAN%,"analog.array%
=",ANALOG.DATA.ARRAY%(SP%+C.PNT%)
1820    'VOLTAGE!    =    (ANALOG.ARRAY%(SP%+C.PNT%)    *
SCALED.LSB!)+SCALED.LOW!
1825 TIME=TIME + 1/REQUESTED.FREQ
1829 GOSUB 2000
1830 IF CHANNEL$="THREE" AND TEMPERAT>LIMIT THEN BTIME=TIME
:PRINT #1, BTIME,TEMPERAT
1831 IF CHANNEL$="THREE" THEN CHANNEL$="TWO"  : GOTO 1835
1832 IF CHANNEL$="TWO" AND TEMPERAT>LIMIT THEN BTIME=TIME
:PRINT #2, BTIME,TEMPERAT
1833 IF CHANNEL$="TWO" THEN CHANNEL$="THREE"
1835 'AVERAGE=AVERAGE+VOLTAGE :PRINT CHANNEL$,BTIME,TEMPERAT
1840 NEXT C.PNT%
1850 NEXT SCAN%
1855 AVERAGE=AVERAGE/(NUMBER.OF.SCANS%*2)
1870 'VOLT!=((( CJADATA% * .04) /4096) - .02)
1880 'PRINT #1, "CJ VOLTAGE =",VOLT!
1885 'PRINT #1, "CJ TEMPERATURE =",CJTEMP
1886 SUM=VOLT!+VOLTAGE!
1887 'PRINT #1,"voltage!= ",VOLTAGE!
1888 'PRINT #1,"TOTAL VOLTS= ",SUM
1889 'PRINT #1,"AVERAGE = ",AVERAGE
1890 CLOSE #1 : CLOSE #2
1891 PRINT " End of A/D conversion"  :  SYSTEM    '   END
1                  9                    9                  9
```

```
'*************************************************************
2000 '      subroutine to convert from volts to temperature
2005 '   correlations are only good for tungsten-rhenium
termocouples
2010  IF  VOLTAGE!  <  1.01/1000  THEN  TEMPERAT=31.8727  +
128.4919 * VOLTAGE!*1000
2020 IF VOLTAGE! >=1.01/1000 AND VOLTAGE!<9.390001/1000 THEN
TEMPERAT=155.0759*(VOLTAGE!*1000)^.8279
2030  IF  VOLTAGE!  >=9.390001/1000  AND  VOLTAGE!<19.947/1000
THEN TEMPERAT=107.6579+94.4076*VOLTAGE!*1000
2040 IF VOLTAGE! >=19.947/1000 AND VOLTAGE!<28.953/1000 THEN
TEMPERAT=76.3295*(VOLTAGE!*1000)^1.0892
2050 IF VOLTAGE! >=28.953/1000 AND VOLTAGE!<35.978/1000 THEN
TEMPERAT=922.4559*EXP(.0407*VOLTAGE!*1000)
2060    IF    VOLTAGE!    >=35.978/1000    THEN
TEMPERAT=11.3566*(VOLTAGE!*1000)^1.6366
2070 '
2080 '
2090 TEMPERAT= (TEMPERAT-32)*5/9 + 273          'CONVERTS TO
DEGREES KELVIN
2095 TEMPERAT=TEMPERAT+45     ' calibrates for cold juntion
temperature
2100 RETURN
```